NASA TECHNICAL TRANSLATION NASA TT F-16,367

CALCULATION OF AIRCRAFT ENGINE TURBINES: (GASDYNAMIC CALCULATION — BLADE PROFILING)

S. Z. Kopelev and N. D. Tikhonov

(NASA-TT-F-16367) CALCULATION OF AIRCRAFT ENGINE TURBINES. (GASDYNAMIC CALCULATION: BLADE PROFILING) (Scientific Translation Service) 330 p HC $9.50 CSCL 21E N75-29120

G3/07 Unclas 33019

Translation of "Raschet turbin aviatsionnykh dvigateley (gazodinamicheskiy raschet profilirovaniye lopatok)", "Mashinostroyeniye" Press, Moscow, 1974, pp. 1-268

AUG 1975
RECEIVED
NASA STI FACILITY
INPUT BRANCH

NATIONAL AERONAUTICS AND SPACE ADMINISTRATION
WASHINGTON, D. C. 20546 AUGUST 1975

STANDARD TITLE PAGE

1. Report No.	2. Government Accession No.	3. Recipient's Catalog No.
NASA TT F-16,367		

4. Title and Subtitle	5. Report Date
CALCULATION OF AIRCRAFT ENGINE TURBINES (GASDYNAMIC CALCULATION — BLADE PROFILING	AUGUST 1975
	6. Performing Organization Code
7. Author(s)	8. Performing Organization Report No.
S. Z. Kopelev and N. D. Kikhonov	
	10. Work Unit No.
	11. Contract or Grant No. NASw-2483
9. Performing Organization Name and Address SCITRAN Box 5456 Santa Barbara, CA 93108	13. Type of Report and Period Covered Translation
12. Sponsoring Agency Name and Address National Aeronautics and Space Administration Washington, D.C. 20546	14. Sponsoring Agency Code

15. Supplementary Notes

Translation of "Raschet turbin aviatsionnykh dvigateley (gazodinamicheskiy raschet profilirovaniye lopatok)", "Mashinostroeniye" Press, Moscow, 1974, pp. 1-268.

16. Abstract

A generalization of various methods of gas-turbine design is presented, including an evaluation of methods of gasdynamic calculation of turbine stages, methods of blade profiling, and methods of calculating cooled blades. The size and weight characteristics of a turbine and their dependence on the main engine parameters are considered, and the relation between gasdynamic and strength parameters of a turbine is discussed, with allowance for its structural features and fabrication technology, paying special attention to choice of the layout and dimensions of the air-gas flow area and to the profiling of both nozzle and rotor blades. To facilitate understanding of the theory, a number of examples of specific calculations based on given numerical values of the initial parameters are presented which pertain to single-stage and multistage gas turbines of turbojet engines.

17. Key Words (Selected by Author(s))	18. Distribution Statement
	Unclassified - Unlimited

19. Security Classif. (of this report)	20. Security Classif. (of this page)	21. No. of Pages	22. Price
Unclassified	Unclassified	330	

NASA-HQ

ANNOTATION

Basic questions of the theory and methods of aviation engine turbine and gasdynamic design are presented in the book. The influence of the basic design parameters of a turbine stage on its efficiency is examined. Recommendations are given for turbine flow path configuration selection and flow path dimension determination.

Methods of air cooling of the blades and methods of determining their temperature are examined. Examples of cooled blade and multistage turbine design are presented. Turbine operation in off-design regimes is examined.

The book is intended for specialists working in the aviation industry. It can also be used by students in the aviation institutes.

PREFACE

The continuous development of aircraft gas turbine engines and the accumulation of experience in their design, production and operation necessitates a systematic description of this experience and its presentation to a wide circle of specialists.

Also, a need has arisen for appraisal of the various methods of gasdynamic analysis of turbine stages, profiling stator vanes and rotor blades, and design of cooled blades.

In the present book, practical experience in aviation engine turbine design is presented. The dimensional and weight characteristics of the turbine and their dependence on the fundamental engine parameters are examined; the connection between the gasdynamic and strength parameters of the turbine, keeping in mind its structural characteristics and fabrication technology, is discussed; this pertains especially to selection of the flow path scheme and dimensions and blade profiling. These questions are considered in this book in a series of problems arising in aviation gas turbine design.

Several examples of specific calculations with assigned numerical values of the initial parameters suitable for single-stage and multistage turbines are presented in order to clarify the ideas presented in this book.

The authors considered it advantageous to present the methods for calculating the basic parameters of turbojet aviation engine turbines, so that they can be used in writing programs for electronic digital computer calculations.

The methods presented in the book for determining the basic turbine parameters under off-design conditions are illustrated by sample claculations for a single-shaft, three-stage turbine operating under off-design conditions in a turboprop engine system.

All computation examples are based on hypothetical initial data, and therefore have purely methodological significance.

Chapters II - VII were written by S. Z. Kopelev. Sections 4.1 and 5.2 were written by S. Z. Kopelev and N. D. Tikhonov in collaboration. Chapters I, VIII, and IX were written by N. D. Tikhonov. Chapter VI uses work which was carried out by S. Z. Kopelev in collaboration with S. V. Gurov and M. V. Avilova-Shulgina, and in Chapter V — in collaboration with V. A. Zhuravlev.

The authors thank Candidate of Technical Sciences V. A. Gel'fer for help given during preparation of the book, and Engineer V. S. Zikeyev for valuable comments made during review of the manuscript.

A great deal of help with the book was given by the reviewer, the late G. L. Livshits.

TABLE OF CONTENTS

PREFACE		iv
CHAPTER I.	GENERAL INFORMATION FROM GAS TURBINE THEORY	1
	1.1. Turbine Scheme and Basic Geometric Parameters	1
	1.2. Elementary Turbine Stage. Basic Equations Stage	5
	1.3. Losses in the Turbine and Their Estimation. Turbine Efficiency	14
	1.4. Concept of Turbine Stage Degree of Reaction	26
	1.5. Basic Turbine Stage Governing Parameters	28
II.	BASIC TURBINE PARAMETERS AND THEIR INFLUENCE ON TURBINE EFFICIENCY	33
	2.1. Turbine Stage Loading	
	2.2. Flow Velocity and Direction at the Turbine Outlet	42
	2.3. Kinematics of Flow in Turbine Stage	47
III.	SELECTION OF TURBINE FLOW PATH SCHEME AND DETERMINATION OF BASIC TURBINE DIMENSIONS	52
	3.1 Determination of Number of Stages and Distribution of Work Between Them	53
	3.2. Determination of Basic Flow Path Dimensions at the Turbine Outlet	56
	3.3. Turbine Flow Path Configuration Selection	69
	3.4. Determining Rotor and Stator Cascade Widths	73
	3.5. Axial Clearance Between Blade Rows	82
	3.6. Overlap Between Vane and Blade Rows	84
	3.7. Losses Introduced by a Body Located Ahead of the Stator	88
IV.	GASDYNAMIC CALCULATION OF TURBINE STAGE	91
	4.1. Calculation of Turbine Stage at the Mean Diameter	91
	4.2. Radial Variation of Flow Parameters in Turbine Stage	104
	4.3. Determination of Stage Flow Parameters at the Inner and Outer Radii	116

CHAPTER V. PROFILING TURBINE BLADES 125

5.1. Choice of Basic Cascade and Profile Parameters 125

5.2. Blade Profile Construction 135

5.3. Matching the Individual Section Profiles and Constructing the Profiled Part of the Blade 143

5.4. Techniques for Constructing Blades with Machined Profiled Part 147

5.5. Profiling Cooled Blades 152

VI. COOLING OF GAS TURBINE BLADES AND VANES 156

6.1. Open-Cycle Air Cooling Scheme 156

6.2. Blades with Internal Convective Cooling 164

6.3. Cooling Effectiveness with Heat Transfer in Blades with Transverse Flow Scheme 173

6.4. Determining Cooling Air Flowrate in Blades with Transverse Flow Scheme 181

6.5. Determining Cooled Blade Temperature 188

VII. DEGREE OF LOADING OF TURBINE STAGE WITH COOLED BLADES 207

7.1. Cooled Blade Temperature as Function of Stage Loading Coefficient 207

7.2. Variation of Cooled Blade Strength Margin with Increase of Stage Loading 213

VIII. GASDYNAMIC CALCULATION OF MULTISTAGE TURBINE 220

8.1. Basic Features and Sequence of Multi-stage Gas Turbine Calculation 220

8.2. Two-Stage TJE Turbine Gasdynamic Calculation Example 230

8.3. Example of Approximate Gasdynamic Calculation of Two-Stage TJE Turbine 251

8.4. Profiling Turbine Blades 258

IX. OFF-DESIGN TURBINE OPERATING REGIMES 266

9.1. Basic Concepts of Turbine Operating Regimes and Characteristics 266

9.2. Laws Governing Variation of Basic Turbine Parameters with Turbine Operating Regime Variation 273

9.3. Determination of Basic Turbine Parameters in Off-Design Regimes 282

9.4. Example of Turbine Parameter Calculation in Off-Design Regimes 296

APPENDICES 306

REFERENCES 320

CHAPTER I

GENERAL INFORMATION FROM GAS TURBINE THEORY

1.1. Turbine Scheme and Basic Geometric Parameters

The gas turbine is a bladed machine in which gas flow potential energy is transformed into mechanical work on the turbine shaft. /5*

In aviation gas turbine engines (GTE), the turbine is employed to drive the compressor, propellor, and engine accessories. Turbines are often used in starting systems for turning over the GTE rotor during start-up. The stationary stator and rotating rotor are the fundamental elements of the gas turbine.

The stationary part of the turbine is called the stator, and consists of the frame, nozzle ring, and other nonmoving turbine parts. The nozzle ring transforms the potential energy of the gas into kinetic energy. It consists of a series of vanes positioned radially between two coaxial banding rings (Figure 1.1).

The rotor consists of a rotating working wheel (disk with blades fastened on it) and a shaft.

---

*Numbers in the margin indicate pagination in the original foreign text.

The combination of a stator and a rotor is called a turbine stage. The annular channel from the stator entrance to the rotor exit is called the turbine flow path, and its form in the turbine longitudinal section is called the meridional flow path profile.

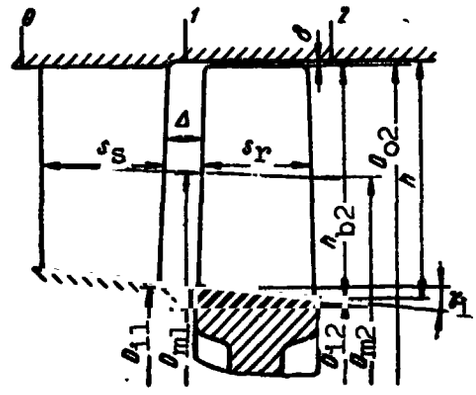

Figure 1.1. Flow path scheme of a single-stage turbine /6

In contemporary turbojet engines (TJE), one-stage, two-stage and three-stage turbines are used. In turboprop (TPE) and turbofan (TFE) engines, where the turbine turns the propellor or fan in addition to the core flow compressor, multistage turbines having four to six or more stages are used.

The process of gas energy transformation is the same in each stage of a multistage turbine. Therefore, it is sufficient to examine the operating principles and energy transformation processes in a turbine using an example of a single stage or an individual one-stage turbine.

In analyzing the processes and designing the turbines, the gas flow parameters and the basic geometric dimensions usually are considered only at three reference sections along the turbine stage path, which are denoted by the following indices:

"0" — denotes stator inlet parameters*;

"1" — denotes parameters in the axial clearance between the stator and rotor;

"2" — denotes rotor exit parameters.

---

*In certain cases, the turbine inlet gas is denoted T_3^*, as is done in examining the turbine in the engine system.

The numerals I, II, III, and so forth, will denote the stage number.

Turbines are divided into axial, radial, and diagonal, depending on the form of the flow path meridional section and the flow direction. Here, only the axial gas turbine is examined, in which the flow path is nearly cylindrical, and the radial velocity components are absent or small in comparison with the axial and circumferential velocity components.

The basic geometrical dimensions of the turbine stage are denoted as follows:

D_o — the outer (peripheral) diameter;

D_i — the inner (root) diameter;

$D_m = \frac{D_o + D_i}{2}$ — is the mean turbine diameter (the diameter of the circle passing through the mean blade sections) (occasionally D_m is the diameter defined by the formula $D_m = \sqrt{\frac{D_o^2 + D_i^2}{2}}$);

h — turbine flow path height;

h_b — blade length (height);

f — turbine flow path section area;

Δ — axial clearance;

δ — radial clearance;

S_s and S_r — the stator and rotor cascade widths; /7

b — the blade chord;

γ_o and γ_i — flow path divergence angles at the blade periphery and root, respectively;

$\bar{h} = h_b/b$ — (or $\bar{h} = h_b/S$) — blade aspect ratio;

$\bar{d} = D_i/D_o$ — relative hub diameter.

The relative length of the turbine blade is characterized by the ratio of the mean diameter to the blade length:

$$\bar{D} = \frac{D_m}{h_b} = \frac{D_o + D_i}{D_o - D_i} = \frac{1 + \bar{d}}{1 - \bar{d}} .$$

All of the above parameters are also denoted by indexes corresponding to the stage design section number. For example, the flow path dimensions at the rotor entrance are denoted by $D_{o\,1}$, $D_{i\,1}$, $D_{m\,1}$, F_1, $h_{b\,1}$; those at the rotor exit — $D_{o\,2}$, $D_{i\,2}$, $D_{m\,2}$, F_2, $h_{b\,2}$.

At some radius r, we cut the turbine blades by a coaxial cylindrical surface, and then we develop this section onto a plane. As a result, we obtain a plane cascade of stator and rotor profiles.

The basic geometric paramaters of the profile cascade (Figures 1.2 and 1.3) are:

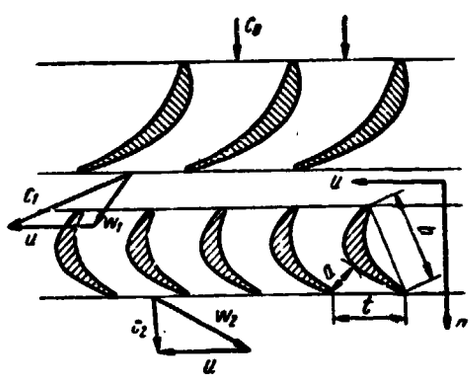

Figure 1.2. Development of annular turbine stage blade section

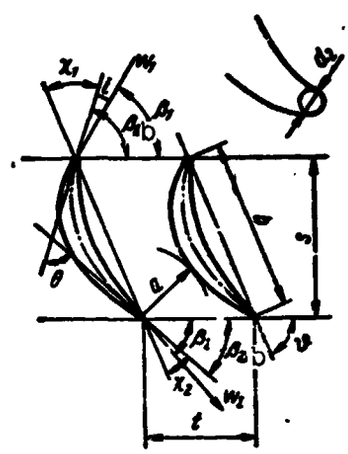

Figure 1.3. Geometrical parameters of the profile cascade

b — blade profile chord;

t — cascade spacing;

$\bar{t} = t/b$ — relative cascade spacing;

$\bar{b} = b/t$ — cascade solidity (reciprocal of the relative spacing); /8

θ — profile setting angle in the cascade;

$\beta_{1\,b}$ — profile entrance angle, formed by the tangent to the profile median line at the leading edge and the cascade front;

$\beta_{2\,b}$ — profile exit angle, formed by the tangent to the median line at the trailing edge and the cascade front;

$\beta_{ap} = \arcsin \frac{a}{t}$ — cascade exit angle.

Flow entrance and exit angles in the stator cascade are denoted by the letter α with the index of the corresponding section.

1.2. Elementary Turbine Stage.
Basic Equations Stage

The gas flow in a turbine has a spatial (three-dimensional) character. To simplify turbine analysis and calculations, the real gas flow pattern is replaced by an approximate scheme. It is assumed that the gas in the turbine flows in coaxial, cylindrical layers whose axes coincide with the turbine axis. An elementary turbine stage, which is the combination of the stator and rotor profile cascades at a given radius, corresponds to each such layer of infinitesimal thickness. The development of the cylindrical section of the turbine onto a plane is called a plane elementary turbine stage.

In the elementary stage, we can consider the parameters of the gas constant along the blade height. This allows us to regard the elementary stage as a plane profile cascade, which significantly simplifies the analysis and computations of the gas flow parameters in the turbine stage.

With known flow parameters in each elementary stage, it is possible to determine the average values of the parameters of the entire stage by integrating these parameters over the blade height. In many cases (for example, with constant work along the blade height), the average parameters are close to the gas parameters at the mean turbine diameter.

1.2.1. Kinematics of flow in an elementary turbine stage

We will assume that the flow at the cascade entrance and exit is stationary and axially symmetric, that is, all gas stream filaments along the front of the cascade have velocities identical in magnitude and direction. In reality, there will be such flow only at a quite large distance ahead of the cascade, where the cascade influence on the unperturbed flow is absent, and behind the cascade /9
where the flow perturbed by the cascade has equalized. Immediately before and behind the cascade, and especially in the inter-blade channel, the flow is not uniform.

As is well known, to characterize the gas flow in the elementary stage, a velocity diagram (triangle) of the gas flowing around the profile cascade is used (Figure 1.4). The flow absolute velocity vectors are denoted by the letter c, the relative velocity vectors — w, and the circumferential velocity vectors — u.

For the stator cascade, the following kinematic flow parameter designations are introduced:

c_0, α_0 and c_1, α_1 — flow velocities and angles at the stator entrance and exit, respectively.

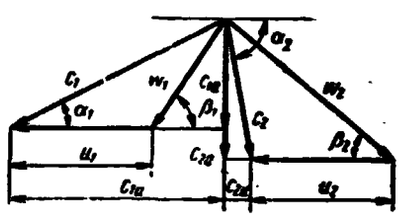

Figure 1.4. Velocity diagram of a turbine stage

For the rotor cascade:

w_1 and β_1 — flow velocity and angle at the cascade entrance in the relative motion;

$i = \beta_{1\,b} - \beta_1$ — angle of attack (with $\beta_{1\,b} > \beta_1$, the angle of attack is considered positive; with $\beta_{1\,b} < \beta_1$, it is negative);

c_2 and w_2, α_2 and β_2 — flow velocities and angles at the cascade exit in the absolute and relative motions;

$\Delta\beta=\beta_2-\bar{\beta}_{2p}$ — flow lag angle, where β_{2p} = arc sin a/t.

The velocity projections on the axial direction are denoted by the index "a", and on the circumferential direction by the index "u"; downstream and rotor rotation directions are considered positive.

The connection between the cascade kinematic parameters is found from the velocity triangles.

It should be kept in mind that the magnitude and direction of the velocities at the cascade inlet and outlet vary in the interblade space. Therefore, we take the average values for the velocities c_1, w_1, w_2, c_2 and flow angles α_1, β_1, β_2, α_2.

The turbine stage working principle is as follows. The gas enters the stator from the combustion chamber with velocity c_0, pressure p_0, and temperature T_0. The stator blades form converging curvilinear channels, in which expansion of the gas and turning of the flow occurs. Due to this, the gas temperature and pressure decrease, but the velocity increases from c_0 to c_1. From the stator, the gas enters the rotor cascade with the relative velocity w_1. The rotor blades, in most cases, also form converging curvilinear channels in which flow turning and further expansion of the gas occurs, /10
accompanied by decrease of its pressure and temperature. The flow relative velocity increases from w_1 to w_2. The gas absolute velocity decreases from c_1 to c_2 in the rotor. The decrease of the absolute velocity in the rotor occurs because a large part of the gas kinetic energy, obtained as a result of the gas expansion in the stator and rotor, is transformed into mechanical work of wheel rotation.

When there is flow around the rotor blades, the pressure on the concave side of the blade becomes larger than on the convex side, due to the turning of the flow in the cascade (Figure 1.5). The result of the pressure and friction forces action on the blade surface is the aerodynamic force. The circumferential components (P_u) of the forces acting on each blade create a torque and drive the rotor, while the axial components (P_a) determine the axial force acting on the turbine rotor.

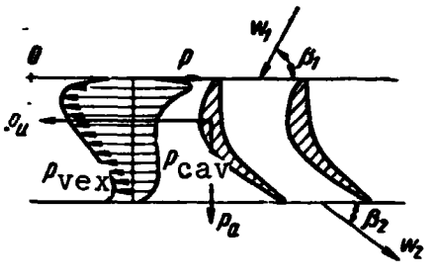

Figure 1.5. Pressure distribution over a profile

It is obvious that the magnitude of the aerodynamic force acting on each blade will be larger, the higher the velocity of the gas flowing around the blades and the larger the flow turning in the grid.

1.2.2. Basic equations of the elementary turbine stage

The connection between the gas parameters at various sections of the turbine flow path is established on the basis of the gas flow equations and the thermodynamic relations between the gas state parameters in the adiabatic expansion process. The basic equations of the turbine stage are: continuity, energy conservation, Bernoulli, and Euler. In writing these equations, several simplifying assumptions are made (the flow is considered steady and uniform; heat exchange with external medium is absent, and so forth), with the goal of obtaining a simpler form of these equations, suitable for engineering calculations. The derivation of the basic equations is given in well known courses on thermodynamics and turbomachine theory [9, 23, 24, 28, and others]. Therefore, we limit ourselves here to examination of the application of these equations to gas flow in the turbine stage.

1. The flowrate (continuity) equation.

For an elementary stage and an individual stream filament, the gas mass flow rate is: /11

$$\Delta G = \varrho_0 c_0 f_0 = \varrho_1 c_1 f_1 = \varrho_2 c_2 f_2,$$

where f_0, f_1, f_2 — cross section areas at the respective stage sections;
$\varrho_0, \varrho_1, \varrho_2$ — gas densities at the respective stage sections;
c_0, c_1, c_2 — normal gas velocity components at the respective stage sections.

For the turbine stage, the gas flowrate is:

$$G = \int_{F_0} \varrho_0 c_0 dF_0 = \int_{F_1} \varrho_1 c_1 dF_1 = \int_{F_2} \varrho_2 c_2 dF_2,$$

where F_0, F_1, F_2 — gas flow cross section areas;
$\varrho_0, \varrho_1, \varrho_2$ and c_0, c_1, c_2 — instantaneous values of the gas density and velocity at the respective sections.

If the flow parameters are constant at each section, the continuity equation will have the form:

$$G = \varrho_0 c_0 F_0 = \varrho_1 c_1 F_1 = \varrho_2 c_2 F_2.$$

The continuity equation will also have this form if we substitute into it the average values of the flow parameters for the flow path section.

The gas flow rate through any turbine flow path section can be expressed in terms of the dimensionless flow density function:

$$q(\lambda) = \frac{c\varrho}{(c\varrho)_{cr}} = f\left(\frac{p}{p^*}\right);$$
$$G = F_i c_i \varrho_i = F_i (c_i \varrho_i)_{cr} q(\lambda_i),$$

where $\lambda = c/a_{cr}$ — reduced velocity;
a_{cr} — critical speed of sound;

$$(c_i \rho_i)_{cr} = m \frac{p_i^*}{\sqrt{T_i^*}}; \quad m = \sqrt{\frac{k}{R}\left(\frac{2}{k+1}\right)^{\frac{k+1}{k-1}}}.$$

For k = 1.33, and R = 289 J/(kg · K);

$m = 0.0396\ (\text{kg} \cdot \text{K/J})^{0.5}$.

Then, $G = m \frac{p_i^*}{\sqrt{T_i^*}} F_i q(\lambda_i)$.

2. Energy conservation equation.

In the absence of heat exchange with the external medium, the gas flow energy conservation equation for the turbine has the form:

$$L_T = i_0^* - i_2^* = c_p (T_0^* - T_2^*)$$

or, /12

$$L_T = c_p (T_0 - T_2) + \frac{c_0^2 - c_2^2}{2},$$

where L_T — work extracted from the gas in the turbine;

i_0^* and i_2^* — total gas enthalpies at the turbine inlet and outlet

An illustration of the gas expansion process in the turbine is presented in Figure 1.6, where the line 0-1-2 is the polytropic gas expansion curve in the stator and rotor;

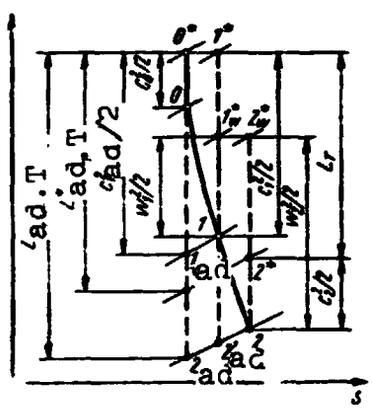

Figure 1.6. Representation of gas expansion process in a turbine on i-s diagram

0*, 1*, 2* — points characterizing the parameters of flow retarded in terms of the absolute velocity at the corresponding stage turbine sections;

1_w^*, 2_w^* — points characterizing the parameters of flow retarded in terms of relative velocity at the rotor inlet and outlet.

For the stator, the energy equation has the form:

$$i_0^* = i_1^* \text{ or } c_p T_0^* = c_p T_1^* = c_p T_1 + \frac{c_1^2}{2}. \tag{1.1}$$

From Equation (1.1), we obtain the formula for determining the gas exit velocity from the stator:

$$c_1 = \sqrt{2c_p(T_1^* - T_1)} = \sqrt{2c_p T_1^* \left(1 - \frac{T_1}{T_1^*}\right)}.$$

Keeping in mind that $\frac{T_1}{T_1^*} = \left(\frac{p_1}{p_1^*}\right)^{\frac{k-1}{k}}$, and $p_1^* = \sigma_s^* p_0^*$, we obtain:

$$c_1 = \sqrt{2c_p T_1^* \left[1 - \left(\frac{p_1}{p_0^* \sigma_s^*}\right)^{\frac{k-1}{k}}\right]}.$$

where σ_s^* — coefficient of total pressure losses in the stator.

The hydraulic losses in the stator are more frequently estimated with the help of the velocity coefficient $\phi = c_1/c_{1\ ad}$, where $c_{1\ ad}$ is the stator exit velocity for adiabatic expansion of the gas;

$$c_{1\ ad} = \sqrt{2c_p T_0^* \left[1 - \left(\frac{p_1}{p_0^*}\right)^{\frac{k-1}{k}}\right]}.$$

Then, /13

$$c_1 = \varphi \sqrt{2c_p T_0^* \left[1 - \left(\frac{p_1}{p_0^*}\right)^{\frac{k-1}{k}}\right]}. \tag{1.2}$$

The energy equation for the rotor:

a) in the absolute motion:

$$L_T = i_1^* - i_2^* = c_p(T_1^* - T_2^*);$$

b) in the relative motion:

$$i_{1w}^* = i_{2w}^*, \quad c_p T_{1w}^* = c_p T_{2w}^*$$

$$\text{or } c_p T_{1w}^* = c_p T_1 + \frac{w_1^2}{2} = c_p T_2 + \frac{w_2^2}{2}. \tag{1.3}$$

From the energy equation, we obtain the expression for the relative gas exit velocity from the rotor:

$$w_2=\sqrt{2c_pT^*_{1w}\left[1-\frac{T_2}{T^*_{1w}}\right]}.$$

Keeping in mind that $T^*_{1w}=T^*_{2w}$, $\frac{T_2}{T^*_{1w}}=\frac{T_2}{T^*_{2w}}=\left(\frac{p_2}{p^*_{2w}}\right)^{\frac{k-1}{k}}$, and $p^*_{2\ w} = \sigma^*_r p^*_{1\ w}$, we obtain:

$$w_2=\sqrt{2c_pT^*_{1w}\left[1-\left(\frac{p_2}{\sigma^*_r\, p^*_{1w}}\right)^{\frac{k-1}{k}}\right]}, \qquad (1.4)$$

where σ^*_r — coefficient of total pressure losses in the rotor.

If the hydraulic losses in the rotor are estimated with the help of the velocity coefficient ψ, equal to the ratio of the actual rotor exit velocity to the adiabatic — $\psi = w_2/w_{2\ ad}$, then,

$$w_2 = \psi w_{2\ ad} = \psi\sqrt{2c_pT^*_{1w}\left[1-\left(\frac{p_2}{p^*_{1w}}\right)^{\frac{k-1}{k}}\right]}$$

or

$$w_2=\psi\sqrt{2c_pT_1\left[1-\left(\frac{p_2}{p_1}\right)^{\frac{k-1}{k}}\right]+w_1^2}.$$

3. Bernoulli equation —

$$L_\tau=\int_2^0 v\,dp-L_r-\frac{c_2^2-c_0^2}{2},$$

where $\int_2^0 v\,dp=L_{pol}=\frac{n}{n-1}RT_0\left[1-\left(\frac{p_2}{p_0}\right)^{\frac{n-1}{n}}\right]$ — polytropic work of gas expansion in the turbine;

L_r — work expended in overcoming hydraulic friction with the flow of 1 kg of gas in the turbine. /14

For the isentropic processes (n = k):

$$\int_{p_2}^{0} v\,dp = L_{ad.T} = \frac{k}{k-1} RT_0 \left[1 - \left(\frac{p_2}{p_0}\right)^{\frac{k-1}{k}}\right].$$

It is possible to represent the polytropic work as the sum of the adiabatic work L_{ad} and the additional work ΔL_s, appearing as the result of increased gas expansion work, because of its heating in flow with hydraulic losses,

$$L_{pol} = L_{ad.T} + \Delta L_s.$$

Then it is possible to write the Bernoulli equation in the form:

$$L_T = L_{ad.T} + \Delta L_s - L_r - \frac{c_2^2 - c_0^2}{2}$$

or, $L_T = L_{ad.T} - L_r' - \frac{c_2^2 - c_0^2}{2}$,

where $L_r' = L_r - \Delta L_s$ — irreversible losses in the turbine.

Thus, the turbine effective work (extracted in the form of mechanical energy) is equal to the adiabatic work of gas expansion minus the hydraulic losses and kinetic energy increase.

4. Euler equation.

On the basis of the angular momentum theorem for the elementary turbine stage, it is possible to write:

$$dM_u = dG(c_{1u} r_1 + c_{2u} r_2), \tag{1.5}$$

where dM_u — elementary stage rotor torque;

dG — gas flowrate through the elementary stage cascade;

c_{1u} and c_{2u} — circumferential components of the gas absolute velocity at the exit from the stator and behind the stage;

r_1 and r_2 — distances between the gas stream filament and the axis rotation at the corresponding stage sections.

It is possible to set $r_1 = r_2 = r$ for axial turbines. The elementary stage work per kilogram of gas:

$$L_{st} = \frac{dM_{\omega}}{dG} = \frac{dM_{u}}{dG}\frac{u}{r}; \tag{1.6}$$

where $\omega = u/r$ — rotor angular velocity.

Then, we obtain from (1.5) and (1.6):

$$L_{st} = u(c_{1u} + c_{2u}) = u\Delta c_{u},$$

where $\Delta c_{u} = c_{1u} + c_{2u}$.

The basic equations considered above for an elementary stage /15
can also be applied to a real stage. In this case, they should have an integral form, since in the turbine stage, the gas parameters usually vary along the blade height.

The initial design of the turbine, using the basic equations, is made for the mean diameter, using at the cascade inlet and outlet the flow parameters averaged over the blade height and considering all losses in the turbine flow path.

1.3. Losses in the Turbine and Their Estimation. Turbine Efficiency

It is possible to divide the losses in the turbine flow path into the following three basic types.

1. Profile losses, including:

a) losses from friction and eddy formation in the boundary layer and during its separation;

b) edge losses, arising in the vortical trailing wake and during mixing of the flows coming from the concave and convex sides of the profile;

c) losses in shock waves and in their interaction with the boundary layer.

2. End losses:

a) from secondary flows (paired vortices) in the stator and rotor cascades, and losses in the boundary layer on the end walls;

b) from leakage flow in the radial clearance.

3. Additional losses (outside the cascade):

a) from friction and eddy formation in the boundary layer on the side walls in the axial clearance;

b) from friction of the disk with the gas;

c) from leakage flow through the labyrinth seals and slots;

d) from mixing of the main flow with the cooling air.

With gas flow in cascades, the hydraulic resistances (losses) reduce the kinetic energy and total pressure of the gas, as a result of which the gas velocities leaving the stator and rotor cascades decrease, and the effective turbine work decreases.

The hydraulic losses in turbine cascades are estimated with the help of the loss coefficient ξ_Σ, which is the ratio of the enthalpy losses in the cascade ΔH to the available isentropic enthalpy in the cascade H_{ad}:

$$\xi_\Sigma = \Delta H/H_{ad} \text{ or } \xi_\Sigma = L_r'/L_{ad},$$

where $\Delta H = L'_r$; $H_{ad} = L_{ad}$, L'_r — irreversible losses in the cascade.

For the stator cascade:

$$L'_{r.s} = \frac{c_{1\ ad}^2 - c_1^2}{2} = \xi_s \frac{c_{1\ ad}^2}{2}, \tag{1.7}$$

for the rotor cascade: /16

$$L'_{r.r} = \frac{w_{2\ ad}^2 - w_2^2}{2} = \xi_r \frac{w_{2\ ad}^2}{2}. \tag{1.8}$$

The cascade loss coefficient can be represented as the sum of the coefficients of separate forms of losses in the cascade:

$$\xi_\Sigma = \xi_{pr} + \xi_{sec} + \xi_\delta = \xi_{pr} + \xi_e,$$

where ξ_{pr} — profile loss coefficient;

ξ_{sec} — secondary loss coefficient;

ξ_δ — coefficient of losses connected with leakage flow in the radial clearance end loss;

$\xi_e = \xi_{sec} + \xi_\delta$ — end loss coefficient.

In calculations of gas flow in turbine cascades, the profile losses are usually accounted for using the velocity coefficients $\phi = c_1/c_{1\ ad}$ and $\psi = w_2/w_{2\ ad}$.

From (1.7) and (1.8), it is obvious that

$$\varphi^2 = 1 - \xi_s \text{ and } \psi^2 = 1 - \xi_r.$$

Sometimes, both the profile losses and the secondary losses are considered with the help of the velocity coefficients ϕ and ψ. In this case, $\phi^2 = 1 - \xi_{pr} - \xi_{sec}$ and $\psi^2 = 1 - \xi_{pr} - \xi_{sec}$.

Total pressure losses in the cascade are estimated with the help of the pressure loss coefficient σ^*:

$$\sigma_s^* = \frac{p_1^*}{p_0^*} \text{ and } \sigma_r^* = \frac{p_{2w}^*}{p_{1w}^*}.$$

The correction between σ^* and ϕ (or ψ) is expressed by the formula:

$$\sigma_s^* = \frac{\pi(\lambda_1/\varphi)}{\pi(\lambda_1)}; \quad \sigma_r^* = \frac{\pi(\lambda_{2w}/\psi)}{\pi(\lambda_{2w})}.$$

Loss coefficients are usually obtained experimentally by flow testing plane or annular turbine cascades.

1.3.1. Profile loss coefficient and its dependence on the basic cascade parameters

Results of experimental investigations show that the profile loss coefficient (ξ_{pr} or the velocity coefficients ϕ and ψ) depends primarily on the following parameters: the profile camber angle $\theta = 180 - (\beta_{1\,b} + \beta_{2\,b})$, the angle characterizing flow turning in the cascade $\varepsilon = 180 - (\beta_1 + \beta_2)$, the degree of convergence of the inter-blade channel K_p, leading and trailing edge thicknesses d_1 and d_2, cascade solidity, and also the angle of attack i, and the M [Mach] and Re [Reynolds] numbers. The cascade convergence is characterized by $K_p = \sin\beta_{1\,b}/\sin\beta_{2\,b}$, and the degree of flow convergency by the /17 ratio of the flow areas at the cascade inlet and outlet $K = f_1/f_2 \approx \sin\beta_1/\sin\beta_2$. For active cascades $K_p = 1$, and for reactive cascades $K_p > 1$. With $K_p < 1$, the cascade will be diffusive. For turbine cascades $K_p \geq 1$.

Experimentally, profile losses are determined as the sum of the friction and edge loss coefficients $\xi_{pr} = \xi_{fr} + \xi_{ed}$. When designing cascades, it is desirable to have separate data on these losses.

For contemporary profiles in subsonic flow, the cascade friction losses as a function of the sum of the angles ($\beta_{1\,b} + \beta_{2\,b}$) and cascade convergence can be determined from the experimental data of G. Yu. Stepanov and V. L. Epshtein [23], and are characterized by the relations presented in Figure 1.7. From this figure, it is obvious that the losses due to friction decrease with increase of the sum of the cascade angles and increase of K_p. Hence, losses in a reactive cascade are significantly smaller than in an active one.

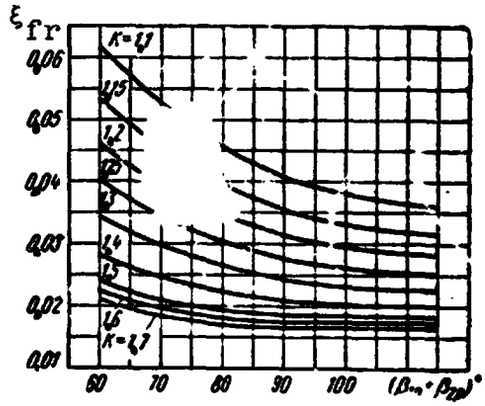

Figure 1.7. Dependence of cascade friction losses on the sum of the angles $\beta_{1p}+\beta_{2p}$

The average losses due to friction presented in Figure 1.7 in plane cascades correspond to optimal relative profile thickness, which depends on the flow turning angle and on the cascade type, on which, in turn, the form of the inter-blade channel and character of the flow in the cascade depend.

G. Yu. Stepanov proposed a formula for determining optimal relative profile thickness:

$$\left(\frac{c_{max}}{b}\right)_{opt} - 1 - A \sin \beta_{1\,b}$$

where A — experimental coefficient equal to 0.8 - 1.0 for active cascades, and 1.0 - 1.1 for reactive cascades. /18

Edge losses arise as a result of the interaction of boundary layers flowing from the concave and convex sides of the profile. They depend on the boundary layer state at the trailing edge. With boundary layer separation, the edge losses increase sharply.

It is recommended in several works [1, 23, 28] that the edge loss coefficient be estimated with the empirical formula:

$$\xi_{cr} = 0{,}2\frac{d_2}{a} = 0{,}2\frac{d_2}{\beta_{2p}}.$$

where a — cascade interblade channel throat width, and

β_{2p} — cascade exit angle.

With known values of the loss coefficients due to friction and edge losses, the profile loss coefficient in a plane cascade with subsonic flow velocities can be determined:

$$\xi_{pr} = \xi_{fr} + \xi_{cr}.$$

On the basis of the above data, the values of ξ_{pr} and the velocity coefficient $\psi = \sqrt{1 - \xi_{pr}}$ are computed in [28] for various flow turning angles and degree of cascade convergence. The relations $\psi_{pr} = f[(\beta_{1\,b} + \beta_{2\,b}), K_p]$, presented in Figure 1.8, can be used to estimate the velocity coefficients ϕ and ψ with subsonic flow velocities in cascades in the region of self-similarity with respect to Re.

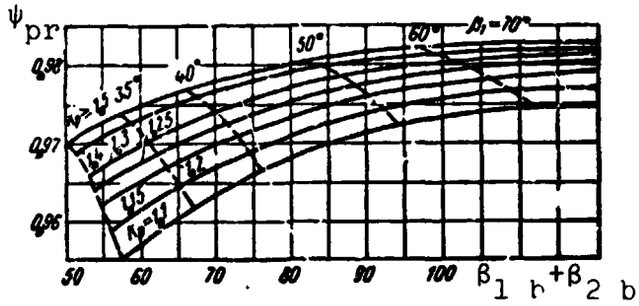

Figure 1.8. Dependence of the velocity coefficient ψ_{pr} on cascade convergence K_p and flow turning angle in the cascade /19

1.3.2. Secondary loss coefficients

The semi-empirical formula (see Figures 3.11 and 3.12):

$$\bar{\xi} = \frac{\xi_{sec}}{\xi_{\Sigma}} = \frac{A}{1 + 0{,}5\tilde{h}}, \qquad (1.9)$$

can be used to evaluate casacde secondary losses on the basis of experimental data. Here, $\xi_{\Sigma} = \xi_{pr} + \xi_{sec}$; $\tilde{h} = h_b/a$;

h_b — blade length; $a = t \sin \beta_{2p}$ ($t \sin \alpha_{1\,p}$); the coefficient $A = 1.0 - 1.1$; the value is smaller ($A = 1.0$) for cascades with

turning angle $\varepsilon = 180 - (\beta_1 + \beta_2) \geqq^{*} 70°$; the value is larger ($A = 1.1$) for cascades with flow turning angle $\varepsilon = 110°$.

Then, the coefficient of secondary loss:

$$\xi_{sec} = \xi_{\Sigma}\bar{\xi} \text{ or } \xi_{sec} = \xi_{pr}\frac{\bar{\xi}}{1-\bar{\xi}}.$$

It is obvious from (1.9) that the smaller $\tilde{h}$ (the shorter the blade), the larger the secondary flow losses.

From the known values of the coefficients ξ_{pr} and ξ_{sec}, it is possible to determine the velocity coefficients ϕ and ψ, taking into account both profile and secondary losses.

1.3.3. Losses from leakage flow in the radial clearance

Depending on the turbine diameter and structural stiffness, the radial clearance between the blade tip and the turbine housing in the cold state is chosen in the limits $\delta = 0.5 - 1.5$ mm. With increase of the radial clearance, the losses in the turbine stage increase and the efficiency decreases. Losses because of the radial clearance are caused by the following:

1) part of the gas exits through the clearance without performing work in the wheel;

2) an eddy zone arises at the trailing edge on the back side of the blade;

3) the pressure differential across the blade decreases in the peripheral part and, correspondingly, the aerodynamic force on the tip of the blade and turbine work decrease.

---

*Translator's note. Ina[illegible] ven as $\leqq$ in the original foreign text.

The loss coefficient ξ_δ, accounting for gas leakage flow through the radial clearance, can be taken to be equal to the ratio of the gas flowrates through the clearance and through the cascade (supposing that the kinetic energy of the gas flowing through the clearance is completely lost). This flowrate ratio in the cascade with blades without shrouds, in turn, is approximately proportional to the corresponding section area ratio [23]:

$$\xi_\delta = \frac{G_\delta}{G} \approx k_G \frac{\delta \delta}{t h_b \sin \beta}, \tag{1.10}$$

where k_G = 0.5 - 0.7 is the discharge coefficient.

The discharge coefficient k_G depends on the hydraulic resistance /20
in the clearance: the larger values of k_G correspond to blades with narrower tip sections.

Computations and experimental data show that increase of the relative radial gap $\bar{\delta} = \delta/h_b$ by 0.01 reduces turbine stage efficiency, on the average, by 1.5 - 2.5% [24]. The experimental dependence of the quantity $(1-\xi_\delta)$ on the radial gap is presented in Figure 1.9.

In the case of blades fitted with shrouds forming a banding ring, ξ_δ is taken equal to zero, and the possibility of gas leakage over the banding ring is almost completely eliminated by using special labyrinth seals. The use of shrouds and labyrinth seals increases turbine efficiency about 2 - 3%. However, the use of shrouds is often limited, since with a large tangential velocity of the blade periphery, low profile cascade solidity, and small thickness of the shrouds, strains develop in them which surpass the allowable levels. In such cases, use of narrow shrouds which do not fully cover the interblade channel may be feasible. Experience shows that the installation of such shrouds also reduces the losses caused by the presence of the radial gap.

In many cases, the blades are banded using wire, to prevent resonant vibrations of the rotor blades. The presence of the banding

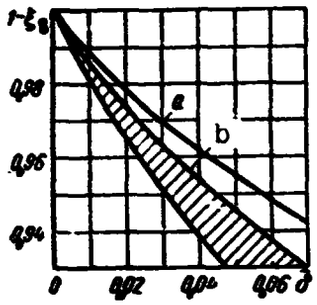

Figure 1.9. Dependence of losses in the radial gap on relative size gap $\bar{\delta} = \delta/h_b$: a — active stage; b — reactive stage

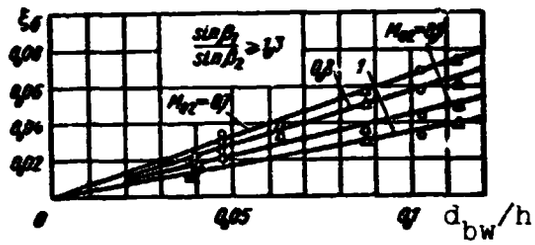

Figure 1.10. Dependence of cascade loss coefficient on relative banding wire diameter

wire in the interblade channel causes additional hydraulic losses. For an estimate of these losses in a turbine stage, attributable to the banding wire, the experimental relation $\xi_\delta = f(d_{bw}/h)$ (Figure 1.10), found in [15], can be used, where d_{bw} is the banding wire diameter. /21

1.3.4. Additional losses

Losses from friction and eddy formation in the boundary layer on the side walls in the axial gap and losses from mixing of the primary flow with the cooling air are small (usually less than 1%); therefore, in approximate calculations, they are usually neglected.

The relations presented for estimating stage profile losses are given for the cases of a flow around cascades at optimal angles of attack. Cascade losses increase with deviation of the attack angles from their optimal values (Figure 1.11).

1.3.5. Dependence of losses on cascade solidity

The influence of cascade solidity on the losses in it appears in the following way. With decrease of cascade solidity, the friction area between the blades and gas and the friction losses in the cascade decrease. However, at the same time, the pressure on the concave (face) side increases, and on the convex (back) side decreases.

This causes increased velocity on the back of the profile and local diffusion of the flow on the aft portion of the convex side of the profile, which can lead to boundary layer separation and, consequently, increased losses.

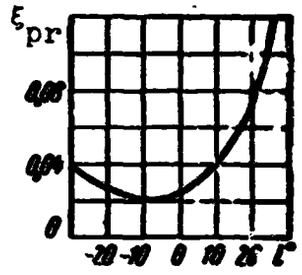

Figure 1.11. Dependence of profile losses on angle of attack

The opposing influence of these two factors means that for each cascade, there is an optimal solidity (relative spacing) for which the losses in it are minimal.

The optimal relative cascade spacing can be determined from the empirical formula proposed by V. I. Dyshlevskiy:

$$(t/b)_{opt} = 0{,}55\left[\frac{180}{180-(\beta_1+\beta_2)}\,\frac{\sin\beta_1}{\sin\beta_2}\right]^{\frac{1}{3}}(1-\bar{c}), \qquad (1.11)$$

where $\bar{c} = c_{max}/b$ — relative profile thickness (c_{max} — maximum profile thickness).

Formula (1.11) gives satisfactory results for angles $\beta_2 < 40°$. For the stator, it is necessary to replace β_1 by α_0 and β_2 by α_1.

It is important to note that (1.11) does not reflect directly the influence of the velocity level in the cascade on $(t/b)_{opt}$. It is obvious that, other conditions being equal, the larger the cascade outlet velocity λ_2, the larger the cascade solidity must be. /22

1.3.6. Turbine efficiency

The effectiveness of a turbine is evaluated by its efficiency.

In aviation turbines, account for all irreversible hydrodynamic losses is usually made with the help of the efficiency, based on total flow parameters:

$$\eta_T^* = \frac{L_T}{L^*_{ad.T}} = \frac{i_0^* - i_2^*}{i_0^* - i_{2ad}^*} = \frac{\Delta i^*}{\Delta i^*_{ad}} \approx \frac{\Delta T^*}{\Delta T^*_{ad}}, \tag{1.12}$$

where $L_T = i_0^* - i_2^*$ — effective turbine work at the wheel circumference;

$L^*_{ad.T} = i_0^* - i_{2ad}^* = c_p T_0^* \left[1 - \left(\frac{p_2^*}{p_0^*}\right)^{\frac{k-1}{k}}\right]$ — adiabatic work of gas expansion in the turbine. This efficiency is convenient for analysis of processes in a gas turbine engine, and for analysis of the combined performance of the turbine and the propulsive nozzle.

We will find the connection between the loss coefficient and the turbine efficiency:

$$\eta_T^* = \frac{L_T}{L^*_{ad.T}} = \frac{L_{ad.T} - L'_{r.T} - (c_2^2/2)}{L_{ad.T} - (c_2^2/2)}.$$

Hence,

$$\eta_T^* = 1 - \frac{\xi_T}{1 - \frac{c_2^2}{2L_{ad.T}}}, \tag{1.13}$$

where

$$\xi_T = \frac{L'_{r.T}}{L_{ad.T}}; \quad L'_{r.T} = \sum L'_{ri} = \sum \xi_i L_{ad\ i};$$

$L'_{r\ i}$ and ξ_i — irreversible losses and loss coefficient in the individual turbine stages.

The efficiency of the turbine stage can also be determined from the known values of the velocity coefficients ϕ and ψ:

$$\eta^*_{st} = \frac{L_{st}}{L^*_{ad.st}} \approx \frac{L_{st}}{L_{st} + L'_{r\ st}} = \frac{1}{1 + (L'_{r\ st}/L_{st})},$$

where $L'_r = L'_{rs} + L'_{rr} = \left(\frac{1}{\varphi^2} - 1\right)\frac{c_1^2}{2} + \left(\frac{1}{\psi^2} - 1\right)\frac{w_2^2}{2}$.

For estimating turbine hydrodynamic effectiveness, the adiabatic efficiency is sometimes used, which is defined in terms of the flow unretarded parameters at the turbine outlet: /23

$$\eta_{ad.T} = \frac{L_T + \frac{c_2^2}{2}}{L_{ad.T}} = \frac{i_0^* - i_2}{i_0^* - i_{2ad}} \approx \frac{\Delta T}{\Delta T_{ad}}. \tag{1.14}$$

For estimating the effectiveness of the turbine as a driving machine (turboprop engine turbines, stationary gas turbines, and accessory drive turbines), along with the efficiencies η_T^* and $\eta_{ad.T}^*$, we use the effective (power) efficiency, defined by the ratio of the effective work which can be taken from the turbine shaft to the available energy of the gas flowing through the machine:

$$\eta_T = \frac{L_T}{L_{ad.T}} = \frac{L_T}{L_{ad.T}^* + \frac{c_2^2}{2}}. \tag{1.15}$$

The effective efficiency characterizes the degree of utilization of the available energy ($L_{ad.T}$) for obtaining shaft work (L_T) in the actual gas expansion process, i.e., all losses in the turbine are accounted for, including those associated with the exit velocity.

All three efficiencies considered above are interconnected. We will find the connection between η_T^*, $\eta_{ad.T}$, and η_T.

Substituting L_T from (1.15) into (1.12) and (1.14), we obtain:

$$L_{ad.T}^* = \frac{c_2^2}{2} \frac{\eta_T^*}{\eta_T^* - \eta_T}; \tag{1.16}$$

$$L_{ad.T} = \frac{c_2^2}{2} \frac{1}{\eta_{ad.T} - \eta_T}. \tag{1.17}$$

Equating the right hand sides of these equations, we obtain, after some manipulation:

$$\eta_{\tau}^{*}=\frac{\eta_{\tau}}{\eta_{\tau}+(1-\eta_{ad.T})} \qquad (1.18)$$

For contemporary aviation gas turbines, the values attained for the above efficiencies in the design regime lie in the following limits: $\eta_{\tau}^{*}=0{,}89\div0{,}93$; $\eta_{ad.T}=0{,}9-0{,}94$; $\eta_{\tau}=0{,}75\div0{,}85$.

The highest efficiencies are achieved in multi-stage turbines. The adiabatic efficiency of the individual turbine stages reaches η^{*}_{st} = 0.91 - 0.925.

Besides the efficiencies examined above, the hydraulic effectiveness of gas turbines is sometimes estimated with the help of the polytropic efficiency, based on total flow parameters: /24

$$\eta^{*}_{pol}=\frac{L_{\tau}}{\int\limits_{2}^{0}\frac{dp^{*}}{\rho^{*}}}=\frac{\frac{k}{k-1}R(T_0^{*}-T_2^{*})}{\frac{n}{n-1}R(T_0^{*}-T_2^{*})}=\frac{\frac{k}{k-1}}{\frac{n}{n-1}},$$

where n — polytropic exponent of the effective process which characterizes the change of the total flow parameters in the turbine.

For actual turbines with various stage loading, the polytropic efficiencies lie in the range η^{*}_{pol} = 0.88 - 0.92. The maximum polytropic efficiency reaches 0.92 - 0.925, and has practically not changed recently.

1.4. Concept of Turbine Stage Degree of Reaction

The gas expansion process occurs in both the stator and rotor of the gas turbine stage. The ratio of the adiabatic work of gas expansion in the stator and rotor of the elementary stage is characterized by the degree of ρ. By stage degree of reaction, we mean the ratio of adiabatic gas expansion work in the rotor to the adiabatic gas expansion work in the entire stage.

$$\rho = \frac{L_{ad.r}}{L_{ad.st}}$$

where

$$L_{ad.r} = c_p T_1 \left[1 - \left(\frac{p_2}{p_1}\right)^{\frac{k-1}{k}}\right];$$
$$L_{ad.st} = c_p T_0 \left[1 - \left(\frac{p_2}{p_0}\right)^{\frac{k-1}{k}}\right].$$

The enthalpy charge equivalent to the adiabatic gas expansion work is called the available (adiabatic) enthalpy $H = L_{ad}$. Correspondingly, the degree of reaction is often defined as the ratio of adiabatic enthalpy in the rotor to the adiabatic enthalpy in the stage: $\rho = H_r/H_{st}$.

The degree of reaction, while defining the ratio of the gas expansion works in the stage ele. nts, is at the same time a parameter which characterized rotor cascade convergence. With increase of ρ, /25 the degree of gas expansion and, consequently, the rotor cascade channel convergence increases.

With $\rho = 1$, the gas expands only in the rotor, while only flow turning occurs in the stator, and the gas pressure does not change ($p_1 = p_0$).

In an active turbine ($\rho = 0$), the gas expands only in the stator, and the gas pressure does not change in the rotor ($p_2 = p_1$).

With $\rho < 0$, static pressure increase, rather than decrease, occurs in the rotor. The interblade channel in such a cascade will be diffusive. In turbine cascades having large flow turning angles, negative reaction can lead to boundary layer separation and additional increase of the cascade losses. Therefore, a negative degree of reaction is not usually allowed in the design regime.

The degree of reaction decreases from the blade periphery toward the blade root for all of the commonly used distributions of the flow parameters along the radius. The nature of ρ variation along the radius depends chiefly on the flow parameter distribution law along the radius (see § 2.4).

In order to avoid negative reaction at the blade root, the value of ρ at the mean radius is chosen in the limits $\rho_m = 0.25 - 0.5$.

The larger values of ρ pertain to the stages which have larger relative blade length (smaller value of the ratio D_m/h_b).

The degree of reaction based on adiabatic enthalpy drops is not directly connected with the flow kinematics. Therefore, in turbine theory, the concept of kinematic degree of reaction is sometimes introduced:

$$\rho_k = 1 - \frac{c_{1u} + c_{2u}}{2u}.$$

The kinematic degree of reaction, which involves the ratios of enthalpy drops equivalent to the actual velocities, is determined by the velocity triangle, that is, it is connected with the flow kinematics in the stage. Therefore, this is a convenient paramet r to use in practical turbine design. With regard to its absolute value, it is somewhat smaller than the degree of reaction based on the ratio of the adiabatic enthalpy drops (by approximately 1.5 - 2%). This difference will be smaller, the less the axial velocity components at the rotor inlet and outlet differ, and the smaller the portion of hydraulic losses in the stage which consist of losses in the rotor. In calculations, ρ_k is chosen in the same limits recommended for the thermodynamic degree of reaction:

1.5. Basic Turbine Stage Governing Parameters

In designing a turbine, the total pressure p_0^*, total temperature T_0^*, gas flowrate G, work L_T, and turbine rotor speed are usually the initial values. /26

In order to design a turbine, it is necessary to select the basic characteristic parameters for each stage which allow us to construct the velocity triangles and ensure that we obtain the required turbine work with high efficiency.

The characteristic parameters are usually chosen for the mean turbine radius. From them, in accordance with the specified initial data, the velocity triangles are computed, and the flow parameter variation in the stage along the blade length is determined.

It is obvious from examination of the velocity diagram (see Figure 1.4) that, for known turbine stage work L_{st}, it is sufficient to know four dimensional or dimensionless characteristic parameters to construct the velocity triangles characterizing the kinematics of the gas flow in the stage.

The losses in a turbine and its efficiency depend on proper choice of the magnitude of the governing parameters.

The following quantities can be taken as the turbine stage governing parameters.

1. The loading coefficient μ, which is the ratio of work taken from the turbine rotor to the parameter u^2 at the corresponding radius:

$$\mu = \frac{L_u}{u^2}.$$

Since usually $L_u \approx L_{st} = u(c_{1u} + c_{2u})$, then

$$\mu = \frac{c_{1u} + c_{2u}}{u}.$$

For given turbine stage work, the loading factor uniquely determines the magnitude of the circumferential velocity $u = \sqrt{L_{st}/\mu}$.

2. Degree of reaction.

The magnitude of the degree of reaction determines the distribution of the pressure ratios between stator and rotor and, in combination with other parameters, allows us to find the kinematic flow parameters and construct the velocity triangles.

3. The Mach number based on the axial velocity at the stage exit M_{2a}. The value of M_{2a} influences the flow section dimensions F_2, the losses in the turbine and in the post-turbine diffuser, the behavior of the characteristics, and the turbine work margin in the GTE system.

By turbine work margin in the GTE system, we mean its ability /27
to increase its work with pressure decrease behind it and with constant turbo-compressor rotational speed. When the effective turbine work in this situation ceases to increase, so-called turbine "choking" with regard to work occurs.

The work margin magnitude is determined by the difference between the maximum work and its value in the design regime.

4. The angle α_2 between the absolute flow velocity vector at the turbine exit and the plane of rotation. The angle α_2 determines the losses in the post-turbine diffuser and engine propulsive nozzle, determines the number M_{2a} at which "stalling" of the turbine with regard to work occurs, and influences the operation of the following stage*.

5. The axial velocity ratio $K_a = c_{1a}/c_{2a}$. The form of the velocity triangles and the form of the turbine stage flow path meridional profile depend on K_a.

---

*The angles α_1 or β_2 can also be used as governing parameters.

6. The parameters u/c_1, u/c_{ad}, or u/c^*_{ad}, where $c_{ad} = \sqrt{2L_{ad.T}}$, $c^*_{ad} = \sqrt{2L^*_{ad.T}}$. The turbine stage load coefficient depends on the values of these parameters:

$$\mu = \frac{L_u}{u^2} = \frac{L^*_{ad.st}\eta^*_{st}}{\delta_r u^2},$$

where $\delta_r = L_{st}/L_u$ — factor accounting for leakage flow in the radial gap and friction between the disk and rim. Usually, $\delta_r = 0.97 - 0.98$. Since:

$$u^2 = \left(\frac{u}{c^*_{ad}}\right)^2 c^{*2}_{ad} = \left(\frac{u}{c^*_{ad}}\right)^2 2L^*_{ad},$$

then $\mu = \frac{1}{2}\,\frac{\eta^*_{st}}{\delta_r (u/c^*_{ad})^2}$.

In aviation gas turbine design, the best approach is to use a computation method based on the following governing parameters:

$$\mu,\ M_{2a},\ \alpha_2,\ K_a \text{ and } \mu,\ \varrho,\ \alpha_1,\ \alpha_2 \text{ (or } M_{2a}).$$

Either of these systems determines the flow kinematics at a given radius.

Besides these, calculation methods are used in which the governing parameters are u/c_{ad} (or u/c_1), ρ, α_1, β_2, or u/c_1, ρ, u, α_1, and other combinations.

For aviation GTE turbines, the system of governing parameters which includes the parameter u/c_{ad} is inconvenient, since for such turbines the effective and not the adiabatic work is given. However, for given effective work L_T and the parameter u/c_{ad} selected as /28
initial parameter, the turbine circumferential velocity, which to a large extent determines its frontal dimensions, cannot be found until the adiabatic work $L_{ad.T}$ is determined as a result of calculation.

Besides this, the magnitudes of the angle α_2 and the number M_{2c} cannot be specified directly when using this system of governing parameters. They are determined as a result of calculations and may turn out to be unacceptable, which makes it necessary to carry out several calculation variants.

The optimal values of the governing parameters are chosen on the basis of analysis of their influence on turbine stage efficiency and work.

CHAPTER II

BASIC TURBINE PARAMETERS AND THEIR INFLUENCE ON TURBINE EFFICIENCY

2.1. Turbine Stage Loading

The gas dynamic loading of a turbine stage is usually characterized by the work or enthalpy drop realized in the stage for a given rotor circumferential velocity. /29

The parameter u/c_{ad} or the stage load coefficient $\mu = L_{ad}/u^2$ is taken in practice as the criterion characterizing turbine stage loading, where u is the circumferential velocity at the stage mean diameter, and c_{ad} is the effective velocity of a flow whose kinetic energy is equal to the available work of gas expansion in the stage:

$$\frac{c_{ad}^2}{2} = L_{ad}.$$

As was said above, use of the parameter u/c_{ad} in GTE turbine design is often extremely unsuitable, since the velocity c_{ad} for an intermediate or final stage of a multistage turbine is a function of many gasdynamic quantities which are obtained as the result of complete turbine analysis and, consequently, are unknown at the beginning of the design.

It is more suitable to use the load coefficient μ, which does not have the above drawback, to characterize turbine stage loading.

The advantages of using the load coefficient as the turbine loading criterion appear especially in analyzing multistage turbines, when the necessity arises to distribute the work for the entire turbine among its stages. This is an important problem, because not only the geometrical dimensions of the turbine flow path or the form of its meridional cross section, but also the operational characteristics of the turbine and engine (turbine efficiency as a function of rotational speed, engine starting, acceleration, and so forth) will be determined by the work distribution between the stages.

For example, in the two-stage turbine of a single-shaft engine /30
with given work of the entire turbine, the higher the first-stage loading, the easier it is to design the second stage with axial gas discharge and the lower the temperature of its rotor blades, which because of greater length undergo higher loads than the first-stage blades from the effect of centrifugal and often the gas forces.

When distributing the work between stages, it is also necessary to consider turbine operation in the off-design regimes. It is known that with decrease of the pressure differential in the turbine, the pressure drop in the last stages decreases most. Therefore, with small loads, particularly in engine regimes near idle, the second stage unloads so much that it can enter the so-called compressor regime in which the work taken from this stage $L_{st} \leqq 0$. The more turbine stages, the greater the degree to which this occurs. In the multistage turbine, the last stage can enter the compressor regime even with comparatively small decrease in the turbocompressor speed compared to its maximum value, since in this case the volumetric gas flowrate through the first turbine stage changes very little, and the greater the pressure ratio in the compressor at maximal speed, the larger the region of compressor slowdown in which the volume flow remains unchanged. Therefore, the pressure differential realized across the first stage also remains practically unchanged. And since the overall pressure differential on the expansion line decreases

with decrease of rotational speed (pressure behind the compressor decreases for constant atmospheric pressure), this occurs at first at the expense of a decrease of the pressure drop in the propulsive nozzle (with constant throat area), and then at the expense of a decrease in the pressure drop in the last turbine stages.

Such a turbine will have poor starting characteristics; this is, engine starting will be difficult. One the basis of these considerations, it is desirable to load the last turbine stage more than the first stages.

On the other hand, overloading the last turbine stages can change the usual nature of turbine efficiency variation with change of rotational speed, so that the maximal efficiency will not be obtained at the maximum speed, but at a lower speed (Figure 2.1) Obviously, the distribution of work between stages also depends on the flow path scheme in the meridional section. If, for example, we take the flow path scheme with constant outer diameter (see Figure 3.7a), it is clear that allocation of more or even the same work to the last stage as to the first is not possible without appreciable decrease in the turbine efficiency at the design maximal speed. Therefore, in the turbine design, the distribution of work between the stages must be made with account for the requirements imposed on the engine as a whole.

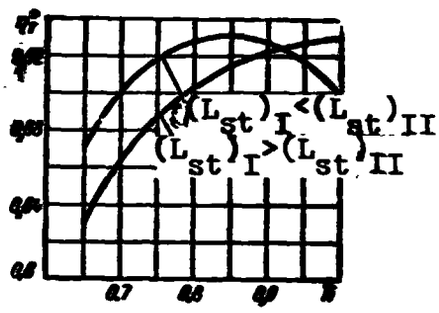

Figure 2.1. Influence of load distribution on two-stage turbine efficiency as a function of rotational speed /31

The load coefficient is one of the parameters which determine turbine stage efficiency. We will find the dependence of efficiency on the load coefficient.

From the expressions for the turbine stage load coefficient and efficiency, we find:

$$\mu = \frac{L_a}{u^2} = \frac{L_{ad}\eta_T}{u^2}$$

or

$$\mu = \frac{L_{ad}\eta_T}{x^2 2L_{ad}} = \frac{\eta_T}{2x^2},$$

where

$$x = \frac{u}{c_{ad}} = \frac{u}{\sqrt{2L_{ad}}}.$$

Then,

$$\eta_T = 2\mu x^2. \tag{2.1}$$

Analogously, is is possible to find the relations $\eta_{ad}(\mu)$ and $\eta_T^*(\mu)$:

$$\mu = \frac{L_u}{u^2} = \frac{L_{ad}\eta_{ad} - c_2^2/2}{u^2},$$

hence,

$$\eta_{ad} = \frac{2\mu u^2 + c_2^2}{2L_{ad}} = 2\mu x^2 + \frac{c_2^2}{2L_{ad}}; \tag{2.2}$$

substituting (2.2) and (2.1) into:

$$\eta_T^* = \frac{\eta_T}{\eta_T + (1 - \eta_{ad.T})}$$

we find:

$$\eta_T^* = \frac{2\mu x^2}{1 - \frac{c_2^2}{2L_{ad}}}. \tag{2.3}$$

We will find the relation $\eta_T^* = f(\mu)$ for corresponding values of α_1, φ, ψ, and ρ.

The effective turbine stage efficiency:

$$\eta_T = \frac{L_{st}}{L_{ad}} = \frac{u(c_{1u} + c_{2u})}{L_{ad}}. \tag{2.4}$$

From the velocity diagram (See Figure 1.4), we have:

$$c_{2u} = w_2 \cos\beta_2 - u_2 = \psi \cos\beta_2 \sqrt{w_1^2 + 2L_{ad.r}} - u_2; \tag{2.5}$$

$$w_1^2 = c_1^2 + u_1^2 - 2u_1 c_1 \cos\alpha_1. \tag{2.6}$$

where $c_{1u} = c_1 \cos\alpha_1$, and $L_{ad.r} = \rho L_{ad.st}$ is the adiabatic gas expansion work in the rotor. /32

It is possible to set $u_1 = u_2$. Then, after substituting the value of w_1 from (2.6) into (2.5), and then substituting the resulting expression for c_{2u} into (2.4), we obtain, after some manipulation:

$$\eta_r = 2x\left[\varphi\cos\alpha_1\sqrt{1-\varrho} + \psi\cos\beta_2\sqrt{\varrho+\varphi^2(1-\varrho)-2x\varphi\cos\alpha_1\sqrt{1-\varrho}+x^2-x}\right]. \tag{2.7}$$

The turbine stage adiabatic efficiency

$$\eta_{ad.T} = \frac{L_{st} + c_2^2/2}{L_{ad.T}}.$$

After substituting the values $c_2^2 = w_2^2 - u^2 - 2uc_{2u}$ and $L_u = u(c_{1u} + c_{2u})$, and some manipulation, we obtain:

$$\eta_{ad.T} = \frac{2uc_{1u} - u^2 + w_2^2}{2L_{ad.st}} \tag{2.8}$$

In turn,

$$\frac{w_2^2}{2} = \psi^2\left(\varrho L_{ad.st} + \frac{w_1^2}{2}\right). \tag{2.9}$$

Then, after substituting (2.9) into (2.8), and dividing numerator and denominator of the resulting expression by $c_1^2 = 2\varphi^2(1-\varrho)\ L_{ad.st}$, and after some manipulation, we obtain:

$$\eta_{ad.T} = \frac{2uc_{1u} - u^2 + \psi^2\left[2\varrho L_{ad.st} + c_1^2 + u^2 - 2uc_1\cos\alpha_1\right]}{2L_{ad}}$$

or,

$$\eta_{ad.T} = \varphi^2(1-\varrho)\left[\psi^2 + \frac{\psi^2}{\varphi^2}\frac{\varrho}{1-\varrho} + (1-\psi^2)(2x_1\cos\alpha_1 - x_1^2)\right], \tag{2.10}$$

where $x_1 = u/c_1$.

This expression is not entirely suitable for analysis of turbine stage operation because the velocity c_1 is not a characteristic parameter. Thus, for same velocity c_1, the enthalpy drop realized in the turbine can be different, and for a constant enthalpy drop, it is possible to have various velocities c_1. Therefore, it is always better to relate the circumferential velocity of the turbine wheel to c_{ad}. The relationship between the velocities c_1 and $c_{1\,ad}$ can be written in the form:

$$\frac{c_1^2}{2}=\varphi^2(1-\varrho)\ \frac{c_{ad}^2}{2} \text{ or } c_1 = \phi c_{ad}\sqrt{1-\varrho}.$$

Then,

$$x_1=\frac{u}{c_1}=\frac{u}{\phi c_{ad}\sqrt{1-\varrho}}=x\frac{1}{\varphi\sqrt{1-\varrho}}. \tag{2.11}$$

Substituting the value of x_1 from (2.11) into (2.10), we obtain, after manipulation: /33

$$\eta_{ad} = \varphi^2\psi^2(1-\varrho)+\psi^2\varrho-(1-\psi^2)(x^2 - 2x\varphi\cos\alpha_1\sqrt{1-\varrho}). \tag{2.12}$$

In the relations obtained for η_T (u/c_{ad}) and, consequently, μ (u/c_{ad}), there appears the angle β_2, whose magnitude depends on many parameters, such as the circumferential velocity u, the angle α_1, the reactivity ρ, and others. This dependence, in general form, is quite complex; therefore, we limit ourselves to its determination for special cases which are characteristic and suitable for further use.

If we assume constant values of the velocity coefficients ϕ and ψ, that is, we disregard their change with change in u/c_{ad}, and also assume definite values of α_1 and ρ, then η_T, η_{ad}, and μ will depend uniquely on u/c_{ad}.

We will examine the case when the reactivity is equal to zero. This pertains to the blade root section, where the stage has very small or zero reaction. For a stage with $\varrho \approx 0$, the rotor cascade inlet and outlet angles are practically equal $(\beta_1 \approx \beta_2)$.

From the velocity triangle, we have:

$$\cos\beta_1 = \frac{c_{1u} - u}{w_1} = \frac{c_1 \cos\alpha_1 - u}{\sqrt{c_1^2 + u^2 - 2uc_1\cos\alpha_1}}. \tag{2.13}$$

Dividing the numerator and denominator of (2.13) by c_1, and expressing x_1 through x, we obtain, after some manipulation:

$$\cos\beta_2 = \cos\beta_1 = \frac{\varphi\cos\alpha_1 - x}{\sqrt{\varphi^2 + x^2 - 2x\varphi\cos\alpha_1}}. \tag{2.14}$$

We substitute the expression for $\cos\beta_2$ from (2.14) into (2.7). Then, for the case $\varrho = 0$, we find, from (2.1) and (2.7):

$$\mu = \frac{(1+\psi)(\varphi\cos\alpha_1 - x)}{x}. \tag{2.15}$$

We see that the load coefficient μ in a quite wide region of α_1 change varies little, and is practically a unique function of u/c_{ad}.

For the case under consideration $(\varrho = 0)$:

$$\eta_1 = 2x[\varphi\cos\alpha_1 + \psi(\varphi\cos\alpha_1 - x) - x] \tag{2.16}$$

and

$$\eta_{ad} = \varphi^2\psi^2 + (1-\psi^2)(2x\varphi\cos\alpha_1 - x^2). \tag{2.17}$$

From examination of these expressions, it is not difficult to convince ourselves that the maxima of the adiabatic and effective efficiencies correspond to essentially different values of u/c_{ad}.

Substituting (2.16) and (2.17) into (2.3), and using (2.15), /34
we obtain:

$$\eta_e^* = \frac{2\mu}{2\psi\mu - (1-\psi^2) + \dfrac{(1-\varphi^2\psi^2)(1+\psi+\mu)^2}{(1+\psi)^2\varphi^2\cos^2\alpha_1}}. \tag{2.18}$$

We see that η_T^* is uniquely connected with the load coefficient only for constant values of the coefficients ϕ and ψ and the angle α_1.

We find the optimal turbine stage load coefficient by investigating (2.18) for a maximum. After computing the derivative of η_T^* with respect to μ and equating it to zero, we find the expression for μ_{opt} at which the turbine stage efficiency will be maximal:

$$\mu_{opt} = \sqrt{(1+\phi)^2 - \frac{(1+\psi)^2(1-\psi^2)}{1-\varphi^2\psi^2}\varphi^2\cos^2\alpha_1}. \qquad (2.19)$$

Analogously to the preceding case ($\varrho=0$), the relation $\eta_T^* = f(\mu)$ is found for $\varrho=0{,}5$, which is represented graphically in $\eta_T^*(\mu)$ Figure 2.2.

All the relations presented above were obtained by neglecting the change in the coefficients ϕ and ψ with change in the load coefficient. In reality, the velocity coefficients ϕ and ψ vary with changes in μ and x. They decrease with increase in the stage loading. Consequently, in the general case, they cannot be assumed constant; however, at the same time, account for their change is too cumbersome. Therefore, it is better to use experimental data to find $\eta_T^* = f(\mu)$.

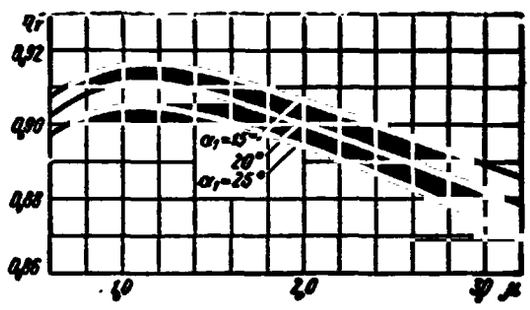

Figure 2.2. Dependence of turbine efficiency η_T^* loading coefficient for ρ = 0.5

We can use the results of an experimental investigation of five different turbines with outer diameter D_o = 600 mm. The turbines are distinguished by the following:

a) blade absolute length (h_b = 40 - 100 mm); /35

b) relative hub diameter ($\bar{d}$ = 0.65 - 0.75);

c) angle α_1 at the mean radius (α_{1m} = 18 - 25° and α_{1m} = 30 - 36°);

d) gas expansion ratio in the turbine ($\pi_T^* = 2.0 - 3.0$);

e) flow path shape in meridional section (from cylindrical to slightly diverging along the inner diameter, $\gamma_i = 0 - 12°$);

f) load coefficient referred to the root section ($\mu_i = 1.5 - 3.0$).

The resultant experimental data permitted us to construct the relationship between the maximal efficiency and the load coefficient at the blade root section for fixed Mach numbers at the turbine outlet (Figure 2.3). For ease of use, these graphs are presented in the form of the relative efficiencies of functions of the load coefficients:

$$\frac{\eta_T^*}{(\eta_T^*)_{max}} = f(\mu_i).$$

The load coefficient at the turbine stage inner diameter μ_i is chosen as a basic initial parameter, because it is more suitable for use in choosing the flow path scheme and also because the values of $M_{1\,w}$ and the flow turning angle in the cascade are usually maximal at the base section, and the degree of convergence of the interblade channels which characterize μ_B is usually minimal.

It will be shown later that for given $M_{2\,c}$, the larger the load coefficient, the larger $M_{1\,w}$, the larger the flow turning angle, and the smaller the difference of the angles $\beta_1 - \beta_2$, which for large values of μ can even become negative. This means that the turbine being designed may have diffusive flow on some part of the blade /36
length, causing the appearance of additional losses.

On this basis, for stages with $M_{2\,c} = 0.5 - 0.6$, and angle $\alpha_{1\,m} = 18 - 25°$, we take $\mu_i \leqq 2.0$, and for $\alpha_{1\,m} = 30 - 36°$, $\mu_i \leqq 2.2$. If the regulation law selected for the engine being designed provides an increase (under flight conditions) of the pressure difference across the turbine, which leads to significant increase in the load

coefficient in the last stage, then for its initial value (under static conditions) μ_1 is chosen smaller than the indicated values.

The value of the load coefficient at the mean diameter can be obtained by simple scaling:

$$\mu_m = \mu_1 \left(\frac{2\bar{d}}{1+\bar{d}} \right)^2.$$

Analysis of turbine stage efficiency as a function of the load coefficient shows that η_T^* changes very little in the region in which μ changes from 1.2 to 1.7. With axial gas discharge from the turbine, the optimal load coefficient lies in the limits $(\mu_m)_{opt}$ = 1.3 - 1.4. With increase of the flow twist at the turbine outlet, the optimal load coefficient increases. For α_2 = 70 - 65°, which can be attained for the stages preceding the last stage, the load coefficient can be increased to $(\mu_m)_{opt}$ = 1.75 - 1.85.

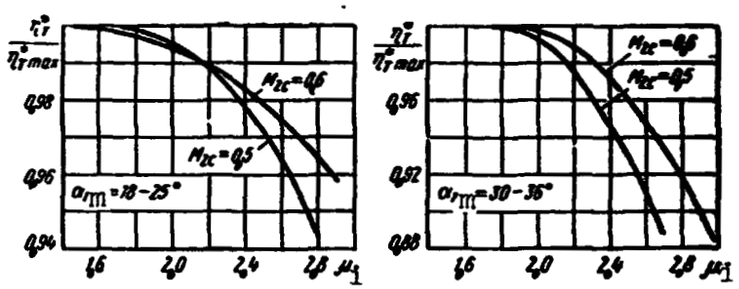

Figure 2.3. Experimental dependence of turbine efficiency on loading coefficient for five turbine stages.

2.2. Flow Velocity and Direction at the Turbine Outlet

First of all, we will examine the influence of outlet velocity on turbine stage efficiency:

$$\eta_T^* = \frac{L_{st}}{L_{ad.T} - \frac{c_2^2}{2}}. \qquad (2.20)$$

The adiabatic work of gas expansion in the stage is $L_{ad.st} = L_{st} + \frac{c_2^2}{2} + L_r'$, where L_r' — irreversible losses in the stage. Since:

$$L_r' = L_r - \Delta L_r = (1-\varphi^2)\frac{c_{1ad}^2}{2} + (1-\psi^2)\frac{w_{2ad}^2}{2},$$

then,

$$L_{ad.st} = L_{st} + \frac{c_2^2}{2} + (1-\varphi^2)\frac{c_{1ad}^2}{2} + (1-\psi^2)\frac{w_{2ad}^2}{2} \qquad (2.21)$$

We will examine the two most characteristic cases: $\rho = 0$ and $\rho = 0.5$. In the case $\rho = 0$, $w_{2\,ad} = w_1$, and $L_{ad.st} = c_{1\,ad}^2/2$. Then, after substituting the corresponding quantities into the original expression (2.20) for the efficiency, and after some manipulation, we obtain: /37

$$\eta_t^* = \frac{2\varphi^2\psi^2 - \varphi^2}{\frac{k-1}{k+1}(\varphi^2-\varphi^2\psi^2)\psi^2(1-\varphi^2)\left[\frac{Rk/(k-1)}{L_{st}/T_3^*} - 1\right]\lambda_{2c}^2 - (1-\psi^2)\frac{2\mu-1}{2\mu} + \psi^2}. \qquad (2.22)^*$$

where $\mu = L_u/u^2$, and T_3^* is the total temperature of the gas flow at the inlet to the turbine.

The condition $\rho = 0.5$ can be realized when $w_{2\,ad}^2 = w_1^2 + c_{1\,ad}^2$. In this case:

$$\eta_t^* = \frac{\psi^2(1+\varphi^2)}{\frac{k-1}{k+1}[2-\psi^2(1+\psi^2)]\left[\frac{Rk/(k-1)}{L_{st}/T_3^*} - 1\right]\lambda_{2c}^2 - (1-\psi^2)\frac{2\mu-1}{\mu} + 2}. \qquad (2.23)^{**}$$

To simplify (2.22) and (2.23), it is assumed that $c_{2\,u} = 0$ in the equation $\mu = c_{1u}/u + c_{2u}/u$.

Analysis of these expressions for the efficiency has shown that change of L_{st}/T_3^* in the region from 180 to 200, which represents the region of interest for practical application in gas turbine stages, influences turbine efficiency very little. Therefore, in calculating the relation $\bar{\eta}_t^*(M_{2c})$, represented in Figure 2.4, the value L_{st}/T_3^* was assumed constant and equal to 200. Here, $\bar{\eta}_t^* = \eta_t^*/\eta_{t0}^*$ is the ratio of the stage efficiency for a given value of $M_{2\,c}$ to the stage efficiency for the optimal value of $M_{2\,c}$. Also plotted on this graph

---

*Translator's note. The plus sign has been omitted between the second and third terms of the denominator, i.e., $(\phi^2-\phi^2\psi^2)+\psi^2$.

**Translator's note. $(1+\psi^2)$ in the second term of the denominator should correctly read $(1+\phi^2)$.

are the experimental points obtained from experiments on three single-stage turbines installed in a gas turbine engine, and the relation (curve a) obtained by V. V. Druzhilovskiy as a result of experiments on a special setup of three turbines differing in the design number $M_{2\ c}$.

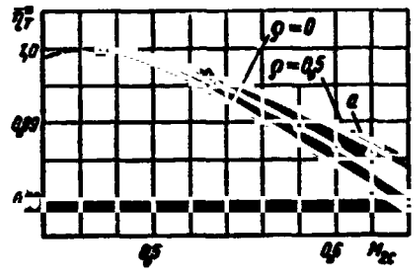

Figure 2.4. Turbine efficiency as function of outlet velocity

The curves presented in Figure 2.4 make it possible to determine turbine efficiency change as a function of outlet velocity magnitude change.

When selecting the design Mach number at the turbine outlet, besides the relation $\bar{\eta}_T^*(M_{2c})$, already considered, we must consider that for a given gas flowrate, $M_{2\ c}$ determines the flow section area F_2, which in turn determines the blade length. With decrease of $M_{2\ c}$, the blade lengths and strains in them increase. Besides this, with blade length increase for a given gas flowrate, the angle α_1 decreases and the flow turning angle increases which for small values of $M_{2c}<0{,}45$ can cause deterioration in the flow around the blades and increased losses in the cascades.

With very long blades, difficulties with profiling the root sections can arise, in which the interblade channel can become diffusive, and a large twist can appear at the wheel outlet. /38

With large outlet velocities, the blade length decreases, but the turbine efficiency decreases, and losses in the post-turbine diffuser grow, especially in presence of flow twist (with $\alpha_2<90°$).

The experimental dependence of the total pressure recovery coefficient in the post-turbine diffuser on the Mach number and the flow twist angle at the turbine outlet is presented in Figure 2.5*.

*Taken from a study of V. V. Druzhilovskiy, "Air Bleed in TJE", Riga, 1958.

Besides this, with large M_{2c}, the turbine margin decreases, since increase of the pressure differential across the turbine only causes increase in the outlet velocity, and not the power. When attempting to increase the turbine throughput, it is not advisable to increase $M_{2c} > 0.7$, since with such large values, the turbine capacity increase and blade length decrease take place very slowly, while the losses in the turbine diffuser grow rapidly.

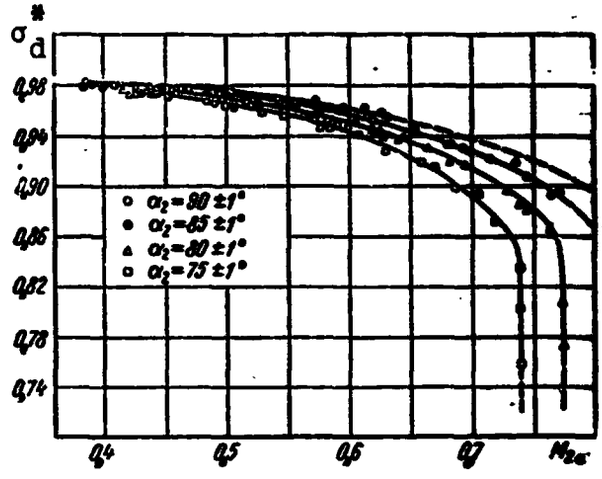

Figure 2.5. Total pressure recovery coefficient in the post-turbine diffusor σ_d^* as function of Mach number and flow direction behind the turbine

Taking into account all the above considerations (obtaining acceptable turbine efficiency, small losses in the post-turbine diffuser, required turbine work margin with consideration for the necessary strength margin and relative hub diameter of the last turbine stage), we recommend that the turbine exit Mach number be chosen in the limits $M_{2c} = 0.45 - 0.55$ in those engine regimes where it attains its maximal value. In turboprop turbines, M_{2c} sometimes reaches 0.7.

The magnitude of the flow twist behind the turbine stage and hence the angle α_2 depends on the stage load coefficient and the degree of reaction. As noted before, in designing the turbine, the load coefficient at the inner radius μ_i is usually specified.

In the blade root section, the reaction is usually close to zero ($\rho_i \approx 0$). In this case, we can assume that $\beta_1 \approx \beta_2$. Since $\operatorname{tg}\beta_1 = \frac{c_{1a}}{c_{1u} - u}$, while $\operatorname{tg}\beta_2 = \frac{c_{2a}}{c_{2u} + u}$, then /39

$$\frac{c_{1a}}{c_{2a}} = K_a = \frac{c_{1a} - u}{c_{2u} + u} = \frac{(c_{1u}/u) - 1}{(c_{2u}/u) + 1}. \qquad (2.24)$$

In turn, $c_{1u}/u = \mu_i - (c_{2u}/u)$, and $c_{2u} = c_{2a}/\mathrm{tg}\,\alpha_2$.

Substituting these values into (2.24), we obtain, after some manipulation:

$$\mathrm{ctg}\,\alpha_2 = \frac{u}{c_{2a}} \frac{\mu_i - K_a - 1}{K_a + 1}. \qquad (2.25)$$

The quantity K_a is usually chosen in the limits 0.8 - 1.0. The smaller value of K_a is taken for turbines with cylindrical flow path or which develop relatively large pressure differentials.

With known values of μ_i, K_a, $c_{2\,a}/u$, and with the condition $\beta_1 \approx \beta_2$, (2.25) allows us to determine the angle α_2 at the blade root section.

The angle α_2 at the turbine mean diemeter is a function of the adopted law of variation of the circumferential velocity components $c_{1\,u}$ and $c_{2\,u}$ along the blade length.

If the computed value of $\alpha_{2\,m}$ is substantially less than 90°, this can lead to increase of the losses in the post-turbine diffuser and decrease of the turbine work margin.

The flow twist at the outlet from the last turbine stage is usually no larger than $(90 - \alpha_2) = 8 - 10°$. At the outlet from the first and intermediate turbine stages, it may reach 20 - 25°.

If large flow twist $(90 - \alpha_2)$ is not desirable, it is necessary /40
to either unload the stage, redistributing part of the work to the other stages, or increase the turbine circumferential velocity.

2.3. Kinematics of Flow in Turbine Stage

In designing turbines, the problem of choosing the stage kinematics which guarantee the highest possible efficiency must be solved.

The turbine stage kinematics, as is well known, are determined by the relations between velocities of the flow passing through it. The relation between the circumferential and axial components of the absolute flow velocity is most characteristic for a turbine in an aviation gas turbine engine. The ratio of the algebraic sum of the circumferential components of the absolute velocity at the rotor blade inlet c_{1u} and exit c_{2u} to the rotor circumferential velocity characterizes turbine stage loading, and the axial component c_a characterizes its handling capacity.

When designing a turbine, its loading $\mu = \frac{(c_{1u} + c_{2u})}{u}$ is usually specified. It is determined for given diametrical turbine dimensions by the work per kilogram of gas passing through it, the magnitude of which is dictated by the required work of the compressor driven by the turbine and its rotative speed. As for the axial component of the absolute velocity, variation is possible within wider limits.

With $c_{1a} \approx c_{2a} = c_a$, which is characteristic for turbines with flow path expanding in the meridional section and with the selected reaction, the form of the velocity triangle, that is, the kinematics of the stage, is defined by the dimensionless coefficients:

$$\varphi = \frac{c_a}{u} \text{ and } \mu = \frac{L_T}{u^2},$$

where L_T is the work extracted from 1 kg of gas in the turbine stage. In this connection, the necessity arises to determine the relation of these coefficients for which losses in the turbine will be minimal, other conditions being equal.

We will examine the process of transformation of the available energy of 1 kg of gas into work in a turbine stage [17].

The available polytropic work per 1 kg of gas expanding in the turbine stator $(L_a)_s$ goes into change of the flow kinetic energy /41
$(L_c)_s$ and into frictional losses in the flow around the blades $(L_{fr})_s$, that is,

$$(L_a)_s = (L_c)_s + (L_{fr})_s \tag{2.26}$$

where $(L_c)_s = \frac{c_1^2 - c_0^2}{2}$.

On the other hand, $(L_c)_s = \omega M_s/G$, and it is possible to express the work of expansion through the projection of forces onto the Y-axis, and the axial velocity component: $(L_a)_s = c_a Y_s'/G$ (Figure 2.6)

where $\omega = \frac{\omega_0 + \omega_1}{2}$ — average angular velocity of the gas flow through the stator profile cascade;

$M_s = z r_{av} X_s'$ — torque applied to the stator cascade;

$G = 2\pi\rho c_a r_{av} h$ — gas flowrate;

z — number of blades.

Using these relations, denoting the ratio of the stator blade chord length to its spacing by $\bar{b}_s = b/t$, and remembering that the blade lift $N_s = \frac{1}{2} C_y \rho c^2 \bar{b}_s h_b$, and drag $T_s = \frac{1}{2} C_x \rho c^2 \bar{b}_s h_b$, it is possible to write:

$$(L_{fr})_s = \frac{1}{2} \frac{\bar{b}_s}{h_b} c^2 \frac{C_x}{\sin\alpha} . \tag{2.27}$$

For the rotor, by analogy with the stator profile cascade,

$$(L_a)_r = (L_T)_r + (L_{fr})_r \tag{2.28}$$

$$(L_{fr})_r = \frac{1}{2} \frac{\bar{b}_r}{h_b} w^2 \frac{C_x}{\sin\beta} . \tag{2.29}$$

If the work expended in overcoming frictional forces in the stator and rotor blades is referred to the effective work L_T extracted by the wheel, we obtain the magnitude of the relative losses due to friction in the stage:

$$\bar{L}_{fr} = \frac{(L_{fr})_s + (L_{fr})_r}{L_T}. \qquad (2.30)$$

The effective work can be expressed through the annular velocity of the rotation of the wheel Ω and the torque applied to the rotor blade cascade (M_r):

$$L_T = \frac{\Omega M_r}{G}. \qquad (2.31)$$

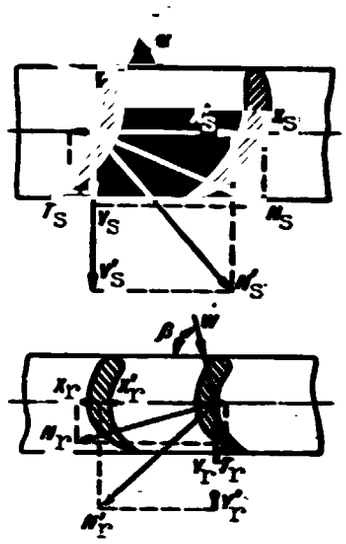

Figure 2.6. Diagram of forces acting on elementary stator and rotor blade cascades

Substituting into (2.30) the values of the quantities appearing in it and assuming that $c_{0u} \approx c_{2u}$, we obtain, after some manipulation: /42

$$\bar{L}_{fr} = \varphi\left[\frac{\varepsilon_s(1+\mathrm{tg}^2\alpha)}{\mathrm{tg}\,\alpha(\mathrm{tg}\,\alpha-\varepsilon_s)} + \frac{\varepsilon_r(1+\mathrm{tg}^2\beta)}{\mathrm{tg}\,\beta(\mathrm{tg}\,\beta-\varepsilon_r)}\right]. \qquad (2.32)$$

where $\varepsilon_s = (C_x)_s/(C_y)_s$ and $\varepsilon_r = (C_x)_r/(C_y)_r$ are the drag-lift ratios of the stator and rotor blade profiles, respectively. If we suppose that $\varepsilon_s = \varepsilon_r = \varepsilon$ (which corresponds to a stage with reaction equal to or near 0.5), the relative frictional losses in the stage will be:

$$\frac{\bar{L}_{fr}}{\varepsilon} = \varphi\left[\frac{1+\mathrm{tg}^2\alpha}{\mathrm{tg}\,\alpha(\mathrm{tg}\,\alpha-\varepsilon)} + \frac{1+\mathrm{tg}^2\beta}{\mathrm{tg}\,\beta(\mathrm{tg}\,\beta-\varepsilon)}\right]. \qquad (2.33)$$

If the values of tg α and tg β from the velocity triangle are substituted into this expression, we obtain:

$$\frac{\bar{L}_{fr}}{\varepsilon} = \frac{\varphi^2 + \left(\frac{\mu_1}{2} - \frac{\mu_0}{2}\right)^2}{\varphi - \left(\frac{\mu_1}{2} - \frac{\mu_0}{2}\right)\varepsilon} + \frac{\varphi^2 + \left(1 - \frac{\mu_1}{2} + \frac{\mu_2}{2}\right)^2}{\varphi - \left(1 - \frac{\mu_1}{2} + \frac{\mu_2}{2}\right)\varepsilon}. \qquad (2.34)$$

Taking $\mu_0 = c_{0u}/u = \mu_2 = c_{2u}/u = 0$, which is most characteristic for aviation engine turbines, it is possible to write: 43

$$\frac{\bar{L}_{fr}}{\varepsilon} = \frac{\varphi^2 + (\mu_1/2)^2}{\varphi - (\mu_1/2)\varepsilon} + \frac{\varphi^2 + [1 - (\mu_1/2)^2]}{\varphi - [1 - (\mu_1/2)\varepsilon]},$$

where $\mu_1 = \mu = c_{1u}/u$ and $\varphi = c_a/u$.

Figures 2.7 and 2.8 present graphs which show the relative frictional losses in a turbine stage as a function of the dimensionless coefficients μ and ϕ for various values of ε.

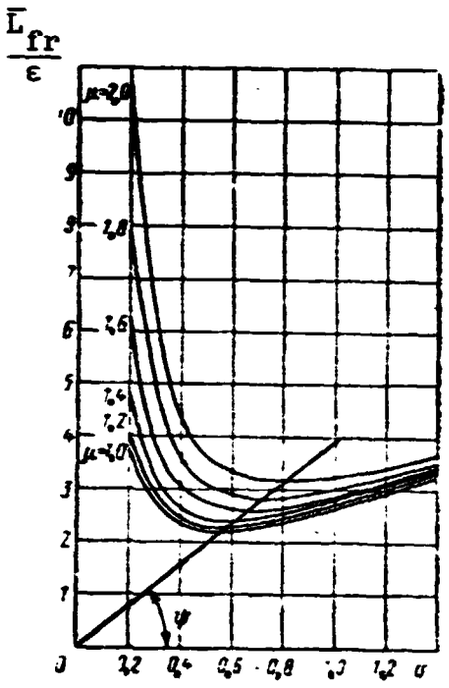

Figure 2.7. Relative frictional losses in a stage as function of the coefficients μ and ϕ for $\varepsilon = 0.1$

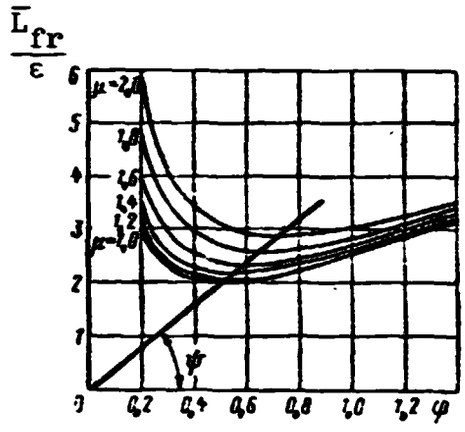

Figure 2.8. Relative frictional losses in a stage as function of the coefficients μ and ϕ for $\varepsilon = 0.01$

The locus of the points of optimal values ϕ_{opt} for various ε is a straight line starting from the coordinate origin with slope:

$$\operatorname{tg} \psi = \frac{(\bar{L}_{fr}/\varepsilon)_{min}}{\phi_{opt}}.$$

This means that the dependence obtained for the relative frictional losses on the coefficients ϕ and μ is general, and does not depend on the magnitude of ε. Consequently, the aerodynamic efficiency of stator and rotor profile cascades will determine only the absolute magnitude of losses in overcoming frictional forces, while their dependence on the velocity ratio will be preserved.

In order to find the relationship between the relative friction loss $\bar{L}_{fr}$ and the conventional turbine stage efficiency, we use (2.26) and (2.28). Then, considering the equality of c_0 and c_2, it is possible to write:

$$(L_a)_s + (L_a)_r = L_T + (L_{fr})_s + (L_{fr})_r.$$

Dividing all terms of this equality by L_T and using (2.30), after some manipulation, we obtain:

$$\eta_T' = \frac{1}{1 + \bar{L}_{fr}}.$$

Since $\eta_{ad} = \dfrac{(L_{fr})_s + (L_{fr})_r}{(L_a)_s + (L_a)_r}$, to within equality of the gas kinetic energy at the turbine outlet, in the adiabatic and actual /44 expansion processes $\eta_T' = \eta_T^*$. A fixed value of ϕ_{opt} corresponds to the minimal value of $\bar{L}_{fr}$ for a given μ. Consequently, it will also be optimal from the viewpoint of maximum turbine efficiency.

Thus to each turbine stage loading characterized for $c_{2\,u} \neq 0$* by the coefficient μ, there corresponds a quite definite value of the discharge coefficient ϕ for which maximum efficiency is realized independently of its absolute value for given concrete conditions (aerodynamic quality of the stator and rotor blade profiles). This value of the discharge coefficient can be found, as was shown, from the relations presented. Consequently, it is possible to find that velocity ratio for which the turbine efficiency will be maximal, all else being equal. Or, using the relations for the coefficients μ and ϕ obtained from turbine analysis or experiment, it is possible to determine how closely the stage kinematics correspond to the optimum from the viewpoint of maximum turbine efficiency.

---

*Translator's note. Inadvertently given in the original for [illegible] text as: $c_{2\,u} = 0$.

CHAPTER III

SELECTION OF TURBINE FLOW PATH SCHEME AND DETERMINATION OF BASIC TURBINE DIMENSIONS

The initial data for designing an aviation gas turbine engine are usually: specified thrust or power, specific fuel flowrate, specific weight, overall dimensions, and the flight height and speed at which the engine is to be used. This determines the choice of the basic engine parameters, which must frequently satisfy conflicting requirements imposed in relation to economy, weight (mass), overall size, reliability, technology, convenience of operation, and so forth. Therefore, the final engine design version is a compromise solution in which the imposed requirements are satisfied as far as possible, subject to the given specific conditions. /45

From the general engine gasdynamic design, the following basic data, which are necessary to design the turbine, are known:

1) gas flowrate through the turbine G_g, kg/sec;
2) gas pressure and temperature ahead of the stator p_0^*, N/m^2 and T_0^*, K;
3) turbine rotational speed n, rev/min;
4) turbine shaft work L_T, J/kg.

The development of contemporary GTE is in the direction of increasing the design compression ratio and improving engine economy. Turbines of such GTE operate with high enthalpy drops, and are usually multistage.

3.1. Determination of Number of Stages and Distribution of Work Between Them

In the previous chapter, it was shown that the allowable increase of the turbine stage loading coefficient has limits, exceeding which causes marked decrease in the turbine efficiency. To obtain acceptable turbine efficiencies, the loading coefficient at the blade root μ_i is chosen in the limits 2 - 2.2. Further increase of the loading coefficient is not feasible, not only because of decreasing efficiency, but also because increase of μ_i above 2.2 practically does not lead to decrease of the turbine weight, although it does /46 provide some (about 3 - 4%) decrease in the external diameter. This is because decrease of the turbine efficiency at constant $\lambda_{2\,c}$ makes it necessary to increase the outlet area F_2 and, consequently, increases the stresses in the rotor blades from the action of the tensile and bending forces [see (3.5) and (3.7) and Figure 3.4]. As a result, for a given safety factor, or what amounts to the same thing, a given value of $\sigma_\Sigma = \sigma_t + \sigma_{bend}$, σ_{bend} must decrease and this means the blade chord must increase. Thus, although increase of μ_i does yield some decrease in the turbine outer and inner diameter, its weight does not decrease. To illustrate, Figure 3.1 shows the results of calculation of the weight variation of a single-stage afterburning TJE turbine with $\bar{D} - D_m/h_b = 5.0$, in the range of loading coefficient variation from 2.1 to 3.4. The design conditions are the following: the magnitude of the thrust developed by the engine is specified, and the reduced velocity of the gas at the turbine outlet $\lambda_{2\,c}$ = const (or $M_{2\,c}$ = const), which is determined by operating conditions of the post-turbine diffuser and afterburner, on the one hand, and by the requirement of equality of the safety factors of the rotor blade and turbine disk, on the other hand. The

rotor speed is also taken constant, due to the constancy of the number of compressor stages and its compression ratio. The relative change in efficiency as a function of the loading coefficient was determined in accordance with Figure 2.3.

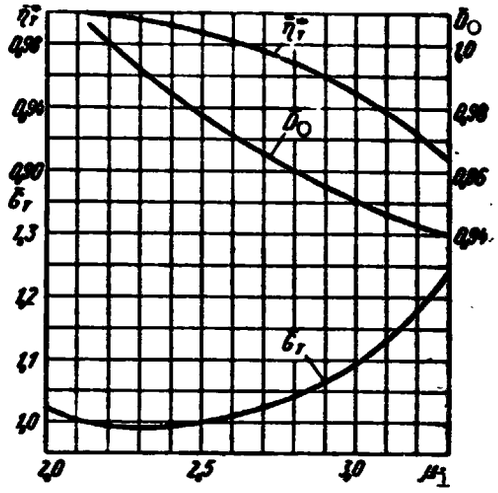

Figure 3.1. Relative efficiency, outer diameter, and weight of turbine as function of blade root loading coefficient

/47

As is obvious, increase of μ_1 above 2.2 causes a decrease in efficiency, and therefore does not reduce the turbine weight.

Experience in constructing TJE gas turbines has shown that moderately loaded stages with circumferential velocities at the mean diameter u_m = 300 - 400 m/sec and turbine stage work L_{st} = (14 - 1[illegible]) · 10^4 J/kg yield the best weight and size characteristics and efficiency.

Consequently, the work obtainable in one turbine stage lies within definite limits. If the required turbine work is higher, we must go to multistage turbines.

Increase in the number of stages with increase of the required turbine work is also dictated by the desire to avoid additional increase in turbine hydraulic losses caused by the increase of the stage loading and the flow velocity in the cascades (development of supersonic velocities) when developing all the enthalpy drop in the turbine in a smaller number of stages.

On the basis of statistical data, it is possible to indicate tentatively the number of turbine stages as a function of the design air compression ratio in the compressor under static sea-level conditions:

a) for TJE with $\pi^*_{\kappa 0} = 4.0 - 5.5$ — one stage;
$\pi^*_{\kappa 0} = 5.5 - 6.0$ — one stage with high circumferential velocity or two stages with relatively low circumferential velocity;
$\pi^*_{\kappa 0} = 6 - 10$ — two stages;
$\pi^*_{\kappa 0} = 10 - 15$ — three stages, or two stages with high circumferential velocity;
$\pi^*_{\kappa 0} \geqslant 15$ — three stages;

b) for FJE with bypass ratio $m = 0.7 - 1.5$, with
$\pi^*_{\kappa 0} = 9 - 10$ — two or three stages;
$\pi^*_{\kappa 0} = 11 - 19$ — three or four stages;
$\pi^*_{\kappa 0} = 20 - 27$ and $m = 4 - 5$ — five or six stages;
$\pi^*_{\kappa 0} = 20 - 27$ and $m = 6 - 8$ — seven or eight stages;

c) for TPE with $\pi^*_{\kappa 0} = 4 - 5$ — two stages;
$\pi^*_{\kappa 0} = 5 - 8.5$ — three stages;
$\pi^*_{\kappa 0} = 8.5 - 16.0$ — four or five stages.

In the first approximation, the effective turbine work can be distributed between the individual stages in proportion to the allowable values of the loading coefficients of the individual stages. As indicated above, it is better to take the value of the loading coefficient at the inner diameter.

With chosen values of the loading coefficients for each turbine stage, the effective work of the first stage is found from the formula: /48

$$(L_{st})_I = \frac{\mu_I}{\mu_I + \mu_{II} + \ldots + \mu_z} L_T \qquad (3.1)$$

Here, we assume that the circumferential velocity at the radius under consideration is approximately constant. We can determine similarly the effective work for the remaining stages.

In the case of two-shaft (two-spool) engines, the distribution of work between spools and also the rotor speed of each spool are

assigned. They are determined as a result of compressor aerodynamic design, prior to the design of the turbine, and as a result of calculations on compatibility of the compressor and turbine parameters. The effective work of a stage in a multistage turbine is also determined by (3.1), in which L_{st} corresponds to the effective shaft work of the given spool.

3.2. Determination of Basic Flow Path Dimensions at the Turbine Outlet

Turbine design begins with choice of the number of stages and the flow path shape in the meridional section. For choice of the turbine flow path shape, we must first know the outer diameter $D_{o\,2}$ and the flow section area at the turbine outlet F_2.

The area of the annular flow path section at the turbine outlet is determined from the [illegible] equation:

$$F_2 = \frac{G_g \sqrt{T_2^*}}{m p_2^* q(\lambda_{2c}) \sin \alpha_2}. \tag{3.2}$$

where $T_2^* = T_0^* - \dfrac{L_T}{\frac{k}{k-1} R}$ — temperature of the gas behind the turbine;

$p_2^* = p_0^* \left(1 - \dfrac{L_T}{\frac{k}{k-1} R T_0^* \eta_T^*}\right)^{\frac{k}{k-1}}$ — total pressure of the gas behind the turbine;

$q(\lambda_{2c})$ — determined from the gasdynamic function tables using the reduced velocity of the gas behind the turbine:

$$\lambda_{2c} = \frac{c_2}{\sqrt{2 \frac{k}{k+1} R T_2^*}};$$

where k = 1.33 and R = 288.4 J/kg · °K; m = 0.0396.

If the flow at the turbine exit is axial or approximately so, at this stage of the design we can take [illegible]. /49

The turbine efficiency is taken in the limits $\eta_T^* = 0.9 - 0.92$. A difference of 1% between the assumed value of η_T^* and the value obtained in the final turbine design is equivalent to a change in the area F_2 at the turbine outlet from 0.5% up to 1.5%.

3.2.1. Turbine blade strength and its connection with the flow path geometry

The choice of the basic turbine parameters should be made with account for ensuring turbine strength. Therefore, after determining the magnitude of the area F_2, it is necessary to determine the maximum strains which arise in the rotor blade root section. It is extremely important to do this now in order to be sure that the basic data for the turbine design and the chosen flow path form can be realized within limits which guarantee the required safety factor.

To determine the safety factor, we first limit ourselves to determination of the magnitude of the tensile stresses from the centrifugal forces.

In the general case, the tensile stress at a distance x from the root section (Figure 3.2a) will be:

$$\sigma_t = \frac{P_c}{F_x} = \rho \frac{\omega^2}{F_x} \int_{r_1+x}^{r_o} f_x (r_1 + x) dx, \qquad (3.3)$$

where P_c — centrifugal force in Newtons;

F_x — blade section area at distance x from the root section, in m^2; /50

ρ — blade material density in kg/m^3;

ω — blade angular velocity in $(sec)^{-1}$;

x — distance from the root section to the selected element in m;

f_x — blade section area at the radius between $r_1 + x$ and r_o;

h_b — blade length in m.

For blades with constant cross section along their height, the maximum tensile stress from centrifugal forces in the root section is:

$$\sigma_{ti} = \rho\omega^2 \frac{r_o^2 - r_i^2}{2}$$

or

$$\sigma_{ti} = 2\rho u_m^2 \frac{h_b}{D_m}, \qquad (3.4)$$

where $D_m = \frac{D_o + D_i}{2}$ — mean turbine diameter;

u_m — circumferential velocity at the mean turbine diameter.

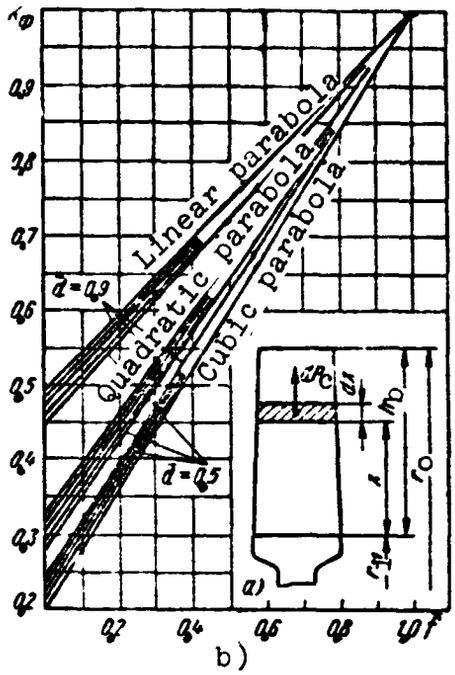

Figure 3.2. Blade form coefficient K_ϕ as function of $\bar{f}$ and $\bar{d}$ for various section area variation laws along the blade length

If we express the circumferential velocity u_m through the turbine speed n, (3.4) takes the form:

$$\sigma_{ti} = 2\rho \frac{\pi^2}{60^2} n^2 D_m h_b$$

Defining the mean diameter at the blade trailing edge, we can express the product $D_m h_b$ through the annular area at the turbine outlet $D_m h_b = F_2/\pi$. Then,

$$\sigma_{ti} = 2\pi\rho \left(\frac{n}{60}\right)^2 F_2. \qquad (3.5)$$

From this formula, it is obvious that the tensile stresses in the turbine blades are directly proportional to the turbine outlet annular area F_2.

The turbine rotor blades are always constructed with variable section along their length, decreasing from the root to the upper pheripheral blade section. Therefore, the tensile stress in the

root section of real blade will be smaller than in blades with constant cross section. This is usually taken into account with the help of the blade form coefficient $K_\phi < 1$:

$$\sigma_t = \sigma_{t1} K_\phi = 2\pi K_\phi \varrho \left(\frac{n}{60}\right)^2 F_s. \tag{3.6}$$

The magnitude of the coefficient K_ϕ depends on the relative blade length D_m/h_b, characterized also by the relative diameter $\bar{d} = D_i/D_o$, and on the ratio of the peripheral (f_o) and root (f_i) blade section areas $\bar{f} = f_o/f_i$, and on the section area variation along the blade length. /51

For linear section area variation along the blade length, $f_x = f_i - \frac{f_i - f_o}{h_b} x$, the coefficient

$$K_\phi = \frac{1+\bar{f}}{2} - \frac{1-\bar{f}}{6} \frac{h_b}{D_m}.$$

The numerical value of the form coefficient K_ϕ for various rules of variation of the area "f" along the blade length can be determined with the help of the graph $K_\phi = \phi(\bar{f})$ (see Figure 3.2b), from which it is obvious that the coefficient K_ϕ varies little in a wide range of variation of the relative diameter $\bar{d}$. For determining K_ϕ, this allows us to assume $\bar{d}$ constant and equal to 0.65, which corresponds approximately to the majority of aviation gas turbines. For most aviation GTE turbine rotor blades, the value of the form coefficient varies in quite narrow limits — K_ϕ = 0.48 - 0.54.

The quantity σ_t constitutes a significant part of the stresses in the blade root section and is very characteristic for evaluating blade strength. However, for a more objective evaluation of blade operational reliability, it is necessary to know the blade strength margin. To this end, we must add to σ_t the residual bending

stresses which are not compensated by the blade foil centrifugal forces*, and determine the allowable stresses based on the blade material stress-rupture strength characteristic, after first finding the temperature of the most highly stressed blade root section.

We note that the minimal strength margin usually occurs not at the blade root section, but rather at a nearby section, which has stresses which differ little in magnitude but higher temperature, because of the fact that this section is located in a zone of higher gas temperature and very little heat is transferred into the base of the blade. Such sections are most frequently located at about one quarter of the blade length from the root section. Their location is determined by the nature of the blade cross section area distribution along its length and by the radial temperature pattern (Figure 3.3).

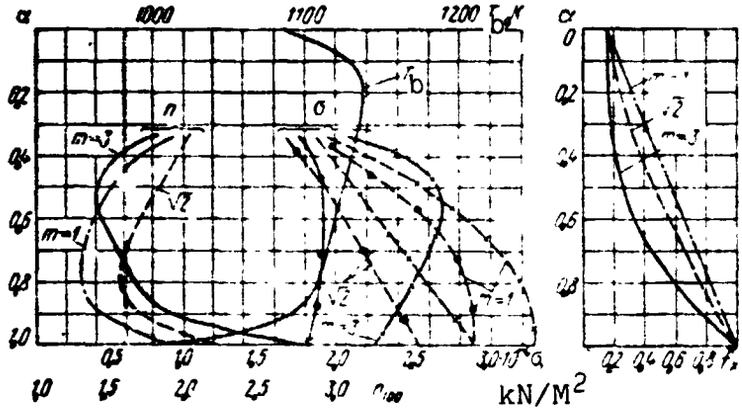

Figure 3.3. Dependence of strength margin on blade cross section area variation along the blade length:

$$\bar{f} = \frac{f_o}{f_i};\ \alpha = \frac{r_o + x}{h_b};\ \bar{f}x = \frac{f_b}{f_i} = \bar{f} + (1 - \bar{f})\alpha^m;$$

T_b — blade temperature; $n_{100} = \sigma_{100}/\sigma_\Sigma$;

$\sigma_\Sigma = \sigma_t + \sigma_{bend}$; —·— — σ_t; —×— — σ_Σ

---

*Uncompensated residual bending stresses arise in the blade foil in the case of a relationship of the gas and centrifugal forces in which the bending stresses from the action of the gas forces are not balanced by the bending stresses from the action of the centrifugal forces.

The magnitude of the uncompensated residual bending stress σ_{bend} in aircraft GTE turbine rotor blades is usually determined by the range of variation of the loading from action of the gas forces. /52 The broader this range, the larger the magnitude of the residual bending stresses.

The variation of the load from the gas forces acting on the blade is determined basically by the variation of the gas flowrate through the turbine. Figure 3.4 shows the ratio σ_{bend}/σ_t as a function of the relative maximal gas flowrate G_{max}/G_0, where G_{max} is the maximal gas flowrate through the turbine over the entire engine operating regime range, and G_0 is the gas flowrate under stand conditions, corresponding to the maximal reduced rotor speed. This graph is constructed on the basis of statistical data and can be used for preliminary calculations.

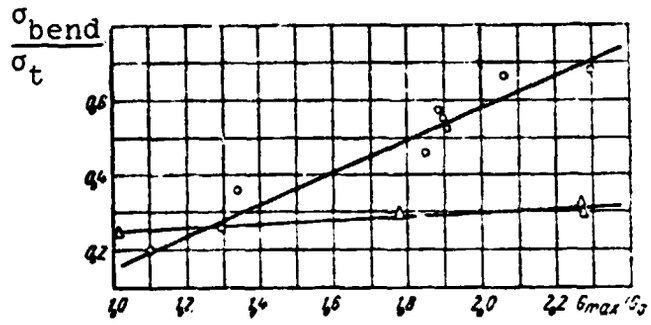

Figure 3.4. Ratio σ_{bend}/σ_t as function of relative maximal gas flowrate G_{max}/G_0:

o — blades without shroud; Δ — blades with wire banding or platform shroud

Then the overall blade stresses:

$$\sigma_{\Sigma} = \sigma_t + \sigma_{bend} = (1 + \frac{\sigma_{bend}}{\sigma_t})\sigma_t. \qquad (3.7)$$

The allowable blade stresses depend on the blade material and the temperature of the most highly stressed lower section blade.

The blade temperature T_b is determined by the total temperature in the relative motion:

$$T^*_{1w} = T_1 + \frac{w_1^2}{2\frac{k}{k-1}R}. \tag{3.8}$$

If we substitute into (3.8) the expressions $T_1 = T^*_{0i} - \frac{c_1^2}{2\frac{k}{k-1}R}$, /53

where T^*_{0i} — gas total temperature ahead of the considered stage, averaged around a circle of given radius, and $w_1^2 = c_1^2 - 2uc_1 + u^2$, we obtain:

$$T^*_{1w} = T^*_{0i} - \frac{u^2}{2\frac{k}{k-1}R}\left(2\frac{c_{1u}}{u} - 1\right). \tag{3.9}$$

From the previous analysis (see Chapter II), we know that $c_{1u}/u = \mu - (c_{2u}/u)$, and for the root section, $(c_{1u}/u)_1 = \mu_1 - (c_{2u}/u)_1$.

From (2.25), we find $\frac{c_{2u}}{u} = \frac{\mu - (1 - K_a)}{1 + K_a}$. Then,

$$\left(\frac{c_{1u}}{u}\right)_1 = \frac{1 - K_a(1 - \mu_1)}{1 + K_a}. \tag{3.10}$$

After substituting (3.10) into (3.9), we obtain:

$$(T^*_{1w})_1 = T^*_{0i} - \frac{u_1^2}{2\frac{k}{k-1}R}\left[2\frac{1 + K_a(1 - \mu_1)}{1 + K_a} - 1\right], \tag{3.11}$$

where $T^*_{0i} = T^*_0 - \frac{L_i - \sum L_{i\,st}}{\frac{k}{k-1}R}$. /54

Here, $\sum L_{i\,st}$ is the overall work of the preceding stages.

When determining the blade temperature variation along its length, we assume that the gas temperature at the combustion chamber exit, averaged around a circle of given radius, i.e., the temperature nonuniformity, retains its nature up to the turbine exit. The total temperature determined in this fashion T^*_{1i} will be close to its actual value with accuracy adequate for evaluating the strength of the material from which the blades are to be made.

Because of heat removal into the disk, particularly when cooling the blade retention area, and addition to the gas stream of the air from the cavity ahead of the turbine disk, the blade temperature in the root region, in contrast with the other sections, is not equal to the temperature of the gas flowing around the blade, and the difference may amount to from 50° to 150°, and in the case of blade airfoil cooling, the difference between the gas temperature and the blade temperature is still larger.

Consequently, the blade temperature at the root section $(T_b^*)_i = (T_{1\,w}^*)_i - \Delta T$, where ΔT is the correction accounting for the nature of the temperature field along the radius, heat removal into the disk, and blade cooling.

The strength characteristic of some materials used in fabricating turbine stator vanes and rotor blades is shown in Figure 3.5, where the stress level $P = 7(\lg \tau + 20)$, τ — loading time to failure, T — temperature in K. Using this characteristic, we can find the allowable stresses σ_a for the selected material as the ratio of the ultimate stress σ_u, determined from the graph (see Figure 3.5), to the normed strength margin. For this, we need to know the blade temperature, the time which the blade must operate at this temperature, and the magnitude of the required strength margin.

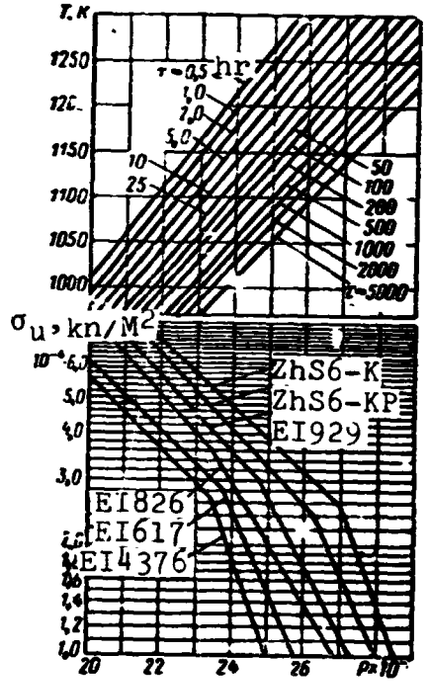

Figure 3.5. Stress-rupture limits of materials

/55

It may happen that in the calculation we obtain $\sigma_a < \sigma_\Sigma$. In this case, the required strength margin will not be provided:

$$n = \frac{\sigma_u}{\sigma_\Sigma} < n_{norm} = \frac{\sigma_u}{\sigma_a} .$$

Then it is necessary to either reduce the blade temperature by introducing special blade cooling, reducing the turbine inlet gas temperature, or reducing σ_Σ. As a rule it is not advisable to reduce σ_Σ by reducing σ_{bend}, since σ_{bend} is not in itself large and its reduction leads to the necessity for a very wide blade and, consequently, increase of the turbine weight (mass), which is extremely undesirable. Therefore, we must reduce σ_t by reducing the exit area F_2, the form coefficient K_ϕ, or the turbine rotational speed. This means that the basic turbine design values, obtained from the general engine design, cannot be realized within the limits of the specified strength margins and weight, and these initial values must be reexamined.

Reduction of turbine exit area F_2

For given p_0^*, T_0^*, G_g, and L_T, the turbine exit area F_2 can be reduced by increasing the gas velocity $M_{2\ c}$. We have noted previously that the maximal permissible value of $M_{2\ c}$ is limited not only by the afterburner chamber and propulsive nozzle operating conditions and the hydraulic resistances in the chamber and nozzle, but also by the magnitude of the allowable losses in the turbine itself. We see from the curves in Figure 2.4 that increase of the gas velocity above $M_{2c}=0{,}5$ leads to reduction of the turbine efficiency. Such important operating characteristics as engine starting, acceleration, and sensitivity to variation of the propulsive nozzle exit (throat) area also depend to a considerable degree on the value of $M_{2\ c}$.

Reduction of the blade form coefficient K_ϕ

It follows from (3.6) that the tensile stresses can be reduced by reducing the form coefficient K_ϕ. We shall see the degree to which this reduction is realistic, and how it is accomplished.

We see from Figure 3.2 that for the blade whose cross section area variation along the length is close to a cubical parabola, the coefficient K_ϕ will be smaller than, for example, for the linear law. The coefficient K_ϕ will also decrease with reduction of the ratio $\bar{f}$ /56 of the upper (tip) f_0 and lower (root) f_i blade section areas. However, we must bear in mind the following.

1. Not all turbine blades can be made with cross sectional area variation along the length close to the cubical parabolic law. This is because of the fact that for blades so designed, with length more than 60 - 70 mm, the maximal overall stresses will occur not at the root section or near the root section, but at approximately one quarter or one third of the blade mean length measured from the root section. This is explained by the fact that for such blades, the bending modulus decreases markedly from the root toward the tip and the uncompensated bending stresses will very large, and also by the fact that in certain cases with variation of the blade cross sectional areas, following the cubical parabola law, the peak tensile stress moves upward from the root section. We must also bear in mind that with increasing distance from the root section, the blade temperature increases and, consequently, the strength margin will decrease to a greater degree than simply because of the increase of the blade stresses.

2. Reduction of $\bar{f}$ is achieved by increasing the blade root section area. This results from the fact that for a definite number of blades and minimal allowable cascade solidity at the outer diameter, the profile chord length is already specified, while the minimal allowable thickness of the leading and trailing edges and

of the profile itself is limited by manufacturing and strength considerations. The minimal allowable edge thickness should be selected from considerations of blade stiffness and material properties (grain size, corrosion resistance, sensitivity to stress concentration, and so on).

However, increase of the blade root section area has certain limits. For example, it is not advisable to increase the area by excessive increase of the leading or, particularly, the trailing edge thickness, since this leads to increase of the hydraulic losses and reduction of the turbine efficiency. Excessive increase of the profile maximal thickness also leads to reduction of the turbine efficiency. In fact, if we make the blade root section profile with maximal thickness greater than:

$$c_{max} = t - a = t(1 - \sin\beta_{1p}),$$

the interblade channel will be divergent (Figure 3.6), and this always leads to greater losses than use of a convergent channel.

Another possibility is to increase the blade root section area by increasing the blade width. This leads to the necessity to make the cascade with excessively large solidity near the blade root, which also leads to the appearance of additional hydraulic losses in the turbine and also to increased turbine weight.

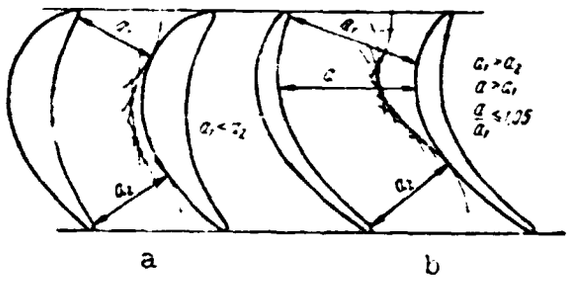

Figure 3.6. Different interblade channel forms: /57

a — divergent channel; b — channel with local divergence

The minimal practically realizable values of $\bar{f} = f_0/f_1$ fall in the range $\bar{f} = 0.2 - 0.25$.

Reduction of rotational speed

It follows from (3.5) that reduction of the turbine rotational speed is an effective technique for reducing the tensile stresses σ_t. However, we must bear in mind that, in this case, the compressor rotational speed also decreases, and therefore the number of compressor stages must be increased in order to maintain the head coefficient.

This still does not mean that the compressor weight necessarily increases. The reduction of the loading on the compressor blades and disks from the action of the centrifugal forces may yield a weight savings which will be equal to or greater than the weight of the added stages. It all depends on the specific engine configuration, engine size, and the magnitude of the rotational speed change.

For twin-spool, bypass, or turboprop engines, rotational speed change leads to still larger structural changes in comparison with the TJE. Therefore, when it beomes necessary to change the rotational speed, it is necessary to make a detailed analysis for each specific case.

3.2.2. Turbine outer diameter selection

As a rule, the maximal turbine outer diameter $D_{0\ 2}$ is limited by the general engine configuration and the conditions of its mounting on the airplane, and is selected with account for ensuring minimal turbine weight.

After using (3.2) to determine the turbine exit flow section area F_2, selecting the blade root section loading coefficient μ_i, and knowing the final stage work L_{st} and the rotor rotational speed /58
n rpm, we find the turbine inner diameter (hub diameter):

$$D_{i\ 2} = \frac{60u_i}{\pi n} = \frac{60}{\pi n}\sqrt{\frac{L_{st}}{\mu_i}}.$$

Since $D_{o\ 2}$ corresponds to the turbine exit, in order to determine it in the case of decreasing hub diameter (Figure 3.7a, c), the loading coefficient can be taken somewhat larger than for the stages with smaller angle γ_i. Thus, in the case of hub taper angle

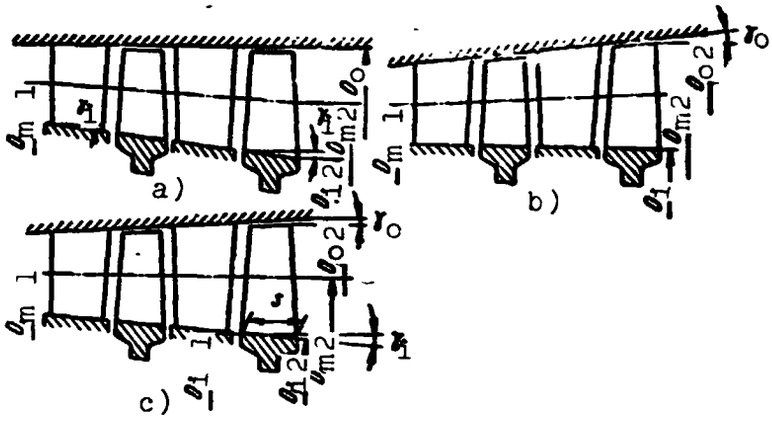

Figure 3.7. Turbine flow path schemes in meridional section

$\gamma_i = \text{arctg}\ \dfrac{D_{i\ 1} - D_{i\ 2}}{2s} = (8 - 10)°$, where s is the disk rim width, the loading coefficient can be taken as $\mu_i \approx 2.2$.

Then the turbine outer diameter

$$D_{o\ 2} = \sqrt{D_{i\ 2}^2 - \frac{4F_2}{\pi}}$$

If the resulting value of $D_{o\ 2}$ does not agree with the general engine configuration, or $D_{i\ 2}$ exceeds the dimensions of the forgings which can be produced on the available equipment, or the blade length $h_b = (D_{o\ 2} - D_{i\ 2})/2$ is so short that the end losses may reduce the turbine efficiency markedly, the number of turbine stages must be increased in order to reduce $D_{i\ 2}$ and $D_{o\ 2}$.

If we assume, for example, uniform division of the work among the turbine stages, then the outer diameter of the last stage, which is also the maximal diameter of the entire turbine, will be:

$$D_{o\ 2} = \sqrt{\left(\frac{60}{\pi n}\right)^2 \frac{L_T}{z\mu} + \frac{4F_2}{\pi}},$$

where z is the number of stages.

It is obvious that the turbine outer diameter can be reduced by /59
reducing the turbine work or increasing the number of stages.

3.3. Turbine Flow Path Configuration Selection

Several flow path schemes in the meridional section can be realized in the limits of the selected value of $D_{o\ 2}$:

a) with constant outer diameter and decreasing inner diameter (see Figure 3.7a)

b) with increasing outer diameter and constant inner diameter (see Figure 3.7b);

c) with varying outer and inner diameters (see Figure 3.7c). A particular case of this scheme is the turbi 'th constant mean diameter.

The scheme with constant outer diameter makes it possible to construct the turbine with smaller number of stages in comparison with the other schemes and, in the case of a single stage, makes it possible to take more work from the turbine for a given loading coefficient. This is explained by the fact that, for the selected maximal outer diameter, the turbine made using the scheme with D_o = const for a given rotational speed has higher circumferential velocities at the mean diameter and, particularly, at the inner diameter of the first turbine stages than in the other schemes. However, in the scheme with D_o = const, the first-stage blades will be shorter than those of the last stages.

The turbine with constant inner diameter, equal to the diameter of the last stage (see Figure 3.7b), has lower circumferential

velocities in the first stages, which may make it necessary to increase the number of stages or increase the loading of the first stages and, consequently, may lead to reduction of the turbine efficiency.

However, the flow path scheme with D_i = const has certain technological advantages, and makes it possible to use a longer first-stage blade than in schemes a and c, which is important for small turbines. For example, absence of taper in the root part of the blade facilitates its machining and simplifies inspection during fabrication; the smaller inner diameter facilitates production of turbine disk castings or forgings, and so on.

The flow path with D_m = const is intermediate between the schemes examined above.

The impression may be created that, since a turbine with D_o = const can be constructed with a smaller number of stages, it will be lighter than the turbine with D_i = const, having a larger number of stages for the same loading of each stage in both turbines. However, in many cases this impression may be misleading, since the weight of the turbines being compared will be determined not only by the number of stages, but also by the degree to which it is possible to reduce the turbine diameter with increase of the number /60 of stages and width of the stator vanes and rotor blades, which in turn is determined by the stator vane attachment design and the allowable rotor blade aspect ratio (ratio of blade length to width of its root section).

The allowable rotor blade aspect ratio is determined, in turn, by the magnitude of the bending stresses in the blades and use of some particular blade banding technique. Finally, the relative weight of these turbines will also depend on their size. Therefore, a comparative weight analysis must be made in each specific case when making the detailed turbine calculations.

In addition to the schemes examined above, wide use is made of intermediate (when all three diameters D_i, D_m, D_o are variable) and combined schemes, when, for example, the first stages are made using the scheme with D_m = const and the last stages — with D_o = const.

For given stage work or heat drop in the turbine stage, the gasdynamic calculation of the turbine yields the magnitude of the required circumferential velocity u. Since different turbine diameters (different relative hub diameters $\bar{d} = D_o/D_i$) correspond to this value of u for different rotational speeds, the question arises of the most rational selection of these quantities.

Theoretical analysis and examination of the result of design refinement of various turbine variants show that for fixed values of u_m and overall blade stresses ($\sigma_t + \sigma_{bend}$ = const), the turbine weight remains practically constant. Therefore, when selecting the turbine diameter, we can be guided by other considerations: overall dimensions, matching of the turbine and compressor characteristics [28], magnitude of the relative hub diameter, and ease of fabrication.

3.3.1. Flow path inner and outer contour taper angles

In practice, it is rarely possible to design a turbine having a flow path with constant outer or inner diameter. If the gas expansion ratio in the turbine $p_0^*/p_2 > 3$, then if we keep the outer or inner diameter constant, the ratio of the annular areas at the turbine entrance and exit may be such that, for a realistically feasible flow path width, the angle γ (see Figure 3.7) is excessive [illegible]. Then, the turbine is made with varying outer and inner diameters. The taper angles γ_o and γ_i of the outer and inner turbine flow path contours in the meridional section are determined by the magnitude /61 of the additional hydraulic losses which may arise in this case, and by considerations of rotor blade strength and, sometimes, by the turbine fabrication and assembly technology.

Experience in developing aircraft engine gas turbines shows that the angles γ_0 and γ_1 for neighboring cascades should not differ by more than 8 - 12°. This ensures smooth variation of the flow path contours and absence of losses which can arise in the case of sharp variation of the flow path profile in the meridional section.

The magnitude of the blade cascade angle γ which is acceptable from the viewpoint of hydraulic losses is defined by the divergence $\bar{F} = F_{en}/(F_{ex} \sin \alpha_1)$, and by the relative interblade channel height h_{ex}/a (h_{ex} — blade length at the exit; a — interblade channel throat width). For stator cascades with axial flow direction at the entrance:

$$\bar{F} = \frac{(D_m h)_{en}}{(D_m h)_{ex}} \frac{1}{\sin \alpha_1}.$$

and for rotor blades:

$$\bar{F} = \frac{(D_m h)_{en}}{(D_m h)_{ex}} \frac{\sin \beta_1}{\sin \beta_2}.$$

Figure 3.8 shows the relative loss coefficient $\bar{\xi}_\Sigma = \xi_\Sigma / \xi_{\Sigma 0}$ as a function of interblade channel divergence $\bar{F}$, obtained from tests of stator profile cascades with endwall slope angles γ up to 45°. The 30° angle was formed in one case by a plane extending from the entrance to the exit (see Figure 3.8a), and in the other case by a curvilinear surface having at the exit a segment parallel to the channel axis (see Figure 3.8b). This segment starts from the narrow section of the interblade channel, as a result of which the degree of divergence in the oblique exit zone decreases.

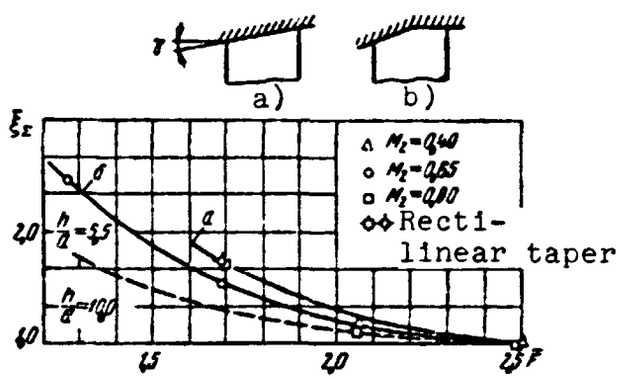

Figure 3.8. Relative cascade loss coefficient $\bar{\xi}_\Sigma$ versus channel divergence $\bar{F}$

/62

We see from the $\bar{\xi}_{\Sigma}(F)$ graph that the cascade with curvilinear taper (curve b) has somewhat smaller losses. Therefore, it is advisable to terminate the blade cascade taper prior to the beginning of the oblique exit segment (section a_2 in Figure 3.6). This applies particularly to cascades having small degree of interblade channel convergence.

The curve $\bar{\xi}(F)$ for h/a = 10 was obtained by scaling the experimental data. Here, it was assumed that the degree of interblade channel convergence remains constant, i.e., the angle α_1 effectively decreases, and the profile losses remain constant within the limits of this reduction (from $\alpha_1=24°$ to $\alpha_1=14°$).

The experiments conducted showed that variation of the Mach number at the exit from the cascade tested in the range $M_{2c}=0.4-0.9$ has very little influence on the losses in the cascade.

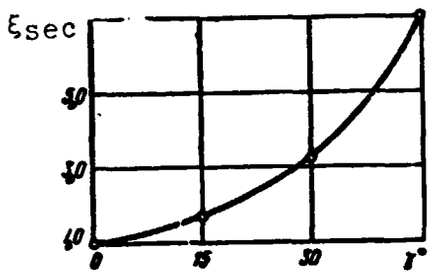

Figure 3.9. Relative cascade secondary loss coefficient versus angle γ

The coefficient of relative secondary loss variation $\bar{\xi} = \xi_{sec}/\xi_{sec\ 0}$ is the difference between the overall cascade loss coefficient ξ_{Σ} and the profile loss coefficient ξ_{pr}. Here, $\xi_{sec\ 0}$ is the magnitude of the secondary losses for $\gamma = 0$. The dependence of $\bar{\xi}_{sec}$ on the angle γ is shown in Figure 3.9. These graphs make it possible to evaluate the turbine stator profile cascade losses in the presence of flow path meridional contour taper.

3.4. Determining Rotor and Stator Cascade Widths

The rotor and stator cascade widths depend on the magnitude of the bending moment acting on the vanes and blades, and the allowable bending stresses, and is determined in the design of already profiled vanes and blades whose geometric characteristics are known,

while the forces acting are determined in the gasdynamic analysis of the turbine.

Therefore, in selecting the flow path scheme, when the complete turbine gasdynamic analysis data and the profile geometric characteristics are not yet known, the rotor and stator cascade widths must be determined approximately. The approximation must obviously be /63 such that after profiling and final calculation, the stator vane and rotor blade widths will not change markedly in comparison with the width determined when selecting the flow path scheme.

This can be achieved when the blade width of the turbine being designed is determined by scaling the width of blades for which all the design data and geometric characteristics are known. These may be either blades of existing or completely designed and analyzed turbines. In practice, the maximal inaccuracy in determining the rotor blade width by this scaling technique does not exceed 5% of their final dimension. Sometime, the blade width is determined during design by comparing the blades with existing blades on the basis of aspect ratio, $\bar{h}_b = h_b/b$, and retaining the same aspect ratio. The technique can be used for similar stages with comparatively small difference of their geometric dimensions. In all other cases, it will lead to significant errors.

As a rule, the rotor blade root section is wider than the other sections, since the bending moment and the centrifugal force load are largest at this section. Therefore, the rotor blade width is found for the root section. The same conclusion applies to cantilevered stator vanes. Their width is determined for the profiled vane section closest to the point of attachment.

The allowable bending stresses σ_a in the rotor blade root section of the turbine being designed I with strength margin n can be found from the formula:

$$(\sigma_{bend})_u = (\sigma_\Sigma)_u - (\sigma_t)_u = n\sigma_a - (\sigma_t)_u.$$

We shall consider that the uncompensated residual bending stress fraction in the blade being designed I is the same as in the blade II selected for scaling. In so doing, we assume that the relative circumferential force variation at the maximal turbine rotor rotational speed is the same for both blades. Then the bending stresses from the action of the gas forces in the blade root section of the turbine being designed will be:

$$(\sigma_{bend}^{(g)})_I = (\sigma_{bend}^{(g)})_{II} \frac{(\sigma_{bend})_I}{(\sigma_{bend})_{II}} .$$

It is well known that the bending stress in the rotor blade root section is directly proportional to the circumferential force acting on the blade (P_u) and the blade length (h_b), and is inversely proportional to the root section profile section modulus W, relative to the axis of minimal moment of inertia, i.e.,

$$\frac{(\sigma_{bend}^{(g)})_I}{(\sigma_{bend}^{(g)})_{II}} = \frac{P_{uI} h_I}{P_{uII} h_{II}} \frac{W_{II}}{W_I}. \qquad (3.12)$$

In turn, /64

$$\frac{P_{uI}}{P_{uII}} = \frac{M_I}{M_{II}} \frac{z_{II}}{z_I} \frac{D_{mII}}{D_{mI}}$$

and

$$\frac{M_I}{M_{II}} = \frac{G_I}{G_{II}} \frac{u_I \Delta c_{uI}}{u_{II} \Delta c_{uII}} \frac{n_{II}}{n_I},$$

where M — torque on the stage shaft;

z — number of blades;

G — gas flowrate through the turbine;

n — rotor rotational speed, and $u\Delta c_u$ can be taken at any radius, since $L_u = u\Delta c_u = f(r) = \text{const}$. Then, substituting these equalities into (3.12), with account for the fact that

$$\frac{n_{II}}{n_I} = \frac{u_{II} D_I}{u_I D_{II}} \text{ and } u_u = u_m \frac{2\bar{d}}{1+\bar{d}},$$

where $\bar{d}$ — hub ratio, after transformation, we obtain:

$$\frac{(\sigma^{(g)}_{bend})_I}{(\sigma^{(g)}_{bend})_{II}} = \frac{G_I}{G_{II}} \frac{h_I}{h_{II}} \frac{z_{II}}{z_I} \frac{(\Delta c_{uI})_I}{(\Delta c_{uII})_I} \frac{\bar{d}_I}{\bar{d}_{II}} \frac{1+\bar{d}_{II}}{1+\bar{d}_I} \frac{W_{II}}{W_I}. \qquad (3.13$$

We can consider that the profile section modulus W is proportional to the chord length and the square of the profile maximal thickness c_{max}. Since the profile width b and chord s are practically equal for the rotor blade root section, we can write:

$$\frac{W_{II}}{W_I} = \frac{b_{II} c^2_{max\,II}}{b_I c^2_{max\,I}} \approx \frac{s_{II}}{s_I} \frac{c^2_{max\,II}}{c^2_{max\,I}}.$$

The rotor [illegible] root section interblade channels are nearly active and are made with practically constant width. Such a channel, characteristic for aircraft engine gas turbines, is shown in Figure 3.10. Therefore we can write:

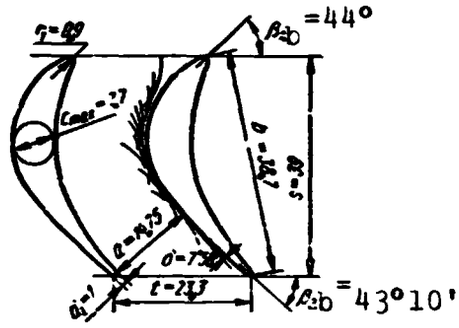

Figure 3.10. Interblade channel at rotor cascade root s[illegible]ion

$$c_{max} = t - a = t(1 - \sin\beta_2).$$

Then,

$$\frac{W_{II}}{W_I} = \frac{s_{II}}{s_I} \frac{t^2_{II}(1-\sin\beta_{2u})^2_{II}}{t^2_I(1-\sin\beta_{2u})^2_I}.$$

Substituting this expression into (3.13), and considering that:

$$\frac{z_{II}}{z_I} = \frac{D_{u\,II}}{D_{u\,I}} \frac{t_I}{t_{II}}, \text{ and } \frac{\Delta c_u}{a} = \mu,$$

after transformation, we obtain: /65

$$\frac{(\sigma^{(g)}_{bend})_I}{(\sigma^{(g)}_{bend})_{II}} = \frac{G_I}{G_{II}} \frac{h_I}{h_{II}} \frac{\bar{d}_I}{\bar{d}_{II}} \frac{1+\bar{d}_{II}}{1+\bar{d}_I} \frac{\mu_{II}}{\mu_{II}} \frac{n_I}{n_{II}} \frac{s_{II}}{s_I} \frac{t_{II}}{t_I} \frac{(1-\sin\beta_{2u})^2_{II}}{(1-\sin\beta_{2u})^2_I} \qquad (3.14)$$

or:

$$s_I = s_{II} \frac{(1 - \sin \beta_{2\,u})_{II}}{(1 - \sin \beta_{2\,u})_I} \times$$

$$\times \sqrt{\frac{G_I}{G_{II}} \frac{h_I}{h_{II}} \frac{\bar{d}_I}{\bar{d}_{II}} \frac{1+\bar{d}_{II}}{1+\bar{d}_I} \frac{\mu_{uI}}{\mu_{uII}} \frac{n_I}{n_{II}} \frac{(\sigma^{(g)}_{bend})_{II}}{(\sigma^{(g)}_{bend})_I} \frac{(b/t)_I}{(b/t)_{II}}}. \qquad (3.15)$$

The gas flow rate is taken as the mean value between the maximal (at the maximal design rotor speed) and the minimal. The angle $\beta_{2\,i}$ is found using (2.25) from the assumed loading coefficient μ_{iI} at the root and the gas velocity c_2 at the turbine exit, known from the preliminary calculation. If the values of the angles $\beta_{2\,i}$ are similar for both cascades, then obviously the ratio $\frac{(1 - \sin \beta_{2u})_{II}}{(1 - \sin \beta_{2u})_I} \approx 1$.

3.4.1. Stator cascade width

The stator cascade width is also determined by scaling existing or completely designed vanes whose geometric characteristics and calculated performance are known. The scaling technique is analogous to that described above. When determining the forces $P_u = G(\Delta c_u/z)$ and $P_a = G(\Delta c_a/z) + \Delta p t h$ acting on the blade in the circumferential and axial directions, we must substitute into the computational formula the maximal value of the gas flow rate G at which the turbine will operate. This operating regime will correspond to the maximal value of the pressure difference Δp across the stator cascade.

The maximal profile thickness of the stator vanes, even if they are cantilevered, is not limited by the intervane channel shape. On the basis of section strength considerations, the relative profile thickness of cantilevered vanes of existing turbines varies in the range 0.1 - 0.06.

The stator vane profile width differs markedly from the chord, whose magnitude is found by scaling. The ratio of the profile width to its chord is determined by the relation $s/b=(1.05-1.1)\,\mathrm{tg}\,\alpha_1$. In the range of variation $\alpha_1=15°-40°$, this relation is confirmed to within ± 3% by a large number of stator vane profiles of existing turbines.

The stator vanes, which are subjected only to the action of bending stresses, permit comparatively free choice of their width. This yields some possibility of selecting the most favorable width from the viewpoint of hydraulic losses in the cascade.

Other conditions being the same, the secondary losses in the cascade are inversely proportional to the ratio of blade length to intervane channel throat width $\tilde{h} = h_b/a$ /66

It is well known that if the vane length reaches 50 mm, further increase of the length does not in itself lead to marked reduction of the losses. For such vanes, we must make certain that the ratio h_b/a is sufficient large. For a selected vane length, this can be achieved by increasing the number of vanes while maintaining the optimal ratio b/t.

When selecting the turbine stator profile cascade solidity, it is not sufficient to satisfy only the requirement for ensuring its optimality from the viewpoint of the profile losses, since experiments show that beginning with $b/t \leqslant 1.25-1.35$, further reduction of the solidity to $b/t=0.9-1.0$ (depending on the flow turning angle in the cascade) does not lead to significant change of the profile loss level. Consequently, the loss dependence on cascade solidity near the optimum point is flat (the optimum essentially extends over a quite broad solidity range); therefore, for more rational selection of the solidity in a stage being designed, we must consider the parameters connecting the spacing with the profile and intervane channel geometric characteristics and their mutual influence on the losses.

It is well known that the profile losses (at subsonic velocities) are made up of the friction losses and the edge losses:

$$\xi_{pr} = \xi_{fr} + \xi_{ed}.$$

If with low solidity it is possible to maintain the profile back surface curvature distribution in limits such that it does not lead to marked increase of the friction losses, then the profile loss variation will be associated with variation of the edge loss contribution. It should be noted that with reduction of the solidity, in spite of the reduced intervane channel "blockage", characterized by the the ratio of the profile trailing edge thickeness to the intervane channel throat dimension d_2/a, the absolute edge losses may increase because of the increase of the difference between the velocities on the convex and concave sides of the profile and the increased kinetic energy losses in mixing of streams with different velocities. Therefore, it is obvious that even in the case of "zero" trailing edge thickness, the edge losses will not be equal to zero. However, with reduction of the cascade solidity, the edge losses will decrease to values of $d_2/a \approx 0{,}03$.

Specially conducted experiments have shown that beginning with $d_2/a \leqslant 0{,}05$, further increase of the spacing does not lead to reduction of the profile losses; but in the case of considerable intervane channel "blockage" $(d_2/a > 0{,}15)$, reduction of the solidity makes it possible to reduce the cascade losses. This is particularly significant for high-temperature-engine gas turbines, whose fabrication technology often does not permit production of thin vane t ing edges. /67

Variation of the cascade solidity also leads ation of the intervane channel relative neigh h_b/a. In this case, the secondary loss contribution aaries directly as the value of h_b/a only in a definite range of variation of the latter. Beginning with some values of h_b/a, these losses increase significantly.

Figure 3.11 shows the magnitude of the secondary losses ξ_{sec} and also the contribution of such losses to the overall losses $\xi_{sec} = \xi_{sec}/\xi_{\Sigma}$ as a function of relative channel height, plotted from the test results of 15 different stator cascades differing in exit angle $\alpha_1 = 9 \div 35°$, flow turning angle $\varepsilon = 65 - 110°$, and solidity $b/t = 1.22 - 2.6$.

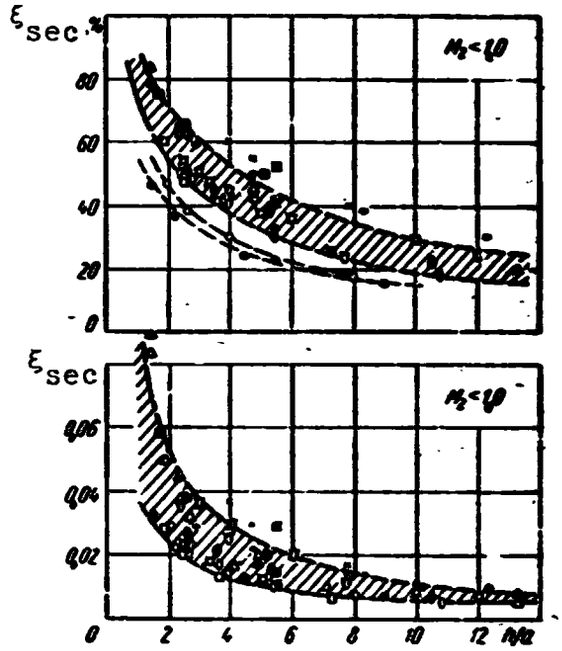

Figure 3.11. Secondary losses in stator cascade versus relative intervane channel height

Analogous relations $\xi_{sec}(h)$ are plotted for the rotor blades (Figure 3.12). These relations can be used when it is necessary to utilize blades with tip shrouds. The values of ξ_{sec} will be larger without the shrouds.

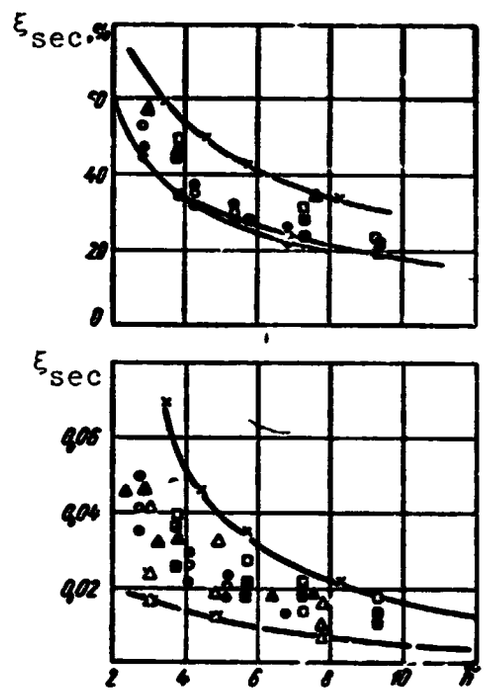

/68

Figure 3.12. Secondary losses in rotor cascade versus relative interblade channel height

We see from examination of these relation $\xi_{sec}(h)$ that the magnitude of the secondary losses is determined by the cascade geometric and operating regime parameters. This dependence can be found from the expression obtained on the basis of the experimental data presented:

$$\xi = \frac{\xi_{sec}}{\xi_{\Sigma}} = \frac{A}{1 + Bh}.$$

Here,

$$\xi_{\Sigma} = \xi_{sec} + \xi_{pr};$$

A = 1.0 - 1.2 and B = 0.4 - 0.5 are constant coefficients. The larger values of A and the smaller values of B correspond, respectively, to cascades with small profile losses (ξ_{pr} = 0.02 - 0.03) and, conversely, the smaller values of A and the larger values of B apply to cascades with relatively large profile losses.

For most profile cascades of existing turbines (or those used in aircraft turbines), the coefficients A = 1.0 - 1.1 and B = 0.5.

Reduction of the stator cascade solidity leads to reduction of the secondary losses from flow nonuniformity at the rotor cascades entrance caused by the stator trailing wakes.

The periodic variation of the flow parameters at the cascade entrance is characterized by the Strouhal number $Sh = \nu L/w$, where ν is the frequency of the flow parameter variation ahead of the cascade, L is the characteristic length, w is the gas velocity.

For number of stator vanes z and shaft speed n in rps, the gas parameters ahead of the cascade vary with the frequency ν - zn Hz.

If we take as the characteristic length the stator vane trailing edge thickness d_2, and as the characteristic velocity the gas velocity at the stator exit c_1, the Strouhal criterion reduces to the form: /69

$$Sh = \sin \alpha_1 \frac{d_2}{a} \frac{u}{c_{ad}} \frac{60}{\varphi \sqrt{1-\varrho}}.$$

Experiments conducted on a turbine stage with D_m/h_b = 3.3, α_1 = 31°, and d_2 = 0.6 mm showed that reduction of the Strouhal number leads to increased turbine efficiency. Thus, with the reduction of Sh by 20%, the turbine efficiency increases by about 1% for

relative axial clearance $\bar{\Delta}=\Delta/\sin\alpha_1=50$. With relative axial clearance approximately half again as large, the turbine efficiency gain from reduction of Sh by this same 20% amounts to only (0.2 - 0.3) %, but in this case the absolute value of η_T^* decreases by about 1%.

Thus, cascade solidity selection must be made not only on the basis of ensuring minimal profile losses, but also with account for the influence on the stage losses of other factors — for example, relative intervane channel height $\tilde{h}$, meridional profile form, relative channel blockage d_2/a, and the magnitude of the angle α_1.

3.5. Axial Clearance Between Blade Rows

When selecting the turbine flow path configuration, the magnitude of the axial clearance between the stator vane and rotor blade rows and the vane and blade cascade widths can be selected only approximately. The final magnitude of the clearance is determined in the working design process, when the rotor and stator locations, rotor and stator temperatures, and the relative displacement of the rotor and stator in both the design and transient turbine operating regimes are known.

There are differing and often contradictory viewpoints on the question of selecting the magnitude of the axial clearance between the turbine stator vanes and rotor blades. Many of these views have been published in the literature and illustrated by corresponding experimental data. For example, experiments have been reported from which the conclusion is drawn that there is a so-called optimal axial clearance, corresponding to maximal stage efficiency. It is concluded from other experiments that variation of the axial clearance in quite wide limits ± 20% from the initial value does not influence the turbine efficiency.

There is also the viewpoint, which has experimental confirmation, that increase of the axial clearance between the stator vanes and rotor blades from practically zero to some small magnitude,

say 5 - 6 mm, does not change the turbine stage efficiency, while for a large clearance, the efficiency decreases and then remains constant up to a clearance equal to 80 mm. Finally, there are experiments made of full-scale gas turbine engine turbines which indicate that increase of the axial clearance between the stator and the rotor inevitably leads to reduction of the turbine efficiency to a degree proportional to the clearance.

This situation is explained basically by the fact that the various studies were made under quite different conditions and on turbines of different construction:

a) in some turbines, labyrinth sealing of the axial clearance /70
between the stator ring and the turbine disk rim was not provided;

b) in other turbines, sealing of the axial clearance was disrupted as the clearance varied, and beginning with some value of the clearance there was no sealing;

c) in certain cases, a spacer was installed between the turbine stator and disk as the clearance was increased;

d) in some cases, there was no so-called "overlap" between the stator and rotor (see section 3.6);

e) some of the turbines had blades with shrouds at the periphery; some had blades without shrouding;

f) nearly all the turbines differed significantly in dimensions and in magnitude of the relative radial clearance between the rotor blade and the turbine case.

From the results of those tests which were conducted on specially designed configurations and under actual turbine operating conditions, we can definitely conclude that if there is reliable sealing between the stator and rotor, and if there is suitable overlapping, the hydraulic losses are smaller, the smaller the clearance. This is

understandable, since the hydraulic losses caused by nonuniform total pressure and velocity fields such as those existing at the stator exit will be smaller for converging flow, i.e., when this flow enters converging interblade rotor channels, than in the case of flow into a cylindrical or diverging annular channel.

Moreover, the smaller the axial clearance, the smaller will be the losses in friction between the swirling gas flow traveling in the axial clearance and the surface bounding the clearance. Therefore, when designing the turbine, we must reduce the axial clearance between the stator vane row and the rotor blade row to the degree permitted by the design configuration and the necessity for ensuring reliability under actual turbine operating conditions. In aircraft engine turbines, this corresponds to a magnitude of the axial clearance between the vane and blade rows equal to about 20% of the rotor blade chord width. These clearance magnitudes are larger than those distances between the vane and blade cascades at which their mutual influence on the flow in the oblique exit region is detected.

Sometimes it is necessary to increase the interblade axial clearance during turbine development, or even during operation, from considerations of rotor blade dynamic strength. This occurs in those cases when there is no way to avoid resonant blade vibrations, and it is necessary to reduce the intensity of these vibrations. It is nearly impossible to predict such cases in advance. However, when designing the turbine, it is necessary to use an axial clearance seal design and establish the vane and blade row overlap so that, if necessary, it will be possible to increase the clearance somewhat in the already constructed turbine without significant reduction of the turbine efficiency.

3.6. Overlap Between Vane and Blade Rows

In the axial clearance between the stator and the rotor, the /71
flow boundaries near the root and periphery of the blades become somewhat diffuse. To ensure that the flow strikes the rotor blades and to minimize the leakage flow through the radial clearance between

the blades and the case, the length of the rotor blade leading edge should be somewhat greater than the length of the stator vane trailing edge. This difference in the lengths is called the overlap.

Overlap is necessary in order that the gas stream traveling from one blade cascade to the other not encounter obstacles along its path, and also in order that this flow not leak through the radial clearance, bypassing the rotor blade. This situation can arise because of deviation in manufacturing the blades, stators, and disks, noncoaxiality of the rotor and stator, assembly inaccuracies, and so on. We differentiate lower overlap δ_1 — the difference between the stator vane cascade exit inner radius and the rotor blade cascade entrance inner radius, and upper overlap δ_2 — the difference between the rotor blade cascade entrance outer radius and the stator vane cascade exit outer radius (Figure 3.13).

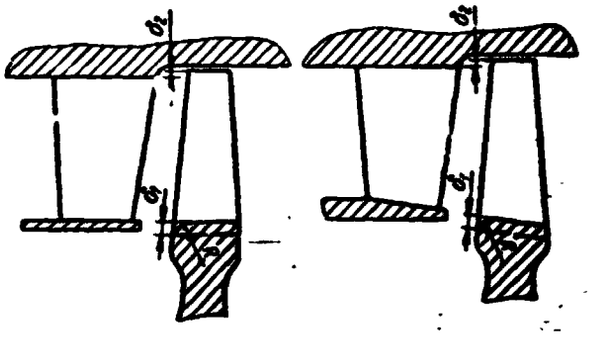

Figure 3.13. Forms of overlap

The hydraulic losses which can occur in the turbine in the absence of overlap are not only associated with the fact that some part of the flow at the stream boundaries loses its kinetic energy as it encounters an obstacle and does not participate in creating work. The primary problem lies in the fact that a disturbance is created /72 which extends into the primary flow and may cause significant losses in the latter. The presence of overlap prevents the appearance of these losses not only in the design turbine operating regime, but also in the transient regimes, when, because of the different temperatures of the stator vane and rotor blade rows, their radial dimensions vary differently. The upper overlap helps reduce the losses associated with presence of the radial clearance in unshrouded rotor blades and in the shrouded blades compensates for flow section

blockage by the fillets at the points of transition from the blade foil to the shroud (Figure 3.14).

Figures 3.15 and 3.16 show turbine efficiency η_T as a function of radial clearance δ for various values of the upper overlap δ_2 and different overlap configurations. These curves were obtained in tests of three turbine stage models [13]. /73

We see from Figure 3.16 that the influence of overlap on stage efficiency is less, the better the radial sealing in the stage.

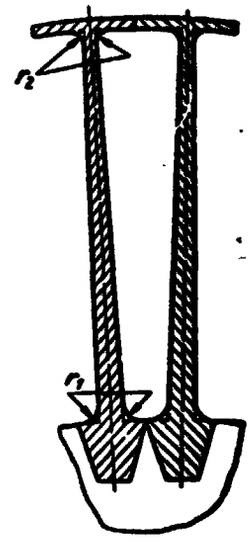

Figure 3.14. Section of interblade channel along height

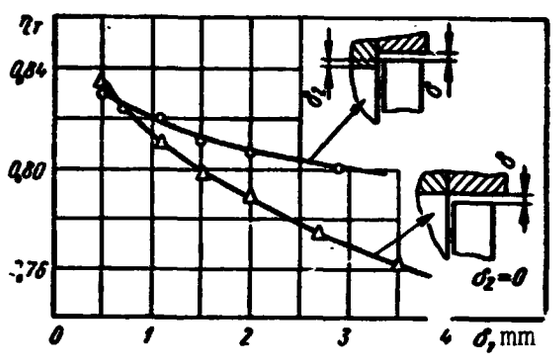

Figure 3.15. Turbine efficiency versus radial clearance for different overlap configurations

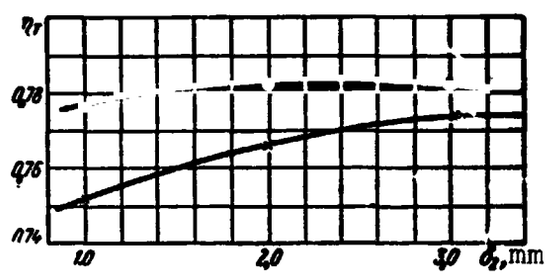

Figure 3.16. Efficiency of active turbine stage versus overlap δ_2 (from Bryansk Institute of Transportation Machinery experiments): ● — with radial seal; × — without radial seal

The magnitude of the upper and lower overlaps may be different, and in each specific case is selected as a function of the axial clearance Δ and the flow angle α leaving the stator (since the distance which the gas flow travels in the axial clearance is directly proportional to the magnitude of the clearance and inversely proportional to sin α_1), the magnitude of the radial clearance δ, the magnitude of the thermal deformations of the rotor and stator in the

different operating regimes, the blade length, the turbine diametrical dimensions, and the manufacturing accuracy adopted.

For example, in turbines with cylindrical flow path contour, unshrouded rotor blades of length 100 - 120 mm, $D_m/h_b = 4-5$, $\alpha_1 = 20°-25°$, radial clearance 0.6 - 0.8 mm (at the design operating regime), and axial clearance between the stator vanes and rotor blades at the mean turbine radius in the range of 6 - 8 mm, the upper overlap should be from 1 to 1.5 mm. If the radial clearance is larger and reaches, say, 1.5 mm (because of different thermal expansions of the stator and rotor in the transient regimes), the upper overlap dimension should be increased to 2 mm. The lower overlap is always made larger than the upper overlap, and in the cited example should be in the 2.5 - 3 mm range. This is explained, on the one hand, by the considerably higher gas discharge velocity from the stator and the larger distance which the gas travels in the axial clearance (smaller angle α_1) than at the outer diameter and the resulting more intense diffusion of the flow boundary near the blade root section in comparison with the peripheral section, and, on the other hand, by the presence (usually) of an extensive region of transition from the blade foil to the lower shroud, which thickens the rotor blade leading edge and tends to block the entrance to the interblade channel (see Figure 3.14).

Upper and lower overlapping should be provided not only in the rotor blade rows, but also in the stator vanes of the following stages. In this case, we need not worry about the appearance of secondary losses from sudden expansion of the flow leaving the cascade, since the downstream stator profile cascade is convergent, thus creating significant resistance, and these losses will be very small. Therefore, we can permit larger overlapping at the entrance to the stator cascades than at the entrance to the rotors. In multistage turbines, this becomes necessary because of the fact that, with minimal initial axial clearance between the first stage stator and rotor, the clearance between the rotor and the following stator must be larger. If this is not done, the rotor and the stator diaphragm may come into contact because of their different thermal expansion.

Obviously, if the overlapping is made too large, the losses from sudden expansion and failure of the flow to fill the entrance segment of the interblade channel will reach a significant magnitude.

The overlapping should be provided as shown by the solid lines /74
in Figure 3.13. If overlap is provided as shown by the dashed lines, the interblade channel will not be filled by the gas flow, and losses associated with this situation will appear. The radius R should fair into the plane bounding the base of the blade row ahead of the point of maximal curvature on the back of the profile in the root section. This is particularly important for the rotor blades, in which diffusive flow and associated secondary losses may appear from the introduction of overlapping in the case of large flow turning angle and an essentially active (constant section) interblade channel.

3.7. Losses Introduced by a Body Located Ahead of the Stator

In many gas turbine engines, the structural members connecting the turbine cases and the bearing must be located ahead of the turbine stator, and they pass either between the combustion chamber flametubes, if individual tubes are used, or in the gas stream, if an annular chamber is used. In the latter case, each structural element is protected against contact with the hot gases by a sleeve of streamlined shape made from a material capable of withstanding the high temperatures.

Thus, in the gas stream ahead of the stator in the the immediate vicinity of the latter. there are bodies which end to block the entrance to the stator cascade and increase the hydraulic losses in the turbine.

The junctures of the individual combustion chambers, located close to the stator (for structural reasons), also introduce disturbance into the gas stream, and may reduce the turbine efficiency. In

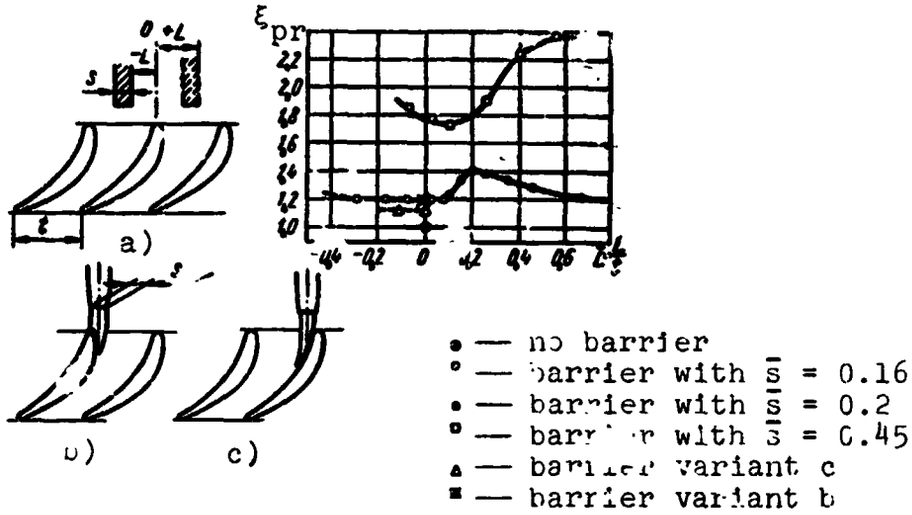

Figure 3.17. Profile loss as function of barrier shape, size, and location

these cases, when designing gas turbine engines, we must solve the problem of rational positioning of these junctures or fairings in relation to the stator cascade intervane channel, and evaluate the losses introduced by these elements.

Figure 3.17 shows the results of an experimental study of a turbine stator vane profile cascade, ahead of which movable barriers with relative thickness $\bar{s}=s/t=0.16$ (see Figure 3.17a) were positioned along the entire blade length, simulating the combustion chamber junction or the fairing edge facing the stator, and transition segments from the barrier to the stator vane of various shapes (see Figure 3.17b and c) were used.

These transition segments were later trimmed off, and the experiments were repeated with the remaining flat barrier segments, which had relative thickness s/t = 0.16 and 0.2, and distance from the cascade front equal to three leading edge radii (5 mm), while in the tests of barriers with relative thickness 0.16 and 0.45, this distance amounted to four leading edge radii (7 mm).

The vane profile cascade was a stator segment with length equal to 100 mm, and solidity $\bar{b} = 1.6$. The barrier location was varied by rotating the segment. The total losses in the cascade were measured at the mean radius along the pitch of two neighboring intervane channels for $\lambda_2 = 0.7$, calculated from the difference between the total pressure ahead of the cascade and the static (barometric) pressure after the cascade. The test result reduction technique normally used in testing plane profile cascades is presented in [6, 23].

It follows from the resulting variation of the relative profile loss coefficient $\bar{\xi}_{pr} = \xi_{pr}/\xi_{pr\,0}$ with barrier location relative to the vane leading edge that the largest losses occur when the barrier is located at the midpoint of the intervane channel, i.e., when the entire disturbance created by the barrier enters the part of the invervane channel located near the back of the vane or directly on the back of the vane, and as this disturbance penetrates into the depth of the channel, it leads to the occurrence of flow separation. This was confirmed by comparing the results of total head loss measurements in the cascade along the pitch of a vane near the back side of which the barrier was located.

The data obtained make it possible to select rational positioning of the combustion chamber junctions or fairings in relation to the stator intervane channel, and evaluate the hydraulic losses which arise in the turbine in this case.

L-2

CHAPTER IV

GASDYNAMIC CALCULATION OF TURBINE STAGE

4.1. Calculation of Turbine Stage at the Mean Diameter

From the general thermal calculation of the gas turbine engine we know the gas flowrate through the turbine G_g kg/s, turbine inlet total pressure and temperature p_0^* N/m^2 and T_0^* K, rotor speed n rpm, and work L_T J/kg. /76

As a result of preliminary calculations to determine the basic turbine stage parameters (see Chapter III), the turbine flow path scheme and number of turbine stages have been selected, the work has been divided between the stages, and preliminary determinations have been made of the gas velocity and total pressure and temperature at the exit from each turbine stage, flow section areas, and turbine diametrical dimensions.

The analysis of the turbine stage at the mean diameter can be made by various techniques, depending on the selected system of characteristic parameters and given basic data. We shall examine some of these techniques.

A. Taking as the basic parameters: μ, M_{2a}, α_2 and K_a (or $\bar{F}_a$)* .

In this case, the calculation can be made in the following sequence.

1. From the assumed value of $M_{2\,a}$ and the known values of the total pressure and temperature at the stage exit, we determine the flow section area F_2 (see section 3.2).

2. Specifying the loading coefficient at the blade root μ_i = 2.0 - 2.2, we determine the circumferential velocity at the blade root and the inner diameter of the flow path at the stage exit:

$$u_{i\,2} = \sqrt{\frac{L_{st}}{\mu_i}} \text{ and } D_{i\,2} = \frac{60u_{i\,2}}{\pi n}$$

We then determine the outer and mean diameters: 77

$$D_{o\,2} = \sqrt{D_{o2}^2 + \frac{4F_2}{\pi}} \text{ and } D_{m\,2} = \frac{D_{o\,2} + D_{i\,2}}{2};$$

the circumferential velocities at these diameters:

$$u_{i\,2} = u_{o\,2}\frac{D_{o\,2}}{D_{i\,2}}, \quad u_{m\,2} = u_{i\,2}\frac{D_{m\,2}}{D_{i\,2}},$$

and refine the previously determined preliminary flow passage shape.

3. We determine the gas absolute velocity at the stage exit:

$$c_2 = \lambda_{2c} a_{cr2} = \frac{\lambda_{2a}}{\sin\alpha_2} a_{cr2}, \quad \text{where } \lambda_{2a} = f(M_{2a});$$

$$a_{cr2} = \sqrt{2\frac{k}{k+1}RT_2^*} \cong 18{,}3\sqrt{T_2^*}; \quad T_2^* = T_0^* - \frac{L_{st}}{\frac{k}{k-1}R};$$

the axial and circumferential components of the absolute velocity at the stage exit:

*The parameter K_a (or $\bar{F}_a$) is used in determining the dimensions of the turbine stage flow path.

$$c_{2z} = c_2 \sin \alpha_2 \quad \text{and} \quad c_{2u} = c_2 \cos \alpha_2;$$

the circumferential component of the relative velocity at the stage exit:

$$w_{2u} = c_{2u} + u_2;$$

the relative velocity at the stage exit:

$$w_2 = \sqrt{c_{2z}^2 + w_{2u}^2};$$

the circumferential component of the gas absolute velocity in the axial clearance:

$$c_{1u} = \frac{L_u - u_2 c_{2u}}{u_1},$$

where $L_u = \xi L_{st}$, $u_1 = u_2 (D_{m1}/D_{m2})$;

$\xi = 1{,}05 - 1{,}025$ — coefficient accounting for the radial clearance and disk friction losses.

The diameter $D_{m\,1}$ and area F_1 are found from the turbine flow path drawing.

For D_m = const, $u_1 = u_2$. We can take approximately $u_1 \approx u_2$ for $D_m \neq$ const, also.

4. We find the angle α_1 and the gas absolute velocity c_1 in the axial clearance:

$$\cos \alpha_1 = \frac{c_{1u}}{c_1} = \frac{\lambda_{c_{1u}}}{\lambda_{1c}}, \tag{4.1}$$

where /78

$$\lambda_{1\,c} = \frac{c_1}{a_{cr\,1}}; \quad \lambda_{c_1\,u} = \frac{c_{1\,u}}{a_{cr\,1}};$$

$$a_{cr\,1} = \sqrt{2 \frac{k}{k+1} RT_1^*} \cong 18{,}3 \sqrt{T_1^*}; \quad T_1^* = T_0^*.$$

From the flowrate equation:

$$\sin\alpha_1 = \frac{G_g\sqrt{T_0^*}}{mF_1 p_0^* \sigma_s^* q(\lambda_{1c})}, \qquad (4.2)$$

where $\sigma_s^* = \frac{p_1^*}{p_0^*} = \frac{\pi(\lambda_{1c}/\varphi)}{\pi(\lambda_{1c})}$ — coefficient of total pressure loss, which can be evaluated with the aid of the graph of $\sigma^* = f(\lambda, \varphi)$ shown in Figure 4.1, taking λ in the range 0.92 - 0.98.

For the combustion products $k = 1.33$, $R = 288.4$ J(kg · K); m = 0.0396.

Solving (4.1) and (4.2) jointly, we find α_1 and λ_{1c}. Then

$c_1 = \frac{c_{1a}}{\cos\alpha_1}$ and $c_{1u} = c_1 \sin\alpha_1$.

5. We determine the relative velocity at the rotor inlet:

$$w_1 = \sqrt{c_1^2 - 2u_1 c_{1u} + u_1^2}.$$

6. We use the value found for λ_{1c} to refine the value of σ_s^* and determine the total pressure at the stator exit:

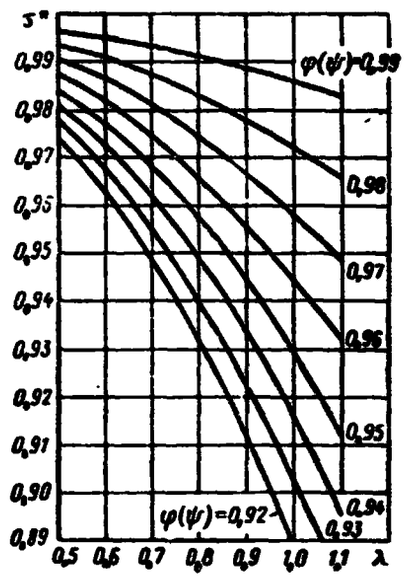

Figure 4.1. Dependence $\sigma^* = f(\lambda, \varphi)$

$$p_1^* = p_0^* \sigma_s^*;$$

The static pressure at the stator exit:

$$p_1 = p_1^* \pi(\lambda_{1c});$$

the static temperature of the gas in the axial clearance:

$$T_1 = T_1^* \tau(\lambda_{1c});$$

the angle of the relative velocity at the rotor inlet:

$$\beta_1 = \operatorname{arctg}\frac{c_{1a}}{c_{1u} - u_1};$$

the angle of the relative velocity at the rotor exit: /79

$$\beta_3 = \operatorname{arctg} \frac{c_{2a}}{c_{2u} + u_2}.$$

7. We determine the degree of flow contraction in the cascade $K = \sin\beta_1/\sin\beta_2$, and the sum of the flow angles $(\beta_1 + \beta_2)$, and then the velocity coefficient ψ

8. We then find:

the adiabatic work of gas expansion in the rotor:

$$L_{ad.r} = \frac{1}{2}\left(\frac{w_2^2}{\psi^2} - w_1^2\right);$$

the gas static pressure at the rotor exit:

$$p_3 = p_1\left(1 - \frac{L_{ad.r}}{\frac{k}{k-1}RT_1}\right)^{\frac{k}{k-1}};$$

the gas temperature at the rotor exit:

$$T_3 = T_1 - \frac{w_2^2 - w_1^2}{2\frac{k}{k-1}R};$$

the gas density at the rotor exit:

$$\rho_2 = \frac{p_2}{RT_2};$$

the axial velocity at the rotor exit:

$$c_{2a} = \frac{G + \Delta G}{F_2\rho_2},$$

where ΔG is the flowrate of the air which cools the blades and then enters the flow path. The density of this additional quantity of air will be different from the main gas stream density ρ_2 (somewhat higher), but this difference can be neclected when finding $c_{2\,a}$.

If $c_{2\,a}$ is found to differ from the value calculated in item 3, another approximation is made (the area F_2 is refined), and the

calculation is repeated until agreement is reached. After this, we can calculate the remaining parameters.

If $u_1 \neq u_2$, then,

$$L_{ad.r} = \frac{1}{2}\left(\frac{w^2}{\psi^2} - w_1^2 + u_2^2 - u_1^2\right)$$

and

$$T_2 = T_1 - \frac{w_2^2 - w_1^2 + u_1^2 - u_2^2}{2\frac{k}{k-1}R}.$$

9. We determine the total temperature based on the relative flow velocity at the rotor cascade entrance: /80

$$T_w^* = T_1 + \frac{w_1^2}{2\frac{k}{k-1}R};$$

the flow turning angle in the rotor cascade:

$$\varepsilon = 180 - (\beta_1 + \beta_2);$$

the Mach number at the turbine exit:

$$M_{2c} = \frac{c_2}{\sqrt{kRT_2}},$$

where

$$c_2 = \frac{c_{2a}}{\sin \alpha_2};$$

the gas total temperature and pressure at the turbine stage exit:

$$T_2^* = T_2 + \frac{c_2^2}{2\frac{k}{k-1}R} \text{ and } p_2^* = p_2\left(\frac{T_2^*}{T_2}\right)^{\frac{k}{k-1}}.$$

This temperature T_2^* is compared with its value obtained in step 1.

If the stage being examined is not the final stage, the quantities T_2^* and p_2^* are the initial values for calculation of the following stages.

10. We calculate the adiabatic work of gas expansion in the stage:

$$L_{ad.st.} = \frac{k}{k-1} RT_0^* \left[1 - \left(\frac{p_2^*}{p_0^*} \right)^{\frac{k-1}{k}} \right];$$

$$L_{ad.st} = \frac{k}{k-1} RT_0^* \left[1 - \left(\frac{p_2}{p_0^*} \right)^{\frac{k-1}{k}} \right];$$

the stage degree of reaction:

$$\rho = \frac{L_{ad.r}}{L_{ad.st}};$$

the turbine stage efficiency:

$$\eta^*_{st} = \frac{L_{st}}{L^*_{ad.st}}.$$

B. Taking as the initial parameters: μ_i, ρ_T, α_2

1. Specifying the loading coefficient at the blade root $u_i \leq$ 2 - 2.2, we find the loading coefficient at the mean radius: /81

$$\mu_m = \mu_i \left(\frac{2\bar{d}}{1+\bar{d}} \right)^2.$$

2. We take the kinematic degree of reaction at the mean radius in the range $\rho_T = (0{,}2 - 0{,}45)$, and find the circumferential components of the gas absolute velocity by joint solution of the equations:

$$c_{1u} + c_{2u} = \frac{L_u}{u}; \quad c_{1u} + c_{2u} = 2u(1 - \rho_T).$$

3. We find the stator exit flow angle α_1.

Direct determination of the angle α_1 for known values of the gas flowrate, mean diameter, and flow path shape is difficult. It is preferable to find the angle α_1 by trial and error. To this end, we first specify three or four values of α_1 in the range 18° - 35°, and

for each specified value of α_1 we determine the axial velocity at the stator exit:

$$c_{1z} = c_{1u} \operatorname{tg} \alpha_1.$$

4. We find the absolute velocity at the stator exit:

$$c_1 = \frac{c_{1z}}{\sin \alpha_1};$$

the reduced gas velocity at the stator exit:

$$\lambda_{1\,c} = \frac{c_1}{a_{cr\,1}},$$

where $$a_{cr\,1} = 18{,}1 \sqrt{T_0^*};$$

the coefficient of total pressure recovery in the stator cascade:

$$\sigma_s^* = \frac{\pi(\lambda_{1c}/\varphi)}{\pi(\lambda_{1c})}.$$

The velocity coefficient ϕ is obtained from experimental cascade flow test data (see Chapter I).

5. We then find the area of the annular flow path section at the stator exit:

$$F_1 = \frac{G_g \sqrt{T_0^*}}{p_0^* \sigma_s^* \, q(\lambda_{1c}) \sin \alpha_1 m},$$

where $m = 0{,}0396$; $q(\lambda_{1c})$ is taken from gasdynamic function tables. /82

6. We plot the relation $F_1 = f(\alpha_1)$. Using the area F_1, calculated from the assumed flow path dimensions, we find the angle α_1.

7. We find the angle of the relative velocity at the rotor entrance:

$$\beta_1 = \operatorname{arctg} \frac{c_{1z}}{c_{1u} - u_1};$$

the relative velocity at the rotor entrance:

$$w_1 = \frac{c_{1a}}{\sin \beta_1};$$

the static pressure at the stator exit:

$$p_1 = p_0^* \sigma_S^* \pi(\lambda_{1c}).$$

8. Specifying the flow exit angle α_2, we determine the absolute velocity at the rotor exit:

$$c_2 = \frac{c_{2a}}{\cos \alpha_2};$$

the reduced velocity at the rotor exit:

$$\lambda_{2c} = \frac{c_2}{\sqrt{2\frac{k}{k+1} RT_2^*}};$$

the circumferential component of the relative velocity at the rotor exit:

$$w_{2u} = c_{2u} + u_2;$$

the relative velocity at the rotor exit:

$$w_2 = \sqrt{c_{2a}^2 + w_{2u}^2};$$

the angle of the relative velocity at the rotor exit:

$$\beta_2 = \operatorname{arctg} \frac{c_{2a}}{w_{2u}}.$$

After this, we find all the remaining parameters as in the first technique, steps 7 - 10.

C. Taking as the basic parameters: μ_1, M_2, ρ

1. From the adopted value of $M_{2\,a}$ and known values of the total pressure and temperature at the stage exit, we determine the flow section area F_2, taking $\alpha_2 \approx 90°$ (see section 3.2).

2. Specifying the loading coefficient at the blade root $\mu_1 \leq$ 2.0 - 2.2, we determine the circumferential velocity $u_{1\,2}$ and the flow passage inner diameter $D_{1\,2}$ at the stage exit. We then find /83

the outer and mean diameters and the circumferential velocities at these diameters (see technique A, step 2).

3. We determine (in the first approximation) the static pressure at the stage exit and the adiabatic work of gas expansion in the stage:

$$p_2 = p_2^* \left(\frac{T_2}{T_2^*}\right)^{\frac{k}{k-1}},$$

where

$$T_2 = \frac{T_2^*}{1 + \frac{k-1}{2} M_2^2},$$

and

$$L_{ad.st} = \frac{k}{k-1} RT_0^* \left[1 - \left(\frac{p_2}{p_0^*}\right)^{\frac{k-1}{k}}\right].$$

4. We specify the degree of reaction at the stage mean radius:

a) for the first stages $\rho_m = 0.2 - 0.35$;

b) for the last stage $\rho_m = 0.35 - 0.45$;

and determine the adiabatic work of gas expansion in the stator:

$$L_{ad.s} = (1 - \rho_m) L_{ad.st}$$

the gas expansion ratio in the stator:

$$\pi_s = \frac{p_0^*}{p_1} = 1 \Big/ \left(1 - \frac{L_{ad.s}}{\frac{k}{k-1} RT_0^*}\right)^{\frac{k}{k-1}};$$

the gas discharge velocity at the stator exit:

$$c_1 = \varphi \sqrt{2 L_{ad.s}}$$

The velocity coefficient φ is selected from experimental cascade flow test data (see Chapter I).

5. We find the stator exit flow angle α_1. The angle α_1 is taken in the range $\alpha_1 = 20 - 35°$ (smaller values of α_1 pertain to the first stages, and larger values — to the last stages), and we then determine the flow path dimensions at the stator exit, or we determine this area from the flow path shape, flow path dimensions, and gas flowrate, known from the preliminary calculation. However, direct determination of the angle α_1 is difficult. It is better to find angle α_1 by trial and error (just as in technique B, step 3). /84

6. We find the angle of the relative velocity at the rotor entrance:

$$\beta_1 = \operatorname{arctg} \frac{c_{1a}}{c_{1u} - u_1};$$

the relative velocity at the rotor entrance:

$$w_1 = \frac{c_{1a}}{\sin \beta_1};$$

the static pressure at the stator exit:

$$p_1 = p_0^* \sigma_{S1}^* \pi(\lambda_{1c});$$

the circumferential component of the relative velocity at the rotor exit:

$$\bar{w}_{2u} = \frac{L_u}{u_m} - w_1 \cos \beta_1;$$

the axial component of the gas relative velocity at the rotor exit:

$$w_{2a} = M_{2a} \sqrt{kRT_2};$$

the angle of the relative velocity at the rotor exit:

$$\beta_2 = \operatorname{arctg} \frac{w_{2a}}{w_{2u}};$$

the circumferential component of the absolute velocity at the rotor exit:

$$c_{2u} = w_{2u} - u_{m\ 2};$$

the angle of the absolute velocity at the rotor exit:

$$\alpha_2 = \operatorname{arctg} \frac{c_{2a}}{c_{2u}}.$$

If this value of $\alpha_2 \leqslant 85°$, we alter M_2, ρ, or the area F_2 by changing the outer diameter, and repeat the calculation beginning with step 5 until the flow parameters at sections 1 and 2 agree.

7. We find the relative gas velocity at the rotor exit:

$$w_2 = \sqrt{w_{2u}^2 + c_{2a}^2}.$$

After this, we determine all the remaining parameters, just as in technique A, steps 7 - 10.

D. Other possible stage calculation techniques

In many cases, it is more convenient to specify the magnitude of the angle α_2 and the ratio of the circumferential velocity components c_{2u}/c_{1u}, since in aircraft engine gas turbines these quantities vary in quite narrow limits: $c_{2u}/c_{1u} = 0 - 0{,}1$ and $\alpha_2 = 90 - 75°$. The smaller values of the ratio c_{2u}/c_{1u} and the larger values of the angle α_2 are characteristic for the last stage. In this case, the calculation sequence will be the same as in technique A, with the difference that: /85

$$c_{2a} = c_{2u} \operatorname{tg} \alpha_2, \text{ and } c_{1u} = \frac{L_s}{u_1 + (c_{2u}/c_{1u})\, u_2}.$$

Agreement of the calculation will also be determined by equality of the axial velocity component downstream of the rotor calculated in step 3 of technique A, and the value determined at the end of the calculation from the flowrate equation $c_{2a} = (G_g + \Delta G)/f_2 \rho_2$.

Other turbine stage calculation techniques can also be used: for example when π_s and π_r are specified. All these techniques make it possible to calculate the turbine at the mean diameter and

determine the parameters required for its design. However, this calculation is still not the final step.

This is explained by the fact that inertial forces which cause change of the velocity and pressure along the radius appear in the gas stream swirled relative to the turbine axis. These changes obey definite laws and cannot be specified arbitrarily. On each particle of mass dm located at the radius r in the axial clearance between the stator and rotor blades, there acts the centripetal force $dP_{c\,1} = dmc_{1u}^2/r$, and downstream of the rotor there acts the force $dP_{c\,2} = dmc_{2u}^2/r$. Consequently, the velocity decreases and the pressure increases toward the blade periphery (with increase of r). Since the circumferential velocity component $c_{2\,u}$ is much less than $c_{1\,u}$, the pressure p_1 increases along the blade length to a considerably greater degree than p_2, and as a result of this, the pressure difference $p_1 - p_2$ at the blade root will be considerably smaller than at the periphery. This means that the degree of reaction decreases with transition to a smaller radius, and may even be negative near the root. Negative degree of reaction means that $p_1 < p_2$, $w_2 < w_1$ and $\beta_1 < \beta_2$, i.e., diffusive flow develops or, as we say, the turbine rotor blade operates in the compressor regime. This naturally leads to increase of the losses and reduction of the turbine efficiency.

Thus, the turbine calculation performed at the mean diameter cannot be considered final until it is verified that, for the flow parameters obtained at the mean diameter, the degree of reaction at the blade root is not negative and the flow swirl angle at the stage exit is not excessive. The latter is very important for the turbine /86
stage downstream of which the discharge diffuser is located.

The flow parameter variation along the blade length must be known in order to design the profile cascade at other radii. This is particularly important for stages with relatively long blades — $D_m/h_b < 10$, where the flow parameter variations along the

blade length are significant and their neglect may lead to marked reduction of the turbine efficiency.

4.2. Radial Variation of Flow Parameters in Turbine Stage

Differences between the flow parameters along the blade length and their values at the mean radius are caused by:

1) variation of the circumferential velocity;

2) presence in the flow of inertial forces caused by flow swirl and streamline curvature in the meridional section;

3) presence of a radial velocity component caused by possible variation of the inner or outer turbine flow path diameter.

In order to obtain high efficiency, it is necessary to ensure flow around the blades at all sections along the length at angles of attack close to the optimal value. This is possible if the cascade is profiled with account for radial variation of the flow parameters.

The streamline curvature and slope in the turbine are usually not large; therefore, when examining the flow in the axial clearances between the stator and rotor rings, we assume that the absolute velocity radial component $c_r \approx 0$, i.e., we consider approximately that the gas particles travel along coaxial cylindrical stream surfaces. It is well known that in this case, radial equilibrium of the centrifugal inertial forces and hydrodynamic pressure forces acting on the gas particles is expressed by the equation:

$$\frac{1}{\varrho}\frac{dp}{dr} \simeq \frac{c_u^2}{r}.$$

For the sections ahead of and downstream of the rotor (sections 1-1 and 2-2 in Figure 1.1), the equations of radial equilibrium have the form, respectively,

$$\frac{1}{\varrho_1}\frac{dp_1}{dr}=\frac{c_{1u}^2}{r} \text{ and } \frac{1}{\varrho_2}\frac{dp_2}{dr}=\frac{c_{2u}^2}{r}. \tag{4.3}$$

Using the Bernoulli equation, we can find the connection between the axial and circumferential velocity components.

We write the Bernoulli equation for the gas stream traveling between sections 0 and 1 (see Figure 1.1), setting the velocity at section 0-0 equal to zero ($c_0 = 0$): /87

$$\frac{c_1^2}{2}=-\int_0^1\frac{dp}{\varrho}-L_{rs}. \tag{4.4}$$

Here, with accuracy to ΔL_r, the friction work $L_{r\,s} \approx L'_{r\,s} = \left(\frac{1}{\varphi^2}-1\right)\frac{c_1^2}{2}$.

Equation (4.4) is valid only along a stream filament, but if we take the gas parameters ahead of the turbine and the losses in all the turbine elements to be constant along the blade length, it can be differentiated along the radius. With account for the fact that $c_1^2=c_a^2+c_u^2$, and $d\varphi/dr=0$, i.e., $\varphi(r)=\text{const}$, we obtain:

$$\frac{1}{2\varphi^2}\frac{d\left(c_{1a}^2+c_{1u}^2\right)}{dr}=-\frac{1}{\varrho}\frac{dp_1}{dr}. \tag{4.5}$$

If in (4.5) we substitute in place of $\frac{1}{\varrho}\frac{dp_1}{dr}$ its value from the radial equilibrium equation (4.3), after transformation we obtain:

$$\frac{1}{\varphi^2}\left(c_{1a}\frac{dc_{1a}}{dr}+c_{1u}\frac{dc_{1u}}{dr}\right)+\frac{c_{1u}^2}{r}=0. \tag{4.6}$$

This equation connects the axial and circumferential velocity components at section 1-1. If we specify the variation of one of the components, we can find how the other will vary.

If we specify a radially uniform rotor blade entrance axial velocity pattern $c_{1a}(r)=\text{const}$, then from (4.6) the circumferential

velocity component variation is defined by the product $c_{1a}r^{\varphi^2}=\text{const}$.

Actually, for $c_{1a}(r)=\text{const}$ $dc_{1a}/dr=0$. Then, from (4.6),

$\frac{1}{\varphi^2}c_{1a}\frac{dc_{1a}}{dr}+\frac{c_{1a}^2}{r}=0$ or $\frac{1}{\varphi^2}\frac{dc_{1a}}{c_{1a}}+\frac{dr}{r}=0$. After integrating this equation, we obtain:

$$\frac{1}{\varphi^2}\ln c_{1a}+\ln r=\text{const} \text{ or } c_{1a}^{1/\varphi^2}r=\text{const},$$

or

$$c_{1a}r^{\varphi^2}=c_{1am}r_m^{\varphi^2}=\text{const}.$$

If we specify the circumferential velocity component variation using the constant circulation law $c_{1u}r = c_{1um}r_m = \text{const}$, and use this condition to solve (4.6), we can find how the axial velocity component varies along the blade length in this case. /88

Since $c_{1a}=c_{1am}\frac{r_m}{r}$, then $\frac{dc_{1a}}{dr}=d\left(c_{1am}\frac{r_m}{r}\right)\Big/dr=-c_{1am}\frac{1}{r^2}$.

Substituting this value into (4.6), we find:

$$\frac{1}{\varphi^2}c_{1a}\frac{dc_{1a}}{dr}-\frac{1}{\varphi^2}c_{1am}^2\frac{r_m^2}{r^3}+c_{1am}^2\frac{r_m^2}{r^3}=0.$$

Integrating this expression, we find

$$\frac{c_{1a}^2}{\varphi^2}+\frac{1}{\varphi^2}c_{1am}^2\frac{r_m^2}{r^2}-c_{1am}^2\frac{r_m^2}{r^2}=C_1. \tag{4.7}$$

We find the integration constant C_1 from the condition that for $r = r_m$, $c_{1a} = c_{1am}$. In this case,

$$C_1=\frac{c_{1am}^2}{\varphi^2}+\frac{c_{1am}^2}{\varphi^2}-c_{1am}^2.$$

Substituting this value of C_1 into (4.7), after transformation we obtain:

$$c_{1a}^2=c_{1am}^2+c_{1am}^2(1-\varphi^2)\left(1-\frac{r_m^2}{r^2}\right). \tag{4.8}$$

We denote the ratios of the instantaneous parameters to their values at the mean radius:

$$\bar{r}=r/r_m; \quad \bar{c}_{1u}=c_{1u}/c_{1u\,m}; \quad \bar{c}_{1a}=c_{1a}/c_{1a\,m}$$

Then the considered law of circumferential velocity component variation along the radius (constant circulation law) is written in the form $\bar{c}_{1u}=1/\bar{r}$.

Dividing both sides of (4.8) by $c^2_{a\,m}$, and bearing in mind that $\frac{c^2_{1u\,m}}{c^2_{1a\,m}}=1/\mathrm{tg}^2\alpha_{1m}$, after transformation we obtain the axial velocity component variation law:

$$\bar{c}_{1a}=\sqrt{1+\frac{(1-\varphi^2)[1-(1/\bar{r}^2)]}{\mathrm{tg}^2\alpha_{1m}}}. \tag{4.9}$$

Let us find the relationship between the variation of the angle α_1 and the velocity components along the radius. To this end, we multiply all terms of (4.6) by dr/c^2_{1u}. Then, after transformations, we obtain:

$$d\ln\left(c_{1u}^{1/\varphi^2}r\right)+\frac{1}{\varphi^2}\frac{c^2_{1a}}{c^2_{1u}}\frac{dc_{1a}}{c_{1a}}=0$$

or /89

$$d\ln\left(c_{1u}^{1/\varphi^2}r\right)+\frac{1}{\varphi^2}\mathrm{tg}^2\alpha_1\, d\ln(\mathrm{tg}\,\alpha_1\cdot c_{1u})=0. \tag{4.10}$$

From this equation, we can determine the variation of the angle α_1 for the adopted circumferential and axial velocity component variation law or, specifying the variation of the angle α_1, we can find the relationship of the velocities $c_{1\,a}$ and $c_{1\,u}$ along the blade length.

Let us determine the variation along the blade length of the angle α_1 for flow swirl, following the constant circulation law.

Replacing in (4.10) $\operatorname{tg}\alpha \cdot c_{1u} = c_{1a}$ and $c_{1a}^{1/\varphi^2} r = c_{1a} r c_{1a}^{(1/\varphi^2)-1}$, with account for the fact that $d\ln(c_{1u} r) = 0$, after transformation, we obtain:

$$\left(\frac{1}{\varphi^2} - 1\right) d\ln c_{1a} + \frac{\operatorname{tg}^2\alpha_1}{\varphi^2} d\ln c_{1a} = 0$$

or

$$\frac{1-\varphi^2}{\operatorname{tg}^2\alpha_1} d\ln c_{1a} + d\ln c_{1a} = 0,$$

hence,

$$\frac{1-\varphi^2}{\operatorname{tg}^2\alpha_1}\frac{dc_{1a}}{c_{1a}} + \frac{dc_{1a}}{c_{1a}} = 0.$$

Using the values of $c_{1a} = c_{1a\,m}\frac{r_m}{r}$ and c_a from (4.8), after integration and transformation, we obtain:

$$\operatorname{tg}^2\alpha_1 = \bar{r}\left[\operatorname{tg}^2\alpha_{1m} + (1-\varphi^2)\left(1 - \frac{1}{\bar{r}^2}\right)\right]. \qquad (4.11)$$

Now let us find how $c_{1\,a}$ and $c_{1\,u}$ vary for a constant angle α_1 along the blade. We recall that constancy of the angle α_1, which defines the flow direction at the stator exit, does not mean constancy of the blade profile geometric angle $\alpha_{1\,b}$. If $\alpha_1(r)$ = const, then $\alpha_{1\,b}(r) \neq$ const.

Equation (4.10) can be written in the form:

$$d\ln\left[(c_{1a}^{1/\varphi^2} r)(\operatorname{tg}\alpha_1 c_{1a})^{\operatorname{tg}^2\alpha_1/\varphi^2}\right] = 0$$

or, after integrating,

$$\ln\left[r c_{1a}^{(1+\operatorname{tg}^2\alpha_1)/\varphi^2}(\operatorname{tg}\alpha_1)^{\operatorname{tg}^2\alpha_1/\varphi^2}\right] = \text{const} = C.$$

We find the integration constant C from the boundary conditions, taking $r = r_m$ and $c_{1\,u} = c_{1\,u\,m}$. Then,

$$\ln\left[r c_{1a}^{(1+\operatorname{tg}^2\alpha_1)/\varphi^2}(\operatorname{tg}\alpha_1)^{\operatorname{tg}^2\alpha_1/\varphi^2}\right] = \ln\left[r_m c_{1a\,m}^{(1+\operatorname{tg}^2\alpha_1)/\varphi^2}(\operatorname{tg}\alpha_1)^{\operatorname{tg}^2\alpha_1/\varphi^2}\right]$$

or

$$r c_{1u}^{1/(\varphi^2 \cos^2 \alpha_1)} = r_m c_{1u\,m}^{1/(\varphi^2 \cos^2 \alpha_1)},$$

hence, /90

$$c_{1u} r^{\varphi^2 \cos^2 \alpha_1} = \text{const}.$$

Since $c_{1a} = c_{1u} \operatorname{tg} \alpha_1$, then $c_{1a} r^{\varphi^2 \cos^2 \alpha_1} = \text{const}$.

It follows from the considered flow swirl examples (characteristic for turbine stages) that for:

1) $c_{1a}(r) = \text{const}$ $\quad c_{1u} r^{\varphi^2} = \text{const}$;
2) $\alpha_1(r) = \text{const}$ $\quad c_{1u} r^{\varphi^2 \cos^2 \alpha_1} = \text{const}$;
3) $\dfrac{c_{1u}}{c_{1u\,m}}(r) = \text{const}$ $\quad c_{1u} r = \text{const}$.

We see that the exponent of r in the product $c_u r$ characterizes the flow swirl variation along the radius. Therfore, in the general case, the swirl variation along the radius can be represented in the form $c_u r^m = \text{const}$. If now, in solving (4.6), we use the condition $c_u r^m = \text{const}$, we obtain the following relations for determining the variation of the axial velocity component and flow direction at the stator exit, respectively:

$$\bar{c}_{1a} = \sqrt{1 + \frac{\left(1 - \frac{\varphi^2}{m}\right)\left(1 - \frac{1}{\bar{r}^{2m}}\right)}{\operatorname{tg}^2 \alpha_{1m}}} \tag{4.12}$$

and

$$\operatorname{tg} \alpha_1 = \bar{r}^m \sqrt{\operatorname{tg}^2 \alpha_{1m} + \left(1 - \frac{\varphi^2}{m}\right)\left(1 - \frac{1}{\bar{r}^{2m}}\right)}. \tag{4.13}$$

Let us examine the variation of the gas parameters at the rotor exit.

We have taken as the first condition the law of circumferential velocity component variation at the stator exit. We usually take as the second condition for aircraft turbines the constancy of the work

along the blade $L_u(r)=\text{const}$. This is done in order to exclude the possibility of the appearance of additional losses because of redistribution of the energy in the flow between the gas stream filaments.

Taking $u_1=u_2=u$, we can write:

$$L_u=u(c_{1u}+c_{2u})=u_m(c_{1u\,m}+c_{2u\,m})=\text{const}.$$

Hence, $c_{2u}=\frac{L_u}{u}-c_{1u}$, or with account for the fact that $c_{1u}r^m=\text{const}$,

$$c_{2u}=c_{1u\,m}\left(\frac{1}{\bar{r}}-\frac{1}{\bar{r}^m}\right)+c_{2u\,m}\frac{1}{\bar{r}}. \tag{4.14}$$

For determining the axial velocity $c_{2\,a}$, we use the Bernoulli equation for the gas stream travelling in the stage from section 0-0 to section 2-2 (see Figure 1.1), taking the velocity at the zero section equal to zero: /91

$$\frac{c_2^2}{2}=-\int_0^2\frac{dp}{\varrho}-L_{st}-L_{r\,st}, \tag{4.15}$$

where the hydraulic work $L_{r\,st}\approx L'_{r\,st}$ is defined by the expression:

$$L_{r\,st}=\left(\frac{1}{\varphi^2}-1\right)\frac{c_1^2}{2}+\left(\frac{1}{\psi^2}-1\right)\frac{w_2^2}{2}=\left(\frac{1}{\varphi^2}-1\right)\frac{c_{1a}^2+c_{1u}^2}{2}+$$
$$+\left(\frac{1}{\psi^2}-1\right)\frac{(c_{2u}+u_2)^2+c_{2a}^2}{2}, \tag{4.16}$$

and the condition of flow radial equilibrium in the axial clearance downstream of the rotor:

$$\frac{c_{2u}^2}{r}=\frac{1}{\varrho}\frac{dp_2}{dr}. \tag{4.17}$$

Using (4.14), (4.16), (4.17), we differentiate (4.15):

$$\frac{dc_{2a}^2}{dr}+\frac{dc_{2u}^2}{dr}+\left(\frac{1}{\varphi^2}-1\right)\psi^2\left(\frac{dc_{1a}^2}{dr}+\frac{dc_{1u}^2}{dr}\right)+\psi^2\frac{2c_{2u}^2}{r}+$$
$$+(1-\psi^2)\frac{d(2c_{2u}u+u^2)}{dr}=0.$$

After integrating, substituting in place of $c_{1\,a}$ its value from (4.12), and transformation, we obtain:

$$\bar{c}_{2a}^2 = c_{2a\,m}^2 + (1-\psi^2)\left[u_m^2(1-\bar{r}^2) - 2c_{1u\,m}u_m(1-\bar{r}^{1-m})\right] + \\ + (1-\psi^2)\left(1-\frac{1}{\bar{r}^2}\right)(c_{1u\,m}+c_{2u\,m})^2 - 2c_{1u\,m}(c_{1u\,m}+c_{2u\,m}) \times \\ \times\left(1-\frac{2}{m+1}\psi^2\right)\left(1-\frac{1}{\bar{r}^{m+1}}\right) + c_{1u\,m}^2\left(1-\frac{\varphi^2\psi^2}{m}\right)\left(1-\frac{1}{\bar{r}^{2m}}\right). \qquad (4.18)$$

If the axial velocity component, by analogy with the preceding analysis, is represented in the form $\bar{c}_{2\,a} = c_{2\,a}/c_{2\,a\,m}$, and the ratio $u_{2\,m}/c_{2\,a\,m} = \operatorname{ctg}\beta_{2\,m} - \operatorname{ctg}\alpha_{2\,m}$, then (4.18) is written as:

$$\bar{c}_{2a}^2 = 1 + (1-\psi^2)\Big[(\operatorname{ctg}\beta_{2m} - \operatorname{ctg}\alpha_{2m})(1-\bar{r}^2) - 2\frac{c_{1u\,m}}{c_{2a\,m}} \times \\ \times (\operatorname{ctg}\beta_{2m} - \operatorname{ctg}\alpha_{2m})(1-\bar{r}^{1-m}) + \frac{(c_{1u\,m}+c_{2u\,m})^2}{c_{2a\,m}^2}\left(1-\frac{1}{\bar{r}^2}\right)\Big] - \\ - 2\frac{c_{1u\,m}(c_{1u\,m}+c_{2u\,m})}{c_{2a\,m}^2}\left(1-\frac{2}{m+1}\psi^2\right)\left(1-\frac{1}{\bar{r}^{m+1}}\right) + \\ + \frac{c_{1u\,m}^2}{c_{2a\,m}^2}\left(1-\frac{\varphi^2\psi^2}{m}\right)\left(1-\frac{1}{\bar{r}^{2m}}\right). \qquad (4.19)$$

Equation (4.19) simplifies if the gas discharge at the mean radius /92 is axial, i.e., if $c_{2\,u\,m} = 0$ and $_2 = 90°$, and the ratio $c_{1\,u\,m}/c_{2\,a\,m}$ is expressed in terms of the loading coefficient μ_m and tg $\beta_{2\,m}$ by the relation:

$$\frac{c_{1\,u\,m}}{c_{2\,a\,m}} = \frac{\mu_m}{\operatorname{tg}\beta_{2\,m}}$$

Then,

$$\bar{c}_{2a}^2 = 1 + (1-\psi^2)\operatorname{ctg}^2\beta_{2m}\left[(1-\bar{r}^2) - 2\mu_m(1-\bar{r}^{1-m})\right] + \\ + \mu_m^2\operatorname{ctg}^2\beta_{2m}\Big[(1-\psi^2)\left(1-\frac{1}{\bar{r}^2}\right) - 2\left(1-\frac{2}{m+1}\psi^2\right)\left(1-\frac{1}{\bar{r}^{m+1}}\right) + \\ + \left(1-\frac{\varphi^2\psi^2}{m}\right)\left(1-\frac{1}{\bar{r}^{2m}}\right)\Big].$$

The variation of the angle β_2 along the blade length is defined by the relation:

$$\operatorname{tg}\beta_2=\frac{c_{2a}}{w_{2u}}=\frac{\bar{c}_{2a}c_{2a}\,m}{c_{2u}+u}=\frac{\bar{c}_{2a}c_{2a}\,m}{c_{1u}\,m\left(1-\frac{1}{\bar{r}^{m-1}}\right)+c_{2u}\,m+u_m\bar{r}}\bar{r}; \qquad (4.20)$$

for axial gas discharge at the mean radius:

$$\operatorname{tg}\beta_2=\operatorname{tg}\beta_{2m}\frac{\bar{c}_{2a}}{\mu_{cp}\left(1-\frac{1}{\bar{r}^{m-1}}\right)+\bar{r}}\bar{r}.$$

The variation of the angle α_2 along the blade length follows the relation:

$$\operatorname{tg}\alpha_2=\bar{r}\operatorname{tg}\alpha_{2m}\frac{\bar{c}_{2a}}{\frac{c_{1u}\,m}{c_{2u}\,m}\left(1-\frac{1}{\bar{r}^{m-1}}\right)+1}; \qquad (4.21)$$

for axial gas discharge at the mean radius:

$$\operatorname{tg}\alpha_2=\bar{r}\frac{\bar{c}_{2a}}{\frac{c_{1u}\,m}{c_{2u}\,m}\left(1-\frac{1}{\bar{r}^{m-1}}\right)}.$$

With the aid of these relations, we can determine how the velocity and the flow angles in the axial clearance and downstream of the rotor will vary along the radius for different flow swirl laws, and also how the other gas parameters will vary. /93

For known gas parameters at the mean radius, we need only specify the value of m and the magnitude of the relative radius $\bar{r}$.

Figures 4.2 - 4.11 show the variation of the flow angles and velocities at the stator cascade and rotor cascade exits. We see that change of m influences most markedly the behavior of the parameters α_1, c_{1a}, c_{1u}, β_1, β_2, α_2, and these variations are more marked, the smaller $\bar{r}$ (closer to the blade root). The other parameters change very little and the degree of reaction ρ remains almost constant with variation of m: thus, for $\bar{r}$ = 0.75, which corresponds to D_m/h = 4, with change of the value of m from m = 1.0 to $m=\varphi^2\cos^2\alpha_1$, (corresponding to

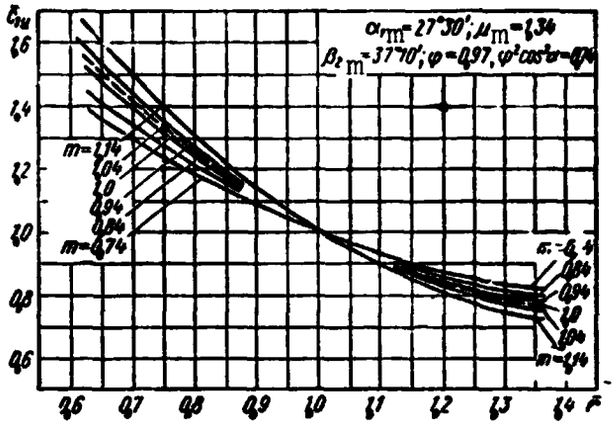

Figure 4.2. Variation of circumferential velocity component downstream of stator along blade length

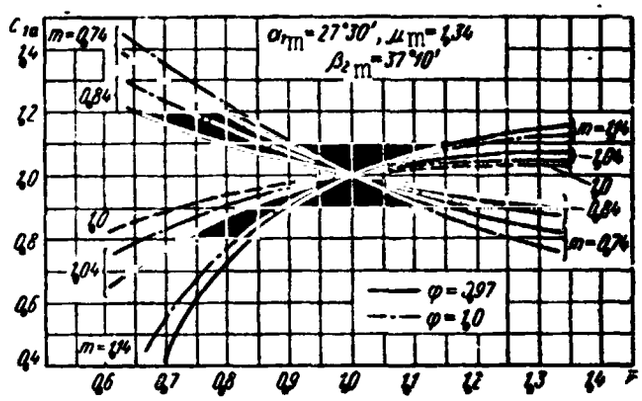

Figure 4.3. Variation of axial velocity component downstream of stator along blade length

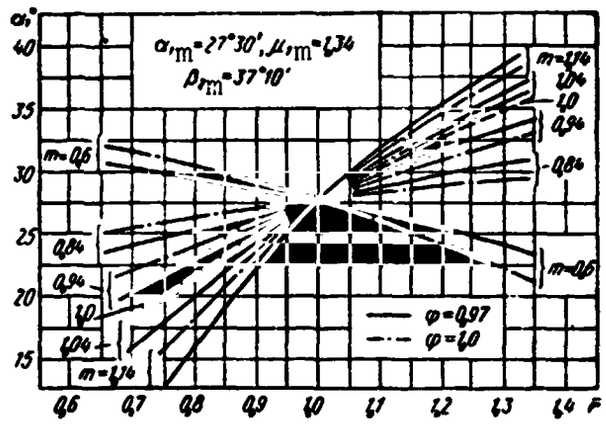

Figure 4.4. Variation of angle α_1 along blade length

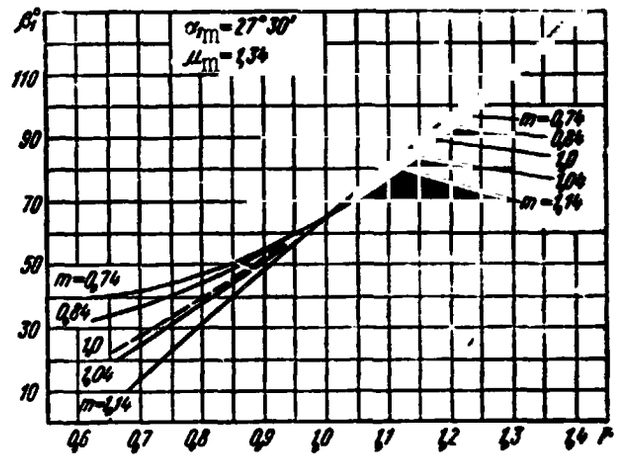

Figure 4.5. Variation of angle β_1 along blade length

α_1 = const), the degree of reaction near the hub changes from 0.5% to 3%. At the same time, near the blade tip at $\bar{r}$ = 1.25, it increases by practically the same magnitude. Nearly the same conclusions apply /95 to another important parameter — the flow turning angle in the rotor cascade $\varepsilon = 180 - (\beta_1 + \beta_2)$. For the same conditions as in the preceding example, the value of ε near the blade root varies from 103° to 97°. This indicates that the variation of m in the indicated limits has very little influence on the degree of rotor blade twist, since with increase of β_1 (near the blade root), β_2 decreases. Further reduction

of $m<\varphi^2\cos^2\alpha_1$ is not desirable because of marked increase of the flow swirl angle downstream of the rotor blades (reduction of the angle α_2) and large nonuniformity of the axial velocity components $c_{1\alpha}$ and c_{2a}. The latter created marked mismatch between the gas flowrate through the stator and rotor cascades in the root and tip sections, which leads to the appearance in the interblade channels of a radial gas velocity component.

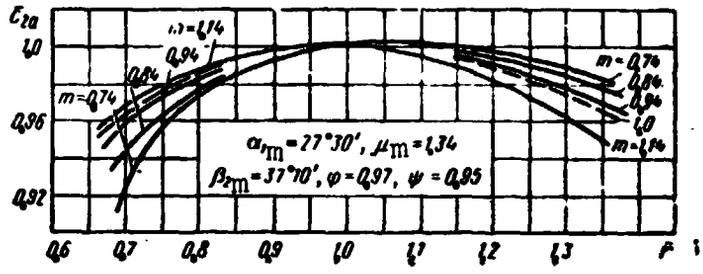

Figure 4.6. Variation of axial velocity component downstream of rotor along blade length

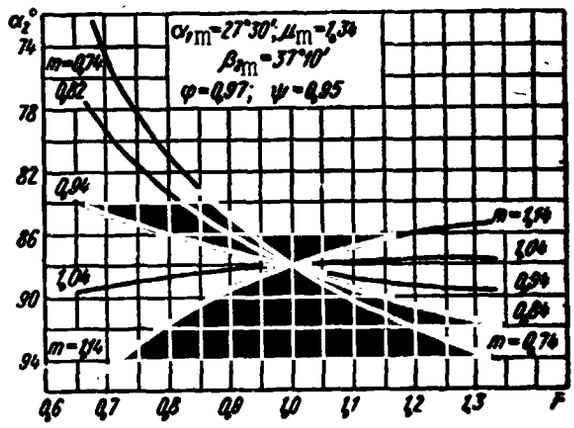

/96

Figure 4.7. Variation of flow angle α_2 along blade length

Values of m greater than one increase the flow turning angle near the blade root, make the degree of reaction negative, increase β_1, create nonuniformity of the axial velocities along the blade, i.e., they lead to deterioration of the gas flow conditions in the turbine. Therefore, when designing turbines, we select m in the range $\varphi^2 \geqslant m \geqslant \varphi^2\cos^2\alpha_1$.

This analysis of the various laws of flow and velocity angle variation along the blade length provids an adequate representation of flow kinematics in the stage, on the basis of which we can select blade angles which are rational from the viewpoint of design and fabrication, and velocity fields and flow directions at the turbine exit which are favorable from the viewpoint of minimal losses in the post turbine diffuser. However, in spite of various considerations of gasdynamic nature, this sort of analysis does not yield adequate bases for judging which of these laws is most favorable for obtaining

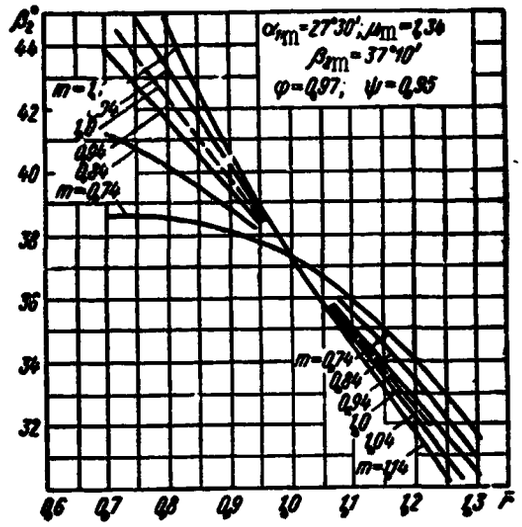

Figure 4.8. Variation of flow angle β_2 along blade length

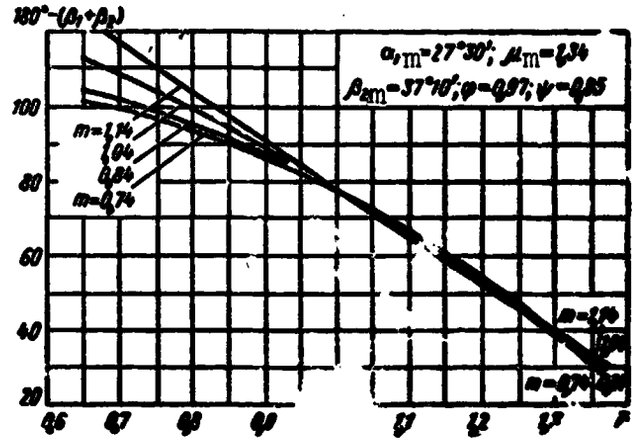

Figure 4.9. Variation of flow turning angle in rotor along blade length

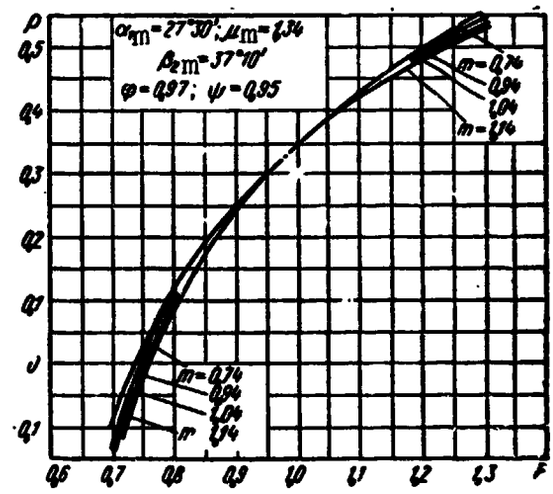

Figure 4.10. Variation of degree of reaction along blade length

maximal stage efficiency. From this viewpoint, each of the laws has its advantages and disadvantages, which affect differently the losses in the stage, and particularly so if the stages also differ in relative and absolute blade length. Therefore, we must resort to experiment in order to select the flow swirl law which provides maximal stage efficiency. Unfortunately, few such experiments have been made, but, together with experience in the design and development of turbines and experimental verification on gas-turbine engines, they lead to the conclusion that the highest efficiency of stages with $D_m/h_b = 4 - 7$ is obtained when the swirl variation is close to the constant circulation law. Therefore, the exponent m is usually taken to be close to ϕ^2. /98

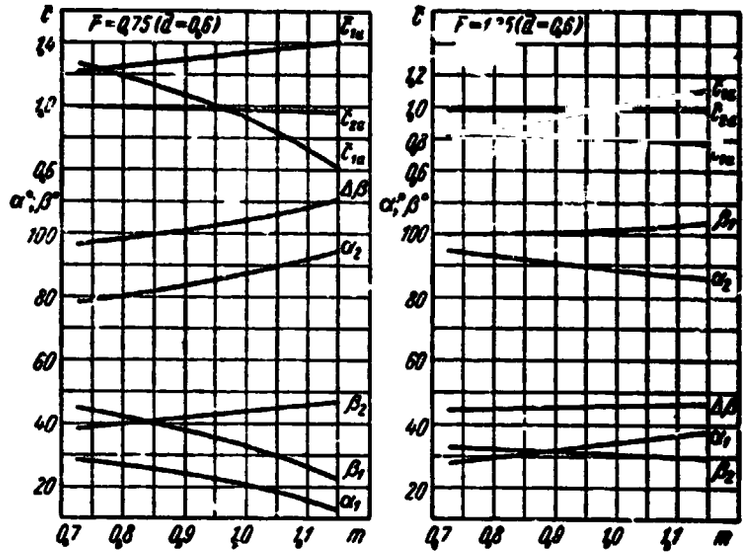

Figure 4.11. Variation of flow angles and velocities as function of exponent m

4.3. Determination of Stage Flow Parameters at the Inner and Outer Radii

After analyzing the turbine at the mean radius, we select the value of the exponent m (law of flow parameter distribution along the radius) and determine the flow parameters at the blade root and tip. Usually, the gasdynamic design of the stage is made at the mean, root, and tip sections.

Using the equations obtained in the preceding section, we calculate the parameters in the following sequence:

1) circumferential velocity component at stator exit:

$$c_{1u}=c_{1u\,m}\frac{1}{r^m};$$

2) axial velocity component at stator exit: /99

$$c_{1a}=c_{1a\,m}\sqrt{1+\mathrm{ctg}^2\alpha_{1m}\left(1-\frac{r^2}{m}\right)\left(1-\frac{1}{r^{2m}}\right)};$$

3) flow angle at stator exit:

$$\alpha_1 = \operatorname{arctg} \bar{r}^m \sqrt{\operatorname{tg}^2 \alpha_{1m} + \left(1 - \frac{\varphi^2}{m}\right)\left(1 - \frac{1}{\bar{r}^m}\right)}$$

or:

$$\alpha_1 = \operatorname{arctg} \frac{c_{1u}}{c_{1a}};$$

4) velocity at stator exit:

$$c_1 = \frac{c_{1a}}{\cos \alpha_1};$$

5) flow angle at rotor entrance:

$$\beta_1 = \operatorname{arctg} \frac{c_{1a}}{c_{1u} - u_1};$$

6) relative velocity at rotor entrance:

$$w_1 = \frac{c_{1a}}{\sin \beta_1};$$

7) static temperature at stator exit:

$$T_1 = T_0^* - \frac{c_1^2}{2\frac{k}{k-1}R};$$

8) static pressure at stator exit:

$$p_1 = p_0^* \left(1 - \frac{c_1^2}{\varphi^2 2\frac{k}{k-1}RT_0^*}\right)^{\frac{k}{k-1}};$$

9) gas total temperature based on relative velocity at rotor entrance:

$$T_{1w}^* = T_1 + \frac{w_1^2}{2\frac{k}{k-1}R};$$

10) circumferential component of absolute velocity at rotor exit:

$$c_{2u} = c_{1u}\, m\left(\frac{1}{\bar{r}} - \frac{1}{\bar{r}^m}\right) + c_{2u}\, m\, \frac{1}{\bar{r}};$$

11) axial velocity component [illegible] rotor exit: /100

$$c_{2u}=c_{2u\,m}\sqrt{1+(1-\psi^2)\left[(\operatorname{ctg}\beta_{1m}-\operatorname{ctg}\alpha_{1m})(1-\bar{r}^2)-2\frac{c_{1u\,m}}{c_{2u\,m}}\times\right.}$$

$$\sqrt{\left.\times(\operatorname{ctg}\beta_{2m}-\operatorname{ctg}\alpha_{2m})(1-\bar{r}^{1-m})+\frac{(c_{1u\,m}+c_{2u\,m})^2}{c_{2u\,m}^2}\left(1-\frac{1}{\bar{r}^2}\right)\right]-}$$

$$\sqrt{-2\frac{c_{1u\,m}(c_{1u\,m}+c_{2u\,m})}{c_{2u\,m}^2}\left(1-\frac{2}{m+1}\psi^2\right)\left(1-\frac{1}{\bar{r}^{m+1}}\right)+}$$

$$\sqrt{+\frac{c_{1u\,m}^2}{c_{2u\,m}^2}\left(1-\frac{\varphi^2\psi^2}{m}\right)\left(1-\frac{1}{\bar{r}^{2m}}\right)}$$

or, if we take approximately $\varphi=\psi=1$, then,

$$c_{2u}=c_{2u\,m}\sqrt{1-2\frac{c_{1u\,m}(c_{1u\,m}+c_{2u\,m})}{c_{2u\,m}^2}\left(\frac{m-1}{m+1}\right)\left(1-\frac{1}{\bar{r}^{m+1}}\right)+}$$

$$\sqrt{+\frac{c_{1u\,m}^2}{c_{2u\,m}^2}\left(\frac{m-1}{m}\right)\left(1-\frac{1}{\bar{r}^{2m}}\right)};$$

for flow without losses ($\varphi=\psi=1$) with m = 1:

$$c_{2u}=c_{2u\,m};$$

12) flow angle at rotor exit in absolute motion:

$$\alpha_2=\operatorname{arctg}\frac{c_{2a}}{c_{2u}};$$

13) flow angle at rotor exit with respect to relative velocity:

$$\beta_2=\operatorname{arctg}\frac{c_{2a}}{c_{2u}+u_2};$$

(14) relative velocity at rotor exit:

$$w_2=\frac{c_{2a}}{\sin\beta_2};$$

(15) static temperature at rotor exit:

$$T_2=T_1-\frac{w_2^2-w_1^2+u_1^2-u_2^2}{2\frac{k}{k-1}R};$$

16) static pressure at rotor exit: /101

$$p_2=p_1\left[1-\frac{(w_2^2\psi^2)-w_1^2+u_1^2-u_2^2}{2\frac{k}{k-1}RT_1}\right]^{\frac{k}{k-1}};$$

17) Mach number based on relative velocity at rotor exit:

$$M_{2w} = \frac{w_2}{\sqrt{kRT_2}}.$$

For flow swirl angles at the stage exit $(90-\alpha_2) \leq 20°$ (usually the swirl does not exceed 15° in actual turbines), the pressure p_2 varies so little along the radius that it can be taken to be constant in turbine calculations. Then the calculation sequence after step 10 will be as follows:

11') adiabatic work of gas expansion in the rotor:

$$L_{ad.r} = \frac{k}{k-1} RT_1 \left[1 - \left(\frac{p_2}{p_1} \right)^{\frac{k-1}{k}} \right];$$

12') relative velocity at rotor exit:

$$w_2 = \psi \sqrt{2L_{ad.r} + w_1^2 + u_2^2 - u_1^2};$$

13') flow angle at rotor exit based on relative velocity:

$$\beta_2 = \arccos \frac{c_{2u} + u_2}{w_2};$$

14') axial velocity at rotor exit:

$$c_{2z} = w_2 \sin \beta_2;$$

15') flow angle at rotor exit based on absolute velocity:

$$\alpha_2 = \operatorname{arctg} \frac{c_{2u}}{c_{2z}};$$

16') absolute velocity at rotor exit: /101

$$c_2 = \frac{c_{2u}}{\cos \alpha_2}.$$

Then T_2 and M_{2w} are determined in accordance with steps 15 and 17.

If the velocity coefficients ϕ and ψ are sufficiently large and differ little from one another (ϕ = 0.97 - 0.98 and ψ = 0.95 - 0.96),

the hydraulic losses can be considered to be practically constant along the blade length $[l_r(r)=\text{const}]$. Then it follows from the Bernoulli /102 equation that for $p_2(r)=\text{const}$, we will also have $c_2(r)=\text{const}$, i.e., $c_2 = c_{2\,m}$.

In this case, the calculation again simplifies, and is made as follows, beginning with step 11:

11") we find the flow angle at the rotor exit based on the absolute velocity:

$$\alpha_2=\arccos\frac{c_{2u}}{c_2};$$

12") the axial velocity at the rotor exit:

$$c_{2z}=c_{2u}\,\mathrm{tg}\,\alpha_2;$$

13") the flow angle at the rotor exit based on the relative velocity:

$$\beta_2=\mathrm{arctg}\frac{c_{2z}}{c_{2u}+u_2};$$

14") the relative velocity at the rotor exit:

$$w_2=\frac{c_{2z}}{\sin\beta_2}.$$

We then find T_2^* and $M_{2\,w}$ in accordance with steps 15 and 17.

There is no need to determine T_2^* at various radii, since for $L_u(r)=\text{const}$ $T_2^*(r)\approx\text{const}$.

The calculation can be considered complete when the angle α_2 at the inner radius is obtained in acceptable limits, and the velocity $w_2>w_1$. However, if we obtain $w_2<w_1$, it is necessary to reduce the loading coefficient at the root section, or increase the degree of reaction at the mean radius (if the value of α_2 still permits this). In other words, we must unload the stage either by reducing the work L_{st}, if the turbine is multistage, or by increasing the diameter.

The stage degree of reaction at the design radii can be determined on the basis of the gas parameter values obtained.

We can also find the relationship between the degree of reaction at the mean and inner radii so that when designing the stage at the mean radius we can select the degree of reaction to ensure a positive value of the latter at the root. If we neglect the variation of ρ_m along the blade length, we can write:

$$\rho_m = 1 - \frac{(L_{ad.s})_m}{L_{ad.st}} \text{ and } \rho = 1 - \frac{L_{ad.s}}{L_{ad.st}} .$$

From joint solution of these equalities, we obtain:

$$\rho = 1 - (1 - \rho_m) \frac{L_{ad.s}}{(L_{ad.s})_m} = 1 - (1 - \rho_m \frac{c_1^2}{c_{1.m}^2} . \qquad (4.22)$$

In turn, /103

$$\frac{c_1^2}{c_{1m}^2} = \frac{c_{1u}^2 + c_{1a}^2}{c_{1u\,m}^2 + c_{1a\,m}^2} = \frac{(c_{1u}^2\, c_{1u\,m}^2) + (c_{1a}^2/c_{1a\,m}^2)}{(c_{1u\,m}^2/c_{1u\,m}^2) + 1} . \qquad (4.23)$$

Replacing in (4.23) the ratio $(c_{1a}^2/c_{1a\,m}^2)$ by its value from (4.12), and considering that $c_{1u} = c_{1u\,m}(1/\bar{r}^m)$, and $c_{1a\,m}/c_{1u\,m} = \mathrm{tg}\,\alpha_{1m}$, after substituting (4.23) into (4.22) and transformations, we obtain:

$$\rho = 1 - (1 - \rho_m)\varepsilon, \qquad (4.24)$$

where

$$\varepsilon = 1 + \frac{\varphi^2}{m}\left(\frac{1}{\bar{r}^{2m}} - 1\right)\cos^2\alpha_{1m}.$$

For m = 1 and $\varphi = 1$ $\varepsilon = \sin^2\alpha_{1m} + \frac{\cos^2\alpha_{1m}}{\bar{r}}$.

Taking as the limiting case at the inner radius $\rho = 0$, we obtain from (4.24):

$$0 = 1 - (1 - \rho_m)\varepsilon \text{ or } \rho_m = 1 - \frac{1}{\varepsilon} .$$

Using this formula, we can find as a function of ϕ, m, and $\bar{r}$ the value of ρ_m to which the value $\rho_i = 0$ at the blade root corresponds. This will be the minimal acceptable value of ρ_m.

However, it is not advisable in practice to design the turbine stage with degree of reaction at the blade root section equal to zero.

Errors which are unavoidable in manufacturing the turbines, even within the tolerances on blade fabrication or on their positioning, may lead to a situation in which the interblade channel flow section area of the finished rotor is somewhat greater than the design area or the same area for the stator vanes is less than the design value. In these cases, the degree of reaction at the blade root section of the actual turbine becomes negative if it was desgined to be equal to zero.

It is well known that a negative degree of reaction, even in the blade root sections, reduces turbine efficiency. This is explained primarily by disruption of the design flow in the root sections of the turbine stage and spreading of this disruption to the adjacent region along the blade length to an extent which is greater, the more negative the degree of reaction, i.e., the larger the portion of the blade along the radius which operates in the negative degree of reaction regime. According to the experimental data of [32], in turbine states with negative degree of reaction at the root, raising /104 of the streamlines in the lower part of the blade and flow separation in the region near the hub are observed.

Moreover, in turbine stages with zero or negative degree of reaction in the blade root sections, reduction of their efficiency because of practically unavoidable air leakage into the axial clearance between the stator and rotor blade rows takes place to a considerably greater degree than in stages with positive degree of reaction. In other words, these stages are more sensitive to entry into the flow passage of air supplied either for cooling of the rotor blades and disks, or for reducing (unloading) the axial force acting on the turbocompressor rotor. Advanced types of labyrinth seals

reduce these leaks, but do not eliminate them entirely, and they still have a negative influence on turbine efficiency. Therefore, when designing turbines, the degree of reaction in the blade root sections must be made positive.

A positive degree of reaction in the blade root sections, particularly in the gasdynamically loaded stages, other conditions being the same, leads to reduction of the relative velocity at the entrance to the rotor blades, which in the root sections reaches very high values, and to increase of the gas flow angle approaching the rotor blades (see Figures 4.5 and 4.10). The latter facilitates blade profiling considerably, particularly blades with internal air cooling.

The design of turbines with positive degree of reaction in the blade root sections encounters certain difficulties in stages with relatively long blades. These difficulties can be overcome by designing the turbine with reduced gradient of the degree of reaction along the blade length: for example, with constant or nearly constant angle α_1 along the blade length (see Figure 4.10), or increase of the overall level of the degree of reaction in the stage, i.e., increase of the degree of reaction at the mean radius. The latter also reduces the gradient of the degree of reaction along the length and, in combination with some deviation from the law of constant circulation, in the direction of the constant angle α_1, practically resolves the problem of designing aircraft engine turbines with positive degree of reaction along the entire blade length.

Other conditions being the same, the higher the overall level of the degree of reaction in the stage, the larger will be the flow deflection at the stage exit from the axial direction. If this occurs in the last turbine stage, the vanes present in the post-turbine diffuser are used to impart an axial direction to the flow. To this end, these vanes are profiled with account for the flow direction leaving the turbine.

Experience shows that the turbine stage with ratio of mean diameter to blade length equal to 4.5, with positive degree of reaction, and with a straightening cascade downstream of the turbine has an overall efficiency 2.5% higher than the same stage but with rotor blades for which the degree of reaction in the root section is negative (-0.12), and the flow direction at the exit is nearly axial. /105

The formulas presented in the present chapter can serve as the basic algorithm in formulating the program for the gasdynamic turbine calculation on a digital computer. It is advisable to utilize the high-speed computer capabilities to select the parameters during the analysis, so that the calculation result will satisfy the specified conditions.

For example, the distribution of the adiabatic work of gas expansion in the stator vanes and rotor blades is selected so that the flow at the rotor exit is axial ($\alpha_2=0$), or the magnitude of the degree of reaction at the inner diameter will be positive; the digital computer can be used to determine the adiabatic work of gas expansion in the stator vanes and rotor blades for given flow angles at the stator vane exit α_1 and rotor blade exit β_2, and to solve many other problems. The use of digital computers for turbine gasdynamic calculation not only reduces the time expended on the calculation, but also makes it possible to perform parametric turbine analysis when designing the engine in order to select the turbine variant which is most rational for the given conditions.

CHAPTER V

PROFILING TURBINE BLADES

5.1. Choice of Basic Cascade and Profile Parameters

The profiling of turbine blades reduces to the construction of /106
several sections which define the form of the profiled part of the blade.

The turbine blades must provide the flow velocity and direction at the cascade exit which are specified by the gasdynamic analysis with minimal hydraulic losses. At the same time, the rotor blade geometric form must satisfy the requirements of strength and producibility, ensuring adequate fabrication accuracy with high production rates.

Several methods for the design of hydrodynamic cascades have been developed in recent years.

Some of these methods permit determining the profile shape which provides a favorable velocity distribution over the profile surface on the basis of specified flow conditions at the cascade entrance and exit. However, these methods do not take into consideration the requirements of blade strength and producibility, and are not used in practice.

Other methods of calculating hydrodynamic cascades make it possible to find the flow conditions and evaluate the losses in the cascade on the basis of the specified form of the profile in a cascade. These methods can obviously be used only after the profiles are already constructed.

Therefore, graphical methods are usually used in profiling turbine blades. The increasing introduction of electronic digital computers in turbomachine design practice will permit broader utilization of the analytic turbine blade profiling methods [2, 10, 11].

The experience accumulated in turbine construction and the theoretical and experimental studies of turbine profiles make it possible to establish for a broad class of cascades, criteria which define cascade operational efficiency. These criteria include: cascade solidity (b/t), blade incidence angle (i); form of the lines describing the profile, shape of the interblade channel; channel throat dimension, and so on. /107

Adherence to the optimal values of these criteria makes it possible to construct confidently profiles with excellent hydrodynamic qualities [18]. The basic recommendations on construction of turbine blade profiles with high efficiencies, developed on the basis of experimental and theoretical studies of various authors, reduce to the following:

1. The profile cascade solidity (b/t) should be as close as possible to the optimal value. The quantity $(b/t)_{opt}$ depends on the flow turning angle in the cascade, cascade type (active or reactive), range of angle-of-attack variation during cascade operation, and so on.

The empirical formula proposed by V. I. Lyshlevskiy can be used to select the cascade solidity, or relative pitch, at the blade root and mean sections:

$$\frac{t}{b}=0{,}55\left[\frac{180}{180-(\beta_1+\beta_2)}\,\frac{\sin\beta_1}{\sin\beta_2}\right]^{\frac{1}{3}}(1-\bar{c}),$$

where $\bar{c}$ is the profile relative thickness.

The dependence of the flow turning angle $\varepsilon=180-(\beta_1+\beta_2)$ on the relative pitch and the angle β_2 (Figure 5.1) can also be used for approximate determination of the cascade solidity.

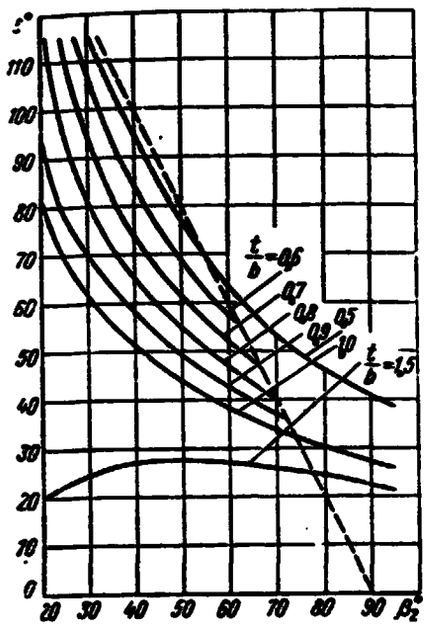

Figure 5.1. Flow turning angle ε in cascade as function of relative pitch t/b and the angle β_2

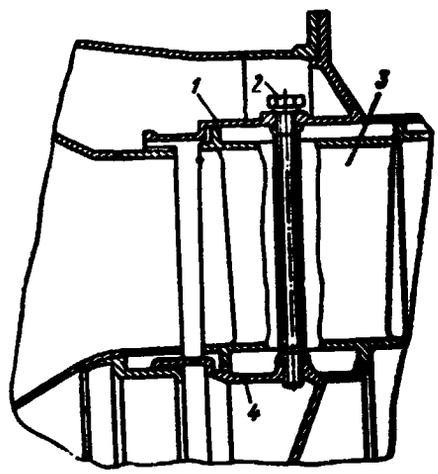

Figure 5.2. Stator construction scheme:

1 — outer case; 2 — structural member; 3 — vane; 4 — inner case

However, in constructing aircraft gas turbine profile cascades, it is sometimes necessary, in order to ensure the required blade strength, to deviate from the optimal solidity in the rotor blade root sections and increase their area, while the tip section profile area is made as small as possible, deviating here in the downward direction from the optimal solidity.

In the stator vanes deviation from the optimal solidity is most often dictated by vane fabrication technology and the structural turbine configuration. For example, if structural members pass through the stator vanes (Figure 5.2), the cascade is wider than

dictated by the optimal chord-to-pitch ratio, particularly at the root section, in order to provide the profile thickness required for passage of the structural member.

Since the optimum with respect to solidity has a relatively flat nature for most profile cascades used in aircraft engine gas turbines, some deviation from the optimal value of b/t does not lead to marked losses. However, reduction of b/t, in relation to the optimal value in limits which are acceptable from the loss viewpoint, may lead to deviation from the calculated flow direction at the cascade exit. This shows up particularly in the rotor cascade near the peripheral blade sections.

2. The interblade channel should be smoothly convergent. If /108
this cannot be accomplished, i.e., realization of a smoothly converging channel contradicts other important requirements imposed not only by considerations of cascade efficiency (minimal losses) but, let us say, by strength or manufacturing considerations or, finally, some combination of the latter, we can permit local divergence of the interblade channel not exceeding 5%. This means that the ratio of maximal channel width to minimal channel width in the segment from the entrance to the point of maximal width should not exceed 1.05. In Figure 3.6b, this is shown as the ratio of a to a_1.

Local channel enlargement of up to 5% in the region of maximal curvature of the back of the profile does not lead to increase of the losses in the cascade, and experience shows that this may even reduce the losses in active channels with large flow turning angle 110° - 120° at transonic and supersonic velocities.

The channels should not be constructed with constant width, since because of the presence of manufacturing deviations during blade production, the channels in the completed turbines become divergent with the minimal section located at any (arbitrary) point of the channel. It is well known that such channels have significant hydraulic losses and do not provide the design flow direction at the exit.

3. The angle of attack i (flow angle approaching the blade) should be in the range from -2° to -6° for reactive, relatively widely spaced cascades with small profile leading edge radius, which is characteristic for rotor blade tip sections and is encountered in the last and next-to-last stage stator vanes. For the root sections, where the cascades are relatively closely spaced with quite large leading edge radius, positive angles of attack up to +12° can be tolerated. Experience shows that for comparatively high inlet gas velocity $M_{1w}=0{,}65-0{,}70$, the rotor blade root section profile cascades have small losses at positive angles of attack. This situation is utilized in cascade profiling in order to obtain a converging interblade channel, since in the root section, where $\beta_1 \approx \beta_2$, the channel is diffusive, even for i = 0°. /109

Variation of the angle of attack in the limits ± 10° has practically no influence on the losses in the cascade for stator vanes, particularly the first stage vanes which have large leading edge radii and low inlet velocities.

4. The curvature of the convex side of the profile downstream of the interblade channel throat is characterized by the trailing edge camber angle δ_b (see Figure 5.6), which may be in the range 5° - 16°, depending on the gas flow Mach number M_2 at the cascade exit (smaller value of the angle δ_b correspond to $M_2 > 1$).

Figure 5.3 shows the results of wind tunnel flow tests of two plane cascades composed of profiles with different angles δ_b. We see that for the cascade with smaller angle δ_b, the losses for $M_2 < 1$ and for $M \geqq 1.0$ are significantly less than for the cascade with larger trailing edge camber angle.

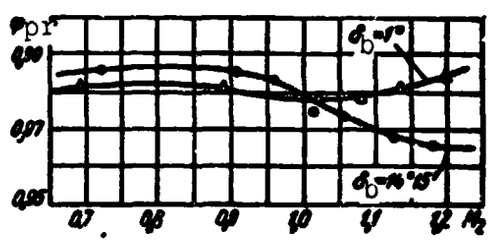

Figure 5.3. Variation of coefficient ϕ_{pr} for profile cascades with angle β_2 = 31° and different angles δ_b

In addition, the variation of the losses with variation of M_2 for the first cascade is smoother than for the second cascade; consequently, the former is less sensitive to variation of M_2. /110

However, we should bear in mind that for cascades composed of profiles with $\delta_b \leqq 3°$, the interblade channels have an excessively small degree of contraction near the exit section, i.e., over some length of the channel upstream from the throat, the channel size varies so little that in the actual turbines the throat displaces within the channel and a diffusive region appears.

If a cascade being designed is intended for operation with $M_2 \leqq 0.8$, it can be made with the angle $\delta_b = 12° - 14°$. For cascades operating with $M_2 > 1$, the magnitude of the angle δ_b can be selected using the graph of $\delta_b = f(M_2)$, obtained by G. D. Grodzovskiy and shown in Figure 5.4.

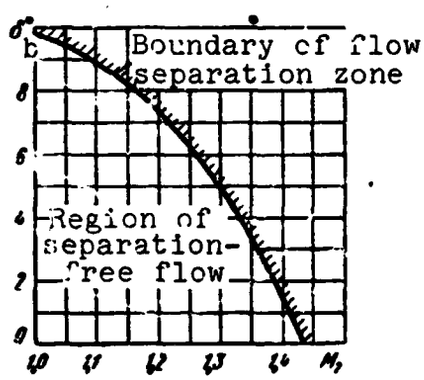

Figure 5.4. Angle δ_b versus M_2 at flow separation boundary:

5. The interblade channel throat width is found from the formula:

$$a = t \sin \beta_{2p}.$$

For subsonic gas discharge velocities $\beta_{2p} = \beta_2 - \Delta\beta$, where $\Delta\beta$ is determined as a function of β_2 and M_2 from the well-known curves of Figure 5.5.

For supersonic discharge velocities, the quantity a is found from the formula $a = tq(\lambda_2)\sin\beta_2$, where $q(\lambda_2)$ is found from the gasdynamic function tables as a function of M_2. For stator cascades, $a = tq(\lambda_1)\sin\alpha_1$.

6. The line describing the convex side (back) of the profile must have a smooth change of the curvature. It will often be

convenient to use as this line a segment of the Bernoulli lemniscate ($\rho = a\sqrt{\cos 2\varphi}$), or sometimes a parabolic segment when there is no straight segment on the back near the trailing edge. The latter is explained by the fact that the junction of a parabola with a straight line does not yield smooth curvature variation. It is not always possible to form the back of the profile by a single lemniscate. Then we can use two or more lemniscates, joining them at points of the same curvature.

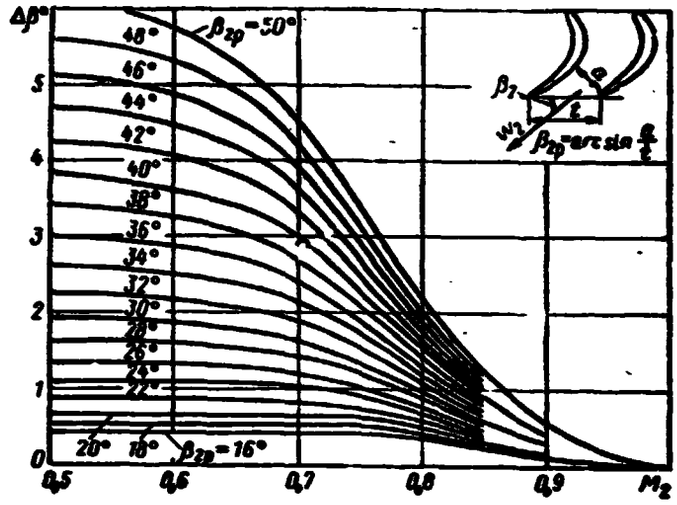

Figure 5.5. Flow lag angle $\Delta\beta = \beta_2 - \beta_{2p}$ as function of Mach number at exit for cascades with different angles β_{2p}

7. The geometric angle $\beta_{2\,b}(\alpha_{1\,b})$ (Figure 5.6) must be equal to the angle $\beta_2(\alpha_1)$, or smaller than the latter by 1° - 1.5°. For the root sections of rotor blades and stator vanes, where the trailing edge relative thickness is comparatively large d_2/a, where $d_2 =$ /111
$2\,r_2$, we can permit $\beta_{2\,b}(\alpha_{1\,b})$ to be somewhat larger than $\beta_2(\alpha_1)$. This is explained by the fact that the larger the ratio d_2/a, the more reduction of $\beta_2(\alpha_1)$ is observed in comparison with $\beta_{2\,b}(\alpha_{1\,b})$.

8. The trailing edge taper angle ϕ_2 should not exceed 6°. For larger values of the angle ϕ_2, the losses in the cascade increase markedly because of increase of the velocity and the total head field nonuniformity at the cascade exit. This effect is particularly marked for relatively thick trailing edges ($d_2/a \geqslant 0{,}1$), characteristic of the blade root sections.

9. The blade trailing edges should be as thin as possible, since the hydraulic losses in the cascade are directly proportional to their thickness. The trailing edge radius is usually taken in the limits $r_2 = (0{,}03 - 0{,}08) c_{max}$ near the root, and $r_2 = (0{,}08 - 0{,}16) c_{max}$ near the tip of the blade.

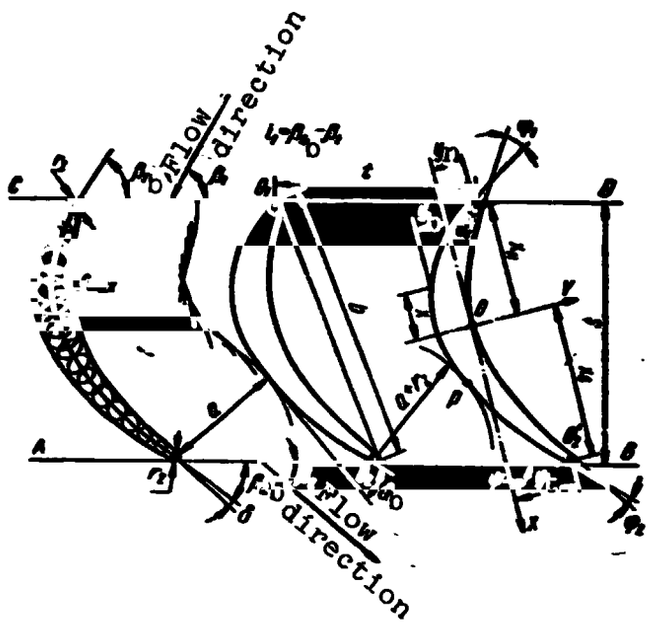

Figure 5.6. Geometric parameters of cascade and profile

However, in spite of this it is sometimes still necessary to make the trailing edges quite thick from considerations of strength and fabrication technology. Therefore, the question of edge thickness selection must be resolved in each specific blade design case. In all cases, we must make certain that the rotor blade trailing edge thickness (this also applies to the leading edge) decreases from the root section toward the tip section enough to preclude thinning of the edge in the /112 lower-lying sections with account for fabrication tolerances. In this way, we eliminate one of the reasons for instability of the finished blade frequency characteristics, which is important from the viewpoint of their dynamic strength.

Blade strength considerations determine both the section dimensions and the relative blade positioning, on which depends to a considerable degree the magnitude of the bending stresses in the profiled part which are not compensated by the centrifugal forces.

Usually, good compensation can be achieved with a blade shape in which the section centers of gravity are located on a straight or nearly straight line.

In addition to having good aerodynamic and strength properties, the turbine blades must be easy to manufacture. This quality is very important, since a considerable portion of the labor involved in gas turbine engine manufacture is expended on the turbine and compressor blades. Therefore, blade profiling must be performed with account for the technique by which they will be fabricated.

Many blade fabrication techniques now used have a definite influence on the form of the profiled part and on the section construction process.

These techniques include the methods for obtaining blades without any machining of the profiled part (for example, by precision casting, stamping, electrochemical and electrospark machining, and so on), and also machining with the use of three-dimensional duplication. When using these fabrication techniques, no special technological requirements are imposed on the form of the profiled part surfaces. In this case, the designer has relative freedom in selecting the profile form for the various blade sections. /113

However, when designing blades, it is not always possible to satisfy completely all the above-listed requirements. For example, it may often be difficult to obtain the blade root section profile areas dictated by the strength requirements. Conversely, the rotor blade tip section profile area for minimal acceptable cascade solidity is determined by the profile thickness, and reduction of this thickness is limited, in turn, by considerations of material structural strength and blade fabrication technology. It is not recommended that the profile relative thickness (ratio of profile maximal thickness to chord) $\bar{c}=c_{max}/b$ be less than 4.5%, since experience in gas turbine development and operation shows that rotor blade tip section profiles with less relative thickness are subject to a much greater degree than others to failures from high-frequency mode resonant vibrations. Thus, the tip section profile area for the blade being designed is essentially already specified, and, since the upper and lower section area ratio is also specified by the magnitude of the allowable tensile stresses (σ_t), in essence the minimal root section

profile area is defined. However, if it is not possible to obtain the required area in the limits allowed by the cascade solidity (further increase of the solidity leads to considerable increase of the losses) and the maximal profile thickness, for which the inter-blade channel section ($c_{max}=t-a$), then we must increase c_{max} by reducing the channel throat section. Then $c'_{max}>c_{max}$, since $a_1<a$.

If $(a-a_1)/a\leqslant 4\%$, and if this reduction of the flow section area in the root part is compensated by corresponding increase of the flow section area in other sections of the blade, experience shows that the resulting flow restructuring (in comparison with the theoretical flow structure) does not lead to marked losses in the stage. For this case, Figure 5.7 shows the experimental relation $\eta_T^* = f(u_m/c_{ad})$ for a turbine stage with $D_m/h_b = 5.6$; h_b = 100 mm and $\alpha_{1\ m} = 22°$.

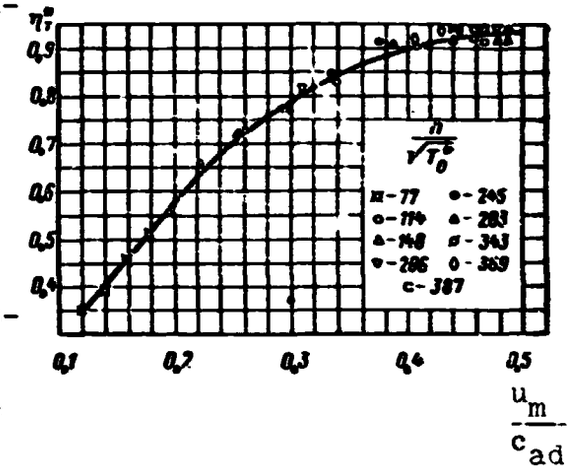

Figure 5.7. Turbine efficiency as function of u/c_{ad}

In many cases, we also encounter difficulty in profiling the stator cascade, in which certain angles should be small δ_b = 5 - 7°, $\delta_2 \leqq 3°$, and the relationship of the geometric and gas angles should be such that $\alpha_{1\ b} \leqq \alpha_1$, since the smaller the selected ϕ_2 is relative to δ_b, the larger $\alpha_{1\ b}$ is relative to α_1.

Many such examples can be cited. They indicate that nearly every aircraft engine gas turbine stator vane or rotor blade design is a compromise solution of the problems presented by the requirements of gasdynamics, strength, and fabrication technology. Preference is given to certain of the requirements listed above, depending on the turbine application, its operating conditions, and the mission of the gas turbine engine as a whole. This also explains why it is /114

not possible in practice to apply directly in a new turbine design the profile cascades which have been developed by the research organizations, no matter how effective they may be. They can only serve as prototypes or models, indicating for a given specific case what means can be used to improve profile aerodynamic efficiency.

5.2. Blade Profile Construction

The following basic data must be available in order to construct the turbine stator vane and rotor blade profiles.

1. Turbine flow passage scheme in the meridional section with the blade width and number selected on the basis of preliminary gas-dynamic and strength calculations.

2. Turbine gas dynamic analysis, including calculation of the velocity triangles at three diameters (root, mean, and tip).

3. Law of blade profile section area variation along the blade length.

4. Structural requirements which affect the profile shape. For example, necessity for the passage of structural members or fuel and oil lines through the stator vanes with indication of the minimal dimensions which the vane cross section must have; presence of rotor /115 blade banding — wire or with the use of shrouds; minimal acceptable stator vane and rotor blade trailing edge thickness, etc.

5. Blade and vane fabrication techniques.

On the basis of these data, we plot for each blade curves (Figures 5.8 and 5.9) of radial variation of the:

a) blade pitch;
b) profile area (for the rotor blades);
c) dimensionless velocities M_{2w}, M_{1c},

d) angles β_1, β_2, $\beta_{2\ p} = \beta_{2\ ef}(\alpha_0, \alpha_1, \alpha_{1\ ef})$,

e) interblade channel throat width a.

We shall present the further description of the profile construction sequence in application to the rotor blade.

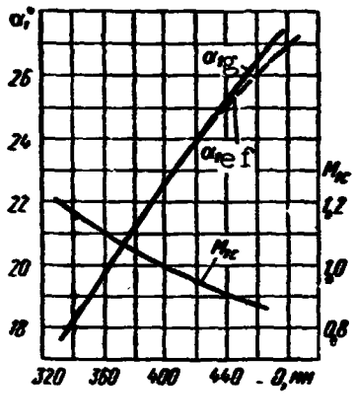

Figure 5.8. Variation of $M_{1\ c}$ and angles α_1 and $\alpha_{1\ ef}$ along blade length

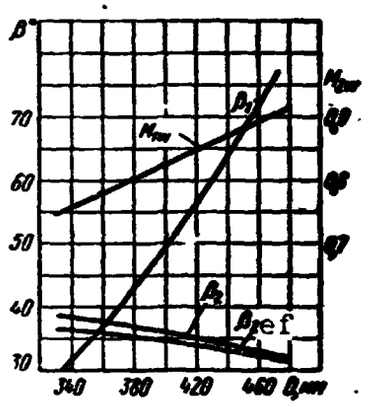

Figure 5.9. Variation of $M_{2\ w}$ and angles β_1, β_2, $\beta_{2\ ef}$ along blade length

We break the blade length down into several sections (Figure 5.10) and, in accordance with the radius at which the particular section is located, we plot them on all the graphs constructed above.

We take the root section at a distance 2 - 3 mm from the beginning of the transitional fillet from the blade airfoil to the platform. This is done so that we can monitor profile fabrication accuracy.

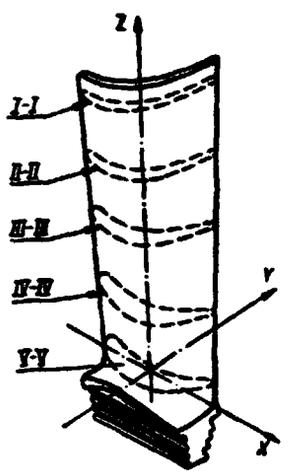

Figure 5.10. Arrangement of coordinate axes and specified blade sections

The size of the transitional fillet is taken as a function of the blade fabrication technique and blade dimensions. Figure 5.11 shows the nature of the dependence of the fillet radius on the blade airfoil length. These data can be used in profiling the blades.

The upper section I - I (see Figure 5.10) is taken 2 - 3 mm below the blade tip. The remaining sections are located at equal distances from one another between the lower and upper sections. Three or five sections are taken for the stator vanes, and no less than five for the rotor blades. Experience shows that for reliable checking of rotor blade fabrication accuracy, the maximal distance between two neighboring sections should not exceed 25 mm. This also applies to the relatively long (twisted) last-stage stator vanes with a section which is variable along the blade length.

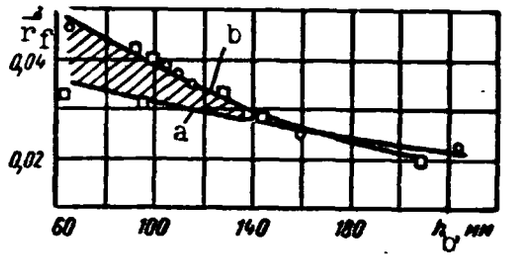

/116

Figure 5.11. Fillet radius (r_f) versus blade length (h_b):

a — machined; b — investment case; o — rotor blades; □ — stator vanes

Therefore, when profiling long blades (h_b > 100 mm), the number of sections for which the profile dimensions must be specified will be more than five.

The number of sections is always odd in order that the middle section, on the basis of which we can judge during profiling the extent to which the law of cross section variation along the blade length differs from the specified law, will be at the midpoint of the blade. In order to work out the blade fabrication technology, the profiles of two additional sections outside the profiled part of the blade (airfoil), located above the tip section and below the root section, are constructed and specified on the drawing for information. These are called technological sections.

We noted above that both analytic and graphical blade profile construction methods are used at the present time.

The essence of the analytic profile construction method lies in describing the curves forming the blade profiles (concave and convex sides) by an nth degree polynomial (n = 5 - 7), whose coefficients

are found from the boundary conditions which are determined by the requirements of hydrodynamics, strength, and blade fabrication technology. This makes it possible to determine analytically, i.e., calculate, the coordinates of the blade profile points which are specified by the drawing and are necessary for fabrication of the blades. Here, use is made of high-speed computers [2, 10, 11]. Experience in application of this method for profiling aircraft engine turbine blades has shown its practical usefulness. /117

We shall examine only the graphical profile construction techniques in which the back side of the profile is described by arcs of lemniscates or parabolas and the concave side is described by arcs of a circle or parabola or also by a lemniscate, i.e., by an essentially arbitrary curve.

5.2.1. Lemniscate profile construction technique

Before drawing the profiles themselves, we must (if we do not have a set of lemniscate French curves) construct on a sheet of heavy paper a family of lemniscates with different pole distance, whose dimension in millimeters is used to number the corresponding lemniscate (Figure 5.12). For example, the lemniscate with pole distance 20 mm will be No. 20, while that with pole distance 80 mm will be No. 80. The scale of these lemniscates usually corresponds to the scale in which the profiles are constructed. Normally, this is a ten-fold scale.

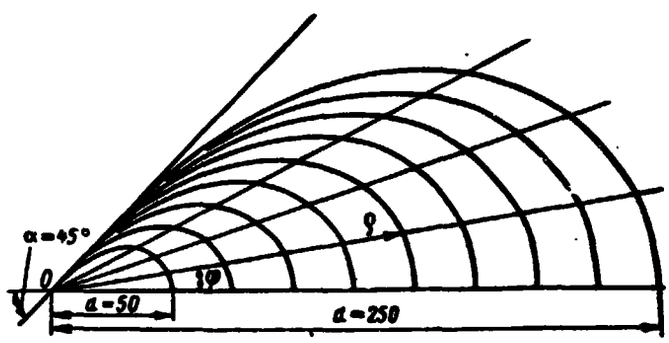

Figure 5.12. Lemniscates $\rho = A\sqrt{\cos 2\varphi}$

The constructed lemniscate family is essentially a template with which we can redraw onto parchment or tracing paper any lemniscate necessary for forming the back side of the profile.

The profile is drawn in the following sequence.

1. We draw two parallel lines AB and CD at a distance equal to the cascade width s (see Figures 5.6, 5.13, 5.14). Two circles tangent to the line AB are drawn with radius $r_2 = d_2/2$ (r_2 = 0.3 - 1.0 mm) at the pitch distance t. Through the centers of these circles /118
O_2 and O_2' at the angle $\beta_{2\,b}$, we draw the straight lines mn (trailing edge centerlines). At the angle $\phi_2/2$ to these straight lines, we draw tangents to the circle describing the trailing edge mfN and mhu.

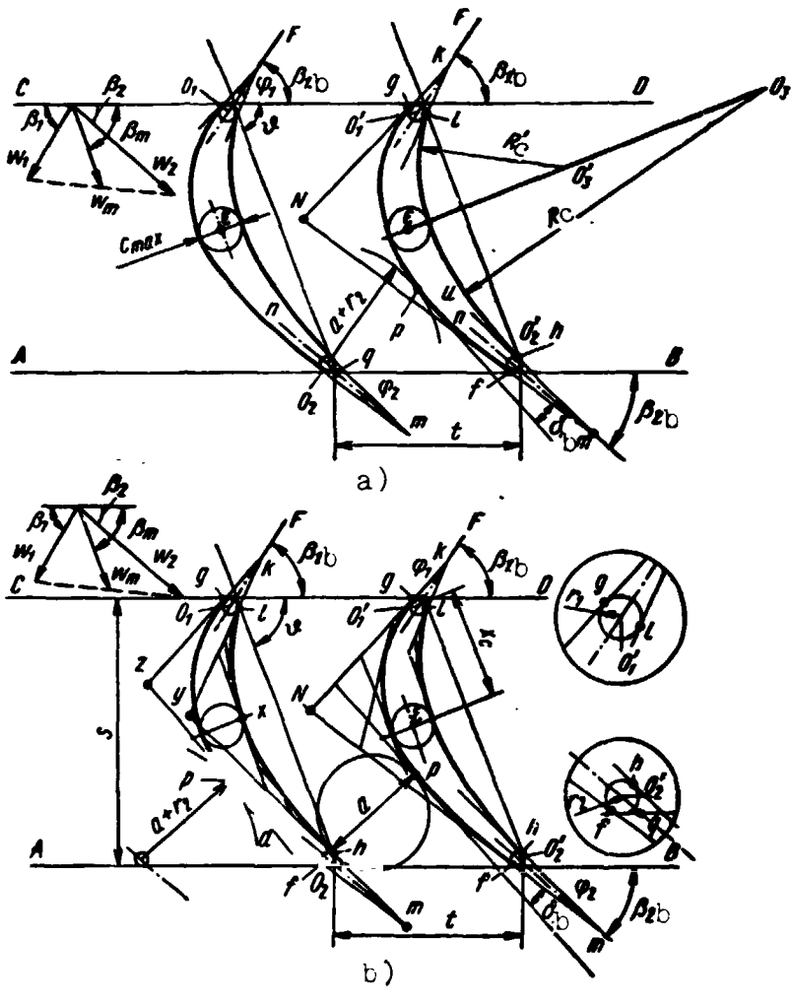

Figure 5.13. Construction of blade profile:
a — using lemniscate arcs (back) and circular arcs (front); b — using parabolic arcs

The points of tangency f and h are the end points of the profile convex and concave surfaces.

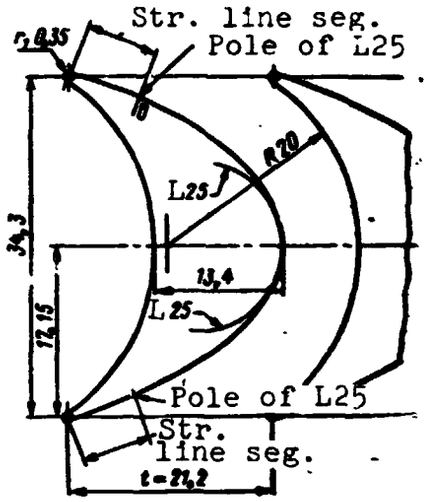

Figure 5.14. Symmetric (lemniscate) profile cascade

2. We find the interblade channel throat width using the formula $a = t \sin \beta_{2p}$. With the radius $r_2 + a$ from the point O_2 defining the interblade channel exit section.

3. We select the profile back side aft segment camber angle δ_b (δ_b = 8 - 10°, but no more than 15°). We draw a tangent to the circular arc of radius $(r_2 + a)$ at an angle equal to $\beta_{2\,b} - \phi_2/2 + \delta_b$ to the line AB. The back side of the profile must pass through the point of tangency p. /119

4. We construct the velocity diagram. We draw the geometric mean velocity vector $\bar{w}_m = \frac{1}{2}(\bar{w}_1 + \bar{w}_2)$, and determine the slope β_m of the geometric mean velocity. We take the magnitude of this angle as the profile setting angle in the cascade $\theta \simeq \beta_m$*.

5. Through a point q (point of intersection of the lines mn and AB), we draw at the angle θ a straight line to intersect the line CD. From the center O_1' with radius r_1, we draw the leading-edge circle, tangent to the cascade front CD. The leading-edge radius r_1 is taken in the limits $(0.12 - 0.15)c_{max}$ in the stator vanes and in the rotor blade root sections, the value $(0.3 - 0.4)c_{max}$ is taken in the rotor blade tip sections.

---

*Statistical data show that $\theta \sim \beta_m$ only for the mean and tip blade sections. For rotor blade root sections, $\theta \sim (0{,}83 - 0{,}85)\beta_m$. For stator vanes with angle $\alpha_1 \leq 20°$ $\theta = \beta_m + (8 - 10)°$.

6. Through the center of the circle O_1 we draw the line O_1F at the angle $\beta_{1\,b}$ to the line CD. Then we draw tangents to the circle of radius r_1 at the angle $\phi_1/2$ to the line O_1F. The leading edge taper angle ϕ_1 varies in the limits $\phi_1 = 10 - 30°$. The larger values of ϕ_1 pertain to the blade root sections. The points of tangency g and l to the circle of radius r_1 are the initial points of the profile convex and concave contours.

7. Using the tracing paper with the lemniscate curves, we select the lemniscate arc so that its straight segment coincides with the line mfN, tangent to the circle of radius r_2, and the lemniscate curve itself contacts the arc of radius $r_2 + a$ at the point p, and is tangent to the line kgN. Here, we must find that position of the lemniscate for which the required angle δ_b is obtained.

If it is not possible to describe the back side of the profile by a single lemniscate, we can use two or three lemniscates, joining them at points of equal curvature.

The back side of active symmetric profiles can be described by a single lemniscate with two mirror-image positions (see Figure 5.14). /120

8. We construct the concave side of the profile. It is described by an arbitrary curve (circle, combination of several circles, lemniscate, parabola, or simply a French-curve shape) which forms an interblade channel of the desired form and required profile area.

Let us examine the construction of the concave side of the profile using two circular arcs.

From point E as the center, we describe a circle of diameter c_{max} (maximal profile thickness), tangent to the back of the profile at the distance $x_c = (0.25 - 0.35)b$* from the center of the circle

*Smaller values of x_c pertain to the blade tip sections.

of radius r_1 describing the profile leading edge (see Figure 5.13). From the point h, we erect a perpendicular to the line mhu. Selecting the radius R_c, we describe from the center O_3 an arc tangent to the line mhu at the point h and to the circle of diameter c_{max}. Then, from the point l, we erect a perpendicular to the line kl, whose point of intersection O_3' with the line O_3E will be the center of the arc of radius R_c', which joins with the arc of radius R_c and with the circle of radius r_1 at the point l.

5.2.2. Profile construction using parabolic arcs

1 - 6. We perform the construction in accordance with steps 1 - 6 of the technique examined above for constructing the lemniscate profile.

7. From point O_2, we draw an arc of radius $r_2 + a$, or a circle of diameter a (see Figure 5.13b).

8. We continue the lines mf and kg to mutual intersection at the point N. We divide the segments gN and Nf into the same number of equal parts and connect the points of division sequentially with one another as shown in Figure 5.13. The envelope of these straight lines is then the sought parabolic arc.

If it is found that the parabola constructed in this fashion does not contact the circle of diameter a (does not pass through the point p), we must alter somewhat the slope of the line mN, which reduces to varying the angles δ_b and ϕ_2, or we must describe the back side of the profile by the two parabolic arcs fp and pg. When constructing the back side using two parabolic arcs, each parabola is inscribed analogously in the angles formed by the segments fd and dp and by the segments pz and zg, respectively.

9. We draw a circle of diameter c_{max} at the distance x_c from the leading edge. Through the point of tangency of this circle with the back side of the blade, we draw a diameter and a normal to the diameter (tangent) at the point x. We continue the segments kl and mh to their mutual intersection at the point y. If it is found that the tangent to the circle at the point x divides the segments ly and yh in halves, the concave side of the profile is described by a single parabolic arc. If each of the segments ly and yh is divided into unequal parts, the concave side of the profile is constructed using two parabolic arcs lx and xh by a technique analogous to the construction of the back side of the blade using two parabolic arcs.

If the area (or $\bar{c} = c_{max}/b$) and section center-of-gravity location based on strength conditions are given, we can vary the quantities $\beta_{1\,b}$, $\beta_{2\,b}$, r_1, r_2, ϕ_2, δ_b, and a in the limits indicated in the preceding discussion in order to obtain profiles of the desired form.

5.3. Matching the Individual Section Profiles and Constructing the Profiled Part of the Blade

After constructing the root, mean, and tip section profile cascade, we construct, using three points, the preliminary graphs of the variation along the blade length of the quantities r_1, r_2, b, s, the lemniscate pole distance, the distance of the point p from the trailing edge, the angles $\beta_{1\,b}$, $\beta_{2\,b}$, and the other quantities required for constructing the profile.

With the aid of these curves (Figure 5.15), we describe the remaining blade section profiles, after which we use one of the well known techniques to determine their centers of gravity. This is /122
often done by two- or three-fold suspension of a profile cut from cardboard or heavy paper on a needle with a plumb bob attached to a vertical board.

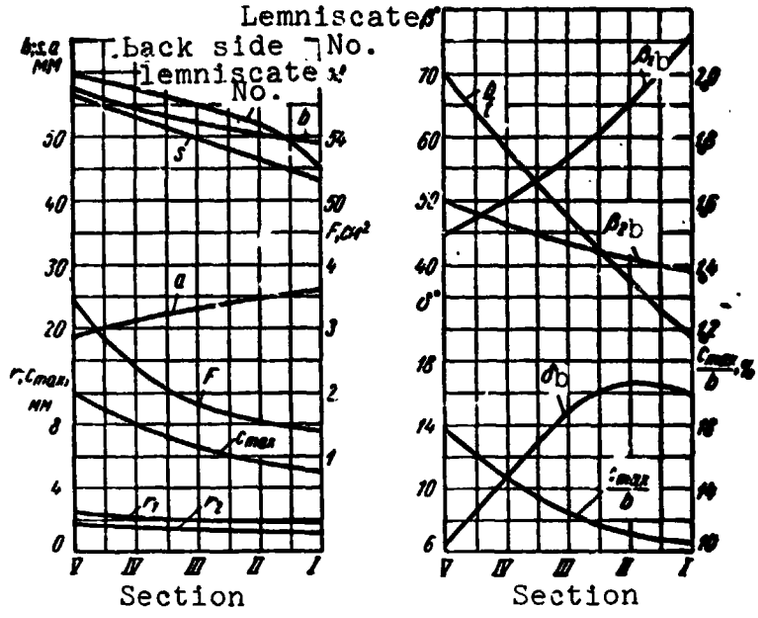

Figure 5.15. Variation of profile geometric characteristics along blade length

In the section construction process, their centers of gravity are adjusted to the required position, and the curves of the quantities r_1, r_2, b, s, and so on, are refined.

After drawing all the sections, the final strength calculation is made, and that position of the blade section center-of-gravity line relative to the disk radius, passing through the root section center-of-gravity, which ensures the required interaction of the aerodynamic and centrifugal forces applied to the blade, is found.

The coordinate system in which the blade section profiles are specified is usually selected so that its origin is located at the root section center-of-gravity, the X axis lies in the plane of symmetry of the fir-tree retention, and the Z axis is directed as shown in Figure 5.10.

If the blade does not have a fir-tree attachment and the X axis location is not dictated by technological considerations, its direction must be selected so that it is approximately parallel to the blade mean section profile chord (see Figure 5.6).

Thus, from the blade strength analysis results, we draw for each section the X and Y axes, relative to which the coordinates of the points lying on the lines describing the profile are measured. The X axis is divided into equal parts, the distances between which are determined by the dimensions of the blade being designed. These distances are usually reduced in the leading edge region. This is explained by the fact that, in the case of large leading edge curvature (small angles $\beta_{1\,b}$), specification of the lines describing the leading edge requires smaller distances between the coordinates along the X axis than for the rest of the profile.

After measuring the coordinates, we verify the leading and trailing edge fairing accuracy. These profile segments are drawn with considerable magnification, usually to a scale of 50 : 1.

Smooth variation of the curvature of the lines describing the back side of the profile is usually verified by calculating the second differences of the coordinates (Figure 5.16), which must vary smoothly (the second derivative must not have discontinuities). This is done because of the fact that in the graphical construction, inaccuracies may occur in drawing the lemniscate, measuring the coordinates, and so on, and these inaccuracies must not be present in the actual profile. We see from the back side profile coordinate table how the Δ_2 values are calculated, and Figure 5.16 shows their behavior.

In addition, in order to verify the entire construction and to avoid waviness along the length of the profiled part of the blade, it is necessary to construct curves of the coordinates $y = f(x)$ for constant values of x (Figure 5.17). These curves can also be used in constructing the profiles of additional blade sections, for /124
example, the upper and lower technological section (by extrapolating the curves), and zero section passing through the blade tip, or the section n' at which it is proposed to make holes for wire banding, and so on.

TABLE OF BLADE BACK SIDE PROFILE COORDINATES*

x	y	Δ_1	Δ_2	x	y	Δ_1	Δ_2
57,5	−13,01			27,5	0,08	1,01	0,04
		1,11				0,97	
55	−11,9		0	25	1,05		0,05
		1,11				0,92	
52,5	−10,79		0	22,5	1,97		0,05
		1,11				0,87	
50	−9,68		0	20	2,84		0,06
		1,11				0,81	
47,5	−8,57		0	17,5	3,65		0,07
		1,11				0,74	
45	−7,46		0	15	4,39		0,07
		1,11				0,67	
42,5	−6,35		0	12,5	5,06		0,08
		1,11				0,59	
40	−5,24		0	10	5,65		0,09
		1,11				0,5	
37,5	−4,13		0,02	7,5	5,15		0,1
		1,09				0,4	
35	−3,04		0,02	5	6,55		0,11
		1,07				0,29	
32,5	−1,97		0,03	2,5	6,84		0,12
		1,04				0,17	
30	−0,93		0,03	0	6,67		
		1,01					

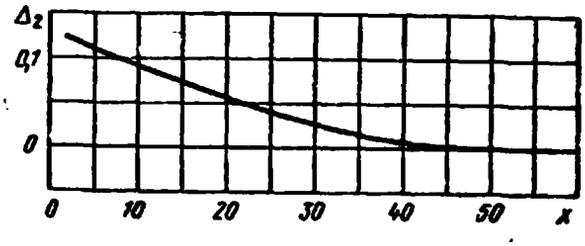

Figure 5.16. Variation of second difference of blade convex surface profile coordinates

*Translator's note. Commas in numbers represent decimal points.

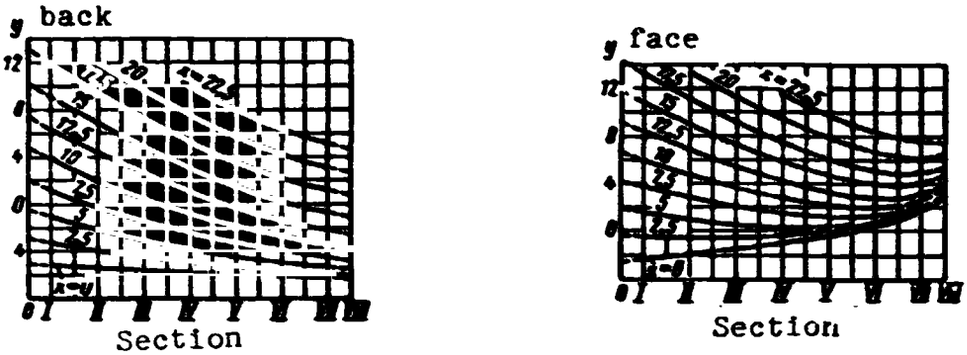

Figure 5.17. Variation of profile convex and concave surface coordinates as function of section number (sections 0 and VIII are technological sections)

For this, it is sufficient to note the section of interest on the Z axis and at this point draw vertically lines of constant x, reading out on the ordinate axis the values of the coordinate y for the given x.

5.4. Techniques for Constructing Blades with Machined Profiled Part

In this case, the blade surfaces must have a form which permits the use of some machining scheme.

Considerable use has been made in recent years of machining of the profiled part of the blade in which the convex (back) side is machined with the use of a three-dimensional template, and the concave (face) side is machined by a cylindrical or shaped cutter with the aid of one or two two-dimensional templates [18].

We shall examine the sequence of turbine rotor blade section profile construction for two concave surface machining techniques:

a) using a cylindrical cutting tool (hobbing cutter) with an adapter having two two-dimensional templates;

b) shaped cutting tool with the use of a single two-dimensional template.

In both cases, the back side of the blade is machined using a three-dimensional template.

When machining the concave surface using these schemes, the cutter and the blade are positioned relative to one another so that the angle between the Y-Z coordinate plane and the cutter axis is equal to some value ϕ, which is held constant during surface generation.

The Y - Z plane is established vertically and remains in this position during milling. /125

As the table moves horizontally, the blade is displaced in the vertical plane with the aid of one of the two-dimensional templates, so that the cutter generates the entire concave surface at one time (Figure 5.18).

The sequence of turbine rotor blade section profile construction, when machining the concave surface using two two-dimensional templates and a cylindrical cutter, is as follows.

1. We obtain the root (V - V) and tip (I - I) section profiles by the technique described above, determine their centers of gravity, and draw the profiles as shown in Figure 5.19. When drawing these section profiles, we must bear in mind that the minimal radius of curvature on the concave surface limits the radius of the cutter used to machine this surface. The cutter radius must be at least 2 - 3 mm less than the minimal radius of curvature of the surface being machined.

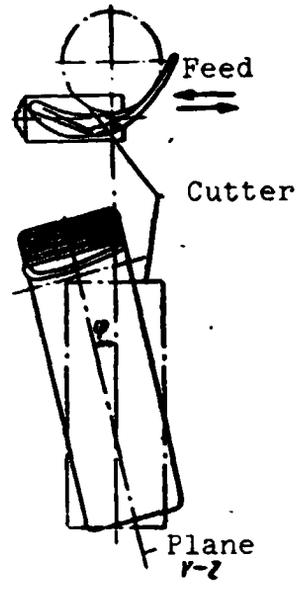

Figure 5.18. Mutual positioning of cutter and blade

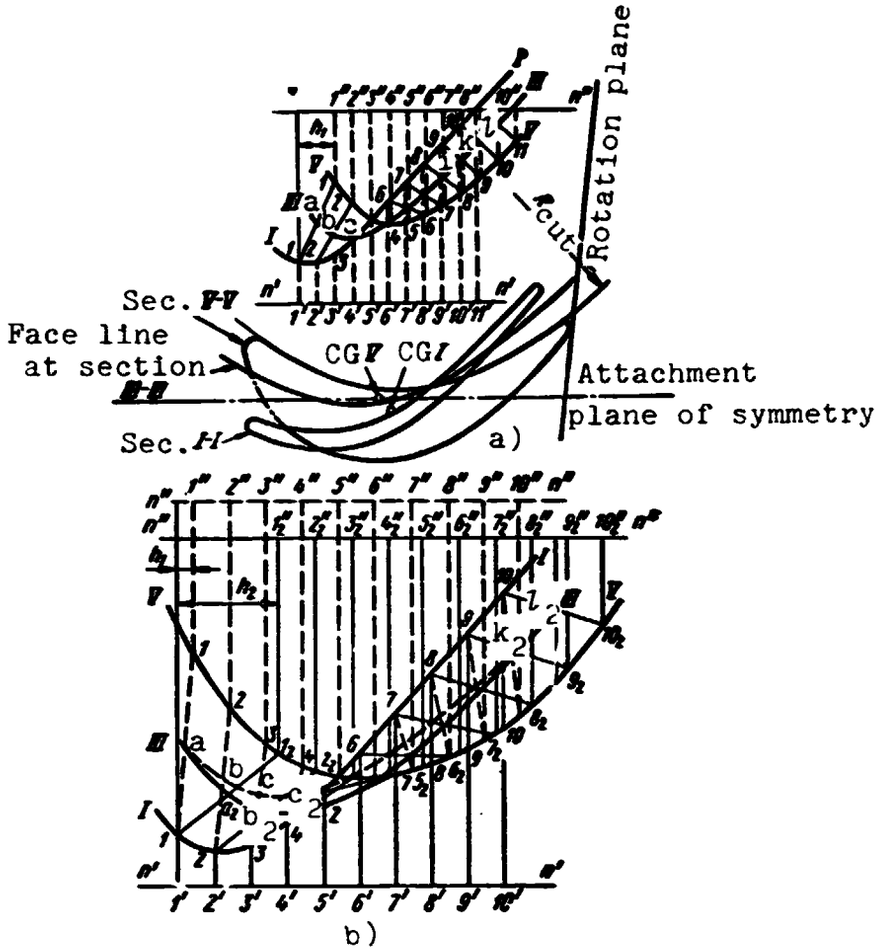

Figure 5.19. Construction of mean section (III - III) concave surface profile when machining using two templates

2. After selecting the cutter radius, we construct the lines I - I, V - V along which the centers of the corresponding cutter sections will travel.

In the machining process, the planes of the specified sections and the axis of the generating cylinder are not perpendicular, and the lines of intersection of these planes and the cylinder are ellipses. The description of the intermediate blade sections and, particularly, the construction of the lines of travel of the centers of the generating cutter sections simplifies considerably if we position the cutter axis perpendicular to the plane of the drawing and consider the cutter sections to be circles whose diameters are

equal to the cutter diameter. The error resulting from replacement of the ellipses by circles is not large and, if necessary, can be eliminated by slight correction of the templates and blade plane setting angle in relation to the cutter axis.

3. In order to construct the line III - III (Figure 5.19a) along which the center of the sections of the cutter generating the mean blade section (III - III) will travel, it is necessary to construct several sequential positions of the cutter axis 1 - 1, 2 - 2, ..., 10 - 10. To do this, taking some initial position 1 - 1, we break the lines n' - n' and n" - n", coinciding with the direction of /126
machine tool table feed during milling, into segments 1' - 2', 2' - 3' ... and 1" = 2", 2" - 3", ... such that all these segments are equal to one another.

Then, we erect at the points 1', 2', ..., 10' perpendiculars to intersect the line I - I, and at the points 1", 2", ..., 10" — to intersect the line V - V.

The points a, b, c, ..., i, k, l, by which the segments 1 - 1, 2 - 2, ..., 10 - 10 are divided in half, correspond to several sequential positions of the center of the section of the cutter generating the mean section profile, and their locus is the line of displacement of this center, analogous to the lines I - I and V - V.

4. The line describing the second mean section surface is drawn /127
equidistant to the line III - III at the distance $R = R_{cut}$ (cutter radius).

The back surface is fitted to this line, i.e., the entire mean section is constructed so as to obtain acceptable areas, center-of-gravity location, angles, and other geometric characteristics.

If for the given form of the concave side it is not possible to obtain satisfactory geometric characteristics of the mean profile, we must shift the cutter axis to a new initial position 1 - 1_2 and

repeat the construction (Figure 5.19b), i.e., again break the line n" - n" into equal segments $1''_2 = 2''_2$, $2''_2 - 3''_2$, ..., $9''_2 - 10''_2$, erect perpendiculars at the points $1''_2$, $2''_2$, ..., $10''_2$ to intersect the line V - V at the points 1_2, 2_2, ..., 10_2. The locus of the points a_2, b_2, ..., k_2, l_2 will correspond to the new form of the line III - III.

We see that for unchanged lines V - V and I - I, the form of the line III - III (a, b, c, ...) corresponding to the first approximation, and the line a_2, b_2, ..., k_2, l_2 corresponding to the variant being considered is determined to a considerable degree by the cutter axis setting angle in relation to the blade Y - Z plane.

The magnitude of this angle is defined as arctg ($h/\Delta z$), where Δz is the distance along the cutter radius between the lower and upper sections. If necessary, the tip and root section can be varied in permissible limits in order to obtain an acceptable mean section.

5. After obtaining the mean section profile, the further construction of the blade is carried out in the sequence described above. The construction of the blade section profiles when machining using /128 a single two-dimensional template is shown in Figure 5.20.

The lines describing the concave surface are segments of several equidistant lines. In Figure 5.20b, the sections are shown as they are projected if we look in the direction of the generating cutter axis. This arrangement of the sections is convenient for the construction. Figure 5.20a shows these sections as they are projected on the X - Y plane if we look in the direction of the Z axis.

In both cases, for simplicity of construction, the section configuration is drawn the same, i.e., we assume that transition from Figure 5.20a to Figure 5.20b is made by plane-parallel displacement of all the sections relative to the lower section by distances proportional to the coordinate z of each section (see Figure 5.10). Shift of the sections for compensation of the bending stresses is accomplished in the same fashion.

The line CC' (see Figure 5.20b), equidistant to the lines describing the concave part of the profiles, is the locus of the centers of the generating circles for all the sections.

The cutter radius for the mean section, just as the radii of all the intermediate sections, is selected so that the section center of gravity, after constructing the back surface, is located on the specified line O_V - O_I. In order to obtain an acceptable form of the generating tool, the variation of the concave side radius along the blade length must be quite smooth.

The further construction of the intermediate section profiles and of the entire blade is made as in the preceeding case.

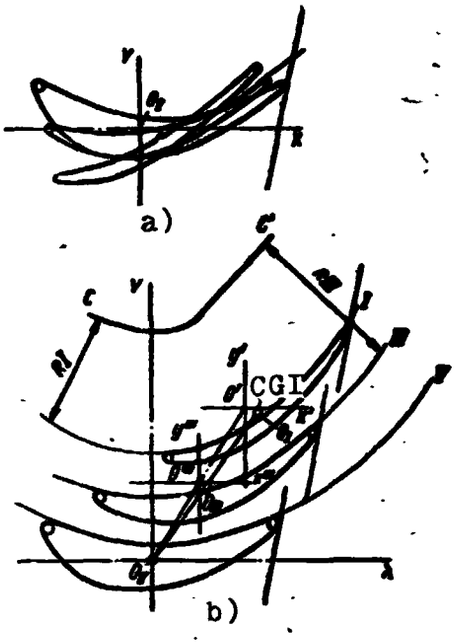

Figure 5.20. Construction of concave surface profile at the mean section (III - III) when machining using a single template. O_V - O^{III} - O'* is the line passi through the coordinate origins of the corresponding blade sections

*Translator's note. The dash between O_V and O^{III} is inadvertently omitted in the original foreign text.

5.5. Profiling Cooled Blades

When profiling cooled stator vanes and rotor blades, along with finding the form and dimensions of the profile external contours at various sections along the blade length, it is also necessary to solve the problem of locating within the blade the channels through which the cooling medium flows. The number of these channels, their form and dimensions are determined by the selected cooled blade construction and by the requirements for high cooling effectiveness. Here, we must take into consideration the technological processes used in fabricating the blades. The capabilities of the particular blade fabrication technique to provide the required accuracy, high

productivity, and reliable quality control methods, and the heat resistance of the materials used are of decisive importance in selecting cooled blade geometry.

The location of the cooling channels within the blade makes it difficult to obtain the cross section area variation along the blade length required by strength considerations and the most rational center-of-gravity location of the individual sections for compensation of the bending stresses. /129

The presence in the blade cooling channels of structural elements (intended for increasing the surface area exposed to the cooling air and intensifying the heat transfer) in the form of transverse ribs, turbulence generators, protuberances, and so on, and the need to increase the form coefficient K_ϕ [see Figure 3.2 and Equation (3.6)], complicate cooled blade profiling in comparison with uncooled blades.

When locating, inside the blade, channels of form specified by the heat transfer conditions and satisfying the strength and fabrication requirements, it is necessary to introduce changes in the generally accepted form of the profile external contour characteristic for uncolled blades, often with simultaneous increase of the losses in the blades. Therefore cooled blades, for which large flow turning angles are characteristic — since they are used in the first turbine stages, usually have thickened leading edges, somewhat greater relative profile thickness c_{max}/b, larger leading and trailing edge taper angles ϕ_1 and ϕ_2, and frequently a thickened trailing edge. Thus, while for uncooled stator vane and rotor blade cascades, the ratio of the leading edge thickness to the chord at the root sections is in the range (5 - 7)% and at the mean sections (4 - 5)%, for the cooled blades, this ratio is (8 - 12)% for the root sections, (7 - 8)% for the mean sections, and reaches 12% in some blades.

The presence of relatively thick leading edges makes it possible to allow positive angles of attack in the sections near the root, where the cascade solidity is also quite high, without any marked

increase of the hydraulic losses. This makes it possible to use profiles with less camber, reduce the gradient of the entrance angle variation along the blade length — which simplifies the blade fabrication process, and makes it easier to install an insert-type deflector inside the blade if it is used.

The profile relative thickness for cooled blades is usually greater than for uncooled blades by a factor of 1.2 - 1.3 (at the mean section).

The trailing edge taper angle for cooled blades is usually (8 - 10)°, and sometimes reaches 12°. This is explained by the desire to improve trailing edge cooling, simplify blade fabrication technology, or both at the same time. In the cooled blade, the radial cooling channels of cylindrical form (see Figure 6.1) can be located closer to the trailing edge, the thicker the edge and the larger the taper angle.

In the blade with cooling air discharge through slots in the trailing edge: the larger the angle ϕ_2, the shorter is the slot segment produced by electrochemical milling, with the minimal possible internal cavity radius based on manufacturing technology (see Figure /130
6.16, variants A and C). Finally, if the trailing edge taper angle in a blade of the same design for a given cooling air discharge slot dimension is larger, the inner core will have greater stiffness, and casting such a blade will be simpler (see Figure 6.16, variant B).

The relative blockage of the profile cascade interblade channels by the trailing edges $2r_2/a$ (see Figure 5.6) for the case of cooling air discharge through slots located in the trailing edges amounts to (10 - 12)%, and in cascades composed of small blade profiles ($b \leq$ 40 mm) reaches 15%. However, in these cases, the edge losses are not so large and are not directly proportional to the relative blockage, as is the case for uncooled blades. This takes place because of the fact that as the air ejected through the slots in the trailing edge mixes with the main flow, the nonuniformity downstream of the

trailing edge equalizes, and the wake downstream of the trailing edge diminishes.

If the amount of air discharging from the slots in the trailing edge amounts to more than one percent of the main flow, the edge losses for such blades decrease markedly [19].

When determining the magnitude of the edge losses for cascades consisting of cooled blades with air discharge through trailing edge slots amounting to no less than 1% of the gas flow through the cascade, we can use the formula $\zeta_{cr} = 0.2(2r_2 - \delta)/a$, where δ is the slot width.

For these reasons, most cooled blade cascade designs are still inferior, with respect to their hydraulic efficiency, to the uncooled blades.

However, increased cooling effectiveness and particularly the introduction into production of new technological processes, which provide the required accuracy and reliable blade inspection methods, are making it possible to create cooled blade cascades without marked deterioration of their hydraulic characteristics in comparison with the uncooled blade cascades.

CHAPTER VI

COOLING OF GAS TURBINE BLADES AND VANES

One way to improve the basic performance of gas turbine engines /131
— increase the specific power, reduce the specific fuel consumption and specific weight — is to increase the turbine inlet gas temperature, which is limited to a considerable degree by the strength of the nozzle vanes and rotor blades. However, increase of the blade and vane strength margins to the values required by operational reliability by reducing the design stresses in the vanes and blades is either not possible or leads to increased engine weight, and reduces significantly the advantages obtained from increasing the gas temperature. The solution of this problem lies in two directions. One is to increase the hot strength of the materials used for the gas turbine engine vanes and blades, and the second is cooling of the vanes and blades to ensure reliable operation at high gas temperatures.

6.1. Open-Cycle Air Cooling Scheme

In comparison with many well-known techniques for cooling gas turbine blades — air cooling using a closed-cycle scheme, internal and external liquid cooling, use of an intermediate coolant and "heat pipes" — the open-cycle scheme for air cooling the gas turbine components in which the air taken from the compressor enters the flow path after cooling the blades has several significant advantages. The primary advantage is simplicity and operational reliability. This has made it the most widely used scheme, and to date the only

scheme which has been realized in practice for cooling aircraft engine turbines. However, in this scheme, the larger the cooling air flowrate, the smaller is the advantage from increasing the gas temperature. Therefore, one basic problem which arises with increase of the turbine inlet gas temperature is the creation of a highly efficient blade design which will require minimal cooling air flowrate for cooling the blade, other conditions being the same.

When using the open-cycle air cooling scheme, the blade temperature can be lowered relative to the temperature of the gas surrounding the blade by internal convective cooling, film (barrier) cooling, /132 and porous cooling.

When using internal convective cooling of the blades, the cooling air flows through specially made channels inside the blade, and is discharged into the flow path. Some configurations of such blades are shown in Figure 6.1 [26].

In the three-channel blade "a", the cooling air enters at the root and rises through the channel along the trailing edge; most of the air discharges through a hole in the upper end of the blade, while the remaining air travels downward through the center channel, and then through the channel running along the leading edge, and discharges through a hole in the upper end of the blade into the radial clearance. This blade with 30-mm-long profiled part is installed in the Tyne TJE turbine, having turbine inlet gas temperature 1240 K. With cooling air flowrate equal to 1% of the gas flowrate, the blade temperature reduction at the mean airfoil section is only 40°. But even this reduction increases engine life by more than a factor of two.

Blade "b" is also three-channel. The cooling air enters and leaves the blade through holes in the base. The air first flows upward along the profiled part, simultaneously through two channels located near the edges and then downward through the central channel.

/133

This blade is installed in the Conway TJE first stage turbine, in which the turbine inlet gas temperature is 1310 K; with cooling airflow rate equal to 1.42% of the gas flowrate, the blade is cooled by 120° at its mean section, with a temperature differential (between the midpoint of the back side and the trailing edge) in this section of about 80°.

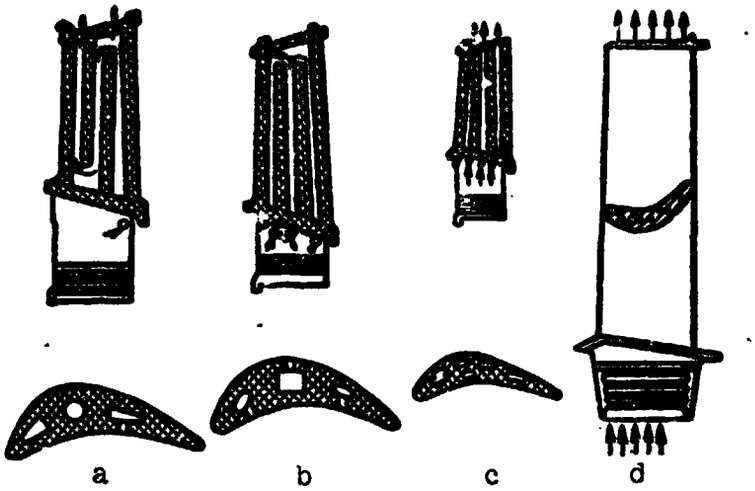

Figure 6.1. Configurations of engine turbine cooled blades:
a — Tyne; b — Conway; c — Spey; d — Olympus

In blade "c", the cooling air enters from both sides of the base, and after flowing through longitudinal (radial) channels of elliptical shape discharges into the radial clearance. The 38-mm-long blade is installed in the Spey TJE turbine, in which the maximal turbine inlet gas temperature does not exceed 1360K. About 2% cooling air flows through the blade, and reduces the temperature at the mean section of the profiled part by 220°, with 200° temperature difference between the middle part of the blade and the trailing edge (at the same section).

Blade "d" has radial channels of 1 - 1.2 mm diameter. The cooling air enters through the attachment part of the blade and, after traveling through the channels, discharges into the radial clearance. The blade is cast from a heat-resistant alloy, and the number of channels may reach 35. In spite of this large number of channels, the difference between the temperatures of the middle part of the blade and the edges in the blade cross section reaches 250°, for temperature of the gas flowing around the blade, 1250 K, and cooling air temperature 310 K, and with cooling air flowrate 1.5 - 18%.

This temperature nonuniformity in the cross section is characteristic for cooled blades with radial channels.

Under the same conditions, the hollow blade with internal deflector (Figure 6.2), i.e., with transverse cooling air flow relative to the airfoil, has a temperature nonuniformity /134
not exceeding 50°.

When using film cooling, the air is blown through specially made slots or holes in the blade surface, creating a protective layer between the gas and the blade surface. As the cooling air layer flows along the blade profile, it is gradually washed away by the gas flow; therefore, rows of similar slots or holes through which new portions of cooling air are introduced (Figure 6.3) must be positioned sequentially at those points of the profile where the film has not yet been washed away. It is obvious that film cooling is preceded by convective cooling, since the cooling air flows through the internal channel before reaching the blade surface. Therefore, in such blades, the convective cooling role is often commensurate with the barrier cooling.

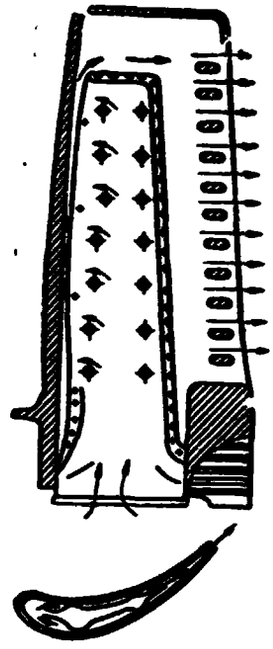

Figure 6.2. Cooled blade with internal deflector [26]

Porous cooling is the most effective type. The essence of porous cooling lies in the fact that, as the air passes through small holes (pores) in the blade wall, it takes heat from the wall and forms a thermoprotective layer on the outer surface (Figure 6.4). The blade consists of an inner load-carrying core 1, with profiled ribs, and a porous shell 2 which forms the profiled part. The shell may be fabricated from metal mesh. The ribs on the core support the shell and form longitudinal channels which provide the required cooling air pressure and flowrate distribution over the blade surface.

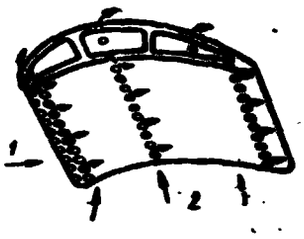

Figure 6.3. Blade with film cooling:

1 — hot gas flow; 2 — cooling air flow [26]

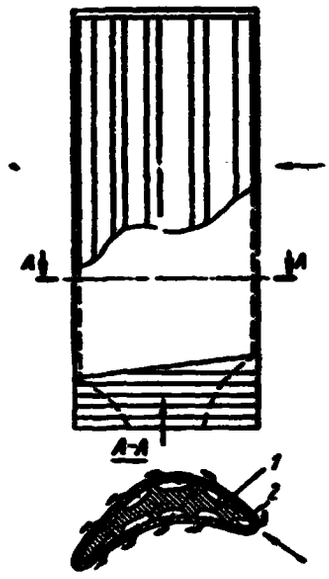

Figure 6.4. Blade with porous cooling:

1 — load-carrying core; 2 — porous shell [26]

We note that the inadequate high-temperature strength of the materials used to date for porous cooling does not permit full realization of the rotor blade temperature reduction effect.

With increase of the pressure ratio in the compressor and the airplane flight speed, the cooling air temperature downstream of the compressor increases, and this degrades the blade cooling conditions. Therefore, with increase of the flight Mach number M_f and π^*_{k0}, the allowable turbine inlet gas temperature decreases for a given blade temperature; this shows up particularly at high values of M_f. For example, /135 for $M_f = 3.0$ and $\pi^*_{k0} = 6.0$, the gas temperature must be reduced by 150° in comparison with the stand regime, and for $\pi^*_{k0} = 9$, it must be reduced by 50° more. In this case, the relative cooling air flowrate in the flight regime is 2%.

We could maintain the same turbine inlet gas temperature (for $\pi^*_{k0} = 6.0$) if we increased the relative cooling air flowrate in the flight regime to 4%, which for a TJE with afterburning would lead, on the one hand, to increase of the specific fuel flowrate by ∿ 1% (under the assumption that η^*_T = const) and, on the other hand, to the necessity for significant increase of the cooling air channel

section area, since for the existing channel flow section areas the relative cooling air flowrate decreases markedly with increase of M_f. This is seen from the following relations: the reduced gas flowrate $\bar{G}_g$ through the turbine and the reduced cooling air flowrate $\bar{G}_a$ through the cooling system are practically constant quantities over the entire range of regime variation as a function of M_f. Consequently,

$$\bar{G}_g = \frac{G_g \sqrt{T_g^*}}{p_g^*} = C_1 \text{ and } \bar{G}_a = \frac{G_a \sqrt{T_a^*}}{p_a^*} = C_2,$$

and the relative cooling air flowrate:

$$G_{cool} = \frac{G_a}{G_g} = \frac{C_2}{C_1} \frac{p_a^*}{p_g^*} \sqrt{\frac{T_g^*}{T_a^*}}.$$

When the cooling air is taken from downstream of the compressor, $P_a^* = p_k^*$ and $T_a^* = T_k^*$.

Since with engine operating regime change to within constancy of the total pressure loss in the combustion chamber:

$$p_k^*/p_g^* = \text{const and } T_g^* = T_{g\,max}^* = \text{const, then } \bar{G}_{cool} = \frac{C_3}{\sqrt{T_k^*}};$$

where C_1, C_2, C_3 — constant quantities.

Thus, the relative air flowrate through the cooling system decreases as the square root of its temperature.

In reality, the coefficients C_2 and C_3 are not constant, but are rather a complex function of the flight regime, since they depend on the Reynolds number in the cooling channels and the ratio of the channel wall and cooling air temperatures. The form of this function is determined, in turn, by the selected cooled blade constructional scheme, i.e., by the cooling channel shape and arrangement.

Figure 6.5 shows the relative cooling air flowrate as a function of flight altitude and speed for $T_g^* = T_{g\,max}^* = \text{const}$, from which /136

we see that for M_f = 3.0 and H = 28 km, $\bar{G}_{cool}$ decreases by a factor of two in comparison with the stand regime, although $\sqrt{T_k^*}$ varies by only a factor of 1.3.

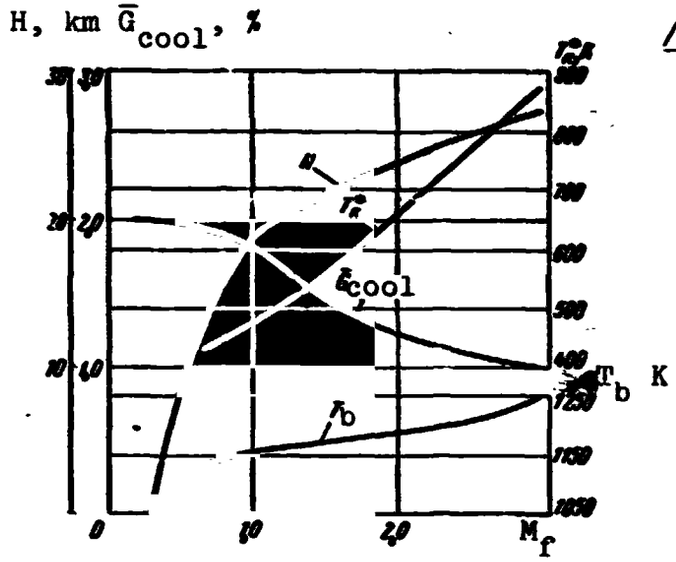

Figure 6.5. Variation of relative cooling air flowrate $\bar{G}_{cool}$ and blade temperature T_b with flight altitude H and speed M_f

/136

Consequently, in order that the blade temperature for M_f = 3.0 not exceed the allowable value based on strength considerations or, what is the same, in order to maintain the same turbine inlet gas temperature, it is necessary in the considered example that the relative cooling air flowrate, determined by the flight conditions, be nearly twice as high under stand conditions. This requires increase of the cooling channel dimensions and associated thickening of the blades and leads to increased hydraulic losses in the turbine.

It is obvious that increase of $\bar{G}_{cool}$ and deterioration of the turbine efficiency lead to reduction of the maximal thrust and increase of the engine fuel flowrate in the takeoff regime at both high and low M_f. Therefore, we see from this example that increase of the turbine inlet gas temperature under flight conditions by increasing the relative cooling air flowrate is not justified.

However, since the reduction of the specific fuel flowrate during engine operation in the partial afterburning regime (afterburning TJE flight in the cruising regime) involves increase of T_g^*, it is still desirable to increase this temperature. In this connection /137
a question arises: can we not solve this problem by taking the cooling air from an intermediate stage where the air temperature is lower, rather than from the compressor exit.

The solution of this problem in general form is very difficult, since it will depend on the engine type, values of the basic engine parameters, engine configuration, operating conditions, cooling scheme, and cooled blade construction.

The blade temperature as a function of air bleed location is shown in Figure 6.6 for the example considered above, in which we assume a cooled blade with transverse flow of the cooling air relative to the airfoil and known relationship between the blade cooling intensity and the cooling air parameters. The higher the number of the stage from which the air is taken, the higher will be the air pressure and flowrate, and consequently the higher the cooling intensity. Therefore, in spite of the fact that when taking the air from the intermediate stages its temperature is lower than T_k^*, the heat removal from the turbine blade wall and, therefore, the allowable turbine gas inlet temperature are no higher than with bleed downstream of the compressor. Consequently, the only way to increase turbine blade air cooling intensity in an engine with high π_{k0}^* and at high flight speeds is preliminary cooling of this air. In this /138 case, air bleed downstream of the compressor is most favorable. The bleed air enters a heat exchanger in which air from the airplane air intake, air after the fan stage, or fuel is used as the cooling medium.

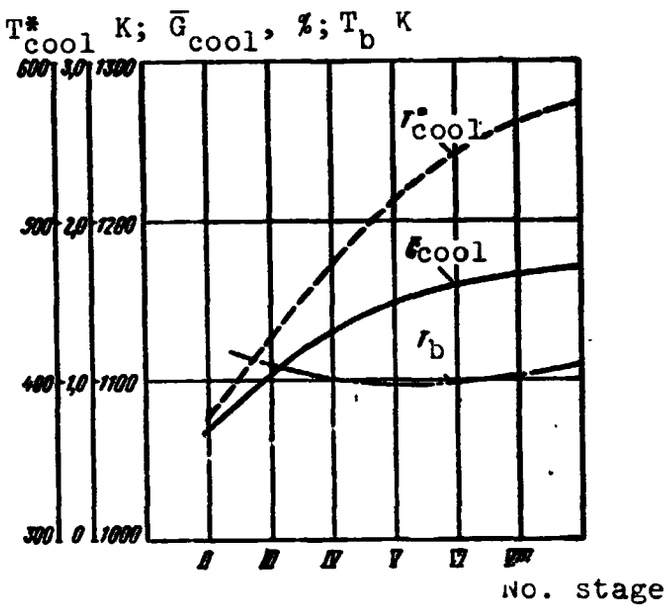

Figure 6.6. Cooled blade temperature as function of cooling air bleed location

Significant increase of the turbine inlet gas temperature for the rotor blade temperature specified by strength conditions can be obtained by reducing the cooling air temperature in a fuel-air heat exchanger.

For example, with pressure ratio in the

compressor corrected to stand conditions $\pi_k^* = 12$, $M_f = 3.0$, at an altitude of H = 23 km, and turbine inlet gas temperature $T_g^* = 1515$ K, reduction of the cooling air temperature (for cooling air flowrate equal to 2.5% of the flowrate through the compressor and blade temperature 1200 K) by 220 K (from 920 to 700 K) makes it possible to increase the turbine inlet gas temperature by 125 K. In this case, the temperature of the fuel usually used for aircraft gas turbine engines increases by about 120° in the heat exchanger. We must bear in mind that the amount of heat which can be absorbed by the fuel is limited by the available difference between the fuel temperature at the engine inlet and the allowable fuel temperature at the heat exchanger exit. Moreover, when using this technique for cooling the air, difficulties arise associated with the influence of starting and off-design engine operating regimes on blade cooling, since the absolute fuel and cooling air flowrates and their ratio change.

If we add to such an engine a second (bypass) contour and locate an air-air heat exchanger in the bypass flow, for the considered conditions we can increase the turbine inlet gas temperature by nearly 90°. But in this case, pressure losses in the bypass flow in overcoming heat exchanger hydraulic resistance are inevitable.

Considerably less effect from cooling the air in the heat exchanger is obtained when air taken from the airplane air intake is used as the coolant.

The decisive factor in evaluating the various techniques for improving the effectiveness of the open-cycle turbine air cooling scheme, with all its advantages and disadvantages, is the degree of improvement of the basic performance of the engine and of the airplane as a whole.

6.2. Blades with Internal Convective Cooling

Reduction of the cooled blade temperature relative to that of the gas flowing over the blade is accomplished by the processes of heat exchange between the gas and the blade, on the one side,

between the blade and the cooling air flowing through the channels /139
within the blade, on the other side, and by heat propagation in the body of the blade itself. In this connection, to determine the temperature field in cooled blades, we must solve the three dimensional problem of heat transfer in a multiconnected region with variable boundary conditions along the contour. Analytic solution of this problem (in general form) is possible only for bodies of very simple form. Therefore, the cooled blade temperature field is usually determined by approximate methods, in which the problem reduces under certain assumptions to a two-dimensional or even one-dimensional problem.

The approximate solution methods and also the electrothermal or hydrothermal analogy methods yield accuracy adequate for practical purposes if the coefficients of heat exchange with the gas and with the air are known sufficiently accurately.

6.2.1. Heat transfer from the gas to the blade

There are several methods which permit finding the coefficient of heat transfer from the gas to the blade if we know the flow regimes in the boundary layer along the profile contour. They assume constant surface temperature and physical constants in the boundary layer, and reduce to calculation of the coefficient with subsequent use of some form of Reynolds number similarity.

One method which has been developed for practical application is that of L. M. Zysina-Molozhen, by which we find theoretical heat transfer coefficients which agree satisfactorily with those obtained experimentally [12] for known distributions along the profile contour of the velocities (pressures) and location of the point (limit) of laminar boundary layer transition into a turbulent layer.

The basic computational equation of this method has the form:

$$Nu_m = \frac{\alpha_g m^b}{\lambda_g} = \left(\frac{\bar{\delta}_{red}}{\Pi \sin \beta_2} \frac{w_{ed}}{w_2} \frac{T_{ed}}{T - T_W} + \varepsilon\right) Pr \cdot Re.$$

where Nu, Pr, Re — Nusselt, Prandtl, and Reynolds numbers;

α_g — coefficient of heat transfer from gas to the blade;

λ_g — thermal conductivity of the gas;

b — blade chord;

$\bar{\Pi}=\Pi/b$ — relative profile perimeter;

$\bar{\delta}^{**}_{ed}=\frac{\delta^{**}_{ed}}{b}$ — relative enthalpy loss at the trailing edge;

β_2 — flow angle downstream of cascade (at the section where the boundary layers come together);

w_2 — velocity in equalized flow downstream of cascade;

w_{ed}, T_{ed} — flow velocity and temperature at the trailing edges; /140

T T_w — flow and wall temperatures;

ε — correction for flow compressibility ($\varepsilon=0$ for $M<0.5$).

The drawback of this method, as of all methods for analytic determination of the coefficients of heat transfer from the gas to the blade, is the fact that it is very labor . even when using a digital computer. In addition, the cooled blade temperatures must be determined in the very early design stage, when the data necessary for calculating the flow around the profile cascade are either not available at all or have not yet been firmly established, and there are no reliable data for determining the limits of the laminar, transitional, and turbulent boundary layers along the cooled blade profile contour, while the calculation accuracy depends to a considerable degree on the location and extent of the transitional zone.

Therefore, the coefficients of heat transfer from the gas to the blade must usually be determined experimentally. After reducing the experimental results and correlating them in accordance with similarity theory, we obtain the criterial heat transfer relations which can be used to determine the coefficients of heat transfer from the gas to the blade, even in the very early blade design stage, when

the gasdynamic calculation of the turbine has been made and only the basic geometric characteristics of the blades have been determined.

The following similarity criteria are generally used in studying the heat exchange process in cooled blades.

1. The Nusselt number, characterizing thermal similarity of the flow:

$$Nu = \frac{\alpha L}{\lambda},$$

where λ — thermal conductivity of the medium;
α — coefficient of heat transfer at the given point;
L — characteristic linear dimension.

2. The Reynolds number, characterizing the ratio of the inertial forces to the viscous forces (molecular friction forces):

$$Re = \frac{w\rho L}{\mu},$$

where w — characteristic flow velocity;
μ — dynamic viscosity of the medium;
ρ — density of the medium.

3. Grashoff number, characterizing the interaction of the viscous forces (molecular friction) and the buoyant force due to the difference of the densities at individual points:

$$Gr = \frac{g\beta a^3 \Delta t}{\nu^2},$$

where g — gravity force acceleration or (in rotating systems) centrifugal force acceleration; /141
β — bulk expansion coefficient;
Δt — temperature difference causing the buoyant force;
$\nu = \mu/\rho$ — kinematic viscosity of the medium;
μ — dynamic viscosity of the medium.

4. Prandtl number, characterizing the thermostatic properties of the medium:

$$Pr = \frac{\nu}{a},$$

where $a = \frac{\lambda}{c\rho}$ — thermal diffusivity, characterizing the rate of temperature equalization in a nonuniformly heated body;

c — specific heat capacity;

ρ — density.

In addition to these criteria, we use the dimensionless relative temperature of a given point:

$$\theta = \frac{T_0 - T}{T_0 - T_1}.$$

where T_0 — heating medium temperature;

T_1 — cooling medium temperature;

T — body temperature at given point.

In spite of the fact that the local heat transfer coefficient variations are not continuous along the profile contour, we can usually divide the blade into segments, along which we can take the heat transfer coefficient to be practically constant, and we can calculate them using the above-mentioned criterial relations obtained experimentally.

The technique in which we determine the mean coefficient of heat transfer from the gas to the blade at the leading edge $\alpha_{g\ I}$, in the middle part of the profile $\alpha_{g\ II}$, and at the trailing edge $\alpha_{g\ III}$ (Figure 6.7) is widely used in cooled blade design practice.

The average heat transfer coefficient in the leading edge region can be determined with accuracy adequate for practical calculations from the data obtained for transverse flow over a cylinder with radius equal to that of the leading edge. Good agreement between the calculated and experimental values for the blade leading edge region is obtained when determining $\alpha_{g\ I}$ from the criterial relation:

$$Nu_{g\ I} = \frac{\alpha_{g\ I} d_I}{\lambda_{g\ I}} = A_I \sqrt{Re_{g\ I}}, \qquad (6.1)$$

where, in determining $Nu_{g\ I}$ and $Re_{g\ I}$, the geometric dimension is taken to be twice the leading edge radius, the characteristic velocity is the approaching flow velocity, and the viscosity and thermal conductivity are defined in terms of the total parameters of the flow approaching the blade. According to the data of various authors, the coefficient A_I varies in the limits 0.635 - 0.82 in the range $Re_{g\ I} = 2.5 \cdot 10^3 - 4 \cdot 10^4$ and for subsonic approaching velocities. The coefficient A_I will also depend on the cooled blade cascade sensitivity to angle-of-attack variation. For most cooled rotor blades and ranges of angle-of-attack variation in the first turbine stages (where cooled blades are used) which are encountered in practice, we can take $A_I = 0.74$ in the region bounded by the angle 70 - 75° from the tangent to the profile centerline at the leading edge, and in the range $2.8 \leqq 10^3 = Re_{g\ I} \leqq 2.8 \cdot 10^4$. If we take the term leading edge to mean the segment described by its radius, we can take A_I equal to 0.635 for determining the average value of $\alpha_{g\ I}$ in the range $Re_{g\ I} = 5 \cdot 10^3 - 4 \cdot 10^4$ and $M_I \leqq 0.9$ for zero angle of attack [3]. /142

We can determine the average heat transfer coefficient $\alpha_{g\ II}$ for the concave and convex sides of the profile using the relation obtained by Golubeva (for $0.5 \cdot 10^5 \leqq Re_{g\ II} \leqq 2 \cdot 10^6$), which has been adequately verified in aircraft gas turbine design practice:

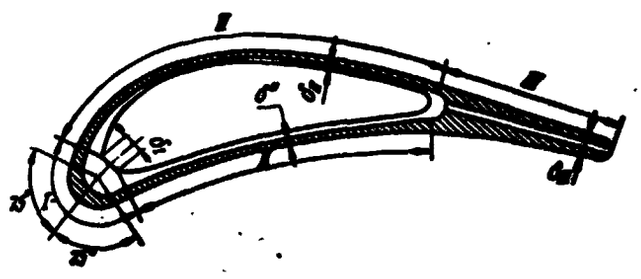

Figure 6.7. Blade profile segments

$$Nu_{g\ II} = \frac{\alpha_{g\ II} b}{\lambda_{g\ II}} = A_{II} Re_{g\ II}^{0.68}. \qquad (6.2)$$

Here, $Re_{g\ II}$ is based on the throat dimension at the cascade exit, the thermal conductivity $\lambda_{g\ II}$ is based on the isentropic total gas temperature, the viscosity is based on the gas temperature at the throat, the blade chord b is taken as the geometric dimension, and /143 the coefficient A_{II} is determined from the curve of Figure 6.8 as a function of the flow turning angle $\varepsilon = 180 - (\beta_1 + \beta_2)$ in the cascade.

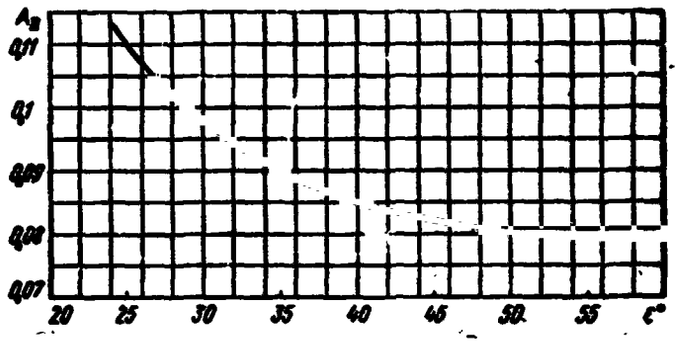

Figure 6.8. Coefficient A_{II} as function of flow turning angle in bladed cascade

The heat exchange between the gas and the blade depends on the entire prehistory of its formation on the preceding profile segments.

Under the assumption that the beginning of transition from the laminar flow regime in the boundary layer to turbulent flow is located about 0.7 of the blade chord from the leading edge, the coefficient of heat transfer from the gas to the blade $\alpha_{g\ III}$ is determined with accuracy satisfactory for practice (for $Re_{g\ II} \geqq 5 \cdot 10^5$) from the criterial relation characteristic for turbulent flow over a flat plate:

$$Nu_{g\ II} = 0.0263\ Re_{g\ II}^{0.8}. \qquad (6.3)$$

The following relation [3] yields good agreement with experiment for Re from $3 \cdot 10^3$ to $3 \cdot 10^4$ when determining the coefficient of heat transfer from the gas to the blade trailing edge on a segment equal to one tenth of the blade chord:

$$Nu = 3{,}25 \cdot 10^{-3}\ Re^{0.93}.$$

Here, the determining parameters are the total gas flow velocity and temperature at the exit from the profile cascade and twice the blade leading edge radius.

6.2.2. Heat transfer from blade to cooling air

The coefficient of heat transfer from the blade to the cooling air is determined by the geometry (shape and dimensions) of the internal channels and the nature of the flow in these channels. The air flow in the channels is a result of the pressure difference between the entrance to and exit from the channels, and in the rotor blades is also influenced by the action of the centrifugal forces. Therefore, this flow is usually turbulent, except for certain regimes realized at high flight altitudes. /144

In most cooled blade designs, the internal channels have relative length $l = l/d$, which is sufficient for use of the criterial relative obtained for straight long tubes of varying section area with turbulent air flow:

$$Nu_a = 0{,}018\, Re_a^{0.8} \cdot e_r \cdot e_l. \qquad (6.4)$$

Here, $Re_a = \frac{w_a d_a}{\nu_a} = \frac{(\rho w)_a d_a}{\mu_a} = \frac{G_a d_a}{F_a \mu_a}$;

ν_a and μ_a — respectively, kinematic and dynamic air viscosities;

$(\rho w)_a = \frac{G_a}{F_a}$ — cooling air flowrate per unit channel section area;

$d_a = \frac{4F_a}{\Pi_a}$ — channel hydraulic diameter;

Π_a — channel wetted perimeter;

F_a — channel cross section area;

e_r and e_l — coefficients accounting for the influence of channel curvature and relative length, taken from [21].

Considering the usual configuration of longitudinal (radial) internal channels in the cooled blades (see Figure 6.1), we can take $\varepsilon_r = 1{,}0$ and $\varepsilon_l = 1{,}2$;

ε_t — coefficient reflecting the influence of the first ψ and second ψ' temperature factors [33],

where $\psi = T_b/T_a^*$ — first temperature factor;

$\psi = T_a^*/\text{const}$ — second temperature factor; for blade temperature equal to or greater than 1000 K, $\varepsilon_t \approx 1.0$.

In cooled blades with transverse cooling air flow relative to the airfoil and jet impingement of the cooling air on the leading edge inner surface, α_a is determined (by analogy with α_g) for the different segments of the profile inner contour. An example of such a blade is the hollow thin-wall blade with internal insert-type deflector (see Figure 6.2) [26]. In this blade, the cooling air is fed inside the deflector and flows through holes in the deflector onto the inner surface of the blade leading edge. Then, after turning through 180°, it enters the channels between the deflector and the inner surface of the blade, flows over the concave and convex surfaces of the blade, and discharges into the turbine flow path through /135
slots (holes) in the trailing edge.

The heat transfer coefficient α_ε in the blade leading edge region, according to [4], is found from the criterial relation tained for $1.7 \cdot 10^3 \leqq Re_{a\ I} \leqq 6 \cdot 10^3$:

$$Nu_{a\ I} = 0{,}0984\, Re_{aI}^{0{,}71} \left[\frac{d_{aI}}{l} \; \frac{\mu_{III} F_{aIII}}{\mu_I F_{aI}} \right]^{0{,}208} \varepsilon_{II}. \qquad (6.5)$$

Here, $Re_{a\ I}$ is based on the air parameters at the exit from the holes in the base of the deflector;

$d_{a\ I} = 4F_{a\ I}/\Pi$ — hydraulic diameter, taken as the characteristic dimension;

$\varepsilon_{t\ I} = 1.0$ (for $T_b \geq 1000$ K);

$l/d_{a\ I}$ — maximal relative distance from deflector hole exit to inner surface of the blade leading edge;

$F_{a\ I}$ and $F_{a\ III}$ — respectively, areas of holes in deflector and in blade trailing edge;

μ_I and μ_{III} — discharge coefficients for air flow through the deflector holes and trailing edge slots.

If the holes in the deflector are made, as is usually done, in the form of convergent nozzles, and if special devices (for example, turbulence generators in the form of small pins and the like) are not provided in the trailing edge slots to significantly increase their hydraulic resistance, we can take the discharge coefficients to be equal, in other words, $\mu_{III}/\mu_I \cong 1{,}0$.

For the cooling channels in the blade concave and convex segment and in the trailing edge region, we can use the criterial relation (6.4), which can be used for $0{,}5 \cdot 10^3 \leq Re_{a\ II} \leq 10 \cdot 10^3$ (extension of the turbulent flow regime into the low Re region is associated with one-sided heat input in the channel and turbulization of the flow at the entrance to the channel) and $Re_{a\ III} \geq 15 \cdot 10^3$. Then, $\varepsilon_r = 1 + 1{,}77\ d_a/r$ and $\varepsilon_l = f(Re, l/d)$ [21], and the influence of one-sided heat input is accounted for by the coefficient $\varepsilon_q = 0{,}7 - 0{,}85$ (which corresponds to T_b = 1250 - 1100 K).

6.3. Cooling Effectiveness and Heat Transfer in Blades with Transverse Flow Scheme

The effectiveness of blade cooling with air discharge into the turbine flow path is determined by two factors: the cooling intensity and the magnitude of the losses associated with the introduction of

cooling. These two factors are interrelated: the higher the cooling intensity, the smaller the amount of air taken from the compressor for cooling and the larger the amount of air which participates in the expansion process in the turbine. Moreover, with decrease of /146 the cooling air flowrate, the hydraulic losses in the turbine associated with introduction of the cooling air into the flow path and mixing with the gas flow decrease.

For given gas T_g and cooling air T_a temperatures at the blade entrance (or at some blade segment), the cooling intensity can be characterized by the ratio of the differences between the gas and blade temperatures (in the considered region) to the difference between the gas and air temperatures:

$$\theta = \frac{T_g - T_b}{T_g - T_a}. \tag{6.6}$$

If we suppose that with change of the heat exchange conditions characteristic for cooled blades, the blade temperature varies analogously to the temperature of a thin plane wall exposed to the same conditions, then for each considered blade segment, we can write:

$$\frac{T_g - T_b}{T_b - T_a} = K_\phi \frac{T_g - T_{pw}}{T_{pw} - T_a}, \tag{6.7}$$

where K_ϕ — form factor accounting for the difference between the blade temperature and that of the thin flat wall.

It follows from the conditions of thermal balance between the gas and the cooling air that the amount of heat transferred to the cooling air $Q_a = \alpha_a(T_{pw} - T_a)S_a$ is equal to that taken from the gas $Q_g = \alpha_g(T_g - T_{pw})S_g$, and for $S_a \approx S_g$, we obtain:

$$\frac{T_g - T_{pw}}{T_{pw} - T_a} = \frac{\alpha_a}{\alpha_g}. \tag{6.8}$$

Then, (6.6) with account for (6.7) and (6.8) can be written as:

$$\theta = \frac{T_g - T_b}{T_g - T_a} = \frac{K_\phi(\alpha_a/\alpha_g)}{K_\phi(\alpha_a/\alpha_g) + 1} . \qquad (6.9)$$

For a flat wall and thick wall cylinder, the form factor is defined by the relations

$$K_{\phi.pw} = \frac{1}{1 + \frac{\alpha_a \delta_{pw}}{\lambda_{pw}}} , \quad K_{\phi.cyl} = \frac{r}{R} \frac{1}{1 + \frac{\alpha_a r}{\lambda_{cyl}} \ln \frac{R}{r}} ,$$

where δ_{pw} — thickness of the plane wall;
r and R — inner and outer radii of the cylinder.

Under the heat exchange conditions characteristic for cooled turbine blades, the magnitude of the heat transfer coefficient has very little influence on the variation of K_ϕ, and for the considered /147 blade design it is practically constant. Then, from (6.9):

$$\theta = f(\frac{\alpha_a}{\alpha_g}). \qquad (6.10)$$

The ratio (6.6) is convenient for comparing the cooling intensity of different blades. It makes it possible to determine the temperature of the considered blade region for a given turbine operating regime, and the larger the coefficient θ, the less the blade temperature will differ from the cooling air temperature and, consequently, the better the blade is cooled.

Since for physical properties of the gas and air which vary little under the heat exchange conditions, for definite geometry of the profile scade and the cooling air channels, and for given gas and cooling air temperatures determined by the turbine operating regime, the right side of (6.10) depends on the relative air flowrate, the coefficient θ is represented graphically as a function of the ratio of the air G_a and gas G_g flowrates.

Figure 6.9 shows a comparison of the cooling intensity (θ) of the profile midsection of some aircraft turbine blade designs.

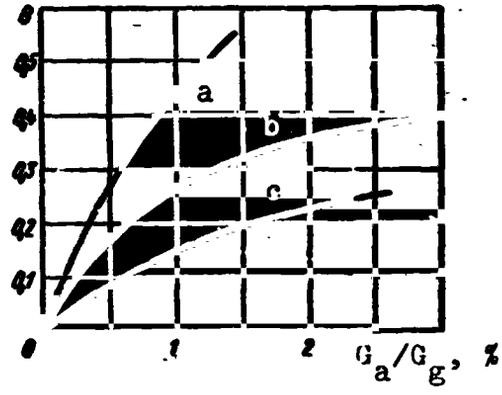

Figure 6.9. Comparison of intensity of different variants of blde profile midsection cooling:

a — porous cooling; b — blade with insert-type deflector; c — blade of Conway type with radial cooling air flow

Under the actual heat exchange conditions determined by the engine operating regime, the physical properties of the air and gas do not remain constant. With accuracy adequate for practice, their variation can be expressed as a power function of the absolute temperature [5]:

$$\mu = f_1(T^{0.64}); \ \lambda = f_2(T^{0.75}). \qquad (6.11)$$

A single-valued relation is obtained between the complexes /148

$(T_g/T_a)^p$ and $\bar{G}_a Re^q \mathcal{F}$ [14], which can be used to determine blade cooling effectiveness.

The criterial relations presented in sections 6.2 and 6.3 can be written in the form:

$$Nu_a = A_a Re_a^n \text{ and } Nu_g = A_g Re_g^m.$$

In turn, $\alpha_a = A_a Re_a^n \frac{\lambda_a}{d_a}$ and $\alpha_g = A_g Re_g^m \frac{\lambda_g}{d_g}$.

If the kinematic viscosity μ and thermal conductivity λ are expressed as functions of the temperature using (6.11), the ratio of the coefficients of heat transfer with the air and gas for geometrically similar blades can be represented by the expression:

$$\frac{\alpha_a}{\alpha_g} \sim \left(\frac{G_a}{G_g}\right)^n \left(\frac{T_a}{T_g}\right)^q Re_g^{n-m}.$$

According to (6.10), the quantity θ is determined by the ratio of the heat transfer coefficients α_a/α_g. Consequently,

$$\theta = f\left[\left(\frac{G_a}{G_g}\right)^{n} \cdot \left(\frac{T_a}{T_g}\right)^{e} \cdot Re_g^{e-m}\right].$$

This dependence will be different for the different blade segments, having according to (6.1) - (6.5) different values of the Re exponents. Thus, according to [14], for the leading edge region:

$$\left.\begin{array}{l}
\dfrac{\lambda_a}{\lambda_a}\left(\dfrac{\mu_g}{\mu_a}\right)^{0,71} \sim \left(\dfrac{T_a}{T_g}\right)^{0,305} \text{ and } \theta_I = f_I\left[\bar{G}_{cool}\left(\dfrac{T_a}{T_g}\right)^{0,305} Re_g^{0,21\varepsilon_I}\right]; \\
\text{for the middle region} \\
\dfrac{\lambda_a}{\lambda_g}\left(\dfrac{\mu_g}{\mu_a}\right)^{0,8} \sim \left(\dfrac{T_a}{T_g}\right)^{0,2} \text{ and } \theta_{II} = f_{II}\left[\bar{G}_{cool}\left(\dfrac{T_a}{T_g}\right)^{0,2} Re_{g\,II}^{0,8\varepsilon_I}\right]; \\
\text{for the trailing edge region:} \\
\theta_{III} = f_{III}\left[\bar{G}_{cool}\left(\dfrac{T_a}{T_g}\right)^{0,2\varepsilon_I}\right].
\end{array}\right\} \quad (6.12)$$

In determining the exponent for the middle region of the blade and the trailing edge, we assume that $\lambda = f(T^{0,71})$.

Expressions (6.12) are valid for geometrically similar blades because of the fact that in their derivation we assumed the ratios of the characteristic dimensions appearing in the criterial relations for Nu and Re to be constants.

If we introduce into the relations obtained the ratios of the characteristic dimensions for the different blade regions, in accordance with (6.1) - (6.5), these relations can be used for determining the cooling intensity of blades of different geometry [14].

Then the expressions for the blade segment cooling intensity will have the form: /140

a) leading edge $\theta_I\left(\dfrac{T_g}{T_a}\right)^{0,305} = f_I\left[\bar{G}_{cool}\, Re_{g\,I}^{0,21\varepsilon_{II}} \mathcal{F}_I\right]$, (6.13)

where

$$\mathcal{F}_I = \left(\frac{F_{gI}}{zF_{aI}}\right)^{0.71} \frac{d_{gI}^{0.29}}{l^{0.305}} \left(\frac{\mu_{III} F_{aIII}}{\mu_I F_{aII}}\right)^{0.305} \varepsilon_{II}. \tag{6.14}$$

Here, $F_{g\ I}$ — annular area swept by the blades at the cascade entrance;

$d_{g\ I} = 2R_I$ — leading edge hydraulic diameter;

$R_I = L/\Pi$ — equivalent leading edge outer radius (Figure 6.10);

l — maximal distance between deflector hole exit and blade leading edge inner surface;

z — number of blades;

b) middle part of the profile:

$$\theta_{II}\left(\frac{T_g}{T_a}\right)^{0.2} = f_{II}\left[\bar{G}_{cool}\, Re_{gII}^{0.15}\, \mu_{II}\, \mathcal{F}_{II}\right]. \tag{6.15}$$

where

$$\mathcal{F}_{II} = \left(\frac{F_{gII}}{F_{aII}^2}\right)^{0.8} \left(\frac{d_{gII}}{d_{aII}}\right)^{0.2}. \tag{6.16}$$

Here, $F_{a\ II} = 2\delta_{II} h_{DII}$ — flow section area between blade inner surface and deflector;

δ_{II} — distance (clearance) between blade inner surface and deflector;

$h_{D\ II}$ — deflector length

$d_{a\ II} = 2\delta_{II}$ — hydraulic diameter of clearance between deflector and blade inner surface;

$F_{g\ II} = F_I \sin \alpha_1$ and

$F_{g\ II} = F_I \sin \beta_2$ — respectively, stator and rotor interblade channel throat areas;

$d_{g\ II} = b$ — characteristic geometric dimension — the blade chord;

c) trailing edge:

$$\theta_{III}\left(\frac{T_g}{T_a}\right)^{0.2} = f_{III}\left[\bar{G}_{cool}\,\varepsilon_{III}\mathcal{F}_{III}\right]. \tag{6.17}$$

where /150

$$\mathcal{F}_{III} = \left(\frac{F_{gII}}{F_{aIII}\varepsilon^2}\right)^{0.8}\left(\frac{d_{gII}}{d_{aIII}}\right)^{0.2}. \tag{6.18}$$

Here, $d_{a\ III} = \frac{4F_{III}}{\Pi}$ — hydraulic diameter of the holes (slots) in the trailing edge.

These functional relations were obtained by correlating the theoretical and experimental quantities appearing in them. This minimizes the error in determining blade temperature because of inaccuracies made in selecting the numerical values of the coefficients in the formulas $Nu_a = f(Re_a)$ and $Nu_g = f(Re_g)$. The ratios of these coefficients were used /151 as the abscissa scale.

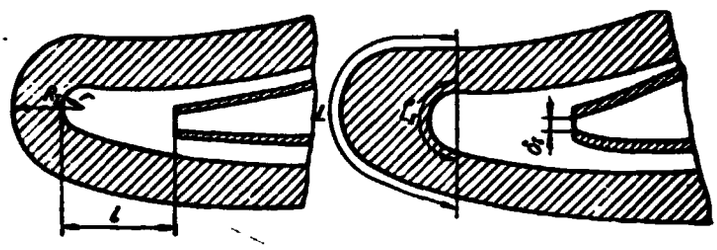

Figure 6.10. Characteristic dimensions of leading edge segment of blade with internal deflector

The exponents of the relative cooling air flowrate $\bar{G}_{cool}$ was taken equal to one, which leads to significant simplification in the calculations.

These relations are shown in graphical form in Figure 6.11, 6.12, and 6.13 [14]. In plotting these curves, it was assumed that the leading edge can be made in several variants, differing in form and ribbing on the inner surface. Therefore, the magnitude of the η factor was taken as the parameter, and the presence of ribbing was accounted for by the coefficient η_r [31], i.e., $\bar{K}_\phi = \eta_r K_\phi$.

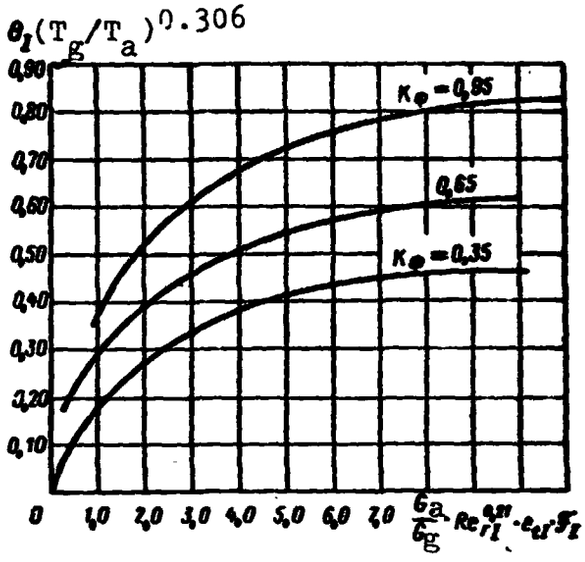

Figure 6.11. Relation for determining temperature of cooled blade leading edge region

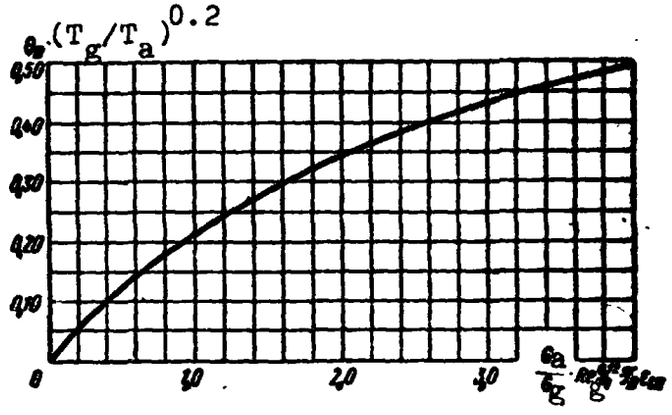

Figure 6.12. Relation for determining temperature of cooled blade profile middle segment

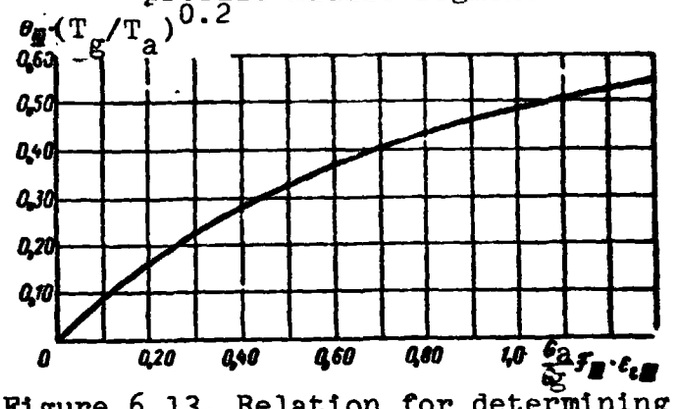

Figure 6.13. Relation for determining temperature of cooled blade trailing edge segment

If there are no ribbing or other structural elements on the inner surface of the middle segment of the blade profile which intensify the heat transfer and alter the form of the blade wall so that it becomes significantly different from a thin plane wall, then the form factor will be practically constant for a broad class of blades, and in many cases differs very little from one. Therefore, for each of these blade profile segments with small and relatively invariant wall thickness (1.2 - 1.8), we can very well make use of a single curve (see Figures 6.12, 6.13).

Moreover, since the experimental data reduction was based on the cooling air temperature T_a at the blade entrance, when using these curves, we assume similarity of the heating of the air in the tested and analyzed blades, and that this heating is independent of the amount of cooling air flowing through the blade. Tests of a large number of blades, differing in their dimensions by more than a factor /152

of [illegible], showed that these assumptions do not introduce any significant error into calculation of the temperature of deflector-type blades operating with specific surface thermal flux densities $q = (10 - 15)\ 10^5\ W/m^2$, and relative cooling air flow rate $\bar{G}_{cool} = 1.5 - 3.0\%$, which are characteristic for aircraft engine turbines.

Using these curves, when designing the blade we can select for the given conditions the cooling air channel dimensions and determine the blade temperature in the various engine operating regimes. In so doing, of course, we need to know the cooling air flowrate.

6.4. Determining Cooling Air Flowrate in Blades with Transverse Flow Scheme

In gas turbine engines, the difference between the pressures at the inlet to and exit from the cooled blade is limited. Its magnitude is determined by the pressure difference developed across the stator vanes and rotor blades for a given pressure ratio in the compressor. Under these conditions, the amount of air which can be passed through the cooled blade depends on the dimensions and hydraulic resistance of all the series and parallel connected channels of different length and configuration.

The existing methods [22] make it possible to perform hydraulic calculations of cooling systems of practically any complexity. However, for their broad application, particularly to deflector-type blades, it is necessary to have reliable data on the hydraulic characteristics of the individual cooling path elements and their mutual /153 influence under actual operating conditions.

Usually, the experimental determination of cooling channel hydraulic resistance is accomplished by flow testing blades, specially instrumented for measurements [16]. In both the thermal and hydraulic calculations, we divide the blade up into three basic segments: leading edge — from the deflector inner cavity to the entrance to the slots in the concave or convex part of the profile (segment I),

slots of the concave or convex part of the profile (segment II), and trailing edge (segment III). The coefficients of hydraulic resistance of each segment are determined from the difference between the total pressures at the entrance to and exit from the segment:

$$\zeta_j^{(0)} = \frac{\Delta p^*}{\varrho_0 w_0^2/2} = \frac{p_0 - p_1}{\varrho_0 w_0^2/2} - \frac{\varrho_0}{\varrho_1}\left(\frac{F_0}{F_1}\right)^2 + 1.$$

Here, $p_0, p_1, \varrho_0, \varrho_1, F_0, F_1$ are the static pressure, density, and flow section area at the entrance to and exit from the considered segment. If the total head losses are referred to the flow kinetic energy at some other section F_i, the coefficient of hydraulic resistance is defined by the relation:

$$\zeta_i = \zeta_j^{(0)} \frac{\varrho_i}{\varrho_0}\left(\frac{F_i}{F_0}\right)^2.$$

For isothermal flow, this relation can be reduced to the form:

$$\zeta_i = \zeta_j^{(0)}\left(\frac{F_i}{F_0}\right)^2 \frac{1}{\pi}.$$

Here, the index "0" refers to the section at the entrance to the considered segment, and $\pi = p_0/p_i$.

Experiments made on blades differing in dimensions by more than a factor of two, with $l = 5-10$ in a wide range of regime variation ($p_0 = 20-250$ кПа, T_g = 330 - 1100 K and T_a = 280 - 620 K) [16] showed the following.

1. The total pressure loss in the entrance to the deflector and in its internal cavity does not exceed 3 - 5%. The difference in the pressures within the deflector along its height were within the measurement accuracy limits.

2. For isothermal gas and air flow in the temperature range 300 - 920 K, the leading edge segment hydraulic resistance coefficient, referred to the velocity head at the exit from the holes in the deflector nose for $l = l/d_1 \geqslant 2.0$ (where l is the maximal distance between the holes in the deflector nose and the blade leading edge inner surface, and d_1 is the hydraulic diameter), is practically

independent of the pressure ratio in the limits $\pi \leqslant 3{,}5$ and of the Reynolds number $Re_I = (0{,}15-4{,}0)\cdot 10^4$ based on the air parameters at the exit from the holes in the deflector nose. We take as the defining geometric parameter, the hydraulic diameter of a single hole (slot) at the exit from the deflector $d_1 = 4F_1/\Pi$ and $\zeta_I^{(0)} = 2{,}8-3{,}0$. We assume that segment I (leading edge) terminates where the formation of losses associated with flow turning terminate. This corresponds, as is known, to $\bar{x} = x/\delta_{II} \approx 10$, where δ_{II} is the width of the slot between the deflector and the blade in the concave (convex) part of the profile. /154

For isothermal flow, the hydraulic resistance coefficient dependence on the flow parameters in general form can be written as:

$$[\zeta_I^{(0)}]' = f(Re, Pr, \psi, \psi'),$$

where $\psi = T_b/T_0^*$ — so-called first temperature factor;

$\psi' = T_0^*/\text{const}$ — second temperature factor.

Considering that the coefficient of hydraulic resistance of segment I for isothermal flow is independent of the operating regime parameters, we find its dependence on the cooling air temperature at the entrance to the blade T_0^* and the blade temperature T_b in the form $\zeta_I/\zeta_I^{(0)} = f(T_b/T_0^*)$.

For the stabilized turbulent gas flow regime in a turbine, corresponding to very large Re, this dependence is known [20] in the form:

$$\frac{[\zeta_I^{(0)}]'}{\zeta_I^{(0)}} = \left(\frac{2}{\sqrt{\psi}+1}\right)^2.$$

Analytic description of the turbulent exchange mechanism under conditions applicable to the leading edge is very difficult; therefore this dependence is obtained experimentally — directly from total head loss measurements in this segment with blade temperature variation from 300 to 1100 K. The increase of the leading edge

segment hydraulic resistance with heating is explained primarily by the influence of gas viscosity in the vortical zones which forms at the leading edge. If the air viscosity dependence on its absolute temperature is represented by the first equality (6.12), we can write:

$$\frac{[\zeta^{(0)}]'}{\zeta^{(0)}}=\left(\frac{T_g}{T_0^*}\right)^{0.64} \text{ or } \frac{[\zeta^{(0)}]'}{\zeta^{(0)}}=\varphi^{0.64}.$$

This relation is shown in Figure 6.14. We see that it not only reflects correctly the physical essence of the phenomenon, but also yields quite good agreement with the experimental data.

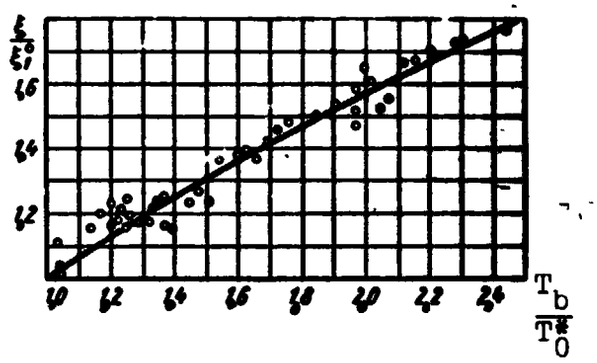

/155

Figure 6.14. Leading edge segment hydraulic resistance versus ratio of blade temperature and cooling air temperature at entrance to the blade

Figure 6.15 shows the relation $\frac{\zeta_{II}}{(l/d)}=f(\mathrm{Re})$ for the concave (convex) middle profile segment, obtained from total head loss measurements for isothermal flow and flow with heat input. Twice the clearance (slot) width is taken as the hydraulic diameter d. Also shown is the relation $\frac{\zeta_{fr}}{(l/d)}=f(\mathrm{Re})$, from [33]. We see that the influence of heating on the frictional resistance is very slight, and can be neglected. The influence of flow turbulization near the leading edge and one-sided heat input caused the turbulent flow regime to extend into the region of small Re (down to Re = 650 for channel aspect ratio $l/d=23$).

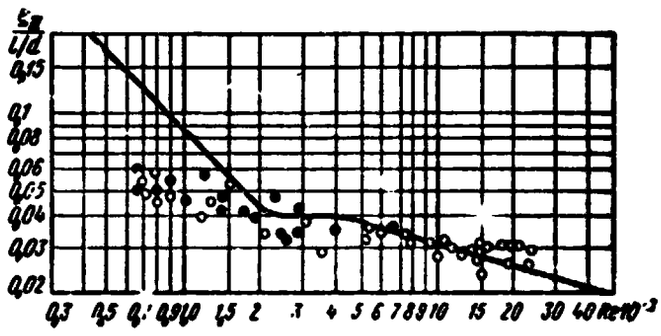

Figure 6.15. Coefficient of hydraulic resistance of blade profile middle segment air channels versus Re:

o — isothermal flow; ● — flow with heating; --- — from [33]

Experimental study of the hydraulic resistance of the channels in the trailing edge in the Re range $1\cdot10^3 \leq Re_{III} \leq 5\cdot10^4$, showed that it is a local resistance and is independent of Re; the value of ζ_{III} depends on the construction and techniques used to obtain the cooling channels, and for variants A, B, C, shown in Figure 6.16, ζ_{III} = 1.05, 0.5, and 1.6, respectively. /156

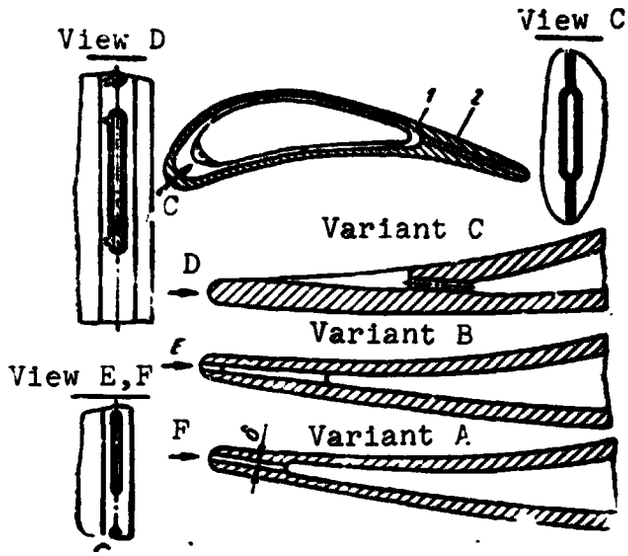

Figure 6.16. Cooled blade trailing edge configurations

The ratio of the cooling air flowrate through the blade for flow with heating G_a' to the flowrate for isothermal flow G_a can be written as:

$$m = \frac{G_a'}{G_a} = \sqrt{\frac{\zeta_I + \zeta_{II} + \zeta_{III}}{\zeta_I + \zeta_{II}' + \zeta_{III}'}} \sqrt{\frac{T_0^*}{T_0^* + \Delta T}}.$$

Here, the hydraulic resistance coefficients are referred to the velocity head at the exit from the blade.

Considering that $\zeta_\Sigma = \zeta_I + \zeta_{II} + \zeta_{III}$; $\zeta_{II}' \approx \zeta_{II}$ (because of their smallness) and $\zeta_{III}' \approx \zeta_{III}$, we obtain:

$$m = \frac{1}{\left[1 + (\zeta_I/\zeta_\Sigma)\left(\frac{T_0^*}{T_0^* + \Delta T}\psi^{0.64} - 1\right)\right]^{0.5}} \sqrt{\frac{T_0^*}{T_0^* + \Delta T}} \qquad (6.19)$$

With account for the fact that: /157

$$\zeta_I = \zeta_I^{(0)}\left(\frac{F_{III}}{F_0}\right)^2 \frac{1}{n}, \qquad (6.20)$$

and $F_0 = F_I$, we can reduce (6.19) to the form:

$$m=\left[1+\frac{\zeta_I^{(0)}}{\zeta_{II}}\left(\frac{F_{III}}{F_I^*}\right)^2\left(\frac{T_0^*}{T_0^*+\Delta T}\psi^{0.64}-1\right)\frac{1}{\pi}\right]^{-0.5}\sqrt{\frac{T_0^*}{T_0^*+\Delta T}}. \qquad (6.21)$$

where ΔT — air temperature rise in the blade.

Then, the cooling air flowrate through the blade:

$$G_a^*=m\mu F_{III}\varphi\frac{p_0^*}{\sqrt{RT_0^*}}.$$

where $\varphi=\sqrt{\frac{2k}{k-1}\left[\left(\frac{p_{III}}{p_0^*}\right)^{\frac{2}{k}}-\left(\frac{p_{III}}{p_0^*}\right)^{\frac{k+1}{k}}\right]}$.

The discharge coefficient μ is determined by the sum of the resistances of all three blade segments. Neglecting compressibility, we can write:

$$\mu=\frac{1}{\sqrt{\zeta_I+\zeta_{II}+\zeta_{III}}}.$$

Correlating the flow parameters at the exit from the concave (convex) profile segment with the flow parameters at the exit from the blade, and considering that the total pressure at the exit from this segment p_{II}^* is equal to the total pressure at the entrance to the cooling channels in the trailing edge, i.e.,

$$\frac{\zeta_{II}}{\zeta_{II}^*}=\frac{F_{III}}{F_{II}}\frac{w_{II}}{w_{III}}=\frac{F_{III}}{F_{II}}\frac{\lambda_{II}}{\lambda_{III}}.$$

where $\lambda=w\Big/\sqrt{\frac{2k}{k+1}RT^*}$,

we obtain:

$$G_a^*=m\varphi F_{III}\left\{\zeta_I^{(0)}\left(\frac{F_{III}}{F_I}\right)^2\frac{1}{\pi}+\left[\zeta_{II}^*\frac{F_{III}}{F_{II}}\frac{\lambda_{II}}{\lambda_{III}}+\zeta_{III}\right]\right\}^{-0.5}\frac{p_0^*}{\sqrt{RT_0^*}}. \qquad (6.22)$$

Here, ζ_{II}'' is the hydraulic resistance coefficient, which can be found from the curve of Figure 6.15, or from the data of [20];

$$T_{II}^*+\Delta T_{II}=T_0^*+\Delta T;$$

T^*_{II} — air temperature at entrance to trailing edge cooling air channel; /158

ΔT_{III} — air temperature rise in trailing edge segment;

the quantity λ is defined by the relation (in gasdynamic functions)

$$q(\lambda_{III})=24.7\frac{G_a\sqrt{T_0^*}}{p_{III}F_{III}};$$

$$q(\lambda_{II})=24.7\frac{G_a\sqrt{T_0^*}}{p_{II}^*F_{II}};\quad p_{II}^*=\left[0.37q(\lambda_{III})\lambda_{III}\zeta_{III}+\frac{1}{\pi(\lambda_{III})}\right]p_{III};$$

λ_{III} and $\pi(\lambda_{III})$ — found from gasdynamic function tables.

The magnitudes of the air temperature rise in the blade ΔT and in the profile segments ΔT_{II} and ΔT_{III} are specified on the basis of preliminary calculations, and are refined during detailed thermal analysis of the blade.

The air flowrate appears in implicit form in the right side of (6.22), and is determined by successive approximations.

If we consider blades in which the flow characteristics are determined by the leading edge segment hydraulic resistance, then for sufficiently high temperatures T_0^*, T_g, T_b and pressure p_{III}:

$$\zeta_I^{(0)}\left(\frac{F_{III}}{F_I}\right)^2\frac{1}{\pi}\gg\zeta_{III};\ m\approx\text{const}$$

and

$$\frac{G_a\sqrt{T_0^*}}{p_{III}F_{III}}=f'(\pi)\ \text{or}\ \frac{G_a\sqrt{T_0^*}}{p_0^*F_{III}}=f''(\pi).$$

In many existing blade designs with deflectors, the friction losses in the cooling channels of the middle part of the blade are small. Then the reduced cooling air flowrate, referred to parameters at the blade exit, will be:

$$\bar{G}_a=\frac{G_a\sqrt{T_0^*}}{mp_{III}F_{III}}\left[\zeta_I^{(0)}\left(\frac{F_{III}}{F_I}\right)^2\frac{1}{\pi}+\zeta_{III}\right]^{0.5}=f(\pi). \qquad (6.23)$$

C-3

This relation is normally used for correlating experimental data when determining the flow characteristics of cooled blades.

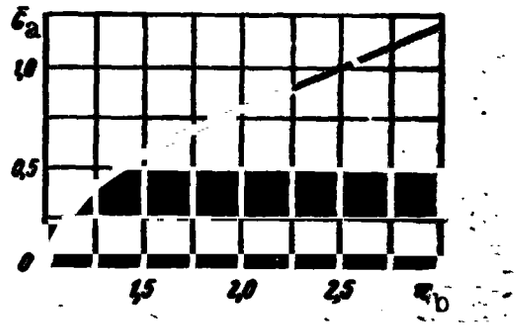

Figure 6.17. Cooling air flowrate (referred to parameters at the exit) through the internal channels of a blade with deflector, obtained from results of tests with heating

The curve of Figure 6.17 shows this experimentally confirmed relation. typical for deflector-type blades, where the $\bar{G}_a$ scale is magnified by a factor of ten.

It is well known that rotor rotation influences the hydraulic resistance in cooling systems. Rotor rotation causes compression of the air in the blade, and also the appearance of mass forces as a result /159 of centripetal and Coriolis accelerations. However, rotor rotation can be neglected for blades of the configuration examined here [16]. This has been confirmed by the results of comparative tests (under static and rotating conditions) of three turbine rotors differing in dimensions.

Thus, the relations obtained make it possible to determine the shape and dimensions of the cooling air channels in blade design, and also make it possible to perform check calculations, including those for existing blades, in different gas turbine engine operating regimes.

6.5. Determining Cooled Blade Temperature

6.5.1. Example of rotor blade temperature calculation

We shall use the relations presented in the preceding sections to determine cooled rotor blade temperature in the engine operating regimes determined by its operational conditions.

The basic data for the calculation are: cooling air and gas parameters, obtained from gasdynamic analysis of the turbine with account for heating of the air in the system supplying the air to the blade and for the gas temperature field averaged for the radius at which the blade section being analyzed is located; section geometric characteristics, including profile cascade and cooling channel dimensions. These parameters are shown in Table 6.1.

TABLE 6.1.*

Parameter	Symbol	Dimension
Diameter of blade mean section	D_m	0,8 m
Length of blade profile part (airfoil)	h	$95 \cdot 10^{-3}$ m
Area of annular section at bladed cascade inlet	$F_{gI}=\pi D_m h$	0,239 m²
Hydraulic diameter of leading edge	$d_{gI}=\frac{2L}{\pi}$	$4,0 \cdot 10^{-3}$ m
Area of holes in deflector	$F_{aI}=\delta_I k_I$	$30,0 \cdot 10^{-6}$ m²
Hydraulic diameter of holes in deflector	$d_{aI}=\frac{2\delta_I k_I}{k_I+\delta_I}$	$1,0 \cdot 10^{-3}$ m
Maximum distance from leading edge inner surface to deflector holes	l	$5,0 \cdot 10^{-3}$ m
Reduced leading edge outer radius	$R=\frac{L}{\pi}$	$2 \cdot 10^{-3}$ m
Reduced leading edge inner radius	$r=\frac{L_I}{\pi}$	$0,70 \cdot 10^{-3}$ m
Characteristic dimension of blade middle segment (profile chord)	$d_{g\ II}$	$50,0 \cdot 10^{-3}$ m
Profile cascade interblade channel throat area	$F_{g\ II}$	0,12 m²
Hydraulic diameter of gap between deflector and blade inner surface	$d_{aII}=2\delta_{II}$	$1,1 \cdot 10^{-3}$ m

(Table continued on following page)

TABLE 6.1. (continued)

Parameter	Symbol	Dimension
Cross section area of gaps between deflector and blade	$F_{aII}=2b_{II}h_{II}$	$99,0\cdot10^{-6}$ м²
Slot area in blade trailing edge	$F_{aIII}=b_{III}h_{III}$	$45,0\cdot10^{-6}$ м²
Hydraulic diameter of slots in trailing edge	$d_{aIII}=\frac{4F_{III}}{H}$	$1,19\cdot10^{-6}$ м
Slot width in blade trailing edge	b_{III}	$0,6\cdot10^{-3}$ м
Blade wall thickness in middle segment	δ	$1,8\cdot10^{-3}$ м
Geometric entrance angle	β°_{1g}	69°
Geometric exit angle	β°_{2g}	39°
Number of blades	z	82

*Translator/s note. Commas in numbers represent decimal points.

Note. h_I, h_{II}, h_{III} are the length over which holes are located /161
in the deflector, the deflector length inside the blade, and the length of the slot in the trailing edge, respectively.

We take from the gasdynamic analysis the required data, corresponding to the turbine operating regime for which the blade temperature is to be calculated.

The gas flowrate through the first (cooled) turbine stage stator is G_s = 157 kg/s, and since the air which cools the stator vanes enters the main stream, the flowrate through the rotor blades will be greater and in the considered example G_r = 160 kg/s, i.e., approximately 2% of the gas flowrate is used to cool the stator vanes.

The mass-average turbine stator inlet gas temperature T_3^* = 1373 K, the temperature in the relative motion at the rotor blade entrance T^*_{1w} = 1246 K, the air temperature at the compressor outlet, where it

is taken for blade cooling $T_k^* = 710$ K, and the air temperature at the engine entrance $T_H^* = 313$ K.

The pressure ratios in the rotor blade cooling system π_{cool} and in the turbine stage π_T are approximately the same and equal to 2.28.

The temperature T_g of the gas approaching the rotor blades, which is used in determining the blade temperature, differs from the total gas temperature in the relative motion $T_{1\,w}^*$ by a magnitude equal to the difference between the temperature averaged over the diagram at the given radius T_g^* and the mass-average temperature T_3^*, which is characterized by the quantity $\tau\% = \frac{T_3^* - T_g^*}{T_3^* - T_k^*} 100 = \frac{\Delta T_{diag}}{T_3^* - T_k^*} 100$,

on the one hand, and by the amount of added air which has cooled the stator vanes, on the other hand.

With accuracy to equality of the air and gas specific heats, we can write: /162

$$T_{mix}^* = \frac{T_3^* + \bar{G}_S T_k^*}{1 + \bar{G}_S}, \quad \text{and} \quad (T_{1\,w}^*)_{mix} = T_{mix}^* - \Delta T_w \frac{T_{mix}^*}{T_3^*},$$

where $\Delta T_w = T_3^* - T_{1w}^*$; $\bar{G}_S = \frac{(G_a)_S}{G_g}$.

Then, the temperature of the gas approaching the rotor blades $T_g = (T_{1\,w}^*)_{mix} + \Delta T_{diag}$.

For our example, $\tau = 5.0\%$; then,

$$T_{mix}^* = \frac{1373 + 0{,}02 \cdot 710}{1 + 0{,}02} = 1360\ \text{K}; \quad (T_{1w}^*)_{mix} = 1360 - 127 \frac{1360}{1373} = 1234\ \text{K}$$

and

$$T_g = 1234 + \frac{1373 - 313}{100} 5{,}0 = 1287\ \text{K}.$$

Along the path to the rotor blades, the cooling air is heated in the supply channels because of heat input from the more highly heated elements with which the air comes into contact, which experience shows amounts to 10 - 20°, and as a result of addition to the air of the work expended in giving the air a velocity equal to the blade circumferential velocity. For circumferential velocity at the mean blade section u = 340 m/s, this temperature rise is $\Delta T = \frac{340^2}{2815} = 50°$. Thus, we can consider that the temperature of the cooling air approaching the blade T_a = 710 + 20 + 50 = 780 K.

We could reduce the cooling air temperature by swirling it in the direction of rotation of the rotor blades. This swirling of the air is accomplished during its expansion in a profile cascade analogous to the stator ring. Here, part of the available pressure difference is expended in the cascade which swirls the air, and the remainder is expended in overcoming the hydraulic resistance of the channels through which the air flows.

Therefore, use of such a cascade, if there are no limitations of constructional or technological nature, is advisable if there is a pressure differential sufficient to ensure the air flowrate through the blades required for their cooling.

If the cooling air passing through the preswirl cascade is imparted a velocity such that its circumferential component is equal to the circumferential velocity of the disk rim at the location of the channels supplying the air to the root part of the blade, then the cooling air temperature decreases by 35° (u = 280 m/s and $\alpha_{1\,p}$ = 10°), which corresponds to temperature reduction in comparison with absence of swirl by about 70°.

Taking in the present example $\mu_I \approx \mu_{III}$ (see section 6.4), and specifying the relative cooling air flowrate in the considered regime equal to 1.6%, we find the parameter groups appearing in the functional relations (6.13), (6.15), (6.17):

$$\mathcal{F}_I = \left(\frac{F_{g_I}}{zF_{a_I}}\right)^{0.71} \frac{d_{g_I}^{0.29}}{l^{0.306}} \left(\frac{F_{g_{II}}}{F_{a_I}}\right)^{0.306} = \left(\frac{0.239}{82\cdot 30\cdot 10^{-6}}\right)^{0.71} \times$$

$$\times \frac{(4.0\cdot 10^{-3})^{0.29}}{(5.0\cdot 10^{-3})^{0.306}} \left(\frac{45\cdot 10^{-6}}{30\cdot 10^{-6}}\right)^{0.306} = 29.6;$$

$$Re_{g_I} = \frac{G_{g_I} d_{g_I}}{F_{g_I}\mu_g} = \frac{160\cdot 4\cdot 10^{-6}}{0.239\cdot 4.9\cdot 10^{-7}} = 54.5\cdot 10^3;$$

$$\bar{G}_{cool} Re_{g\ I}^{0.21} \mathcal{F}_I = 1.6\,(54.5\cdot 10^3)^{0.21}\, 29.6\cdot 10^{-2} = 4.73.$$

In most cooled blades encountered in practice, we can assume adequate accuracy (~2%) that $K_{\theta I} \approx r/R$. Then, for the considered blade /163

$K_{\theta I} = 0.35$, and we find from Figure 6.11, $\theta_I \left(\frac{T_g}{T_a}\right)^{0.306} = 0.41$, since $\left(\frac{T_g}{T_a}\right)^{0.306} = \left(\frac{1287}{780}\right)^{0.306} = 1.167$, then $\theta_I = \frac{0.41}{1.167} = 0.352$.

This corresponds to a blade leading edge temperature:

$$T_b = T_g - \theta_I(T_g - T_a) = 1287 - 0.352\,(1287 - 780) = 1109\,K.$$

For the middle part of the blade (concave and convex sides)

$$Re_{g\ II} = \frac{G_g d_{g\ II}}{F_{g\ II}\mu_g} = \frac{160\cdot 50\cdot 10^{-6}}{0.12\cdot 4.9\cdot 10^{-7}} = 13.55\cdot 10^5;$$

$$\mathcal{F}_{II} = \left(\frac{F_{g\ II}}{zF_{a\ II}}\right)^{0.8} \left(\frac{d_{g\ II}}{d_{a\ II}}\right)^{0.2} = \left(\frac{0.12}{82\cdot 90\cdot 10^{-6}}\right)^{0.8} \left(\frac{50\cdot 10^{-3}}{1.1\cdot 10^{-3}}\right)^{0.2} = 20.0;$$

$$\bar{G}_{cool} Re_{g\ II}^{0.12} \mathcal{F}_{II} = 1.6\,(13.55\cdot 10^5)^{0.12}\, 20\cdot 10^{-2} = 1.74.$$

We find from Figure 6.12 that $\theta_{II}\left(\frac{T_g}{T_a}\right)^{0.2} = 0.32$, and since $\left(\frac{T_g}{T_a}\right)^{0.2} = \left(\frac{1287}{780}\right)^{0.2} = 1.103$, then $\theta_{II} = \frac{0.32}{1.103} = 0.29$, and the blade temperature will be:

$$T_{b\ II} = T_g - \theta_{II}(T_g - T_a) = 1287 - 0{,}29\,(1287 - 780) = 1140\ \text{K}.$$

For the trailing edge segment:

$$\mathcal{F}_{III} = \left(\frac{F_{g\ II}}{zF_{a\ III}}\right)^{0.8} \left(\frac{d_{g\ II}}{d_{a\ III}}\right)^{0.2} = \left(\frac{0{,}12}{82{\cdot}45{\cdot}10^{-6}}\right)^{0{,}8} \left(\frac{50{\cdot}10^{-3}}{1{,}19{\cdot}10^{-3}}\right)^{0{,}2} = 34{,}2.$$

$$\bar{G}_{cool}\,\mathcal{F}_{III} = 1{,}6{\cdot}34{,}2{\cdot}10^{-2} = 0{,}548.$$

We find from Figure 6.13 that $\theta_{III}(T_g/T_a)^{0.2} = 0.345$, and $\theta_{III} = \frac{0{,}345}{1{,}103} = 0{,}312$, and then the blade temperature:

$$T_{b\ III} = T_g - \theta_{III}(T_g - T_a) = 1287 - 0{,}312\,(1287 - 780) = 1129\ \text{K}.$$

If the temperature of any blade segment is greater than can be allowed on the basis of strength, it can be reduced somewhat by increasing the cooling air flowrate, for example, from 1.6 to 2.0%. In our example, this increases θ_I from 0.29 to 0.335, and reduces the blade temperature by 23°. In order to pass through the blade an additional amount of cooling air above the amount for which it was designed, it is necessary to increase the area of the channel sections limiting this flowrate, after which we check the resulting temperature change on the other blade segments. /164

The blade temperature in regimes differing from that considered can be determined by finding the values of $Re_{g\ I}$, $Re_{g\ II}$, and $\bar{G}_a$ corresponding to the new regime and using the same graphs.

Let us assume that in the cruising regime of interest we have $T_g^* = 1110$ K, $T_a^* = 660$ K, $G_g = 143$ kg/s, and the relative cooling air flowrate remains the same as before $\bar{G}_a = 1.6\%$. Then, by analogy with the preceding discussion:

$$Re_{g\ I} = 48{,}6{\cdot}10^3;\quad \bar{G}_{cool}\,Re_{g\,I}^{0.21}\,\mathcal{F}_I = 1{,}6\,(48{,}6{\cdot}10^3)^{0.21}\,29{,}6{\cdot}10^{-2} = 4{,}56;$$

$$\Theta_I (T_g/T_a)^{0.306} = 0{,}405;\ \theta_I = 0{,}346 \text{ and } T_{g\ I} = 954 \text{ K};$$

$$Re_{g\ II} = 13{,}8 \cdot 10^5;\ \bar{G}_{cool} Re_{g\ II}^{0.12}\ \mathcal{F}_{II} = 1{,}6\,(13{,}8 \cdot 10^5)^{0{,}12}\, 20{,}0 \cdot 10^{-2} = 1{,}74;$$

$$\theta_{II} (T_g/T_a)^{0.2} = 0{,}32;\ \theta_{II} = 0{,}289;\ T_{g\ II} = 980 \text{ K};$$

$$\bar{G}_{cool}\ \mathcal{F}_{III} = 0{,}548;\ \theta_{III} (T_g/T_a)^{0.2} = 0{,}345;\ \theta_{III} = 0{,}312;\ T_{g\ III} = 970 \text{ K}.$$

We see that the resulting blade profile segment temperatures are less than 1000 K. This indicates that they must be considered the first approximation, since for their determination we took $\varepsilon_{II} = \varepsilon_{III} = \varepsilon_{IIII} = 1$. The second and usually sufficient approximation will be determination of the blade temperature with account for the influence of the temperature factor, which for the temperatures $T_{b\ I}$, $T_{b\ II}$, $T_{b\ III}$, obtained in accordance with [4], will be $\varepsilon_{II} = 1{,}07$ and $\varepsilon_{III} = \varepsilon_{IIII} = 1{,}03$.

This refinement does not alter the blade temperature very much (up to 5°), which is already quite low. This makes it possible in the cruising regimes to improve engine economy by cutting off the air supply to the cooled blades. In this case, the maximal temperature on any part of the blade will not exceed the temperature of the gas approaching the blade.

Such termination of the cooling air supply has found application in some aircraft engine designs (see, for example, British patent General Motors No. 1,286,785, 1970).

When discharging the cooling air through slots in the blade trailing edge, the edges themselves must be made considerably thicker than usual, which increases the edge losses. Cooling air discharge through slots in the trailing edge aids considerably in reducing the edge losses. Thus, with discharge through trailing edge slots of an amount of air equal to about 1% of the air flowrate through the interblade channels, the edge loss coefficient ξ_{ed} decreases by about a factor of two in comparison with its value in the absence of discharge [19]. Therefore, complete cutoff of the cooling air is not advisable,

particularly since the possibility of gas leakage into the blades and the associated contamination of the channels and slots through which the cooling air flows is not precluded. /165

It remains to be seen whether the relative cooling air flowrate used in the analysis, with its parameters determined by the engine operating regime, will flow through the blade inner cavity. Relations (6.19) - (6.22) make it possible to determine the cooling air flowrate through the blade for given blade geometry and air parameters. For this, we need to know the magnitude of the air temperature rise in the heat exchange process, which is determined from detailed calculation of the blade temperature.

This calculation was not made in the example cited above. Therefore, we can specify the magnitude of the air temperature rise in the blade, which in the practical range of variation of relative cooling air flowrates 1.5 - 2.5% and surface thermal flux densities q = (12 - 16) $\cdot$ 10^5 W/m^2 amount to 150° - 250° (for the stator vanes — 250° - 350°). Then, we determine the cooling air flowrate using (6.23). We shall calculate the quantities appearing in this expression.

According to (6.20), the hydraulic resistance coefficient in the leading edge region:

$$\zeta_l = \zeta_l^{(0)} (F_{a\ III}/F_{a\ I})^2 \frac{1}{\pi_b} = 3\left(\frac{45\cdot 10^{-6}}{30\cdot 10^{-6}}\right)^2 \frac{1}{2{,}28} = 2{,}96,$$

where π_b = 2.28 — ratio of the cooling air pressure at the entrance to the blade to the pressure at the exit from the blade.

For cooling air discharge through the blade trailing edge slots, this is the ratio of the pressure at the entrance to the blade to the pressure downstream of the stage, equal in practice to the pressure ratio developed across the stage, i.e., $\pi_b \approx \pi_T$.

Using Figure 6.15, we find the hydraulic resistance coefficient in the middle segment of the blade. For

$$Re_{a\ II} = \frac{G_a d_{a\ II}}{zF_{a\ II}\mu} = \frac{2{,}56\cdot 1{,}1\cdot 10^{-3}}{82\cdot 90\cdot 10^{-6}\cdot 36{,}8\cdot 10^{-6}} = 10{,}38\cdot 10^3; \quad \frac{\zeta^{\bullet}_{II}}{l/d} = 0{,}031;$$

and

$$\zeta^{\bullet}_{II} = 0{,}031\,\frac{l}{d_{aII}} = 0{,}031\,\frac{0{,}66\cdot 50\cdot 10^{-3}}{1{,}1\cdot 10^{-3}} = 0{,}93.$$

$$g(\lambda_{III}) = 24{,}7\,\frac{0{,}0312\sqrt{780}}{45\cdot 10^{-6}\cdot 0{,}54\cdot 10^6} = 0{,}886$$

$$\lambda_{III} = 0{,}535;\ \pi(\lambda_{III}) = 0{,}843;$$

$$p^{\bullet}_{II} = 0{,}54\cdot 10^6(0{,}37\cdot 0{,}886\cdot 0{,}535\cdot 1{,}5 + 1/0{,}843) = 0{,}783\ \text{MPa};$$

$$q(\lambda_{II}) = 24{,}7\,\frac{0{,}0312\sqrt{780}}{0{,}783\cdot 10^6\cdot 90^{-6}} = 0{,}305;^{*}$$

$$\lambda_{II} = 0{,}197;\quad \zeta_{II} = 0{,}93\cdot\frac{45\cdot 10^{-6}}{90\cdot 10^{-6}}\cdot\frac{0{,}197}{0{,}535} = 0{,}17.$$

Here we have assumed that the segment in which the channels between the deflector and blade inner surface are located amount to 66% of the profile chord.

The hydraulic resistance coefficient of all the internal blade channels $\zeta_2 = \zeta_I + \zeta_{II} + \zeta_{III} = 2{,}96 + 0{,}17 + 1{,}5 = 4{,}63$.

In accordance with (6.21), the ratio of the air flowrates through the blade for flow through the blade heated by the gas and for isothermal flow when $T_g = T_a = T_b$, will be:

$$\dot{m} = \frac{\sqrt{T^{\bullet}_0/(T^{\bullet}_0 + \Delta T)}}{\left\{1 + \frac{\zeta^{(0)}}{\zeta_2}\left(\frac{F_{aIII}}{F_{aI}}\right)^2\left[\frac{T_a}{T_a + \Delta T}\left(\frac{T_b}{T_a}\right)^{0{,}64} - 1\right]\frac{1}{\pi_b}\right\}^{0{,}5}} =$$

$$= \frac{\sqrt{780/930}}{\left\{1 + \frac{3{,}0}{4{,}63}\left(\frac{45\cdot 10^{-6}}{30\cdot 10^{-6}}\right)^2\left[\frac{780}{930}\left(\frac{1100}{780}\right)^{0{,}64} - 1\right]\frac{1}{2{,}28}\right\}^{0{,}5}} = 0{,}9.$$

From Figure 6.17, for $\pi_b = 2.28$, we find $\bar{G}_a = 0.09$, and using (6.23): /166

---

*Translator's note. In this equation, the last term of the denominator (90^{-6}) should correctly be $90 \cdot 10^{-6}$.

$$G'_a = \frac{m\bar{G}_{a\,I}\,{}_{II}F_{III}}{\sqrt{T_a}\left[\zeta_I^{(0)}\left(\frac{F_{a\,III}}{F_{a\,I}}\right)^2\frac{1}{\pi_g} + \zeta_{III}\right]^{0,5}} =$$

$$= \frac{0,9\cdot 0,09\cdot 0,54\cdot 10^6\cdot 45\cdot 10^{-6}}{\sqrt{780}\left[3\cdot\left(\frac{45\cdot 10^{-6}}{90\cdot 10^{-6}}\right)^2\frac{1}{2,28} + 1,5\right]^{0,5}} = 0,0334\,\text{kg/s}$$

$$\bar{G}_{cool} = \frac{G'_{az}}{G_g}\,100\% = \frac{0,0334\cdot 82}{160}\,100 = 1,71\%.$$

Here, $\Delta T = 150°$ — air temperature rise in the blade;

$$p_{III} = p^*_g/\pi_b = \frac{1,23\cdot 10^6}{2,28} = 0,54 \text{ MPa}.$$

If 20° larger air temperature rise were used in the calculation, i.e., $\Delta T = 180\,K$, the relative cooling air flowrate would be 1.67%.

This result indicates that the cooling air flowrate used in calculating the blade temperature actually will flow through the blade.

In cooled blade design practice, we may encounter cases in which it will be difficult to evaluate the magnitude of the air temperature rise in the blade, or in which more exact determination of the relative cooling air flowrate will be required. Then it is necessary to utilize (6.22) which, in turn, requires — as noted previously — detailed calculation of the heat exchange process in the blade.

This problem can be solved more simply using the dependence of the ratio (m) of the cooling air flowrates through the blade for isothermal flow and under real blade operating conditions on the temperature of the air and the blade, obtained as a result of experimental study of cooled blades with air pressure ratio $\pi_b \approx 2.2 - 2.5$ (Figure 6.18).

To this end, we calculate the flow characteristic of the blade of given dimensions with isothermal flow; from it, we determine the unheated (cold) air flowrate $G_{a\ cold}$ for the pressure ratio corresponding to the conditions under which the blade operates, and /167

introduce a correction to the value of m taken from Figure 6.18. The calculation sequence is as follows.

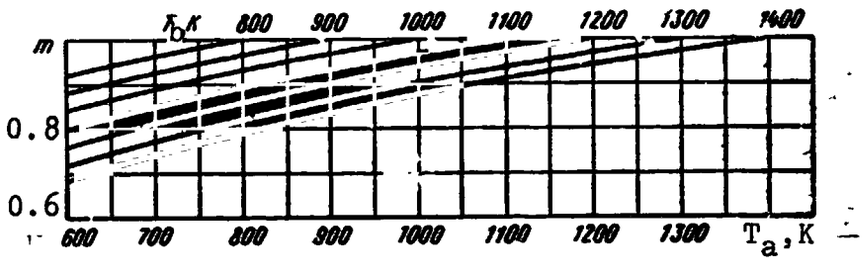

Figure 6.18. Coefficient m as function of blade temperature and cooling air temperature for π_b = 2.2 - 2.5 and $p_2 \geqq B_0$

We take various pressure ratios and, assuming that the exit pressure is barometric (ISA) and the air temperature T_a = 288 K, find the air flowrate through the blade from the equation:

$$G_{a\ cold} = \mu m\ (p_a^*/\sqrt{T_a^*})F_{a\ III}q(\lambda)\ \text{kg/s for } k = 1.4,\ m = 0.0404.$$

We determine the coefficient of air flowrate through the blade, neglecting the hydraulic resistance in the middle segment of the blade because of its smallness, from the relation:

$$\mu = \frac{1}{\left[\zeta^{(0)}\left(\frac{F_{a\,III}}{F_{a\,I}}\right)^2 \frac{1}{\pi_b} + \zeta_{III}\right]^{0,5}} = \frac{1}{\left[3\left(\frac{45,0\cdot 10^{-6}}{30\cdot 10^{-6}}\right)^2 \frac{1}{\pi_b} + 1,5\right]^{0,5}}.$$

The calculation data are summarized in Table 6.2, and are represented graphically in Figure 6.19.

The cooling air flowrate through a single blade for G_{cool} = 1.6% in the design regime, reduced to the design parameters: /168

$$\bar{G}_a = \frac{G_a\sqrt{T_a}}{p_{III}\pi_b} = \frac{0,0312\sqrt{780}}{0,54\cdot 2,28\cdot 10^6} = 0,709\cdot 10^{-6}.$$

TABLE 6.2.*

Pressure ratio π_b	1,5	2,0	2,5	3,0
Flow coefficient μ	0,408	0,453	0,485	0,517
Air flowrate $G_{a.cold}$	$6{,}36\cdot10^{-3}$	$9{,}8\cdot10^{-3}$	$12{,}60\cdot10^{-3}$	$15{,}5\cdot10^{-3}$

*Translator's note. Commas in numbers represent decimal points.

Here,

$$G_a = \frac{0{,}016\,Gr}{z} = \frac{0{,}016\cdot160}{82} = 0.0312 \text{ kg/s.}$$

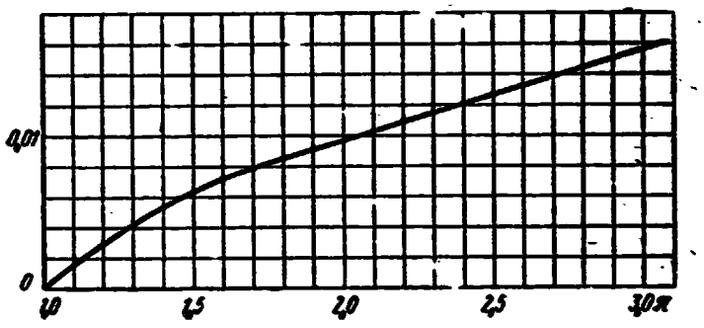

Figure 6.19. Flowrate through internal air cooling channels of analyzed blade with deflector

The difference between the reduced cooling air flowrates through the blade for isothermal flow $G_{a\ cool}$ and for flow with heating G_a' is accounted for by the coefficient m, which for the considered example is equal to 0.89 (see Figure 6.18). Then:

$$\bar{G}_a' - \bar{G}_a/m = \frac{0{,}709\cdot10^{-6}}{0{,}89} = 0{,}796\cdot10^{-6}.$$

Reduced to standard atmospheric conditions (B_0, T_0):

$$G_{a\ ref} = \frac{\bar{G}_a' B_0 \pi_b}{\sqrt{T_0}} = \frac{0{,}796\cdot10^{-6}\cdot1{,}0134\cdot10^5\cdot2{,}28}{\sqrt{288}} \approx 0{,}01[illegible] \text{ kg/s.}$$

Thus, if this air flowrate passes through the blades with the given pressure ratio, then in the design regime the blades will pass the amount assumed in the calculation $\bar{G}_{cool}$ = 1.6%. We see from Figure 6.19 that the air flowrate $G_{a\ cool}$ = 0.0113 kg/s corresponds to the pressure ratio π_b = 2.28. Consequently, an amount of air

which ensures cooling of the blades to the specified temperature will pass through the blades (0,0143>0,0108).

This technique for determining the cooling air flowrate through the blade is less exact than use of (6.22) or (6.23); however, it is adequate for preliminary design calculations and for entry on the blade working drawing. The latter is necessary in order to evaluate the correspondence of the cooling channel flow section areas to those given by the drawing with respect to air flowrate through the finished blade pressure ratio between the blade entrance and exit (for example, $\pi_b = 2.0$). Usually the air flowrate is measured by flow testing a blade positioned in a special adapter using "shop" air, and is compared with the flowrate shown on the drawing.

6.5.2. Example of stator vane temperature calculation

When calculating the stator vane temperature, we determine the gas temperature with account for temperature field nonuniformity at the exit from the combustion chamber. The degree of this nonuniformity is characterized by the coefficient τ, which is the ratio of the difference between the maximal $T^*_{g\ max}$ and mass-average $T^*_{g.mav}$ temperatures to the magnitude of the air temperature rise in the combustion chamber, defined by the temperature difference $T^*_{g.mav} - T^*_k$: /169

$$\tau_{max} = \frac{T^*_{g\ max} - T^*_{g.mav}}{T^*_{g.mav} - T^*_k} .$$

This definition of the degree of gas temperature field nonuniformity at the exit from the combustion chamber assumes that, for constant τ_{max}, the difference between the maximal and mass-average temperatures will be smaller, the less the air is heated in the combustion chamber.

Consequently, if we take an engine regulation law such that with flight speed increase the mass-average turbine inlet gas temperature remains constant, then for a given degree of nonuniformity, the

maximal temperature will decrease. In turn, the quantity τ_{max} also depends on the degree of air temperature rise in the combustion chamber and increases with increase of the latter. This is associated with the fact that the combustion chamber in this case begins to operate with richer mixtures, i.e., with less excess air.

In the considered calculation example, we assume that τ_{max} = 0.25; then $T_g^* = T_{g.mav}^* + \tau(T_{g.mav}^* - T_k^*) = 1373+0.25(1373-710) \approx 1540$ K. The temperature of the cooling air entering the vane with account for temperature rise along the supply path $T_a^* = T_k^* + \overline{20^\circ} = 730$ K.

The vane and internal channel characteristic dimensions in the notations used for the rotor blades are summarized in Table 6.3.

TABLE 6.3.*

Symbol	Dimension	Symbol	Dimension
d_{gI}	$6{,}2\cdot10^{-3}$ м	d_{gII}	$75{,}0\cdot10^{-3}$ м
F_{gI}	0,21 м²	$F_{gII}=F_{gIII}$	0,09 м²
d_{aI}	$1{,}8\cdot10^{-3}$ м	d_{aII}	$1{,}2\cdot10^{-3}$ м
F_{aI}	$55\cdot10^{-6}$ м²	F_{aII}	$70\cdot10^{-6}$ м²
l	$5{,}0\cdot10^{-3}$ м	d_{aIII}	$1{,}1\cdot10^{-3}$ м
r	$2\cdot10^{-3}$ м	F_{aIII}	$36\cdot10^{-5}$ м²
R	$3{,}1\cdot10^{-3}$ м	z	52

Translator's note. Commas in numbers represent decimal points.

To determine the temperature of the characteristic vane segments, we specify the relative cooling air flowrate $\overline{G}_{cool}$ = 1.8%, and by analogy with the rotor blade temperature calculation, we use the functional relations (6.13), (6.15), (6.17), represented graphically in Figures 6.11 to 6.13, respectively. /170

We calculate the quantities appearing in these expressions:

$$\mathcal{F}_I = \left(\frac{F_{gI}}{zF_{aI}}\right)^{0.71} \frac{d_{gI}^{0.29}}{l^{0.305}} \left(\frac{\mu_{III} F_{aIII}}{\mu_I F_{aI}}\right)^{0.305} =$$

$$= \left(\frac{0.21}{52 \cdot 55 \cdot 10^{-6}}\right)^{0.71} \frac{(6.2 \cdot 10^{-3})^{0.29}}{(5.0 \cdot 10^{-3})^{0.305}} \left(\frac{36 \cdot 10^{-6}}{55 \cdot 10^{-6}}\right)^{0.305} = 21.3;$$

$$Re_{g\ I} = \frac{G_{gI}}{F_{gI}} \frac{d_{gI}}{\mu_g} = \frac{157}{0.21} \frac{6.2 \cdot 10^{-3}}{50 \cdot 10^{-6}} = 92.8 \cdot 10^3;$$

$$\bar{G}_{cool} Re_{gI}^{0.21} \mathcal{F}_I = 1.8 (92.8 \cdot 10^{-3})^{0.21} 21.3 \cdot 10^{-2} = 4.22; \quad K_{\phi I} \approx \frac{r}{R} = 0.65.$$

From Figure 6.11, $\theta_I \left(\frac{T_g}{T_a}\right)^{0.305} = 0.52$; $\theta_I = 0.52 \left(\frac{730}{1540}\right)^{0.305} = 0.416$.

Then, $T_{g\ I} = T^*_{g\ max} - \Theta_I (T_{g\ max} - T^*_a) = 1540 - 0.416 (1540 - 730) = 1205$ K; ;

$$\mathcal{F}_{II} = \left(\frac{F_{gII}}{zF_{aII}}\right)^{0.8} \left(\frac{d_{gII}}{d_{aII}}\right)^{0.2} = 29.4; \quad Re_{gII} = \frac{G_g}{zF_{gII}} \frac{d_{gII}}{\mu_g} = 2.62 \cdot 10^3;$$

$\bar{G}_{cool} Re_{gII}^{0.12} \mathcal{F}_{II} = 2.84$. From Figure 6.12, $\theta_{II} \left(\frac{T_g}{T_a}\right)^{0.2} = 0.425$;

$\theta_{II} = 0.425 \left(\frac{730}{1540}\right)^{0.2} = 0.37$ and $T_{b\ II} = 1540 - 0.370 (1540 - 730) = 1240$ K.

$\mathcal{F}_{III} = \left(\frac{F_{gIII}}{zF_{aIII}}\right)^{0.8} \left(\frac{d_{gII}}{d_{aIII}}\right)^{0.2} = 49.8$; $\bar{G}_{cool} \mathcal{F}_{III} = 0.896$ and from Figure 6.13,

$$\theta_{III} \left(\frac{T_g}{T_a}\right)^{0.2} = 0.46; \quad \theta_{III} = 0.46 \left(\frac{730}{1540}\right)^{0.2} = \quad ;$$

$$T_{g\ III} = 1540 - 0.4 \cdot 810 = 1216 \text{ K}.$$

The calculation of the amount of air which flows through the vane is made just as for the rotor blade.

Let us see how much the temperature of the blade segments changes in flight with $M_f = 2.2$ at an altitude of H = 11 km. Here, we neglect the change of the relative cooling air flowrate because of change of the flow regime in the cooling system channels, and consider only the influence of the cooling air temperature, In other words, we consider that the relative cooling air flowrate varies inversely as the square foot of the temperature ratio. Consequently,

$$\bar{G}_{cool.f} = \bar{G}_{cool} \sqrt{\frac{T^*_u}{T^*_{u.f}}} = 1.8 \sqrt{\frac{313}{426}} \cong 1.55\%.$$

The mass-average turbine inlet gas temperature increases and becomes equal to $T^*_{3\ mav}$ - 1395 K, the compressor exit air temperature increases to T^*_k = 823 K, and the degree of gas temperature nonuniformity at the turbine inlet decreases. We assume that τ_{max} = 0.20. /171

Then, $T^*_{g\ max} = T^*_{g\ mav} + \tau(T^*_{g\ mav} - T^*_k) = 1395+0.20(1395-823)=1510$ K.

Thus, the design (maximal) temperature of the gas approaching the stator vanes decreases in comparison with the preceding regime by ∿ 30°. If we neglect the change of the Reynolds numbers $Re_{g\ I}$ and $Re_{g\ II}$, associated with the kinematic viscosity reduction, and the influence of this change on the magnitude of the dimensionless groups plotted on the abscissa axes of Figure 6.11 and 6.12, where they appear to the powers 0.21 and 0.12, respectively, we find that the values of these groups vary in proportion to the relative air flowrate.

Consequently,

$$(\bar{G}_{cool} Re_{g\ I}^{0.21} \mathcal{F}_I)_f = 4.22 \frac{1.55}{1.8} = 3.63;$$

$$\theta_I \left(\frac{T_g}{T_b}\right)^{0.306} = 0.49;\ \theta_I = 0.49 \left(\frac{823}{1510}\right)^{0.306} = 0.408.$$

Then, the blade leading edge temperature will be $T_{b\ I} = 1510-0.408\cdot 687 = 1230$ K, i.e., it decreases by 25°.

For the middle part of the blade:

$$(\bar{G}_{cool} Re_{g\ II}^{0.12} \mathcal{F}_{II})_f = 2.84 \frac{1.55}{1.8} = 2.44;\ \theta_{II} \left(\frac{T_g}{T_b}\right)^{0.2} = 0.39$$

and $\theta_{II} = 0.346$, and $T_{b\,II} = 1510-0.346\cdot 687 = 1273$ K also increases by 33°. And for the blade trailing edge, $\bar{G}_{cool} \mathcal{F}_{III})_f$ = 0.77; $\theta_{III}(T_g/T_b)^{0.2}$ = 0.42; θ_{III} = 0.372, and $T_{b\ III}$ = 1255 K, which exceeds the temperature of the trailing edge segment in comparison with the stand regime by ∿ 40°.

This example shows how we can determine the cooled blade temperature in various engine operating regimes using the relations (6.13), (6.15), and (6.17).

These relations make it possible to evaluate the influence on cooling effectiveness of deviations of the blade element characteristic dimensions from the values used in the design, which is very important for selecting methods for inspecting the blades and justifying the magnitude of the allowable deviations during blade manufacture. Let us assume that when fabricating the stator vane, whose calculation was made as the example, the clearance δ_{II} between the vane inner surface and the deflector in the blade concave and convex segment increases by 0.2 mm. Increase of this clearance does not influence the blade flow characteristic, since in this case the section limiting the air flowrate through the cooling channels is the section at the blade trailing edge, and the change of the considered blade segment resistance does not have any marked influence on the flow coefficient , since it is very small in comparison with the hydraulic resistance of the leading and trailing edges. Consequently, the relative cooling air flowrate remains unchanged with this variation of the clearance δ_{II}. Only the blade geometric characteristic changes, which is reflected in the parameter $\mathcal{F}_{II}$, which includes $d_{a\ II}$ and $F_{a\ II}$.

For the new values $d_{a\ II} = 1.6 \cdot 10^{-3}$ m, and $F_{a\ II} = 93.5 \cdot 10^{-6}$ /172
m^2; $\mathcal{F}_{II} = 14.1$, $\bar{G}_{cool} Re_{g\ II}\ \mathcal{F}_{II} = 1.36$. This corresponds (see Figure 6.12) to $\theta_{II}(T_g/T_a)^{0.2} = 0.270$, and $\theta_{II} = 0.249$, and the blade temperature $T_b = T_g^* - \theta_{II}(T_g^* - T_a^*) = 1346$ K. Thus, the blade temperature in the considered segment increases by 70° in comparison with the design value $\delta_{II} = 0.6$ mm.

Increase of the deflector hole size in comparison with the design value would have still greater influence on the blade temperature in the leading edge region. For example, with increase of the width

of these holes by only 0.2 mm, their area would increase by 25%, and the hole hydraulic diameter $d_{a\ I}$ would increase by approximately the same percentage, while the group $\bar{G}_{cool} Re_{g\ I}^{0.21} \mathcal{F}_I$ would decrease from 4.22 to 3.34. Here, we have considered that increase of δ_I in the indicated limits has practically no influence on the cooling air flowrate change. The value of $\theta_I (T_g/T_a)^{0.306} = 0.475$, obtained from Figure 6.11, in this case corresponds to $\theta_I = 0.379$ and $T_{b\ I} =$ 1233 K, i.e., the leading edge will have a temperature 30° higher.

We see from these examples the severity of the requirements which must be imposed on cooled blade fabrication accuracy.

CHAPTER VII

DEGREE OF LOADING OF TURBINE STAGE WITH COOLED BLADES

7.1. Cooled Blade Temperature as Function of Stage Loading Coefficient

To determine the temperature of the gas flowing over the turbine rotor blade as a function of the magnitude of the loading coefficient, characterizing the turbine stage loading, we use (3.11), writing it in the form: /173

$$(T_w^*)_1 = T_0^* - \frac{a_1^2}{2\frac{k}{k-1}R}\left(\mu_1 \frac{2K_a}{K_a+1} + 1\right).$$

hence the difference between the total gas temperature ahead of the stator and the total gas temperature in the relative flow approaching the rotor blade will be

$$\Delta T_w = T_0^* - (T_w^*)_1 = \frac{a_1^2}{2\frac{k}{k-1}R}\left(\mu_1 \frac{2K_a}{K_a+1} + 1\right). \tag{7.1}$$

We see from these expressions that the larger μ_1, the larger ΔT_w and the lower the temperature of the gas approaching the rotor blade for a fixed value of T_0^*.

We can increase the turbine stage loading either by reducing the circumferential velocity, i.e., for example, we can for fixed rotor rotational speed, frequently determined by the compressor, reduce the turbine diameter, or, for fixed circumferential velocity, we can increase the work extracted per kilogram of gas flowing through the turbine.

In both cases, the load coefficient $\mu_i = L_T/u^2$ will increase. Obviously, if the load coefficient is increased by reducing the circumferential velocity, the temperature of the gas approaching the blades will not decrease, but will increase because of the fact that ΔT_w will decrease. Therefore, there is no need to examine this case, since it is not encountered in practice.

Increase of the load coefficient for fixed value of the circumferential velocity will always lead to increase of ΔT_w, and therefore reduction of T_w^*. /174

Figure 7.1 shows the variation of $(\Delta T_w)_i = (\Delta T_w)_i/(\Delta T_w)_{i0}$ with increase of the load coefficient from $\mu_{i0} = 2.0$, which corresponds to $(\Delta T_w)_{i0}$, to $\mu_i = 2.6$. Here, the coefficient $K_a = c_{1a}/c_{2a}$ is taken equal to unity, i.e., we assume that with increase of the load coefficient, the magnitude of the reaction at the inner diameter of the considered stage remains unchanged and close to zero. If K_a has a value differing from one ($K_a < 1$), the relative temperature change $(\Delta T_w)_i$ will be smaller than shown in Figure 7.1, and if necessary, it can be considered.

We see from Figure 7.1 that with increase of the turbine stage loading by 20%, i.e., for $\mu_i = 2.4$, the relative temperature reduction is 13%. If we take, for example, $u_i = 400$ m/s, the temperature reduction of the gas approaching the rotor blades will be 27°, while for $u_i = 300$ m/s, the reduction will be only 15° (Figure 7.2). If

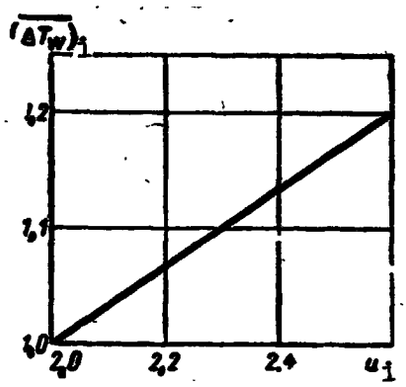

Figure 7.1. Relative differences between gas temperatures ahead of turbine and on rotor blade as a function of the load coefficient

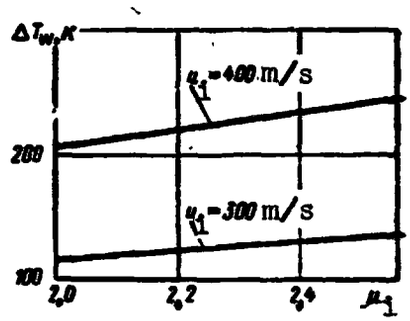

Figure 7.2. Temperature difference ΔT_w as function of load coefficient

the blade were uncooled, then with accuracy to constancy of the recovery coefficient its temperature would decrease by the same amount.

As is well known, the cooled blade temperature variation does not follow directly the temperature variation of the gas flowing over the blade, but rather depends on the ratio of the gas and air temperatures and on the cooling intensity.

For a given turbine operating regime, characterized in the present case by the temperatures of the gas T_w^*, and of the cooling air /175
T_i^*, this relationship is defined by the ratio $\theta = (T_w^* - T_b^*)/(T_w^* - T_i^*)$, which with account for (7.1) can be transformed to

$$T_b = (1-\theta)(T_0^* - \Delta T_w) + \theta T_i^*, \qquad (7.2)$$

where T_0^* — stator inlet gas temperature.

We see from (7.2) that the smaller the cooling intensity θ, the more the blade temperature T_b decreases for fixed T_0^* and T_i^* with increase of the turbine degree of loading, i.e., with increase of ΔT_w. However, the absolute blade temperature will increase.

For example, for $T_0^* = 1490$ K, $T_i^* = 810$ K, $u_i = 400$ m/s, $\mu_{i0} = 2.0$ and $\theta = 0.5$, the blade temperature will be 1046 K. With increase of the loading coefficient μ_i by 20%, ΔT_w increases by 13% (see Figure 7.1), and the blade temperature will be $T_b = 1033$ K, i.e., it decreases by 13°. If, with all other conditions remaining the same, the cooling intensity were $\theta = 0.4$, when $T_b = 1093$ K, then increase of the stage loading by the same 20% would lead to blade temperature reduction from 1093 to 1077 K, i.e., by 16°. We see that in this case the absolute blade temperature increased by $\sim 45°$.

In this example, we assumed that with increase of the loading coefficient, the cooling intensity remains fixed and equal to its value for $\mu_{i0} = 2.0$. In reality, increase of the loading on the turbine stage with cooled blades is accompanied by increase of the cooling intensity θ. This is explained primarily by the fact that with increase of the loading, the gas expansion ratio π_{st} in the stage increases, and consequently the pressure ratio π_{cool} in the cooling system increases. Therefore, for fixed form and dimension of the channels through which the cooling air flows, its velocity increases. The air flowrate increases in proportion to the velocity increase, since the hydraulic resistance of the cooling channels remains practically unchanged (see section 6.4).

The relative expansion ratio $\bar{\pi}_{st} = \pi_{st}/\pi_{st0}$ is shown in Figure 7.3 as a function of turbine stage loading. In constructing this figure, we considered the variation of the stage efficiency with increase of μ_i, in accordance with Figure 2.3. /176

The dependence of the cooling intensity of the various blade segments along the profile contour of the blade with internal deflector on the relative cooling air flowrate is characterized by the curves shown in Figures 6.10, 6.11, and 6.12. If we use these curves, the dependence of the relative gas expansion ratio in the

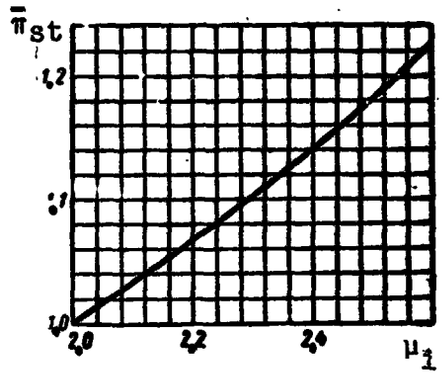

Figure 7.3. Relative gas expansion ratio in turbine stage as function of loading coefficient

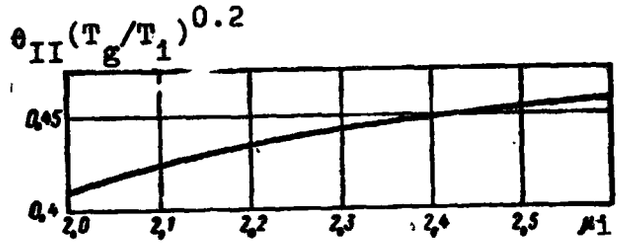

Figure 7.4. Blade profile middle segment cooling intensity as function of loading coefficient

stage $\bar{\pi}_{st}$ on the magnitude of the loading coefficient μ_i, and the flow characteristic of the considered blade $\bar{G}_i = f(\pi_{cool})$ (see Figure 6.17), then with accuracy to constancy of $Re_{g\,I}^{0.21}$ and $Re_{g\,II}^{0.12}$ we can obtain the dependence of the cooling intensity θ on the magnitude of the loading coefficient.

This dependence for the middle blade segment along the profile contour (concave and convex part) is shown in Figure 7.4.

Consequently, in order to determine the degree to which we can reduce the cooled blade temperature by increasing the turbine stage degree of loading, we must substitute into (7.2) the value of θ corresponding to the change $\Delta T_w = f(\mu_i)$.

We shall show this by an example.

Assuming that in the engine operating regime which determines the minimal allowable cooled blade strength margin, the turbine inlet gas temperature $T_0^* = 1550\,K$, the blade cooling air temperature $T_i^* = 810\,K$, the circumferential velocity at the turbine rotor inner diameter (at the blade root section) u_i = 400 m/s, and the loading coefficient μ_i = 2.0.

In accordance with (7.1), the difference between the temperatures of the gas flow ahead of the turbine stator T_0^* and the gas

flow approaching the rotor blades $(T_w^*)_i$ for $K_a = 1.0$ (i.e., the maximal temperature difference)*

$$\Delta T_w = \frac{400^2}{2\frac{1,3}{1,3-1}\cdot 288,4}(2,0+1) \cong 210\,\text{K},$$

and

$$(T_w^*)_1 = T_g = 1550 - 210 = 1340\,\text{K}.$$ /177

From Figure 7.4 for $\mu_i = 2,0\ \theta_{II}\left(\frac{T_g}{T_1}\right)^{0,3} = 0,41$; hence,

$$\theta_{II} = \frac{0,41}{(1340/810)^{0,3}} = 0,371.$$

Then, in accordance with (7.2), the blade temperature will be $T_b = (1-0,371)\ (1550-210)+0,371\cdot 810 = 1144\,\text{K}$.

If we make such calculations for different values of μ_i, we can determine the cooled blade temperature variation as a function of μ_i, represented graphically in Figure 7.5 (in the present case, for the middle segment of the blade profile). We see from this figure that with increase of μ_i by 20% (from $\mu_{i0} = 2.0$ to $\mu_i = 2.4$), the blade temperature decreases, not by 13 or 16° as in the preceding example, but rather by 34°.

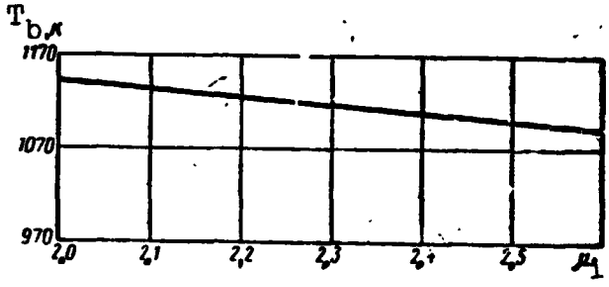

Figure 7.5. Cooled blade temperature as function of loading coefficient

This rotor blade temperature reduction would make it possible to increase the turbine inlet gas temperature if this is permitted by stator vane strength. This increase of the gas temperature can be determined using Figures 7.2 and 7.4 and Equation (7.2),

*The notations are the same as in Chapter VI: $T_w^* = T_g$; $T_i^* = T_i$.

reducing the latter to the form:

$$T_0^* = \frac{(T_g + \Delta T_w) - \theta(T_1 + \Delta T_w)}{1 - \theta}.$$

Then, for $\mu_1 = 2{,}4$, $\Delta T_w = 235$ and $\theta_{11} = 0{,}407$,

$$T_0^* = \frac{(1144 + 235) - 0{,}407\,(610 + 235)}{1 - 0{,}407} = 1610\,\text{K}.$$

Consequently, since the specified strength margin for blade material temperature equal to 1143 K is ensured, the turbine inlet gas temperature can be increased by $\Delta T = 1610 - 1550 = 60°$.

If this gas temperature increase cannot be used because of stator blade strength considerations, or if this increase is prevented by other circumstances — such as, for example, large temperature field nonuniformity at the exit from the combustion chamber, necessity for introducing cooling of the last turbine stage blades, and so on — then reduction of the rotor blade temperature by increasing the turbine loading may make it possible to reduce the turbine weight while retaining the specified strength margin. 78

However, before utilizing this possibility, we must examine the degree to which the stresses in the blade increase because of the increase of the annular area F_2 swept by the rotor blades, caused by the necessity for retaining the allowable value of the dimensionless velocity λ_{2c} or Mach number M_{2c} at the turbine exit.

7.2. Variation of Cooled Blade Strength Margin with Increase of Stage Loading

Using (3.2) with account for (2.25) and the relation $\eta_T^* = f(\mu_1)$ in accordance with Figure 2.3 for $M_{2c} = 0.5$, we can determine the relative area change $F_2 = F_2/F_{2\,0}$ with increase of the turbine loading. This relative area change in application to the considered example is shown graphically in Figure 7.6, from which we see that with increase of the turbine loading coefficient by 20% from

μ_{10} = 2.0 to μ_1 = 2.4, while retaining M_{2c} unchanged, the turbine exit area F_2 must be increased by 14%. According to (3.5), the stresses from centrifugal force action increase to the same degree. For unchanged ratio of the residual uncompensated bending stresses to the tensile stresses σ_{bend}/σ_t, determined by the ratio G_{max}/G_0 (see Figure 3.4), the overall stresses also increase in direct proportion to the turbine rotor blade exit area increase $\bar{F}_2$. This follows from (3.7), in accordance with which:

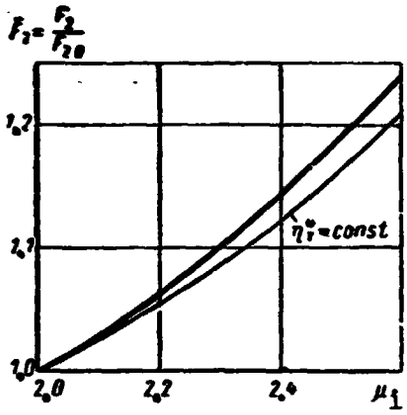

Figure 7.5.. Relative variation of annular area swept by rotor

$$\sigma_\Sigma = \sigma_t(1+m), \tag{7.3}$$

where $m = \sigma_{bend}/\sigma_t$.

In turn, /179

$$\sigma_{bend} = \sigma_{bend}^{(g)} = \sigma_{bend}^{(c)}, \tag{7.4}$$

Here, $\sigma_{bend}^{(g)}$ — bending stresses caused by the bending moments M_g from the gasdynamic forces;

$\sigma_{bend}^{(c)}$ — bending stresses caused by the moments M_c from the centrifugal forces;

σ_{bend} — residual uncompensated bending stresses caused by the gasdynamic and centrifugal forces $M_g - M_c$.

Substituting (7.4) into (7.3) and transforming, we obtain

$$m = \frac{\sigma_{bend}^{(g)}}{\sigma_t}(1 - K), \tag{7.5}$$

where $K = \sigma_{bend}^{(c)}/\sigma_{bend}^{(g)}$.

Consequently, by introducing compensation, we can select that value of K for which the coefficient m will remain constant with change of the quantities $\sigma_{bend}^{(g)}$ and σ_t, associated with variation of μ and L_T.

In most cooled blades, the relative length is small (first turbine stage) and the relative thickness is large, and thus the bending resistance moment is comparatively large, so that the contribution of the uncompensated residual bending stresses to the overall stresses is small. Therefore, constancy of the coefficient m will correspond in practice to the most favorable compensation conditions, for which the strength margin will not be less than the allowable value in the off-design engine operating regimes.

If the bending stresses $\sigma_{bend}^{(g)}$ are relatively high, then under the condition m = const, the absolute uncompensated bending stresses may increase in the other engine operating regimes to such a large magnitude that the overall stresses exceed the allowable values. In these cases, the variation of the allowable residual uncompensated bending stresses must be determined by detailed calculations, which are usually made during production design.

As shown above, reduction of the blade temperature from 1144 to 1110 K by increasing the turbine degree of loading leads to increase of the stresses in the blde by 14%.

For a blade made from the ZhS6-K alloy, for example, we see from Figure 3.5 that such reduction of its temperature increases the ultimate stresses for an engine operating time in the considered regime of 100 hours from $37 \cdot 10^4$ to $43 \cdot 10^4$ kN/m^2, i.e., by 16%. Consequently, in our example, the magnitude of the strength margin in the blade remains practically unchanged.

The lower the hot strength of the material, the more sensitive /180
it is to temperature variation. If the blade were fabricated from a less temperature-resistant alloy — EI929, for example — and had

the required strength margin in the considered temperature range, then for conditions such as those in the considered example, its ultimate stresses would increase from $24.5 \cdot 10^4$ to $32 \cdot 10^4$ N/m^2, i.e., by 30%. This could be used either to reduce the turbine weight or to increase the turbine inlet gas temperature.

In this connection we note that the more heat resistant the material from which the cooled blade is fabricated, the larger the effect from increasing its cooling intensity. This is clearly shown by Figure 7.7, where the abscissa axis is the magnitude of the temperature increase, characterizing the blade material strength increase, i.e., the allowable blade temperature increase and the ordinate axis is the magnitude of the corresponding turbine inlet gas temperature increase.

If the blade is uncooled ($\theta=0$), its fabrication from a material allowing increase of the temperature by 50°, for example, would make it possible to increase the turbine inlet gas temperature by the same amount. However, if we make the cooled blade from this same material, then the higher its cooling intensity, the larger the magnitude by which we can increase the gas temperature. Thus, for $\theta=0{,}5$, increase of the allowable blade temperature by the same 50° makes it possible to increase the turbine inlet gas temperature (for ΔT_w=idem) by 100°, i.e., twice as much. Consequently, the more heat resistant the material, the more favorable is the utilization of cooled blades with high cooling intensity.

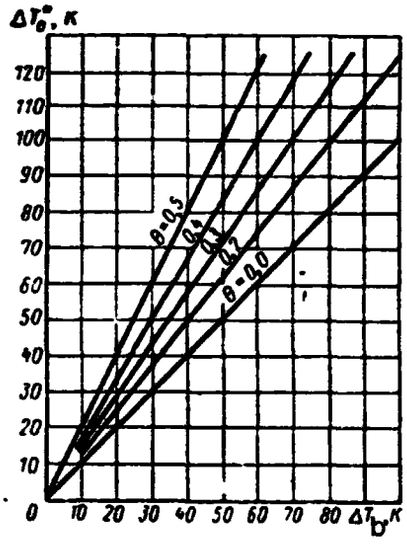

Figure 7.7. Turbine inlet gas temperature increase as function of allowable cooled blade temperature increase

Let us increase, in the above example, the degree of turbine loading to 30%, and determine by analogy with the preceding analysis the associated blade temperature reduction and blade stress increase. As a result of

calculation made by analogy with the preceding analysis, we find that the blade stresses increase by 24%, and the ultimate stresses /181 increase by the same amount. Consequently, the strength margin remains unchanged, but the turbine efficiency deteriorates.

Increase of the degree of loading of a turbine in which the circumferential velocity at the inner diameter is less than 400 m/s, say 300 m/s, will have a different effect on the strength margin variation in our example. We change the turbine inlet gas temperature T_0^* and the cooling air temperature simultaneously, such that the blade temperature for $\mu_{10} = 2.0$, just as in the preceding example, will be equal to 1144 K.

If we increase the loading coefficient in such a stage by 20%, this will lead to reduction of the blade temperature by only 20° and reduction of the strength margin by 4%. In order to maintain the strength margin, we must either increase the blade width, which leads to increased turbine weight, or reduce the gas temperature.

In all these examples, we have examined the lower section of the blade, under the assumption that this section has the minimal strength margin. We use this approach to evaluation of the influence of the degree of loading of the turbine stage with cooled blades on blade temperature, regardless of what section along the blade length has the minimal strength margin. The magnitudes of the defining parameters must be taken for the respective section being examined.

The cooled blade temperature can be reduced with practically unchanged turbine efficiency by increasing the work L_T removed per kilogram of gas flowing through the turbine if the degree of loading remains unchanged. This means that the square of the circumferential velocity will increase in proportion to the increase of L_T, and ΔT_w will increase to the same degree, in accordance with (7.1).

The rotor blade circumferential velocity can be increased in two ways — by increasing the rotor diameter with fixed rotational speed or by increasing the rotational speed with fixed diameter.

Theoretical analysis, in application to the first stage of a turbine with cooled blades of a conventional two-shaft engine, showed that if we increase the turbine diameter with constant rotational speed and, in order to maintain the same turbine efficiency, we not only retain the loading coefficient μ unchanged, but also leave M_{2c} constant and the relative cascade pitch t/b at the mean diameter constant, then increase of L_T above a definite magnitude while retaining the same strength margins in the rotor blade and disk leads to increase of the turbine weight. Here we have assumed that the rotor blade width also remains constant, i.e., the blade dimensions (other than length) and the dimensions of the internal channels through which the cooling air flows remain unchanged. Consequently, the number of blades increases in proportion to the diameter increase.

The results of these calculations are shown graphically in Figure 7.8, from which we see that increase of ΔL_T by 20% leads to increase of the overall turbine weight G by 25%. This takes place basically because of increase of the disk weight.

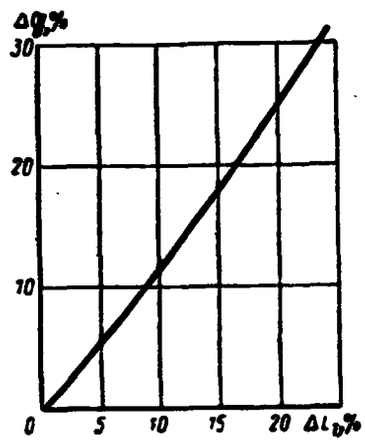

/182

Figure 7.8. Weight of turbine with cooled blades as function of increase of work L_T

Translator's note. Ordinate of figure should be Gothic G to agree with text.

Increase of the circumferential velocity by increasing the rotor rotational speed with constant turbine diameter leads to still greater (by a factor of two) increase of the turbine weight. Since in this case the stress increase in the blade [see (3.5)] exceeds the allowable stress increase associated with reduction of the blade temperature, in order to retain the

same strength margin in the blade, we must also reduce the stator inlet gas temperature.

We see from this analysis that the rational magnitude of the degree of loading of the turbine stage with cooled blades is determined by the cooling intensity, hot strength of the blade material, allowable blade temperature, contribution of the residual uncompensated bending stresses to the overal stresses in the blade, hydraulic resistance of the cooling system channels, blade circumferential velocity, allowable dimensionless gas velocity at the turbine exit, efficiency variation as a function of the loading coefficient, number of stages, work distribution among the stages, number of stages with cooled blades, and the engine type and mission.

If only the first stage of a four-stage turbine has cooled blades, the deterioration of its efficiency, associated with increased degree of loading and, consequently, with increased relative cooling air flowrate, may not have any marked influence on the efficiency of the entire turbine. Or for an afterburning jet engine operating primarily in the afterburning regimes, the turbine efficiency deterioration resulting from increased loading of the stage with cooled blades may not have in practice any marked influence on the engine altitude-speed characteristics.

Consequently, the degree of loading of the turbine with cooled blades must be determined in each specific case with account for all the above-mentioned factors.

CHAPTER VIII

GASDYNAMIC CALCULATION OF MULTISTAGE TURBINE

We shall examine the basic features and sequence of gasdynamic calculation of multistage turbines. /183

8.1. Basic Features and Sequence of Multistage Gas Turbine Calculation

The initial data for the calculation are:

gas flowrate G_g, kg/s;

stator inlet gas total parameters p_0^* and T_0^*;

turbine rotational speed n, rpm;

required turbine work L_T or power N_T.

Turbine design includes selection of the flow path scheme, number of stages and distribution of the work among them, selection of the basic stage design parameters, determination of the stator and rotor dimensions of all the stages, and determination of the turbine exit gas parameters. In selecting the basic turbine and stage design parameters, the objective is to obtain the specified power with minimal losses, minimal weight, and minimal overall turbine dimensions, and also to match the turbine and compressor parameters.

In calculating the individual stages, we must consider the following characteristics of multistage turbines.

1. Total flow parameters based on the absolute gas velocity at the exit from the preceding stage are the initial total flow parameters for the calculation of the next stage.

2. Because of heat loss recovery, the efficiency of the entire multistage turbine is higher than that of each individual stage. This is physically explained by the fact that the heat released as a result of hydraulic resistances in the preceding stage increases the enthalpy and, consequently, the available gas expansion work in the following stages.

The heat loss recovery and corresponding increase of the multistage turbine efficiency in comparison with the stage efficiency will be greater, the higher the gas expansion ratio in the turbine and larger the number of stages. However, for all values of π_T^* and η_{st}^*, it is advisable to increase the number of stages only up to some limit above which the efficiency gain will be very small. /184

The connection between the turbine efficiency and the mean stage efficiency can be represented in the form:

$$\eta_T^* = (1+\alpha)\eta_{st}^*, \tag{8.1}$$

where α — heat loss recovery coefficient.

The quantity α can be determined from the Abiants formula [1]:

$$\alpha = \frac{1-\eta_{st}^*}{z}\left(\frac{1}{1+a} + \frac{2}{2+a} + \ldots + \frac{z-1}{z-1+a}\right),$$

where z — number of turbine stages, $a = \frac{z}{\pi_T^{\frac{k-1}{k}} - 1}$. For the mean stage efficiency $\eta_{st}^* = 0.9$ and $\pi_T^* = 4 - 16$, the heat loss recovery coefficient lies in the range 0.01 - 0.025.

3. In the multistage turbine, the axial gas velocity component should increase from the first stage to the last. If this is not done, the gas density decrease along the turbine flow path may lead to excessive flow path divergence in the meridional section. For large flow path divergence angles ($\gamma > 20°$), flow separation, increase of the losses, and reduction of turbine efficiency may take place.

If the axial velocity increases, the angles α_1 and β_2 increase from stage to stage. In the first stage, the angle α_1 is in the range 16° - 25°, while in the last stages it may reach 30° - 35° or more (depending on the gas expansion ratio in the turbine).

Usually the flow Mach number rather than the magnitude of the axial velocity is specified in turbine design. Here, we must keep in mind that, because of the gas temperature reduction along the turbine flow path, the flow Mach number increases from the first to the last stage more rapidly than the axial velocity increases. In the first stage, the Mach number based on the axial velocity component is in the range $M_{2a} = 0{,}25 - 0{,}35$, while at the exit from the last stage $M_{2a} = 0{,}5 - 0{,}6$, or more. The value of M_{2a} in the intermediate stages is selected so as to obtain a smooth flow path form.

If blade strength and turbine dimensions permit, it is desirable in all cases to reduce the Mach number at the turbine exit to $M_{2a} = 0{,}45 - 0{,}50$, and for lowly loaded stages — to $M_{2a} = 0{,}4 - 0{,}45$.

4. The flow path form has significant influence on the work distribution among the turbine stages. For example, in the case of identical loading coefficients of all the stages for the single-shaft /184 turbine, $L_{st} = \mu u^2 = \text{const}\, \mu D^2$. This implies that for the same values of μ, the stage work will be larger, the larger the diameter. In this case, for a constant mean diameter D_m = const, the work may be distributed uniformly among the stages. In the increasing mean diameter case, the last stages may be loaded more than in the case with D_m = const.

For the case D_i = const and μ = const, the work will decrease from stage to stage. Consequently, for selected values of the loading coefficient, in order to increase the work of the turbine stages and reduce the number of stages, it is advisable to increase the turbine outer diameter to the magnitude allowed by rotor strength or to the degree permitted by the overall diameter of the engine flow path.

5. The degree of reaction of the multistage turbine stages increases at the mean diameter from the first stage to the last, just as does the axial velocity. The magnitude of the reaction at the mean radius is determined by the minimal allowable reaction at the blade root $\rho_i \geqq 0$. On the basis of these consideration, the reaction at the mean radius in the first stage, which has the shortest blades, is usually selected in the range $\rho_m = 0.2 - 0.3$.

The blades of the last stages have considerably greater relative length than those of the first stages. Therefore, in order to avoid negative reaction at the blade root, the reaction at the mean radius in the last stages is increased to $\rho_m = 0.35 - 0.5$. Smaller values of the reaction in the first stages make it possible to take for these stages larger values of the loading coefficients for moderate flow swirl at the exit.

The calculation of the multistage turbine can be carried out in the following sequence.

1. We select the number of stages and distribute the work among the stages (see section 3.1).

We take the maximal allowable loading coefficient at the stage inner radius $\mu_i = 2.0 - 2.2$.

2. We determine the total temperature and total pressure at the turbine exit:

$$T_2^* = T_0^* - \frac{L_T}{\frac{k}{k-1}R}; \quad p_2^* = p_0^*\left(1 - \frac{L_T}{\frac{k}{k-1}RT_0^*\eta_T^*}\right)^{\frac{k}{k-1}}.$$

The turbine efficiency is selected in the range $\eta_T^* = 0{,}91 - 0{,}93$. We can also specify the stage efficiency in the range $\eta_{st}^* = 0{,}89 - 0.9$, and determine the turbine efficiency from (8.1).

3. We specify the turbine exit Mach number and use the flow equation (3.2) to find the flow section area: /186

$$F_2 = \frac{G_g\sqrt{T_2^*}}{mp_{2c}^* q(\lambda_{2c})\sin\alpha_2}.$$

The angle α_2 in the first approximation is taken in the range 85° -95°.

4. We specify the loading coefficient at the last stage blade root and determine:

— the inner diameter at the turbine exit

$$D_{i2} = \frac{60}{\pi n}\sqrt{\frac{L_{st}}{\mu_i}},$$

where n and L_{st} — last turbine stage rotative speed and work;

— the last stage outer diameter

$$D_{o2} = \sqrt{D_i^2 + \frac{4F_2}{\pi}};$$

— the blade length

$$h_b = \frac{D_{c2} - D_{i2}}{2}.$$

5. We make a preliminary check of the stresses in the last stage blade root section in order to determine the degree to which the selected parameters and resulting geometric dimensions satisfy the rotor blade strength conditions.

The tensile stresses in the last turbine stage rotor blade root section can be found from (3.6):

$$\sigma_t = K_\Phi \sigma_{t\,r} = K_\Phi \cdot 1.745 \cdot 10^{-3} \rho_b n^2 F_\Phi,$$

where K_Φ — blade form factor, determined using Figure 3.2;

ρ_b — blade material density in kg/m^3.

The overall stresses in the blades from (3.7):

$$\sigma_\Sigma = \sigma_t + \sigma_{bend} = (1 + \frac{\sigma_{bend}}{\sigma_t})\sigma_t,$$

where σ_{bend}/σ_t is found from Figure 3.4 for the ratio of the maximal air flowrate to the design flowrate G_{max}/G_d known from the engine analysis.

The resulting value of σ_Σ is compared with the allowable stress σ_a for the selected blade material at the blade temperature $T_b \approx (0.9 - 0.95)\,(T^*_{1\,w})_i$, where for $K_e \approx 1$,

$$(T^*_{1w})_i = T^*_0 - \frac{u_i^2(\mu_i + 1)}{2\frac{k}{k-1}R}.$$

Here, $u_i = \pi D_i n/60$; /187

T^*_0 — total temperature at the inlet to the last stage.

The allowable stress $\sigma_a = \sigma_{sr}/n$, where σ_{sr} is the blade material stress-rupture strength at the given temperature, n is the strength safety factor.

Frequently, the preliminary verification calculation of the blade strength is made approximately, considering only the tensile stresses.

In this case, the allowable tensile stress:

$$\sigma_{at} = \frac{\sigma_{sr}}{n},$$

where $n \geqslant 2{,}0$.

If the stresses are found to be within allowable limits, the calculation can be continued. However, if the blade stresses σ_Σ (or σ_t) are excessive, they must be reduced, either by reducing the area F_2 by increasing M_{2c}, or by reducing the coefficient K_Φ or the rotative speed n (see section 3.2).

6. We select the flow path shape and make a preliminary determination of the basic flow path dimensions.

The flow path form is determined to a considerable degree by the ratio of the flow path areas at the turbine inlet and exit F_0/F_2, the cascade width, and the magnitude of the axial clearance (see section 3.5). However, in the preliminary calculation, when selecting the flow path form, the rotor and stator cascade width can be determined approximately (see section 3.4).

The flow path area ratio F_0/F_2 depends on the gas expansion ratio in the turbine $\pi_\tau^* = p_0^*/p_2^*$, and the relative stream densities at the turbine inlet and exit.

From the flow equation written for the turbine flow path inlet and outlet sections, we have:

$$\frac{F_0}{F_2} = \frac{q(\lambda_2)}{\pi_\tau^{*\frac{n+1}{2n}} q(\lambda_0)} = \frac{q(\lambda_2)/q(\lambda_0)}{\pi_\tau^* \sqrt{1-\left[1-\left(\frac{1}{\pi_\tau^*}\right)^{\frac{k-1}{k}}\right]\eta_\tau^*}} \qquad (8.2)$$

From the statistical data for existing turbines, the quantities $q(\lambda_2)$ and $q(\lambda_0)$ vary in the limits $q(\lambda_2) = 0{,}7 \div 0{,}84$ $(M_2 = 0{,}45 - 0{,}6)$ and $q(\lambda_0) = 0{,}30 \div 0{,}46$ $(M_0 = 0{,}18 \div 0{,}22)$.

The quantity π_T^* increases with increase of the air compression ratio in the compressor π_k^* and the engine bypass ratio. With increase of the turbine inlet gas temperature, π_T^* decreases.

The dependence of the turbine flow section area ratio F_2/F_0 on the air compression ratio in the compressor on the stand π_{k0}^* and the gas temperature T_0^*, obtained as a result of calculation for the condition $G_g = G_a$, $q(\lambda_0)/q(\lambda_2) = 0{,}5$; $\eta_r^* = 0{,}9$ and $\eta_k^* = 0{,}84 - 0{,}86$, is shown in Figure 8.1. /188

The turbine flow path width:

$$s_T = \sum s_i + \sum \Delta_i,$$

where $s_i = (s_s + s_r)_i$ and Δ_i — axial clearance of the ith stage. If we introduce the mean values of s_i and Δ_i for all the stages, then,

$$s_T = z_{row} s_i + (z_{row} - 1)\Delta_i = z_{row} \frac{h_b}{\bar{h}} + (z_{row} - 1)\frac{h_b}{\bar{h}_b}\bar{\Delta}_i, \quad (8.3)$$

where z_{row} — number of blade rows;

$\bar{h}_b = h_b/s_r$ — rotor blade aspect ratio;

$\bar{\Delta} = \Delta/s_r$ — relative axial clearance.

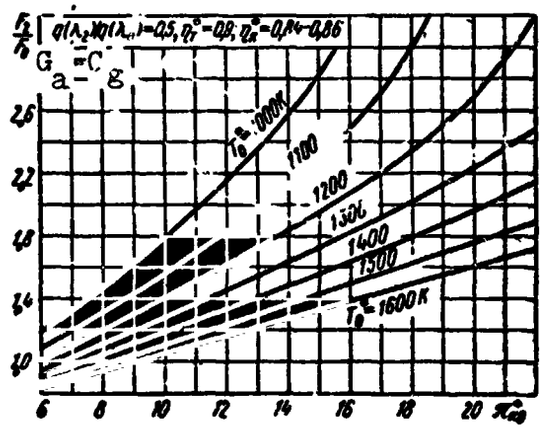

Figure 8.1. Turbine flow path area ratio F_2/F_0 as function of air compression ratio in compressor and turbine inlet gas temperature

In preliminary calculations, the mean value of $\bar{h}_b$ can be taken in the range $\bar{h}_b = 3 - 4$*, and the mean value of the relative axial clearance — $\bar{\Delta} = 0{,}2 \div 0{,}3$.

*For stages with shrouds, the value of $\bar{h}_b$ reaches 6 - 7.

The flow path divergence angle of a turbine made with constant outer diameter D_o = const:

$$\gamma = \operatorname{arctg}\frac{h_2 - h_0}{s_r} = \operatorname{arctg}\frac{1-(h_0/h_2)}{z_{row}\frac{(1+\bar{\Delta}_l)}{\bar{h}_b} - \left(\frac{\bar{\Delta}_l}{\bar{h}_b}\right)}, \tag{8.4}$$

where /189

$$h_0 = \frac{D_o - D_{i0}}{2}; \quad D_{i0} = \sqrt{D_o^2 - \frac{4F_0}{\pi}}.$$

For D_m = const,

$$\gamma = \operatorname{arctg}\frac{1-\left(\frac{h_0}{h_2}\right)}{2\left(z_p\frac{1+\bar{\Delta}_l}{\bar{h}_b} - \frac{\bar{\Delta}_l}{\bar{h}_b}\right)},$$

where

$$h_0/h_2 = F_0/F_2; \ \gamma_i = \gamma_o = \gamma.$$

This value of γ should lie in acceptable limits (see Chapter III).

During detailed analysis of the individual stages, it may become necessary to alter the selected flow path shape and dimensions. Therefore, the preliminary calculation of the basic flow path dimensions should be considered only as the first approximation, necessary for determining the required initial parameters for calculating the individual stages.

7. For selecting the number of stages, distributing the work among the stages, and determining the basic turbine flow path dimensions, we turn to detailed calculation of the first and subsequent stages at the mean diameter. Each stage is calculated using one of the methods presented in Chapter IV, with account for the multistage turbine calculation procedures examined above.

If the detailed calculations are restricted to only a single turbine stage (for example, in an academic course or diploma design),

usually the last stage is analyzed; in the first stages, we only determine the flow parameters at the inlet to and outlet from the stages and their flow path geometric dimensions; we also verify the rotor blade stresses and strength margins, since in the first stages the stress-rupture strength and the magnitude of the allowable stresses in the blades decrease (along with reduction of the blade length) because of the higher gas temperature and blade temperature. If the strength margins are unacceptably low, we must change the blade material or use blade cooling. Turbine cooling introduces certain changes into the technique for calculating the flow parameters and turbine flow path dimensions (see Chapter VI).

8. After calculating all the stages at the mean diameter, we determine the efficiency of the entire turbine:

$$\eta_{\text{т}}^{*}=\frac{\sum L_{\text{т}}}{L_{\text{ad.T}}^{*}}.$$

The adiabatic gas expansion work in the multistage turbine in terms of total parameters is: /190

$$L_{\text{ad.T}}^{*}=\frac{k}{k-1}RT_{0}^{*}\left[1-\left(\frac{1}{\pi_{\text{т}}^{*}}\right)^{\frac{k-1}{k}}\right],$$

where $\pi_{\text{т}}^{*}=p_{0}^{*}/p_{2}^{*}$ is the gas expansion ratio in the turbine in total parameters, and the pressure p_{2}^{*} is determined from the refined data after the detailed calculation of all the stages.

If the detailed turbine calculation is restricted to only calculation of the last stage, the turbine efficiency is not verified.

If the turbine efficiency is unacceptably low, we must reexamine the selection of the individual stage parameters with the objective of increasing their efficiency.

9. After calculating the turbine stages at the mean diameter, we select for each stage the flow parameter distribution along the blade height, and determine the flow parameters at the inner and

outer diameters, as shown in Chapter III. Then we select the cascade parameters, construct the blade profiles for various sections along the blade length, and determine the blade setting angles in the cascade on the basis of the requirements for obtaining the design velocity triangles, and on the basis of strength and producibility considerations.

8.2. Two-Stage TJE Turbine Gasdynamic Calculation Example

As an example, we shall calculate a single-shaft two-stage turbojet engine (TJE) turbine.

We assume that the following initial data for the turbine calculation are known from the general gasdynamic engine calculation:

gas flowrate G_g = 92 kg/s;

turbine outlet gas total pressure p_0^* = 1.2 MPa;

turbine inlet total temperature T_0^* = 1300 K;

required turbine shaft work L_T = 358,000 J/kg;

turbine rotor speed n = 7340 rpm;

adiabatic exponent k = 1.33;

compressor outer diameter $(D_o)_k$ = 0.89 m.

The turbine calculation is made in the following sequence.

1. We first determine the flow parameters and flow section area at the turbine outlet.

The total temperature and total pressure at the turbine outlet:

$$T_2^* = T_0^* - \frac{L_T}{\frac{k}{k-1}R} = 1300 - \frac{358000}{1155} = 990\ \text{K};$$

$$p_2^* = p_0^*\left(1 - \frac{L_T}{\frac{k}{k-1}RT_0^*\eta_T^*}\right)^{\frac{k}{k-1}} = 1.2\left(1 - \frac{358000}{1155 \cdot 1300 \cdot 0.91}\right) = 0.355 \text{ MPa},$$

where in the first approximation we have taken $\eta_T^* = 0.91$.

We assume the turbine outlet Mach number $M_{2c} = 0.52$, and the flow leaving angle $\alpha_2 = 86°$. From the flow equation (3.2), we determine the flow section area at the turbine outlet: /191

$$F_2 = \frac{G_g\sqrt{T_2^*}}{m p_2^* q(\lambda_{2c}) \sin\alpha_2} = \frac{92\sqrt{956}}{0.0396 \cdot 0.355 \cdot 10^6 \cdot 0.765 \cdot 0.9976} = 0.27 \text{ m}^2.$$

2. On the basis of the general engine layout and considerations relative to the allowable turbine diametrical dimension, we select the maximal turbine outer diameter D_o = 0.93 m, and for the last-stage turbine, we determine:

outlet inner diameter

$$D_1 = \sqrt{D_o^2 - \frac{4F^2}{\pi}} = \sqrt{0.93^2 - \frac{4 \cdot 0.27}{3.14}} = 0.72 \text{ m};$$

rotor blade length

$$h_2 = \frac{D_o - D_1}{2} = \frac{0.93 - 0.72}{2} = 0.105 \text{ m};$$

mean diameter

$$D_m = \frac{D_o + D_1}{2} = 0.825 \text{ m};$$

circumferential velocity at the inner diameter

$$u_i = \pi D_i n/60 = \frac{3.14 \cdot 0.72 \cdot 7340}{60} = 276 \text{ m/s}.$$

For the given work $L_T = 358$ kJ/kg in accordance with the recommendations in section 3.1, we take two turbine stages.

3. Selecting the loading coefficient at the second stage inner diameter μ_i = 2.1 (see Chapter II), we find its work:

$$(L_{st})_{II} = \mu_i u_i^2 = 2{,}1 \cdot 276^2 = 159000 \text{ J/kg.}$$

Then the first-stage work:

$$(L_{st})_I = L_T = (L_{st})_{II} = 358\,000 - 159\,800 = 198\,200 \text{ J/kg.}$$

4. In the first approximation, we determine the inner diameter at the outlet of stage I. Taking $\mu_i = 2.2$ for this stage, we find:

$$D_i = \frac{60}{\pi n}\sqrt{\frac{(L_{st})_I}{\mu_i}} = \frac{60}{3{,}14 \cdot 7340}\sqrt{\frac{198200}{2{,}2}} = 0{,}7 \text{ m.}$$

5. We make a preliminary determination of the maximal stresses in the root section of the stage II rotor blade.

We maximal tensile stress is found from the formula:

$$\sigma_t = K_\Phi \cdot 1{,}745 \cdot 10^{-3} \rho_b n^2 F_2 \text{ N/m}^2$$

For the rotor blade, we select the EI929 alloy, whose density is $\rho_b = 8.4 \cdot 10^3$ kg/m^3.

We take a linear law of variation of the section area along the blade height and the form factor $K_\Phi = 0.625$ (see Chapter III, Figure 3.12).

Then,

$$\sigma_t = 0{,}625 \cdot 1{,}745 \cdot 10^{-3} \cdot 8{,}4 \cdot 10^3 \cdot 7340^2 \cdot 0{,}27 = 133 \text{ MN/m}^2 .$$

We determine the overall rotor blade stresses (with account for the bending stresses) from the formula:

$$\sigma_\Sigma \cong \left(1 + \frac{\sigma_{bend}}{\sigma_t}\right)\sigma_t = (1 + 0{,}32) \cdot 133 = 175{,}5 \text{ MN/m}^2,$$

where $\sigma_{bend}/\sigma_t = 0.32$ is determined from Figure 3.4 for the ratio of the maximal flowrate to the design flowrate $G_{max}/G_t = 1.4$, known from the general engine calculation. /192

The resulting stress σ_Σ is compared with the allowable stress σ_a for the selected material at the blade root temperature $T_b \approx 0.93(T^*_{1\ w})_i$. To determine the flow temperature $T^*_{1\ w}$, we take $\alpha_0 = 90°$.

In this case,

$$(T^*_{1w})_i = T^*_{0H} - \frac{u_i^2(\mu_1+1)}{2310} = T^*_0 - \frac{(L_{st})_H}{1155} - \frac{u_i^2(\mu_1+1)}{2310}.$$

Then,

$$(T^*_{1w})_i = 1300 - \frac{196200}{1155} - \frac{276^2(2,1+1)}{2310} \cong 1030\ \text{K}$$

and the blade temperature $T_b = 0,95 \cdot 1030 = 980$ K .

We assume the engine operating life $\tau = 5000$ hours, and for the given blade temperature and selected material EI929, we find from Figure 3.5 the stress-rupture strength:

$$\sigma_{sr} = 412\ \text{MN/m}^2.$$

The blade strength margin:

$$n = \frac{\sigma_{sr}}{\sigma_a} = \frac{412}{175,5} = 2,35.$$

This value of n is acceptable $(n>2)$; therefore, the turbine calculation can be continued.

6. We initially take the flow path form with constant outer diameter D_o = const.

We specify the turbine inlet Mach number $M_0 = 0,22$, and determine the flow path area F_0 and stator vane height h_0:

$$F_0 = \frac{G_g \sqrt{T_0^*}}{m p_0^* q(\lambda_0)} = \frac{92\sqrt{1300}}{0.0396 \cdot 1.2 \cdot 10^6 \cdot 0.385} = 0.181 \text{ м}^2;$$

$$D_{1b} = \sqrt{D_0^2 - \frac{4F_0}{\pi}} = \sqrt{0.932 - \frac{4 \cdot 0.181}{3.14}} = 0.795 \text{ м};$$

$$h_0 = \frac{D_0 - D_{1b}}{2} = 0.067 \text{ м}.$$

The cascade width can be determined using the technique presented in section 3.4. The cascade width can be taken approximately on the basis of statistical data for existing turbines. For multistage turbines, $\bar{h}_b$ = 2.5 - 6.5. The smaller values of $\bar{h}_b$ pertain to the first stages, and the larger values — to the last stages. The stator vane relative length is usually taken somewhat less (the difference between $\bar{h}_r$ and $\bar{h}_s$ reaches 30 - 40%, or more).

In accordance with these values, we take

$$(\bar{h}_s)_I = 1.6; \ (\bar{h}_r)_I = 3.0; \ (\bar{h}_s)_{II} = 3.1; \ (\bar{h}_r)_{II} = 4.$$

We determine the cascade width and the minimal possible magnitude of the axial clearances on the basis of relative displacement of the rotor and stator (see section 8.1), and then draw the turbine flow path to the desired scale (Figure 8.2).

The resulting flow path divergence angle ($\gamma_{i.m}$ = 12°50') is in acceptable limits (see Chapter III); therefore, we finally take the flow path form with D_o = const.

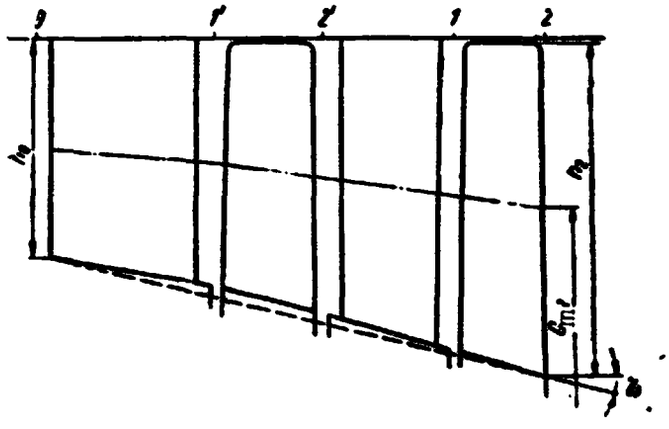

/193

Figure 8.2. Turbine flow path

After selecting the flow path scheme and making the preliminary determination

of the basic flow path dimension, we perform the detailed calculations of the first and second turbine stages*.

8.2.1. Gasdynamic calculation of first turbine stage at the mean diameter

From the preliminary turbine calculation, we know: stage work $(L_{st})_I$ = 198,200 J/kg, rotor speed n = 7340 rpm, stage inlet flow parameters ($T_0^* = 1300$ K, $p_0^* = 1.2$ MPs), and the flow path shape and dimensions.

We shall make the calculation using the technique in which the initial parameters are M_{2c} and α_2.

1. We determine the flow parameters at the exit from stage I:

$$T_2^{*\prime} = T_0^* - \frac{(L_{st})_I}{1155} = 1300 - \frac{198200}{1155} = 1128 \text{ K};$$

$$p_2^{*\prime} = p_0^* \left[1 - \frac{(L_{st})_I}{1155\, T_0^* (\eta_{st}^*)}\right]^{\frac{k}{k-1}} = 1.2\left[1 - \frac{198200}{1155 \cdot 1300 \cdot 0.895}\right]^4 = 0.633 \text{ MPa}.$$

2. From the flow path diagram, we find:

$$D'_{o2} = D_o = 0.930 \text{ m}; \quad D'_{i2} = 0.760 \text{ m}.$$

The exit section mean diameter $D'_{m2} = \frac{D_o - D'_{i2}}{2} = 0.845$ m. The flow path area at the stage outlet:

$$F'_2 = \frac{\pi}{4}\left[D_o^2 - (D'_{i2})^2\right] = \frac{3.14}{4}(0.93^2 - 0.76^2) = 0.225 \text{ m}^2$$

3. From the flow equation, we find the relative stream density: /194

*In approximate turbine calculations (during preliminary design, for example), detailed calculation is sometimes made of only the last stage turbine; this calculation variant will be presented below.

$$q(\lambda_{2c}) = \frac{G_g\sqrt{T_2^{*}}}{mF_2'p_2^{*}\sin\alpha_2} = \frac{92\sqrt{1128}}{0{,}0396\cdot 0{,}225\cdot 0{,}633\cdot 10^6\cdot 0{,}9659} = 0{,}567,$$

and then the gas velocity at the stage exit*, where the flow angle at the stage exit is taken equal to $\alpha_2' = 75°$. From the tables we find $\lambda_{2c} = 0{,}38$. Hence:

absolute gas velocity at the stage exit

$$c_2 = \lambda_{2c}\sqrt{2\frac{k}{k+1}RT_2^{*}} = 0{,}38\sqrt{2\cdot\frac{1{,}33}{1{,}33+1}\cdot 289\cdot 1128} = 232 \text{ m/s};$$

axial and circumferential components of the absolute velocity

$$c_{2a} = c_2\sin\alpha_2 = 232\cdot 0{,}9659 = 224 \text{ m/s};$$
$$c_{2u} = c_2\cos\alpha_2 = 232\cdot 0{,}2588 = 60 \text{ m/s};$$

circumferential velocity at the mean diameter

$$u_{m2} = \frac{\pi D_{m2}n}{60} = \frac{3{,}14\cdot 0{,}845\cdot 7340}{60} = 324 \text{ m/s}$$

circumferential component of the relative velocity

$$w_{2u} = c_{2u} + u_{m2} = 60 + 324 = 384 \text{ m/s}$$

relative gas velocity

$$w_2 = \sqrt{c_{2a}^2 + w_{2u}^2} = \sqrt{224^2 + 384^2} = 445 \text{ m/s}.$$

4. We shall find the flow path dimensions in the axial clearance.

From the flow path diagram, we find $h_1' = 0.007$ m, and then determine:

$$D_{m1}' = D_O - h_1' = 0{,}930 - 0{,}077 = 0{,}853 \text{ m};$$
$$D_{i1}' = D_O - 2h_1' = 0{,}930 - 2\cdot 0{,}077 = 0{,}776 \text{ m};$$

the flow path section area in the axial clearance

$$F_1' = \frac{\pi}{4}\left[D_O^2 - (D_{i1}')^2\right] = \frac{3{,}14}{4}(0{,}930^2 - 0{,}776^2) = 0{,}205 \text{ m}^2.$$

---

*In the following, we shall denote gas velocity without the prime symbol.

5. We find the circumferential component of the absolute gas velocity in the axial clearance:

$$c_{1u} = \frac{(L_{st})_I - u_2' c_{2u}}{u_1'} = \frac{198200 - 324 \cdot 60}{328} = 547 \text{ m/s}$$

where

$$u_1' = \frac{\pi D_{m1}' n}{60} = \frac{3{,}14 \cdot 0{,}853 \cdot 7340}{60} = 328 \text{ m/s}$$

6. We determine the angle α_1 and the absolute gas velocity c_1 in the axial clearance *.

From the flow equation written for the section 1' - 1', we find the relation $\alpha_1 = f[q(\lambda_{1c})]$:

$$\alpha_1 = \arcsin \frac{G_g \sqrt{T_0^*}}{m F_1' p_0^* \sigma_{S_1}^* q(\lambda_{1c})} = \arcsin \frac{C}{\sigma_{S1}^* q(\lambda_{1c})}, \tag{8.5}$$

where G_g = 92 kg/s, and the constant /195

$$C = \frac{G_g \sqrt{T_0^*}}{m F_1' p_0^*} = \frac{92 \sqrt{1300}}{0{,}0396 \cdot 0{,}205 \cdot 12 \cdot 10^5} = 0{,}3405.$$

As the second equation, we use the relation:

$$\lambda_{c1} = \frac{\lambda_{c_{a1}}}{\cos \alpha_1}, \tag{8.6}$$

where

$$\lambda_{c_{a1}} = c_{1u}/a_{cr\,1} = \frac{547}{655} = 0{,}835;$$

$$a_{cr\,1} = \sqrt{2 \frac{k}{k+1} R T_0^*} = 18{,}3 \sqrt{T_0^*} = 18{,}3 \sqrt{1300} = 655 \text{ m/s}.$$

We shall solve the system of equations (8.5) and (8.6) graphically. We take several values of λ_{1c}, and for each of them we

---

*The angle α_1 can also be determined using the technique described on pages 97 - 99.

determine the velocity coefficient ϕ; from the graph of $\sigma^* = f(\lambda, \bar{\varphi})$ (see Figure 4.1), we determine σ_s^*; and then from (8.5) and (8.6), we find the angle α_1.

We summarize the calculation results in Tables 8.1 and 8.2.

TABLE 8.1. CALCULATION USING (8.5)*

λ_{1c}	0,86	0,88	0,90	0,92
$q(\lambda_{1c})$	0,9769	0,9630	0,9483	0,9325
σ_s^*	0,977	0,976	0,975	0,974
$\sin\alpha_1$	0,354	0,353	0,351	0,3504
α_1	20°44′	20°40′	20°33′	20°30′

*Translator's note. Commas in numbers represent decimal points.

TABLE 8.2. CALCULATION USING (8.6)*

λ_{1c}	0,86	0,88	0,90	0,92
$\cos\alpha_1$	0,972	0,9475	0,9275	0,9070
α_1	13°30′	18°39′	21°55′	24°49′

*Translator's note. Commas in numbers represent decimal points.

We plot the relation $\lambda_{1c} = f(\alpha_1)$ (Figure 8.3). The intersection of the curves $\lambda_{1c}(\alpha_1)$ determines the sought value of $\alpha_1 = 20°36'$ and $\lambda_{1c} = 0{,}892$.

The absolute gas velocity: /196

$$c_1 = \lambda_{1c} a_{cr\ 1} = 0{,}892 \cdot 655 = 584 \text{ m/s}$$

the axial velocity component c_1:

$$c_{1a} = c_1 \sin \alpha_1 = 584 \cdot 0{,}3518 = 205 \text{ m/s};$$

the relative gas velocity at the rotor inlet:

$$w_1 = \sqrt{c_1^2 - 2u_1 c_{1u} + u_1^2} = \sqrt{584^2 - 2 \cdot 328 \cdot 547 \cdot 328^2} = 298 \text{ m/s}$$

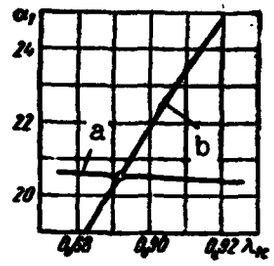

Figure 8.3. Dependence of the angle α_1 on λ_{1c} for the first stage:

a — from (8.5)
b — from (8.6)

7. We find the stator exit static pressure and temperature

$$p_1 = p_1^* \pi(\lambda_{1c}) = p_0^* \sigma_s^* \pi(\lambda_{1c}) = 1{,}2 \cdot 0{,}973 \cdot 0{,}6177 = 0{,}72 \text{ MPa},$$

where σ_s^* is determined from Figure 4.1 for the assumed value $\varphi = 0{,}975$ (with account for the losses from the secondary flows and in the boundary layer on the end walls):

$$T_1 = T_0^* \tau(\lambda_{1c}) = 1300 \cdot 0{,}8873 = 1154 \text{ K}.$$

8. We determine the total temperature at the rotor inlet:

$$T_{1w}^* = T_1 + \frac{w_1^2}{2310} = 1154 + \frac{298^2}{2310} = 1192 \text{ K}.$$

9. We verify the stage I rotor blade strength margin.

The blade temperature $T_b \approx 0{,}92 T_{1w}^* = 0{,}92 \cdot 1192 = 1100$ K; the blade root section stresses:

$$\sigma_t = K_\phi 1{,}745 \cdot 10^{-3} \rho_b n^2 F_2 = 0{,}65 \cdot 1{,}745 \cdot 10^{-3} \cdot 8{,}4 \cdot 10^3 \cdot 7340^2 \cdot 0{,}205 = 105{,}2 \text{ MN/m}^2$$

$$\sigma_\Sigma = \left(1 + \frac{\sigma_{bend}}{\sigma_t}\right) \sigma_t = (1 + 0{,}32) \cdot 105{,}2 = 139{,}1 \text{ MN/m}^2$$

For the stage I rotor blade, we select the ZhS6-K alloy. We take the blade operating life $\tau = 5000$ hours. From Figure 3.5, we find the stress-rupture strength σ_{sr} = 31 kgf/mm^2 = 304 MN/m^2.

The blade strength margin:

$$n = \frac{\sigma_{sr}}{\sigma_3} = \frac{304}{139,10} = 2,18.$$

The value of n is in acceptable limits without blade cooling; therefore, the calculation can be continued*.

10. We find the relative velocity angles at the rotor inlet and outlet:

$$\beta_1 = \operatorname{arctg} \frac{c_{1a}}{c_{1u} - u_1} =$$

$$= \operatorname{arctg} \frac{205}{547 - 328} = 43°06';$$

$$\beta_2 = \operatorname{arctg} \frac{c_{2a}}{c_{2u} + u_2} = \operatorname{arctg} \frac{224}{60 + 324} = 30°18'.$$

11. We determine the degree of flow contraction: /197

$$K = \frac{\sin \beta_1}{\sin \beta_2} = \frac{0,6833}{0,5045} = 1,35.$$

From the graph of $\psi = f(K; \beta_1 + \beta_2)$ (see Figure 1.8), for K = 1.35 and $\beta_1 + \beta_2 = 73°24'$, we find $\psi \approx 0,97$. With account for the losses in the radial clearance $\psi_\delta^2 = \psi^2 - \xi_\delta$, where ξ_δ is the coefficient of losses in the radial clearance. Taking the relative radial clearance $\bar{\delta} = 1,5\%$, from Figure 1.9 we find $\xi_\delta = 0,025$. Then, $\psi_\delta^2 = 0,97^2 - 0,025 = 0,915$.

12. We find the adiabatic gas expansion work in the rotor $(u_2 \approx u_1)$:

$$L_{ad.r} = \frac{1}{2}\left(\frac{w_2^2}{\psi_\delta^2} - w_1^2\right) = \frac{1}{2}\left(\frac{445^2}{0,915} - 298^2\right) = 63800 \text{ J/kg};$$

the pressure and temperature at the rotor exit:

$$p_2 = p_1\left(1 - \frac{L_{ad.r}}{1155 \cdot T_1}\right)^{\frac{k}{k-1}} = 0,72\left(1 - \frac{63800}{1155 \cdot 1154}\right)^4 = 0,59 \text{ MPa}$$

$$T_2 = T_1 - \frac{w_2^2 - w_1^2}{2310} = 1154 - \frac{445^2 - 298^2}{2310} = 1106 \text{ K};$$

*Blade cooling must be used in the case of blade material with lower stress-rupture strength or for $\tau > 5000$ hours.

the air density at the rotor exit:

$$\varrho_2 = \frac{p_2}{RT_2} = \frac{0{,}59 \cdot 10^6}{289 \cdot 1106} = 1{,}846 \text{ kg/m}^3.$$

13. We verify the magnitude of the gas velocity at the rotor exit $(u_2 \approx u_1)$:

— axial component of the absolute velocity,

$$c_{2a} = \frac{G_g}{F_2 \varrho_2} = \frac{92}{0{,}225 \cdot 1{,}846} = 221 \text{ m/s};$$

— absolute gas velocity,

$$c_2 = \frac{c_{2a}}{\sin \alpha_2} = \frac{221}{0{,}9659} = 229 \text{ m/s},$$

— Mach number at stage exit,

$$M_{2c} = \frac{c_2}{\sqrt{kRT_2}} = \frac{229}{\sqrt{1{,}33 \cdot 289 \cdot 1106}} = 0{,}351.$$

The difference between the velocity c_2 obtained and that assumed in the beginning of the calculation is 1.3%. If this difference does not exceed 2%, we can use the first approximation and continue the calculation. If the gas velocity difference is larger, we must correct the area F_2 in order to obtain a velocity value equal to that obtained in step 13.

14. We determine the total temperature and total pressure at the rotor exit:

$$T_2^* = T_2 + \frac{c_2^2}{2310} = 1106 + \frac{228^2}{2310} = 1128 \text{ K};$$

$$p_2^* = p_2 \left(\frac{T_2^*}{T_2}\right)^{\frac{k}{k-1}} = 0{,}59 \left(\frac{1128}{1106}\right)^4 = 0{,}636 \text{ MPa}$$

the temperature and static pressure at the stage inlet: /198

$$T_0 = T_0^* \tau(\lambda_0) = 1300 \cdot 0{,}99205 = 1290 \text{ K};$$

$$p_0 = p_0^* \pi(\lambda_0) = 1{,}2 \cdot 0{,}9685 = 1{,}162 \text{ MPa}$$

where $\tau(\lambda_0)$ and $\pi(\lambda_0)$ are found from the tables for the previously assumed value of $M_0 = 0.22$.

15. We find the adiabatic gas expansion work in the stage:

$$(L^*_{ad.s})_I = \frac{k}{k-1} RT_0^* \left[1 - \left(\frac{p_2^*}{p_0^*}\right)^{\frac{k-1}{k}}\right] = 1155 \cdot 1300 \left[1 - \left(\frac{0,636}{1,2}\right)^{0,25}\right] = 220500 \text{ J/kg};$$

$$(L_{ad.s})_I = \frac{k}{k-1} RT_0 \left[1 - \left(\frac{p_2}{p_c}\right)^{\frac{k-1}{k}}\right] = 1155 \cdot 1290 \left[1 - \left(\frac{0,59}{1,162}\right)^{0,25}\right] = 234200 \text{ J/kg}.$$

16. We calculate the stage reaction at the mean diameter

$$\rho_m = \frac{63800}{234200} = 0,273;$$

the stage efficiency

$$(\eta^*_{st})_I = \frac{(L_{st})_I}{(L^*_{ad.st})_I} = \frac{196200}{220500} = 0,9.$$

After calculating the stage at the mean diameter, we select the flow parameter distribution along the blade length, and determine the flow parameters at the inner and outer radii.

8.2.2. Determination of flow parameters at the first stage inner and outer radii

We take the variation of the circumferential velocity component in the axial clearance and at the exit from the rotor, in accordance with the constant circulation law $c_{1u}r$ = const and $c_{2u}r$ = const.

We summarize the calculation results in Table 8.3.

8.2.3. Gasdynamic calculation of second turbine stage at the mean diameter

The initial data for the calculation are: stage work $(L_{st})_{II}$ = 158,900 J/kg; rotor speed n = 7340 rpm; flow parameters at stage inlet ($p_0^{*\prime} = 0,636$ MPa, $T_0^{*\prime} = 1128$ K, $p_0' = 0,59$ MPa, $T_0' = 1106$ K, $\alpha_2' = 75°$), and the flow path shape and dimensions.

TABLE 8.3.*

Parameter and formula	Dimension	Design diameter D_2', m		
		0,768	0,845	0,926
$\bar{r} = \frac{r}{r_m}$	—	0,910	1	1[illegible]
$c_{1u} = (c_{1u})_m \frac{1}{\bar{r}}$	m/s	601	547	498
$c_{1a} = \sqrt{(c_{1a}^2)_m + (c_{1u}^2)_m (1-\varphi^2) \times \sqrt{\left(1 - \frac{1}{\bar{r}^2}\right)}}$	m/s	198	205	210
$\alpha_1 = \mathrm{arctg} \frac{c_{1a}}{c_{1u}}$	deg	18°12′	20°36′	22°53′
$u_1 = u_{1m}\bar{r}$	m/s	298	328	356
$\beta_1 = \mathrm{arctg} \frac{c_{1a}}{c_{1u} - u_1}$	deg	33°11′	43°06′	55°55′
$w_1 = \frac{c_{1a}}{\sin \beta_1}$	m/s	362	298	253
$c_1 = \sqrt{c_{1a}^2 + c_{1u}^2}$	m/s	632	584	540
$T_1 = T_0^* - \frac{c_1^2}{2310}$	K	1127	1154	1173
$p_1 = p_0^* \left(1 - \frac{c_1^2}{\varphi^2 \cdot 2310 T_0^*}\right)^4$	Mpa	0,657	0,720	0,779
$T_{1w}^* = T_1 + \frac{w_1^2}{2310}$	K	1184	1192	1201
$c_{2u} = (c_{2u})_m \frac{1}{\bar{r}}$	m/s	66	60	55

(Table continued on following page)

TABLE 8.3. (continued)

Parameter and formula	Dimension	Design diameter D_2', m		
		0,768	0,845	0,926
$u_2 = u_{2m}\bar{r}$	m/s	295	324	356
$c_{2u} = \sqrt{(c_{2u}^2)_m + (1-\psi^2)\left[(1-\bar{r}^2)u_m^2 + \left(1-\frac{1}{\bar{r}^2}\right)(c_{2u}^2)_m\right] + (1-\varphi^2)\psi^2\left(1-\frac{1}{\bar{r}^2}\right)(c_{1u}^2)_m}$	m/s	222	224	225
$\alpha_2 = \operatorname{arctg}\frac{c_{2u}}{c_{2z}}$	deg	73°12′	75°	76°05′
$\beta_2 = \operatorname{arctg}\frac{c_{2z}}{c_{2u}+u_2}$	deg	31°33′	30°18′	28°42′
$w_2 = \frac{c_{2z}}{\sin\beta_2}$	m/s	425	445	468
$c_2 = \sqrt{c_{2u}^2 + c_{2z}^2}$	m/s	232	232	232
$T_2 = T_2^* - \frac{c_2^2}{2310}$	K	1105	1105	1105
$L_{ad.r} = \frac{1}{2}\left[\left(\frac{w_2}{\psi_2}\right)^2 - w_1^2\right]$	J/kg	33200	63800	87600
$p_2 = p_1\left[1 - \frac{(w_2/\psi_2)^2 - w_1^2}{2310T_1}\right]$	MPa	0,589	0,590	0,595
$L_{ad.s} = \frac{k}{k-1}RT_0\left[1-\left(\frac{p_2}{p_0}\right)^{\frac{k-1}{k}}\right]$	J/kg	233000	234200	230200
$\varrho = \frac{L_{ad.r}}{L_{ad.s}}$	—	0,1425	0,273	0,380

*Translator's note. Commas in numbers represent decimal points.

In addition, in the preliminary calculation, we assume the Mach number at the stage exit $M_2=0{,}52$ $(\lambda_2=0{,}55)$ and the flow angle $\alpha_2=86°$.

We shall calculate the second stage using the same technique as used for the first stage.

1. We determine the gas velocity at the stage exit:

— the absolute gas velocity

$$c_2 = \lambda_2 a_{cr2} = \lambda_2 \cdot 18{,}3\sqrt{T_2^*} = 0{,}55 \cdot 18{,}3\sqrt{990} = 314 \text{ m/s},$$

where /201

$$T_2^* = T_0^{*\prime} - \frac{(L_{st})_{II}}{1155} = 990 \text{ K};$$

— the axial and circumferential components of the absolute velocity

$$c_{2a} = c_2 \sin\alpha_2 = 314 \cdot 0{,}9976 = 313 \text{ m/s};$$
$$c_{2u} = c_2 \cos\alpha_2 = 314 \cdot 0{,}0698 = 22 \text{ m/s};$$

— the circumferential component of the relative velocity

$$w_{2u} = c_{2u} + u_2 = 22 + 317 = 339 \text{ m/s},$$

where

$$u_2 = \frac{\pi D_m n}{60} = \frac{3{,}14 \cdot 0{,}825 \cdot 7340}{60} = 317 \text{ m/s};$$

— the relative gas velocity

$$w_2 = \sqrt{c_{2a}^2 + w_{2u}^2} = \sqrt{313^2 + 339^2} = 461 \text{ m/s}.$$

2. We find the circumferential component of the absolute gas velocity at the rotor inlet:

$$c_{1u} = \frac{(L_u)_{II} - u_2 c_{2u}}{u_1} = \frac{159800 - 317 \cdot 22}{320} = 477 \text{ m/s},$$

where

$$(L_u)_{II} \cong (L_{st})_{II};$$

$$\lambda_{c_{1a}} = \frac{c_{1a}}{18{,}1\sqrt{T_0^*}} = \frac{477}{18{,}1\sqrt{1128}} = 0{,}784.$$

3. We determine the flow angle α_1 and absolute gas velocity c_1 in the axial clearance.

From the flow equation, we find:

$$\alpha_1 = \arcsin \frac{\bar{G}_g}{\sigma_S^* \, q(\lambda_{1c})}. \tag{8.7}$$

where the constant

$$\bar{G}_g = \frac{G_g\sqrt{T_0^*}}{mF_1 p_0^*} = \frac{92\sqrt{1128}}{0{,}0396 \cdot 0{,}2537 \cdot 0{,}636 \cdot 10^6} = 0{,}483;$$

$$F_1 = \frac{\pi}{4}(D_0^2 - D_{i1}^2) = \frac{3{,}14}{4}(0{,}93^2 - 0{,}736^2) = 0{,}2537 \text{ m}^2$$

We take as the second equation, the relation:

$$\lambda_{1c} = \frac{\lambda_{c_{1a}}}{\cos\alpha_1} = \frac{0{,}784}{\cos\alpha_1}. \tag{8.8}$$

We solve the system of equations (8.7) and (8.8) graphically (see section 8.2.1). As a result of the graphical solution (Figure 8.4), we find:

$$\alpha_1 = 29°54', \quad \lambda_{1c} = 0{,}905.$$

Hence, the absolute gas velocity: /202

$$c_1 = \frac{c_{1a}}{\cos\alpha_1} = \frac{477}{0{,}8669} = 550 \text{ m/s};$$

the axial component of the absolute velocity:

$$c_{1a} = c_1 \sin\alpha_1 = 550 \cdot 0{,}4985 = 274 \text{ m/s}.$$

4. We determine the static pressure and static temperature at the stator exit:

$$w_1 = \sqrt{c_1^2 - 2u_1c_{1a} + u_1^2} = \sqrt{550^2 - 2 \cdot 320 \cdot 477 + 320^2} = 316 \text{ m/s}.$$

5. Let us calculate the static pressure and static temperature at the exit from the stator

$$p_1 = p_0^* \sigma_S^* \pi(\lambda_{1c}) = 0{,}636 \cdot 0{,}978 \cdot 0{,}6084 = 0{,}378 \text{ MPa};$$

$$T_1 = T_1^* \tau(\lambda_{1c}) = 1128 \cdot 0{,}884 = 997 \text{ K}.$$

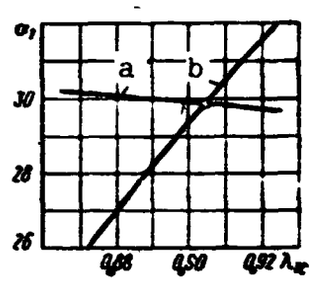

Figure 8.4. Dependence of the angle α_1 on λ_{1c} for second stage:
a — from (8.5)
b — from (8.6)

6. The relative velocity angles at the rotor inlet and exit:

$$\beta_1 = \operatorname{arctg} \frac{c_{1a}}{c_{1u} - u_1} = \operatorname{arctg} \frac{274}{477 - 320} = 60°12';$$

$$\beta_2 = \operatorname{arctg} \frac{c_{2a}}{w_{2u}} = \operatorname{arctg} \frac{313}{339} = 42°42'.$$

7. We determine the degree of flow contraction:

$$K = \frac{\sin \beta_1}{\sin \beta_2} = \frac{0{,}8678}{0{,}6782} = 1{,}28$$

and the sum of the angles $\beta_1 + \beta_2 = 60°12' + 42°42' = 102°54'$, and then from the graph of $\psi = f(K;\ \beta_1 + \beta_2)$ (see Figure 1.8), we find $\psi \approx 0{,}97$.

With account for the losses in the radial clearance:

$$\psi_\Sigma^2 = \psi^2 - \xi_\delta = 0{,}97^2 - 0{,}025 = 0{,}915.$$

8. We find the adiabatic gas expansion work in the rotor:

$$L_{ad.r} = \frac{1}{2}\left[\frac{w_2^2}{\psi_\Sigma^2} - w_1^2\right] = \frac{1}{2}\left[\frac{461^2}{0{,}915} - 316^2\right] = 66220 \quad \text{J/kg};$$

the pressure and temperature at the stage exit:

$$p_2 = p_1\left(1 - \frac{L_{ad.r}}{\frac{k}{k-1} RT_1}\right)^{\frac{k}{k-1}} = 0{,}378\left(1 - \frac{66220}{1155 \cdot 997}\right)^4 = 0{,}298 \quad \text{MPa};$$

$$T_2 = T_1 - \frac{w_2^2 - w_1^2}{2310} = 997 - \frac{461^2 - 316^2}{2310} = 948 \text{ K};$$

$$T_2^* = T_2 + \frac{c_2^2}{2310} = 948 + \frac{314^2}{2310} = 991 \text{ K};$$

$$p_2^* = p_2\left(\frac{T_2^*}{T_2}\right)^{\frac{k}{k-1}} = 0{,}298\left(\frac{991}{948}\right)^4 = 0{,}354 \text{ MPa}.$$

9. We determine the adiabatic gas expansion work in the second stage: /203

$$(L^*_{ad.s})_{II} = \frac{k}{k-1} RT_0^{*''} \left[1 - \left(\frac{p_2^*}{p_0^{*''}}\right)^{\frac{k-1}{k}}\right] = 1155 \cdot 1128 \left[1 - \left(\frac{0,354}{0,636}\right)^{0,25}\right] =$$
$$= 177600 \text{ J/kg}$$

$$(L_{ad.s})_{II} = \frac{k}{k-1} RT_0' \left[1 - \left(\frac{p_2}{p_0'}\right)^{\frac{k-1}{k}}\right] = 1155 \cdot 1106 \left[1 - \left(\frac{0,298}{0,59}\right)^{0,25}\right] =$$
$$= 200600 \text{ J/kg}$$

— the stage reaction at the mean diameter:

$$\rho_m = \frac{L_{ad.r}}{L_{ad.st}} = \frac{66220}{200600} = 0,33;$$

— the stage efficiency:

$$(\eta^*_{st})_{II} = \frac{(L_{st})_{II}}{(L^*_{ad.st})_{II}} = \frac{159000}{177600} = 0,898.$$

10. We refine the adiabatic gas expansion work and the turbine efficiency:

$$L^*_{ad.T} = \frac{k}{k-1} RT_0^* \left[1 - \left(\frac{p_2^*}{p_0^*}\right)^{\frac{k-1}{k}}\right] = 1155 \cdot 1300 \left[1 - \left(\frac{0,354}{1,20}\right)^{0,25}\right] =$$
$$= 395200 \text{ J/kg}$$

$$\eta_T^* = \frac{L_T}{L^*_{ad.T}} = \frac{358000}{395200} = 0,908.$$

This efficiency and the value assumed at the beginning of the turbine calculation practically coincide.

8.2.4. Determination of flow parameters at second stage inner and outer radii

We take the variation of the circumferential velocity component in the axial clearance and at the rotor outlet following the constant circulation law: $c_{1u}r$ = const and $c_{2u}r$ = const.

We summarize the calculation results in Table 8.4.

TABLE 8.4.*

Parameter and formula	Dimension	Design diameter, m		
		0,730	0,825	0,926
$\bar{r} = \frac{r}{r_m}$	—	0,885	1,0	1,135
$c_{1u} = (c_{1u})_m \frac{1}{\bar{r}}$	m/s	539	477	421
$c_{1a} = \sqrt{(c_{1a}^2)_m + (c_{1u}^2)_m \times (1-\varphi^2)\left(1-\frac{1}{\bar{r}^2}\right)}$	m/s	269	274	278
$c_1 = \mathrm{arctg}\,\frac{c_{1a}}{c_{1u}}$	deg	26°31′	29°54′	33°30′
$u_1 = u_{1m}\bar{r}$	m/s	283	320	363
$\beta_1 = \mathrm{arctg}\,\frac{c_{1a}}{c_{1u} - u_1}$	deg	46°24′	60°12′	78°12′
$w_1 = \frac{c_{1a}}{\sin\beta_1}$	m/s	372	316	284
$c_1 = \sqrt{c_{1a}^2 + c_{1u}^2}$	m/s	602	550	504
$T_1 = T_0^{*1} - \frac{c_1^2}{2310}$	K	971	997	1010
$p_1 = p_0^{*1}\left(1 - \frac{c_1^2}{\varphi^2 \cdot 23107 T_0^{*1}}\right)$	MPa	0,338	0,378	0,415
$T_{1w}^* = T_1 + \frac{w_1^2}{2310}$	K	1028	1037	1042
$c_{1u} = (c_{1u})_m \frac{1}{\bar{r}}$	m/s	35	22	19

(Table continued on following page)

TABLE 8.4. (continued)

Parameter and formula	Dimension	Design diameter, m		
		0 730	0,825	0,926
$u_2 = u_{2m}\bar{r}$	m/s	280	317	360
$c_{2a} = \sqrt{(c_{2a}^2)_m + (1-\psi^2)\left[(1-\bar{r}^2)\times u_m^2 + \left(1-\frac{1}{\bar{r}^2}\right)(c_{2u}^2)_m\right] + (1-\varphi^2)\psi^2\left(1-\frac{1}{\bar{r}^2}\right)(c_{1u}^2)_m}$	m/s	312	313	314
$\alpha_2 = \mathrm{arctg}\,\frac{c_{2u}}{c_{2a}}$	deg	85°25′	86°	86°32′
$\beta_2 = \mathrm{arctg}\,\frac{c_{2a}}{c_{2u}+u_2}$	deg	45°38′	42°42′	38°39′
$w_2 = \frac{c_{2a}}{\sin\beta_2}$	m/s	437	461	492
$c_2 = \sqrt{c_{2a}^2 + c_{2u}^2}$	m/s	313,5	314	314,6
$T_2 = T_2^* - \frac{c_2^2}{2310}$	K	948,5	948,3	948,2
$p_2 = p_1\left[1 - \frac{\left(\frac{w_2}{\psi}\right)^2 - w_1^2}{2310T_1}\right]^4$	MPa	0,296	0,298	0,299
$L_{ad.s} = \frac{1}{2}\left[\left(\frac{w_2}{\psi}\right)^2 - w_1^2\right]$	J/kg	35200	66200	91800
$L_{ad.st} = \frac{k}{k-1}RT_0'\left[1-\left(\frac{p_2}{p_0'}\right)^{\frac{k-1}{k}}\right]$	J/kg	202500	200600	200000
$Q = \frac{L_{ad.r}}{L_{ad.st}}$	—	0,174	0,33	0,459

*Translator's note. Commas in numbers represent decimal points.

Calculation of the flow parameters in the turbine stages at various radii using the constant circulation law (under the condition $\phi < 1$ and $\psi < 1$) showed that:

1) for large relative hub diameters (in the present example, $\bar{d}_I = 0{,}829$, $\bar{d}_{II} = 0{,}787$) the axial flow velocity components c_{1a} and c_{2a} vary little along the radius: $(\Delta c_{1a})_I = 5{,}8\%$; $(\Delta c_{1a})_{II} = 3{,}3\%$; $(\Delta c_{2a})_I = 1{,}4\%$; $(\Delta c_{2a})_{II} = 0{,}8\%$.

2) the variation of c_{1a} and c_{2a} along the radius increases with increase of the flow swirl and with reduction of the relative hub diameter $\bar{d}$. For example, calculations of the second stage showed that for the same flow parameters at the mean radius and reduction of the relative hub diameter $\bar{d}_{II}$ from 0.787 to 0.6, the variation of the axial velocities along the radius increases correspondingly: Δc_{1a} — from 3.3% to 10.7%, and Δc_{2a} — from 0.8% to 2.8%, respectively.

This example shows that for large relative stage hub diameters (for relatively short blades), in the calculations of the flow parameters along the radius using the law Γ = const, we can take c_{1a} and c_{2a} to be approximately constant along the radius.

8.3. Example of Approximate Gasdynamic Calculation of Two-Stage TJE Turbine

In many cases, the student is not required to perform detailed calculations of all the multistage turbine stages to satisfy the objective of the academic course or diploma project. In this case, detailed calculations are made only for a single turbine stage, usually the last stage. We shall examine the technique of this approximate calculation in the following example. /206

We take the initial data for the calculation to be the same as in the example considered above (G_g = 92 kg/s: p_0^* = 1.2 MPa; T_0^* = 1300 K; L_T = 358,000 J/kg, n = 7340 rpm; k = 1.33).

We determine the number of turbine stages, distribute the work among the stages, select the flow path shape, and determine its dimensions (see steps 1 - 5 of the example considered above and the flow path scheme of Figure 8.2)*.

As a result of the calculations, we obtain:

$(L_{st})_I$ = 198,200 J/kg; $(L_{st})_{II}$ = 159,800 J/kg; T_2^* = 990 K;

p_2^* = 0.355 MPa; D_o = 0.93 m; D_{i2} = 0.73 m; D_{m2} = 0.825 m.

8.3.1. Gas dynamic calculation of second stage turbine at the mean diameter

The initial data for the stage calculation are: stage work $(L_{st})_{II}$ = 159,800 J/kg, rotor speed n = 7340 rpm, flow parameters at stage outlet p_2^* = 0.355 MPa, T_2^* = 990 K, flow path form and dimensions.

We shall make the calculation using the technique in which the initial parameters are taken to be λ_{2c} = 0.55 and α_2 = 86°.

1. We determine the gas velocity at the stage exit:

the absolute gas velocity

$$c_2 = \lambda_{2c} 18.3 \sqrt{T_2^*} = 0.55 \cdot 18.3 \sqrt{990} = 314 \text{ m/s};$$

the axial and circumferential components of the absolute velocity

$$c_{2a} = c_2 \sin \alpha_2 = 314 \cdot 0.9976 = 313 \text{ m/s}$$
$$c_{2u} = c_2 \cos \alpha_2 = 314 \cdot 0.0698 = 22 \text{ m/s}$$

the circumferential component of the relative velocity

$$w_{2u} = c_{2u} + u_2 = 22 + 317 = 339 \text{ m/s},$$

---

*The turbine parameter calculation technique in steps 1 - 5 and the results of the calculation are exactly the same as those examined above in steps 1 - 5.

where

$$u_2 = \frac{\pi D_{m2} n}{60} = \frac{3,14 \cdot 0,825 \cdot 7340}{60} = 317 \text{ m/s};$$

the relative gas velocity

$$w_2 = \sqrt{c_{2u}^2 + w_{2u}^2} = \sqrt{313^2 + 339^2} = 461 \text{ m/s}.$$

2. We determine the circumferential component of the absolute gas velocity at the rotor inlet.

We take approximately $u_1 \cong u_2 = u = 317$ m/s.

Then, /207

$$c_{1u} = \frac{(L_{st})_{II}}{u} - c_{2u} = \frac{159800}{317} - 22 = 482 \text{ m/s};$$

$$\lambda_{c_{1u}} = \frac{c_{1u}}{18,3\sqrt{T_1^*}} = \frac{482}{18,3\sqrt{1128}} = 0,791,$$

where

$$T^* = T^* - \frac{(L_{st})_I}{1155} = 1300 - \frac{198200}{1155} = 1128 \text{ K}.$$

3. We find the flow angle α_1 and the absolute gas velocity c_1 in the axial clearance.

From the flow equation, we find:

$$\alpha_1 = \arcsin \frac{\bar{G}_g}{\sigma_s^* \, q(\lambda_{1c})}, \tag{8.9}$$

where the constant

$$\bar{G}_g = \frac{G_g \sqrt{T_1^*}}{m F_1 p_2^{*\prime}} = \frac{92\sqrt{1128}}{0,0396 \cdot 0,2537 \cdot 0,635 \cdot 10^6} = 0,484;$$

the flow section area

$$F_1 = \frac{\pi}{4}(D_o^2 - D_i^2) = \frac{3,14}{4}(0,930^2 - 0,730^2) = 0,2537 \text{ m}^2;$$

the total pressure at the second stage inlet

$$p_2^{*\prime} = p_0^*\left(1 - \frac{(L_{st})_I}{1155\ T_0^*(\eta_{st}^*)_I}\right)^4 = 1{,}2\left(1 - \frac{198200}{1155\cdot 1300\cdot 0{,}9}\right)^4 = 0{,}635 \quad \text{MPa}.$$

The first stage efficiency was taken equal to $(\eta_{st}^*)_I = 0.9$.

As the second equation, we use the relation:

$$\cos\alpha_1 = \frac{\lambda_{c_{1u}}}{\lambda_{1c}} = \frac{0{,}791}{\lambda_{1c}}. \tag{8.10}$$

We solve the system of equations (8.6) and (8.10) graphically (see section 8.3.1), and find $\alpha_1 = 30°$, $\lambda_{1c} = 0{,}91$. Then,

the absolute gas velocity

$$c_1 = \frac{c_{1u}}{\cos\alpha_1} = \frac{482}{0{,}866} = 556 \text{ m/s};$$

the axial component of the absolute velocity

$$c_{1a} = c_1 \sin\alpha_1 = 556\cdot 0{,}5 = 278 \text{ m/s};$$

the relative velocity at the rotor inlet

$$w_1 = \sqrt{c_1^2 - 2u_1c_{1u} + u_1^2} = \sqrt{556^2 - 2\cdot 317\cdot 482 + 317^2} = 327 \text{ m/s}.$$

4. We determine the pressure and temperature at the stator exit:

$$p_1 = p_2^{*\prime}\sigma_{S_1}^*\pi(\lambda_{1c}) = 0{,}635\cdot 0{,}978\cdot 0{,}6048 = 0{,}375 \text{ MPa}.$$
$$T_1 = T_1^*\tau(\lambda_{1c}) = 1128\cdot 0{,}8827 = 995 \text{ K}.$$

5. We find the relative velocity angles at the rotor inlet and exit: /208

$$\beta_1 = \operatorname{arctg}\frac{c_{1a}}{c_{1u} - u_1} = \operatorname{arctg}\frac{278}{482 - 317} = 59°19';$$
$$\beta_2 = \operatorname{arctg}\frac{c_{2a}}{w_{2u}} = \operatorname{arctg}\frac{313}{319} = 42°42'.$$

6. We determine the temperature and pressure at the stage exit:

$$T_2 = T_2^*\tau(\lambda_{2c}) = 990\cdot 0{,}9572 = 947 \text{ K};$$
$$p_2 = p_2^*\pi(\lambda_{2c}) = 0{,}355\cdot 0{,}8382 = 0{,}297 \text{ MPa}.$$

Then, the adiabatic gas expansion work in the rotor:

$$L_{ad.r} = 1155T_1\left[1-\left(\frac{p_2}{p_1}\right)^{0,25}\right] = 1155\cdot 995\left[1-\left(\frac{0,297}{0,375}\right)^{2}\right] = 65200 \quad J/kg;$$

the adiabatic gas expansion work in the stage:

$$L_{ad.s} = 1155T_0^{*'}\left[1-\left(\frac{p_2}{p_0^{*'}}\right)^{0,25}\right] = 1155\cdot 1128\left[1-\left(\frac{0,298}{0,635}\right)^{0,25}\right] = 225200\ J/kg;$$

the stage reaction at the mean radius

$$\rho_m = \frac{L_{ad.r}}{L_{ad.st}} = \frac{65200}{225200} = 0,289.$$

After calculating the stage at the mean diameter, we select the flow parameter variation along the blade length and determine the flow parameters at the inner and outer radii.

8.3.2. Determination of flow parameters in stage at inner and outer radii

We take the variation of the absolute velocity circumferential component in the axial clearance and after the rotor following the law $c_u r$ = const and c_a = const.

For convenience of actual blade profile verification with the aid of templates, we take as the design sections D_o = 0.926 m, D_m = 0.825 m, D_i = 0.730 m.

The calculation is made under the assumption that p_0^* = const and T_0^* = const along the blade length. In this case for L_{st} = const and constant losses the flow parameters P_2^* and T_2^* will also be constant along the blade length. Moreover, in calculating $L_{ad.st}$, we take approximately $T_0^{*'}$ = const along the blade length.

We summarize the calculation results in Table 8.5.

TABLE 8.5.*

Parameter and formula	Dimension	Design diameter, m		
		0,730	0,825	0,926
$\bar{r} = \frac{r}{r_m}$	—	0,885	1,0	1,135
$c_{1u} = c_{1u\,m} \frac{1}{\bar{r}}$	m/s	545	482	425
$c_{1a} = \text{const}$	m/s	278	278	278
$\alpha_1 = \text{arctg} \frac{c_{1a}}{c_{1u}}$	deg	26°45′	30°	32°54′
$u_1 \approx u_2 = u_m \bar{r}$	m/s	280	317	360
$\beta_1 = \text{arctg} \frac{c_{1a}}{c_{1u} - u_1}$	deg	46°24′	59°19′	76°51′
$w_1 = \frac{c_{1a}}{\sin \beta_1}$	m/s	384	322	285
$c_1 = \sqrt{c_{1a}^2 + c_{1u}^2}$	m/s	610	556	503
$T_1 = T_0^{*\prime} - \frac{c_1^2}{2310}$	K	967	995	1018
$p_1 = p_0^{*\prime} \left(1 - \frac{c_1^2}{\varphi^2 \cdot 2310 \cdot T_0^{*\prime}}\right)^4$, where $\varphi = 0{,}97 = \text{const}$	MPa	0,335	0,375	0,411
$c_{2u} = c_{2u\,m} \frac{1}{\bar{r}}$	m/s	25	22	20

(Table continued on following page)

TABLE 8.5. (continued)

Parameter and formula	Dimension	Design diameter, m		
		0,730	0,825	0,926
$c_{2a} = \text{const}$	m/s	313	313	313
$\alpha_2 = \text{arctg}\,\frac{c_{2a}}{c_{2u}}$	deg	85°26′	86°	86°20′
$\beta_2 = \text{arctg}\,\frac{c_{2a}}{c_{2u} + u_2}$	deg	45°44′	42°42′	39°30′
$w_2 = \frac{c_{2a}}{\sin \beta_2}$	m/s	437	461	492
$c_2 = \sqrt{c_{2a}^2 + c_{2u}^2}$	m/s	314,1	314	313,7
$T_2 = T_2^* - \frac{c_2^2}{2310}$	K	946,9°	947°	947,4°
$p_2 = p_2^* \left(\frac{T_2}{T_2^*}\right)^4$	MPa	0,297	0,297	0,298
$L_{ad.r} = 11557 T_1 \left[1 - \left(\frac{p_2}{p_1}\right)^{0,25}\right]$	J/kg	33800	65200	91200
$L_{ad.st} = 11557 T_0^* \left[1 - \left(\frac{p_2}{p_0^*}\right)^{0,25}\right]$	J/kg	225200	225200	224300
$\varrho = \frac{L_{ad.r}}{L_{st}}$	—	0,150	0,289	0,406

*Translator's note. Commas in numbers represent decimal points.

8.4. Profiling Turbine Blades

In the present example, we restrict ourselves to construction of the second-stage rotor blade profiles for three cylindrical sections corresponding to D_o = 0.926 m, D_m = 0.825 m, and D_i = 0.730 m (the turbine flow path scheme is shown in Figure 8.2).

We must bear in mind that with this selection of the blade design sections, the reference profile will not be aligned with the streamlines in the flow path. However, the difference between the /211 blade sections along the streamlines and the design sections will be small, and the influence of this on the gas flow in the cascade can be neglected.

The initial data for blade profiling are presented in Table 8.6.

TABLE 8.6.*

Parameter	Design diameter, m		
	0,730	0,825	0,926
β_1	46°24′	59°19′	76°51′
β_2	45°44′	42°42′	39°30′
$\varepsilon = 180 - (\beta_1 + \beta_2)$	87°52′	77°59′	63°39′
$M_{2w} = \frac{w_2}{\sqrt{kRT_2}}$	0,727	0,77	0,817

*Translator's note. Commas in numbers represent decimal points.

Blade profiling is accomplished in the following sequence.

1. We select the basic cadcade and profile parameters:

1) rotor cascade relative spacing at the inner radius, for which we can use the Dyshlevskiy empirical formula:

$$\left(\frac{t}{b}\right)_i = 0{,}55\left[\frac{180}{180-(\beta_1+\beta_2)}\ \frac{\sin\beta_1}{\sin\beta_2}\right]^{\frac{1}{5}}(1-\bar{c}) =$$
$$= 0{,}55\left[\frac{180}{87{,}9}\cdot\frac{0{,}724}{0{,}715}\right]^{\frac{1}{5}}(1-0{,}18) = 0{,}575,$$

where the relative profile thickness at the inner radius in the first approximation is taken equal to $\bar{c}$ = 18%;

2) the angles of attack at the inner radius i_o = -3°, at the mean radius i_m = -1°, and at the outer radius i_i = 2°.

2. From the graph of $\Delta\beta = f(M_{w2}, \beta_2)$ (see Figure 5.5) we determine at the three design radii the flow deviation angle $\Delta\beta$, and then the leaving angle $\beta_{2p} = \beta_2 - \Delta\beta$.

3. We determine the rotor blade chord length at the inner radius, where it differs little from the width; therefore, we can take $b \cong s_i$ = 30 mm for finding the cascade spacing and number of blades:

the rotor cascade spacing at the inner radius

$$t_i = s_i\left(\frac{t}{b}\right)_i = 30\cdot 0{,}575 = 17{,}25 \text{ мм};$$

the number of rotor blades

$$z_r = \frac{\pi D_i}{t_i} = \frac{3{,}14\cdot 730}{17{,}25} = 132{,}5.$$

We take the number of rotor blades z_r = 132 and, correspondingly, t_i = 17.3 mm.

4. We find the cascade spacing and solidity at the mean and outer radii: /212

$$t_m = t_i\frac{D_m}{D_i} = 17{,}3\cdot\frac{0{,}825}{0{,}730} = 19{,}55 \text{ мм};$$
$$t_o = t_i\frac{D_o}{D_i} = 17{,}3\cdot\frac{0{,}926}{0{,}730} = 21{,}98 \text{ мм}.$$

For constant chord b = 30 mm along the blade length, we find:

$$\left(\frac{t}{b}\right)_m = 0{,}652, \quad \left(\frac{t}{b}\right)_o = 0{,}733.$$

5. We determine the interblade channel throat width at the mean radius:

$$a = t \sin \beta_{2p} = 19{,}55 \cdot 0{,}6494 = 12{,}7 \text{ mm},$$

and the relative interblade channel throat height:

$$\frac{h_b}{a} = \frac{105}{12{,}7} = 8{,}27.$$

From the condition of acceptable magnitude of the end losses, the quantity h/a should be no less than 6 - 7.

6. We determine the geometric mean velocity slope β_m at the three design radii from the formula:

$$\beta_m = \operatorname{arctg} \frac{w_1 \sin \beta_1 + w_2 \sin \beta_2}{w_2 \cos \beta_2 - w_1 \cos \beta_1}$$

and the profile setting angle ϑ in the cascade. At the outer and mean radii, we take $\vartheta = \beta_m$, and at the inner radii — $\vartheta = 0{,}85\,\beta_m$.

7. We find the relative profile thicknesses at the design radii. We take at the outer radius $\bar{c}_o$ = 6% or c_o = 1.8 mm. (On the basis of blade vibrational strength at the periphery, c_o should be no less than 4 - 5%, usually, $c_o \geqq 1.5 - 2.0$ mm.)

We can use the approximate relation to find the profile area:

$$f = K \frac{b^2}{s} c,$$

where f — profile area;
K — a coefficient;
b — chord;
$s = b \sin \vartheta$ — cascade width;
c — maximal profile thickness.

From statistical data of several existing turbines K = 0.6 - 0.72 (the larger values of K apply to the blade root sections).

The blade section area at any radius can be found from the formula:

$$f_r = f_i - (f_i - f_o)\bar{x}^m$$

where $\bar{x} = \frac{r - r_i}{h_b}$;

r_i — blade root section radius;

$$h_b = r_o - r_i.$$

For linear blade section area variation along the radius, m = 1.

We determine the relative profile thickness at the inner radius, /213 where $\beta_{1\,b} \approx \beta_{2\,b}$, from the condition that the maximal profile thickness:

$$c_{max} \cong t - a = t(1 - \sin\beta_{2p})$$

and

$$\bar{c} = \frac{c_{max}}{b} < \frac{t(1 - \sin\beta_{2p})}{b}.$$

In the present example,

$$\frac{t(1 - \sin\beta_{2p})}{b} = \frac{17{,}3(1 - 0{,}673)}{30} = 0{,}189.$$

We take the relative profile thickness at the inner radius $\bar{c}_i$ = 0.186, and the maximal profile thickness $c_i = \bar{c}_i b$ = 5.6 mm.

The blade section area ratio at the outer and inner radii for b = const can be taken approximately equal to the profile thickness ratio:

$$\bar{f} = \frac{f_o}{f_i} \approx \frac{c_o}{c_i} = \frac{1{,}8}{5{,}6} = 0{,}32.$$

This value of $\bar{f}$ is close to the value $\bar{f} = 0.3$, previously assumed in calculating the blade strength margin. (If the area ratio $\bar{f}$ is found to be significantly different from the value previously assumed, it is necessary to make an additional check of the blade strength margin.)

For the previously assumed linear blade section area variation along the length, the blade relative thickness at the mean radius:

$$\bar{c}_m \cong \frac{\bar{c}_o + c_i}{2} = \frac{0{,}06 + 0{,}186}{2} \approx 0{,}123.$$

and the profile thickness:

$$c_m = \bar{c}_m b = 0.123 \cdot 30 = 3.69 \text{ mm}.$$

8. We take the leading edge radius (r_1) and the trailing edge radius (r_2), and also the edge taper angles ϕ_1 and ϕ_2, in accordance with the recommendations in Chapter VI.

We summarize the results of the basic cascade and profile parameter determination in Table 8.7.

9. We construct the blade profiles using the initial data presented in Table 8.7 (Figure 8.5).

The blade profiles can be constructed using one of the techniques presented in section 5.2. In the present example, the profile contours at all three design radii were drawn using parabolic arcs. The back of the profile was described by a single parabolic arc, and the front — by two arcs.

We construct the neighboring profile at the cascade spacing at the given section, and verify the interblade channel throat width a.

TABLE 8.7.*

Parameter	Dimension	Value of parameters at sections		
		D_i=0,730 m	D_m=0,825 m	D_o=0,926 m
t/b	—	0,611	0,69	0,776
i	deg	2	—1	—3
β_{2p}	deg	42°18′	40°32′	38°24′
b	mm	30	30	30
t	mm	17,30	19,55	21,98
ϑ	deg	90°54′	103°00′	122°48′
s	mm	30,0	29,2	2[illegible],2
e	mm	5,6	3,69	1,8
r_1	mm	0,9	0,7	0,5
r_2	mm	0,6	[illegible]	0,4
γ_1	deg	24	16	8
γ_2	deg	10	7	5

*Translator's note. Commas in numbers represent decimal points.

The results of the construction show show that the resulting interblade channel throat width satisfies the condition $a = t \sin \beta_{2p}$.

If we find that $a \neq t \sin \beta_{2p}$, we vary the trailing edge shape (vary the angle ϕ_2 or δ) or vary the profile setting angle ϑ to satisfy the condition $a = t \sin \beta_{2p}$. The magnitude of the profile back-side camber angle δ_b downstream of the interblade channel throat must also lie in acceptable limits.

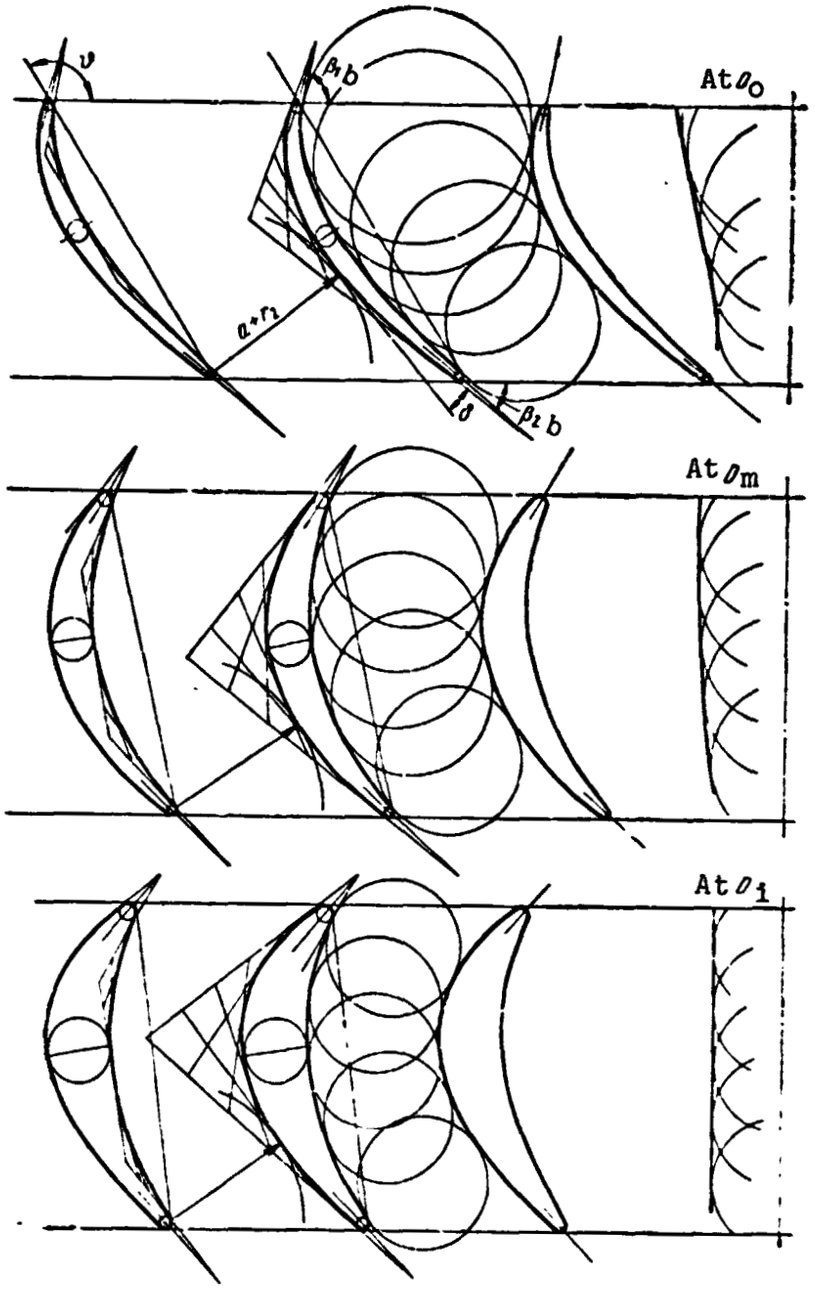

Figure 8.5. Blade profile construction

After this, we verify the flow section variation along the interblade channel length. We see that the interblade channels at the peripheral and mean sections have a smoothly varying convergent form. The root section channel has a slight divergence in the aft segment, /214 but this divergence lies in the allowable limits (see section 5.1).

If the interblade channel flow section area variation is unfavorable (for example, if there is significant local channel divergence), it must be corrected — for example, by shifting the maximal profile thickness location along the blade chord, by varying the magnitude of the leading and trailing edge taper angles, or by an acceptable change of the maximal profile thickness.

After constructing the profiles at the design sections, we match the individual section profiles and construct the profile part of the blade (see section 5.3). Then we prepare the blade working drawing (see Appendix 5) and formulate the specification for its fabrication.

CHAPTER IX

OFF-DESIGN TURBINE OPERATING REGIMES

9.1. Basic Concepts of Turbine Operating Regimes and Characteristics

The combination of basic physical quantities (p^*, T^*, c) characterizing the turbine is called the turbine operating regime. The determination of the basic turbine parameters and flow path dimensions is made for a single operating regime, termed the design regime. /216

As a rule, this regime corresponds to the takeoff or nominal engine operating regime. The values of the gas expansion ratio π_T^*, work L_T, efficiency η_T^*, gas mass flowrate G_g, rotational speed n, and other parameters corresponding to the design turbine operating regime are termed the design parameters.

Separation-free flow around the blades at the optimal angles of attack is provided in the design regime. Depending on the flight regime and the engine operating regime, the turbine inlet gas parameters (p_0^*, T_0^*) and the turbine operating regime may change markedly during turbine operation in the gas-turbine engine system.

In it shown in gas-turbine theory courses [7, 25, 32] that, for a turbine with given geometric dimensions (or for geometrically similar turbines), the operating regime is determined by three

working fluid (gas) parameters p_0^*, T_0^*, and p_2, the rotational speed n, and four parameters characterizing the physical and chemical properties of the gas: specific heat capacity c_p (or ratio of the specific heat capacities k), gas constant R, dynamic viscosity μ, and thermal conductivity λ.

Turbine operating regimes (real gas flows) are termed **gas-dynamically similar if** geometric similarity (constant ratios of all the like dimensions), kinematic similarity (similarity of the velocity fields), and dynamic similarity (similarity of the pressure and temperature fields and, correspondingly, similarity of the pressure, viscous, and inertia forces) are observed.

Steady flows in geometrically similar channels are similar if the ratios of the velocities, pressures, and temperatures at any two comparable points are the same: /217

$$\frac{c_2}{c_1}=\frac{c_2'}{c_1'}=\text{idem};\quad \frac{p_2}{p_1}=\frac{p_2'}{p_1'}=\text{idem};\quad \frac{T_2}{T_1}=\frac{T_2'}{T_1'}=\text{idem}.$$

This implies that the pressure, temperature, and velocity fields at any correspondingly located sections along the turbine flow path are similar.

In similar regimes, not only the ratios of like physical quantities, but also any dimensionless groups formulated from these physical quantities, also remain unchanged.

It is established in similarity theory that, among the various dimensionless groups formulated from the physical quantities, there are groups which define the given phenomenon (or gas flow). Such dimensionless groups are termed <u>similarity criteria</u>.

The following are most often used as similarity criteria in turbomachines:

— adiabatic exponent $k=\frac{c_p}{c_v}$;

— Mach number $M=\frac{c}{a}=\frac{c}{\sqrt{kRT}}$;

— the parameter u/c;

— Reynolds number $Re=\varrho cl/\mu$ (or $Re=\varrho cD/\mu$);

— Prandtl number $Pr=\mu c_p/\lambda$.

The specified values of these five criteria define completely the turbine stage operating regime. In similar regimes

$$k=k'=\text{idem};\ M=M'=\text{idem};\ \frac{u}{c}=\frac{u'}{c'}=\text{idem};$$

$$Re=Re'=\text{idem};\ Pr=Pr'=\text{idem}$$

and all the other dimensionless parameters — for example, the pressure and temperature differences at two comparable sections, turbine efficiencies, and so on — remain the same for any values of the turbine inlet gas parameters.

The magnitude of the adiabatic exponent k depends on the gas temperature and state. In aircraft gas-turbine-engine turbines, in the gas temperature range realizable at the present time, the quantity k can be considered practically constant when analyzing the off-design regimes. Therefore, the adiabatic exponent k is usually excluded from the number of parameters defining the turbine operating regime.

The Prandtl number, characterizing the physical properties of the working fluid, is determined by the number of atoms in the gas molecule, and is independent of the pressure and temperature of the gas. Since the turbine analysis in the off-design regimes is made for definite gases (usually diatomic gases), the influence of the /218
Prandtl number on the turbine operating regime is also usually neglected.

Under these assumptions, similarity of gas flow in the turbine will be determined by the Mach and Reoynolds numbers and by the parameter u/c.

We know from gasdynamics that the Mach number characterizes the influence of fluid (gas) compressibility and the Reynolds number characterizes the influence of fluid (gas) viscosity on the nature of the flow and the hydraulic losses in the turbine; the parameter u/c determines the kinematic similarity of the flows in the turbine (similarity of the velocity diagrams).

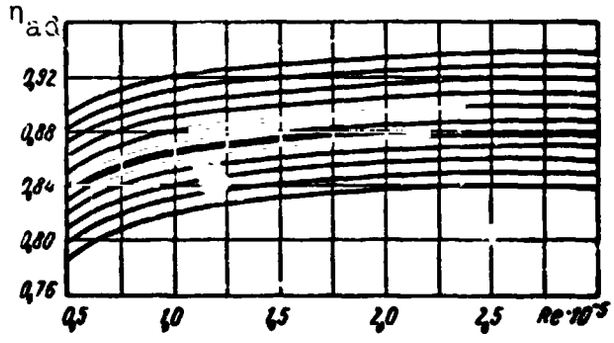

Figure 9.1. Turbine adiabatic efficiency versus Reynolds number

Aircraft gas turbine engine turbines usually operate in the region of self-similarity with respect to the Reynolds number (except for the turbines of lower power GTE and during GTE operation at high altitudes). Therefore, the influence of Re change on the hydraulic losses in the turbine is not considered when calculating the basic turbine parameters in the off-design regimes. If the turbine Reynolds number does not lie in the self-similarity range ($Re < 1{,}5 \cdot 10^5$), corrections for the influence of Re, based on experimental data, must be introduced when determining the efficiency and other turbine parameters. The Akimov relations (Figure 9.1) from [1] can be used to evaluate the influence of Re on turbine efficiency.

For turbine operation in the self-similar regime with respect to Re, turbine operating regime similarity will be determined by only two criteria: the Mach number and the parameter u/c.

The similarity criteria M and u/c can be defined in terms of the parameters at any section along the turbine flow path. It is most convenient to examine these parameters in the turbine axial clearance, i.e., $M_1 = c_1/a_1$ and u_1/c_1. Other critical parameters which are proportional to the criteria M_1 and u_1/c_1 can also be used in practice for determining turbine operating regime similarity.

Bearing in mind that $M_1 \frac{u_1}{c_1} = \frac{c_1}{a_1}\frac{u_1}{c_1} = \frac{u_1}{a_1} = M_{1u}$, we obtain the similarity criteria M_1 and $M_{1\,u}$, and the criteria λ_1 and $\lambda_{1\,u}$, which are uniquely related with the former. /219

In place of the similarity criterion λ_1, we can use the uniquely-related-with-it magnitude of the relative stream density $q(\lambda_1)$, characterizing the gas flowrate through the turbine:

$$q(\lambda_1) = \frac{1}{m\sigma^*_S F_1 \sin\alpha_1}\,\frac{G_g\sqrt{T_0^*}}{p_0^*} \approx \text{const}\,\frac{G_g\sqrt{T_0^*}}{p_0^*}.$$

The similarity criterion $\lambda_{1\,u}$ can be related with the turbine rotational speed:

$$= \frac{u_1}{a_{cr\,1}} = \frac{\pi D}{60\sqrt{2\frac{k}{k+1}R}}\,\frac{n}{\sqrt{T_0^*}} = \text{const}\,\frac{n}{\sqrt{T_0^*}}.$$

In many cases, it is more convenient to use in place of λ_1 the parameter λ_2 (or λ_{2w}) at the rotor exit.

When the turbine operates in the GTE system, the basic parameters characterizing the turbine and determining the engine operating regime on the stand or in a given flight regime are:

1) gas mass flowrate G_g or the parameter $\frac{G_g\sqrt{T_0^*}}{p_0^*} = \sigma^*_S F_1 m q(\lambda_1)\sin\alpha_1$, characterizing the turbine discharge capacity;

2) turbine work L_T, or the parameter L_T/T_0^*;

3) turbine efficiency η_T^*, characterizing the turbine effectiveness as an engine element;

4) gas expansion ratio in the turbine $\pi_T^* = p_0^*/p_2^*$ or $\pi_T = p_0^*/p_2$;

5) turbine rotational speed or the parameter $n/\sqrt{T_0^*}$.

The parameters G_g, L_T, η_T^* characterize turbine operating effectiveness in the given engine operating regime. The parameters π_T^* and n are the regime parameters which determine the gas flow regime in the turbine. In the gas turbine engine operating process, they may vary because of change of the compressor compression ratio, turbine inlet gas temperature, and turbine loading.

The curves of turbine effectiveness parameters G_g, L_T, η_T^* versus the regime parameters π_T^* (or π_T) and n are usually called the turbine characteristics. In order to make the turbine characteristics universal, they must be represented in the form of curves of the criterial parameters:

$$\left.\begin{aligned} \frac{G_g\sqrt{T_0^*}}{p_0^*} &= f\left(\pi_T, \frac{n}{\sqrt{T_0^*}}\right); \\ \frac{L_T}{T_0^*} &= f\left(\pi_T, \frac{n}{\sqrt{T_0^*}}\right); \\ \eta_T^* &= f\left(\pi_T, \frac{n}{\sqrt{T_0^*}}\right). \end{aligned}\right\} \qquad (9.1)$$

or of the reduced parameters /220

$$\left.\begin{aligned} G_{red} &= f(\ _T, n_{red}); \\ L_{T.red} &= f(\ _T, n_{red}); \\ \ _T^* &= f(\ _T, n_{red}); \end{aligned}\right\} \qquad (9.2)$$

where $G_{red} = G_g\sqrt{\frac{T_0^*}{T_{0d}^*}}\,\frac{p_{0d}^*}{p_0^*}$; $n_{red} = n\sqrt{\frac{T_{0d}^*}{T_0^*}}$; $L_{T.red} = L_T\frac{T_{0d}^*}{T_0^*}$,

$p_{0\ d}^*$ and $T_{0\ d}^*$ — turbine inlet pressure and temperature in the design regime.

The experimental characteristic of a single-stage turbine represented by the curves of G_{red} and $L_{T.red}$ for π_T versus π_T for n_{red} = const is shown in Figure 9.2.

The turbine characteristics also may have a different graphical representation, depending on choice of the system of parameters. In several studies [8, 28], the turbine characteristics are represented in the form of the relations:

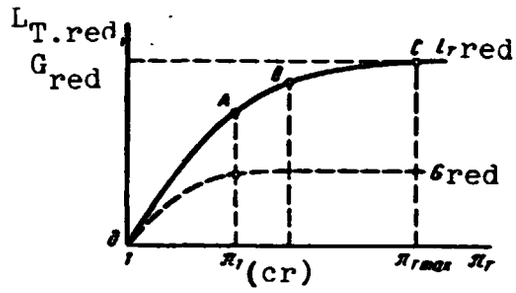

Figure 9.2. Glas flowrate and work versus gas expansion ratio in turbine for n = const

$$\pi_T^* = f\left(\frac{G_g\sqrt{T_0^*}}{p_0^*},\ \frac{n}{\sqrt{T_0^*}}\right);$$

$$\eta_T^* = f\left(\frac{G_g\sqrt{T_0^*}}{p_0^*},\ \frac{n}{\sqrt{T_0^*}}\right).$$

The turbine characteristics can be obtained experimentally (as a result of testing turbines on special stands) or by calculation (analytically). The experimental characteristics are more reliable than the theoretical characteristics, but they can be obtained only for an existing turbine or its model, while the characteristics for both the turbine being designed and the existing turbine can be obtained by calculation.

The off-design regime theory and the turbine characteristic calculation methods have been improved and developed in studies by Kazandzhan, Abiants, Emin, Cherkasov, and other investigators. At the present time, the available analytic calculation methods make it possible to obtain turbine characteristics with adequate accuracy in a comparatively narrow range of turbine operating regime variation. Further accumulation of experimental data and improvement of the methods for calculating turbine characteristics are necessary in order to obtain sufficiently accurate turbine characteristics in a wide range of operating regime variation (particularly of turbines with cooled blades). /221

9.2. Laws Governing Variation of Basic Turbine Parameters with Turbine Operating Regime Variation

Let us first examine the influence of change of the pressure ratio in the turbine stage on the gas flowrate, turbine work, and efficiency for a constant value of the rotational speed n. For simplicity, we shall assume that the turbine inlet gas temperature and pressure (P_0^* and T_0^*) remain constant, and variation of $\pi_T = p_0^*/p$ is accomplished by varying the turbine exit pressure.

9.2.1. Gas flowrate variation

With increase of the pressure ratio in the turbine stage, the pressure ratios in the stator and rotor increase, which is accompanied by increase of the reduced velocity leaving the stator cascade (λ_1) and the rotor cascade ($\lambda_{2\ w}$). This results in increased gas flowrate through the turbine. In fact, it follows from the stator flowrate equation:

$$G_{red} = m \frac{\sigma_s^* p_{0d}^*}{\sqrt{T_{0d}}} F_1 \sin \alpha_1 q(\lambda_1) \qquad (9.3)$$

that G_{red} varies in proportion to $\sin \alpha_1 q(\lambda_1)$. The angle α_1 and $\sin \alpha_1$ remain practically constant with increase of λ_1 to $\lambda_1 \leqslant 0{,}65-0{,}7$ (see Figure 5.5). Therefore, in this flow velocity range, $G_{red} \sim q(\lambda_1)$. With further increase of π_T the gas flowrate increase with increase of π_T slows down, since the flow lag angle in the cascade decreases as π_s increases, and therefore the angle α_1 and $\sin \alpha_1$ decrease and the growth of $q(\lambda_1)$ slows down.

In the case of critical pressure ratio in the stator (π_s = 1.85), the flow velocity in the intervane channel narrow section (throat) reaches the speed of sound ($q_{g.s}$ = 1), and "choking" of the turbine with respect to gas flowrate takes place.

Usually, "choking" of the turbine stator takes place first; however, in turbine stages with a high degree of reaction $\rho \geqslant 0{,}5$, "choking" of the rotor takes place first, when $\lambda_{2w} \geqslant 1$ and $q_{g.r} = 1$.

In the case of a choked stator ($q_{g.s} = 1$), further increase of π_T does not lead to increase of the gas flowrate through the turbine. In this case, with increase of π_T and with corresponding increase of /222
π_s and π_r, there is increase of the stator exit velocity ($\lambda_1 > 1$) because of gas expansion in the stator cascade oblique exit, and the flow deflection in the cascade oblique exit increases in the direction of increasing angle α_1, and the flow velocity (λ_{2w}) at the exit from the rotor cascade increases.

The stator exit flow velocity increases until "choking" of the rotor cascade throat takes place with $\lambda_{2w} = 1$.

For subcritical pressure ratios, the flow deflection angle in the stator (rotor) cascade can be found from Figure 5.5, and for supercritical pressure ratios — from the formula:

$$\sin \alpha_1 = \frac{\sin \alpha_{1p}}{q(\lambda_1)},$$

obtained from the equation of flow continuity between the stator cascade throat section and the stator exit section I - I, where $\sin \alpha_{1p} = a/t$, a is the intervane throat width, and t is the cascade spacing.

The relation $G_{red} = f(\pi_s)$ can be plotted as a result of calculation using (9.3). Figure 9.3 shows the experimental dependence of the relative reduced gas flowrate $\bar{G}_{red} = G_{red}/G_{red.max}$ on π_s for α_1 = const along the radius (taken from [8]). We see that the gas /223
flowrate reaches a maximal value for the critical pressure ratio in the stator ($\pi_s = 1.85$). For the turbine stage with degree of reaction $\rho = 0$, turbine choking with respect to flowrate occurs for

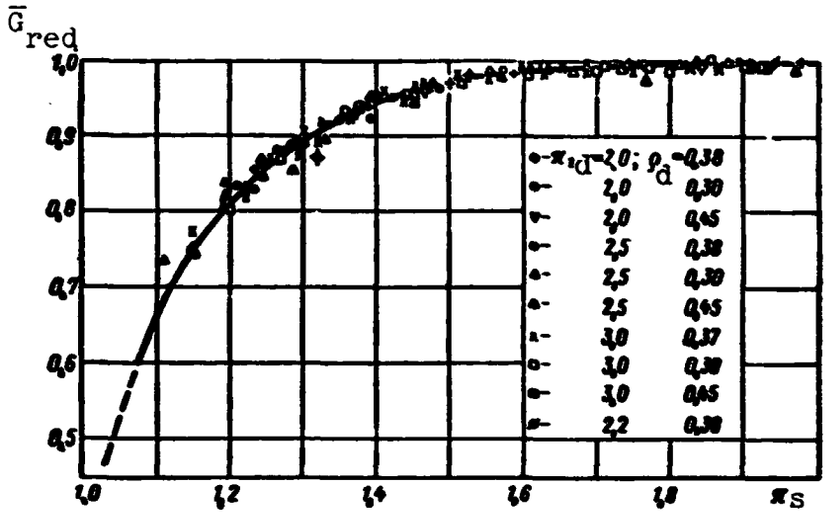

Figure 9.3. Relative reduced flowrate versus turbine stator pressure ratio for various values of the gas expansion ratio and degree of reaction ρ

$\pi_T = \pi_s = 1.85$. With increase of ρ, the turbine "chokes" with respect to the gas flowrate at higher values of π_T.

The nature of the relation $G_{red} = f(\pi_T)$ is determined primarily by the design gas expansion ratio in the turbine stage $\pi_{T.d}$, and depends to a lesser degree on the design turbine reaction ρ_d. When calculating turbine characteristics, it is more convenient to have a single generalized relation $\bar{G}_{red} = f(\bar{\pi}_T)$, where $\bar{G}_{red} = G_{red}/G_{red.d}$, $\bar{\pi}_T = \pi_T/\pi_{T.d}$. As a result of analysis of the relation $G_{red} = f(\pi_T)$ for a turbine with various values of $\pi_{T.d}$ and ρ_d, made in [25], it was found to be possible to present the relations $\bar{G}^2_{red} = f(\bar{\pi}_T)$, obtained for turbines with different values of $\pi_{T.d} = 2 - 3$ and $\rho_d = 0.3 - 0.45$, in the form of a single curve (Figure 9.4) in the coordinates $\bar{G}^2_{red}$ and $A(\pi_T - 1)$, where A — a coefficient obtained by trial and error:

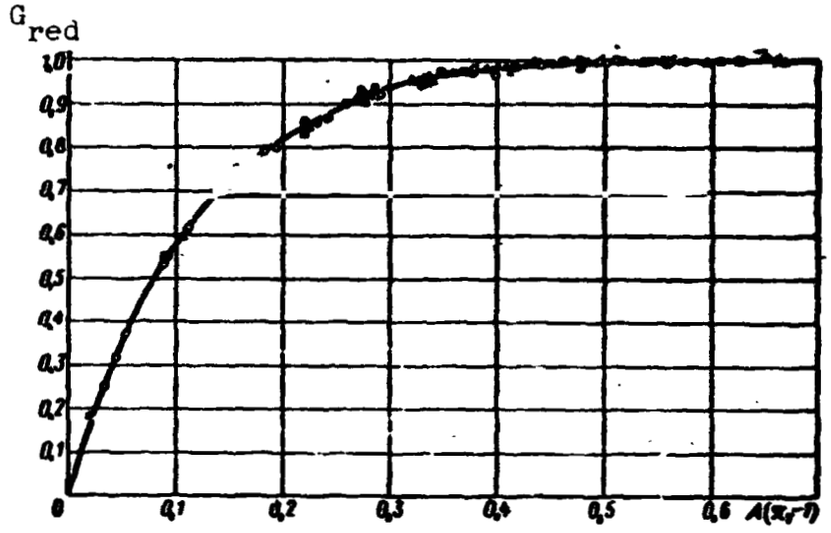

Figure 9.4. Generalized dependence of $\bar{G}^2_{red}$ on π_T (symbols the same as in Figure 9.3)

$$A = \frac{1}{e_d + 1} \left(\frac{e_{cr\ 0}}{e_{cr}}\right)^{1/2} .$$

Here, $e_d = \frac{\pi_{T.d}^{\frac{k-1}{k}}}{}$; e_{cr} — is the effective temperature ratio in the stage, corresponding to the critical pressure ratio in the stator ($\pi_s = 1.85$).

For $k = 1.33$, and assuming that $\rho_{d.cr} \approx \rho_d$, /224

$$e_{cr} = \frac{1-\rho_d}{0,856-\rho_d},$$

where $\rho_{d.cr}$ — is the degree of reaction corresponding to the critical pressure ratio in the stator;

$$e_{cr\ 0} = e_{cr} \text{ for } \rho_d = 0.3.$$

The coefficient A, constant for a given turbine, accounts for the influence of the design values of $\pi_{T.d}$ and ρ_d on the relation $= f(\bar{\pi}_T)$.

We see from Figure 9.4 that all the points for the different turbines lie on a single curve to within 1% when determining $\bar{G}_{red} = f(\bar{\pi}_T)$. The resulting relation $\bar{G}_{red} = f(\bar{\pi}_T)$ can be used with sufficient accuracy for calculating the turbine characteristics using the approximate method. In the range of $\bar{G}^2_{red}$ variation from 0.6 to 1.0, the curve $\bar{G}^2_{red} = f(\bar{\pi}_T)$ can be expressed by the following approximate formula to within 0.5 to 1% when determining $\bar{G}_{red}$:

$$\bar{G}^2_{red} = 1{,}12 - \frac{0{,}06}{A(\pi_T - 1)}.$$

The experimental results show that for a constant value of π_T, turbine rotational speed variation in the limits of ∿ 25% has practically no effect on the gas flowrate through the turbine, and this influence is the smaller, the larger π_T.

9.2.2. Turbine work variation

For any constant turbine rotational speed, increase of the gas expansion ratio π^*_T leads to increase of the turbine work:

$$L_T = 1158 T^*_0 \left[1 - \left(\frac{1}{\pi^*_T}\right)^{\frac{k-1}{k}}\right] \eta^*_T.$$

We shall examine the laws governing the variation of the turbine work L_T with variation π_T for the example of a single-stage turbine (or turbine stage).

With increase of $\pi_T = p_0^*/p_2$, the gas expansion ratios in the stator π_s and in the rotor π_r increase and, consequently, the flow velocities at the stator exit c_1 and at the rotor exit w_2 and c_2 increase. Accordingly, the circumferential velocity components c_{1u} and c_{2u}, and the turbine stage work:

$$L_T = u(c_{1u} + c_{2u}) = u(c_{1u} + w_{2u} - u).$$

increase.

The nature of the turbine stage work variation with π_T is shown in Figure 9.2. Up to point B, the turbine work increases because of increase of the circumferential velocity components $c_{1\,u}$, $w_{2\,u}$. The point A corresponds to the turbine "choking" regime with respect to gas flowrate $M_{1\,c} = 1$. In the region A - B, increase of the velocities c_1 and $c_{1\,u}$ with increase of π_T takes place, only because of gas expansion in the stator oblique exit. For π_T corresponding to point B, the flow velocity in the rotor interblade channel throat reaches the speed of sound $(w_2 = a_2)$. In this case, further increase of π_T does not lead to change of the flow regime or change of the velocit in the stator. /225

Also possible is the case when the velocity c_1 reaches its limiting value first (limit of oblique exit expansion capability, when $c_{1a} = a_1$) with $w_2 < a_2$. However, this case is not characteristic for aircraft GTE turbines. Usually, the rotor throat chokes first, and the velocity c_1 does not reach its limiting value.

For $w_2 \geqslant a_2$ with increase of π_T, increase of the turbine work will take place only as a result of increase of the velocity $w_{2\,u}$, with gas expansion in the rotor cascade oblique exit. In this case, the increase of $w_{2\,u}$ with increase of π_T will be slight, since with increase of the velocity w_2, the flow deflection in the oblique exit increases, which slows the rate of increase of the velocity $w_{2\,u}$.

At the point C, corresponding to $\pi_{T\,max}$, the expansion capacity of the rotor oblique exit is completely utilized $(w_{2a} = a_2)$, and the velocity $w_{2\,u}$ reaches its maximal value. Further reduction of the turbine discharge pressure does not lead to increase of π_T and L_T. At point C, π_T and L_T reach their maximal values, and turbine "choking" with respect to work takes place.

In the design turbine operating regime $L_{T.d} < L_{T.max}$. The difference $L_{T.max} - L_{T.d} = \Delta L_T$ is termed the turbine work margin. The magnitude of the turbine work margin determines the possibility of regulating turbine work during engine development through varying π_T by varying the propulsive nozzle throat area. For small work margins, the turbine becomes practically unregulatable and reacts sluggishly to propulsive nozzle throat area variation.

The turbine work margin depends on the flow Mach number downstream of the turbine in the design regime (M_{2d}). A Mach number M_{2d} no higher than 0.55 - 0.6 must be taken in order to provide the required turbine work margin.

Figure 9.5 shows calculated and experimental values of turbine work versus π_T for various reduced rotational speeds. We see that, depending on the magnitude of π_T, with increase of the turbine rotational speed, the turbine work may either increase or decrease. The nature of the influence of rotational speed n on the turbine work is determined by the nature of the turbine efficiency variation with variation of the rotational speed n.

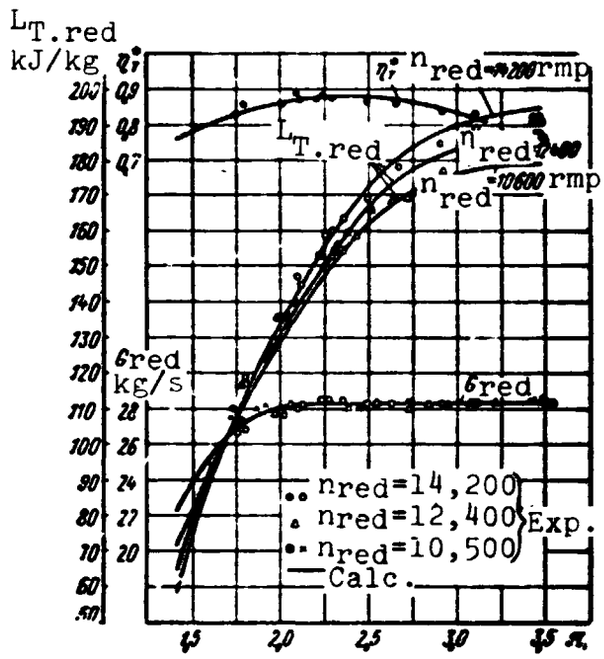

/226

Figure 9.5. Efficiency, reduced gas flowrate, and turbine work versus gas expansion ratio in turbine for various reduced rotor speeds, n_{red}

9.2.3. Turbine efficiency variation in off-design regimes

In the off-design turbine operating regimes, the angles of attack deviate from their design values and, as a result of this, the profile, secondary, and end losses change.

We know from the analysis presented in Chapter 1 that:

$$\eta_T^* = \frac{L_T}{L^*_{ad.T}} = 1 - \frac{L'_{r.T}}{L^*_{ad.T}}. \tag{9.4}$$

For any given value of π_T^*, the turbine adiabatic work $L^*_{ad.T}$ is known. In this case, the turbine efficiency will be determined by the magnitude of the irreversible losses:

$$L'_{r.T} = \left(\frac{1}{\varphi^2} - 1\right)\frac{c_1^2}{2} + \left(\frac{1}{\psi^2} - 1\right)\frac{w_2^2}{2}. \tag{9.5}$$

For simplicity of the analysis, we shall examine only the influence of operating regime change on the turbine profile losses, since the question of operating regime influence on the magnitude of the secondary and end losses has not yet been studied sufficiently. /227

For moderately loaded GTE turbines, the stator velocity coefficient ϕ in a wide range of regime variation can be considered to be practically constant and the rotor velocity coefficient ψ depends primarily on the angle of attack i. In order to determine the variation of the velocity coefficient ψ with change of the angle of attack, we can use the generalized Matkovskiy graph (Figure 9.6).

The flow velocities c_1 and w_2 depend on π_T and on the distribution of the pressure ratios between the stator and rotor in the off-design regimes.

Thus, in any given turbine operating regime with known kinematics of the flow in the stage, we can determine the variation of η_T^*, caused by variation of the profile losses and flow velocities.

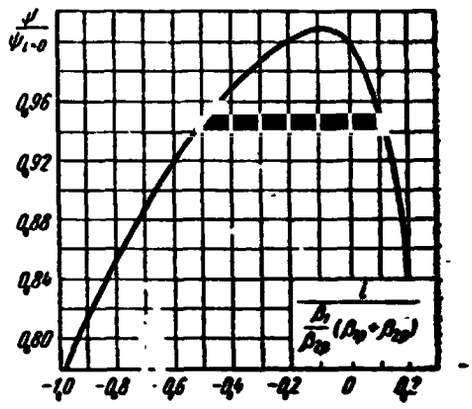

Figure 9.6. Relative velocity coefficient $\psi/\psi_{i=0}$ as a function of angle of attack

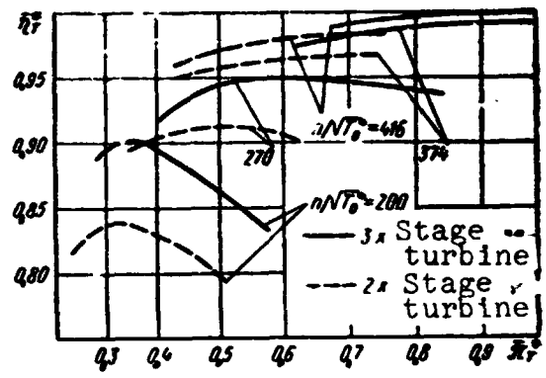

Figure 9.7. Relative efficiency versus gas expansion ratio in turbine for various constant value of the parameter $n/\sqrt{T_0^*}$

The dependences $\bar{\eta}_T^*$ on $\bar{\pi}_T^*$ for various values of the rotational speed parameter $n\sqrt{T_0^*}$ are shown in Figure 9.7. We see from this figure that for any given value of n and a definite value of $\bar{\pi}_T^*$, the turbine efficiency has a maximal value. We see from (9.4) and (9.5) that the reduction of $\bar{\eta}_T^*$ with $\bar{\pi}_T^* > \bar{\pi}_{T.opt}^*$ is caused basically by increase of the flow velocities in the turbine and some reduction of the velocity coefficient ψ. /228

For $\bar{\pi}_T^* < \bar{\pi}_{T.opt}^*$, the reduction of $\bar{\eta}_T^*$ takes place primarily because of reduction of the angle of attack and the velocity coefficient ψ.

Change of the turbine rotational speed wi $\bar{\pi}_T^*$ = const causes change of the angle of attack and the flow turning angle in the rotor, as a result of which the velocity coefficient ψ changes. In the region of $\bar{\pi}_T^*$, values not differing markedly from $\bar{\pi}_{T.d}^*$, with $\bar{\eta}_T^*$, decreases reduction of the turbine rotational speed.

9.3. Determination of Basic Turbine Parameters in Off-Design Regimes

The calculation of the throttling and altitude-speed characteristics of gas turbine engines with subcritical pressure ratios in the propulsive nozzle can be made with adequate accuracy only in the case when the compressor and turbine characteristics are available. In many cases, we can do without the turbine characteristics, whose construction involves the expenditure of a large amount of time, if in each engine operating regime we can determine with adequate accuracy the basic turbine parameters. For this, it is necessary to know the distribution of the pressure ratios between the turbine and the propulsive nozzle, and also between the stages of the multistage turbine.

9.3.1. Division of pressure ratios between the turbine and the propulsive nozzle

For the case of supercritical pressure ratios in the propulsive nozzle ($\pi_{pn} > 1.85$), the pressure ratio in the turbine $\pi_T^* = \text{const}$, and the pressure ratio in the propulsive nozzle $\pi_{pn} = \pi_c \sigma_{cc}^* / \sigma_T^*$, where $\pi_c = p_k^*/p_H$ is the overall air compression ratio in the engine, σ_{cc}^* is the coefficient of total pressure loss in the combustion chamber, p_k^* is the compressor exit total pressure.

The relation $\pi_T^* = f(\pi_c)$ for subcritical pressure ratios in the propulsive nozzle can be found from the condition of equality of the gas flowrates through the turbine first-stage stator and the propulsive nozzle exit (throat) section F_{pn}: /229

$$m\sigma_S^* \frac{p_0^*}{\sqrt{T_0^*}} F_S \, q(\lambda_S) = m\sigma_{pn}^* \frac{p_2^*}{\sqrt{T_2^*}} F_{pn} q(\lambda_{pn}),$$

where $F_S = F_1 \sin \alpha_{1p}$ — minimal stator flow section area, and from the equation of pressure ratio balance along the turbine and propulsive nozzle flow path.

We have from the flowrate equation

$$\frac{p_0^*}{p_2^*}\sqrt{\frac{T_2^*}{T_0^*}}=\frac{\sigma_{pn}^*}{\sigma_s^*}\frac{F_{pn}}{F_s}\frac{q(\lambda_{pn})}{q(\lambda_s)}.$$

Bearing in mind that:

$$\frac{p_0^*}{p_2^*}=\pi_\tau^* \text{ and } \frac{T_2^*}{T_0^*}=\frac{T_0^*-\Delta T_\tau^*}{T_0^*}=1-\left[1-\left(\frac{1}{\pi_\tau^*}\right)^{\frac{k-1}{k}}\right]\eta_\tau^*,$$

we obtain

$$\pi_\tau^*\sqrt{1-\left[1-\left(\frac{1}{\pi_\tau^*}\right)^{\frac{k-1}{k}}\right]\eta_\tau^*}=\frac{\sigma_{pn}^*}{\sigma_s^*}\frac{F_{pn}}{F_s}\frac{q(\lambda_{pn})}{q(\lambda_s)}. \tag{9.6}$$

The magnitude of the relative flow density at the propulsive nozzle throat section $q(\lambda_{pn})$ depends on the propulsive nozzle pressure ratio π_{pn}. For $\pi_{pn} = \sigma_{pn}^* p_2^*/p_H \geqq 1.85$, the relative flow density $q(\lambda_{pn}) = 1$.

The relative flow density at the turbine first stage stator throat section $q(\lambda_s)$ in a wide range of operating regime variation changes very little, and can be taken to be constant in the calculations in the first approximation. Then, (9.6) can be written as:

$$\pi_\tau^*\sqrt{1-\left[1-\left(\frac{1}{\pi_\tau^*}\right)^{\frac{k-1}{k}}\right]\eta_\tau^*}=Cq(\lambda_{pn}), \tag{9.7}$$

where

$$C=\frac{\sigma_{pn}^*}{\sigma_s^*}\frac{F_{pn}}{F_s\,q(\lambda_s)};\quad \sigma_s^*=\frac{p_s^*}{p_0^*};\quad \sigma_{pn}^*=\frac{p_{pn}^*}{p_2^*}.$$

Calculations show that the influence of η_T^* on the relation

$\pi_\tau^*\sqrt{1-\left[1-\left(\frac{1}{\pi_\tau^*}\right)^{\frac{k-1}{k}}\right]\eta_\tau^*}=A=f(\pi_\tau^*)$ is not large.

With accuracy to 1 - 1.2%, we can neglect the influence of η_T^* variation (in the range 0.8 - 0.92) on the parameter A. In the following we shall take $\eta_T^* \cong$ const. when determining the parameter A. Then, /230 two unknowns remain in (9.7): π_T^* and $q(\lambda_{pn})$.

As the additional equations relating π_T^* and $q(\lambda_{pn})$, we take equation of pressure ratio balance in the turbine and propulsive nozzle flow path:

$$\pi_T^* = \pi_c \sigma_{cc}^* \sigma_{pn}^* \pi(\lambda_{pn}), \tag{9.8}$$

and the relation

$$q(\lambda_{pn}) = f[\pi(\lambda_{pn})]. \tag{9.9}$$

Solving (9.7), (9.8), (9.9) jointly for each given value of π_c, we can determine π_T^*, $q(\lambda_{pn})$ and π_{pn} in the case of subcritical pressure ratios in the propulsive nozzle.

Figure 9.8 shows the dependence of π_T^* on $q(\lambda_{pn})$ for various values of π_c and C, plotted using (9.7), (9.8), (9.9). The values of π_T^* for $q(\lambda_{pn}) = 1$ ($\pi_{pn} \geqq 1.85$) are denoted by points in the figure.

For the known value of the parameter C, constant for a given turbine and propulsive nozzle, we use Figure 9.8 to determine for each value of the overall compression ratio π_c the gas expansion ratio in the turbine π_T^* and the relative flow density $q(\lambda_{pn})$, and we then use gasdynamic function tables to find the pressure ratio p_{pn}/p_{pn}^* and the gas expansion ratio in the propulsive nozzle $\pi_{pn} = \frac{1}{\sigma_{pn}^*} p_{pn}^*/p_{pn}$.

The graph shown in Figure 9.8 was plotted for the condition of constant values of the losses in the turbine and propulsive nozzle flowpath and constant value of $q(\lambda_s)$. With variation of the losses

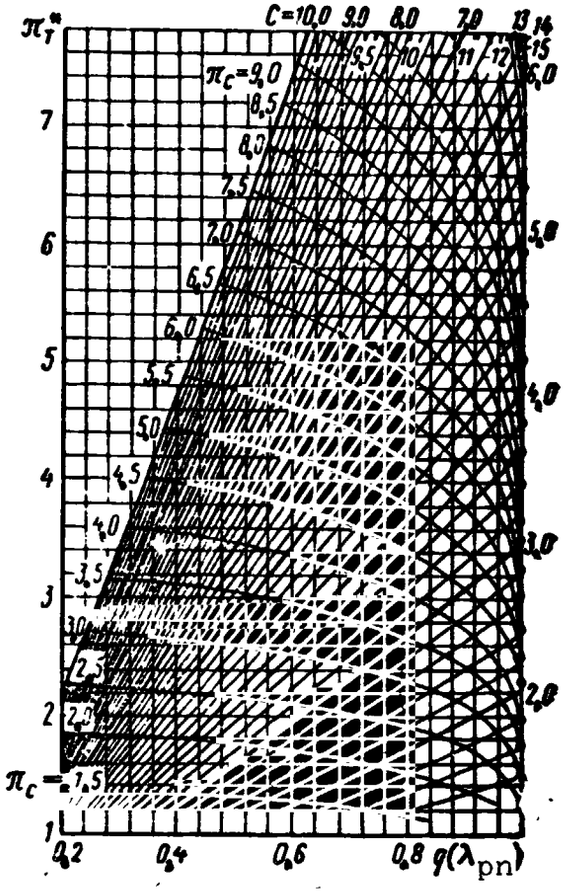

Figure 9.8. Nomogram for determining pressure ratio distribution between the turbine and the propulsive nozzle

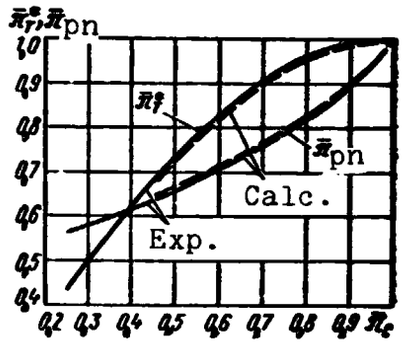

Figure 9.9. Relative variation of gas expansion ratios in the turbine and propulsive nozzle as a function of VK-1 engine compression ratio

and $q(\lambda_s)$, the value of the coefficient C changes with variation of π_c, and the values of π_T^* and $q(\lambda_{pn})$ change accordingly.

Figure 9.9 shows the variations of $\bar{\pi}_T^*$ and $\bar{\pi}_{pn}$ with variation of the compression ratio $\bar{\pi}_c$ for the VK-1 turbojet engine, obtained as a result of calculation using the above technique, where:

$$\bar{\pi}_T^* = \pi_T^*/\pi_{T.d}^*, \quad \bar{\pi}_{pn} = \pi_{pn}/\pi_{pn.d}, \text{ where } \pi_{T.d}^* \text{ and } \pi_{pn.d}$$

— values of the gas expansion ratio in the turbine and in the propulsive nozzle in the design regime. Satisfactory agreement between the theoretical and experimental relations $\bar{\pi}_T^* = f(\bar{\pi}_c^*)$ and $\bar{\pi}_{pn} = f(\bar{\pi}_c)$ in the range of $\bar{\pi}_c$ variations from 1 to 0.5 confirms the validity of the adopted assumptions for the given range of variation of $\bar{\pi}_c$ and the given engine. Good agreement between the theoretical

and experimental relations $\bar{\pi}_t = f(\bar{\pi}_c)$ and $\bar{\pi}_{pn} = f(\bar{\pi}_c)$ has also been obtained for GTE with two-stage and three-stage turbines.

9.3.2. Division of pressure ratios between turbine stages and basic turbine parameters in off-design regimes

In the case of supercritical pressure ratios in the propulsive nozzle and constant propulsive nozzle throat area, the gas expansion in the turbine and in the individual stages remain constant with change of the overall engine compression ratio π_c. /232

In the case of subcritical pressure ratios in the propulsive nozzle, the pressure ratios in the propulsive nozzle, turbine, and individual turbine stages will decrease with reduction of the overall compression ratio π_c. In this case, we use the technique described above to determine the pressure ratio division between the turbine and the propulsive nozzle, and then find the gas expansion ratio in the individual turbine stages.

The basic data for the calculation are:

— the geometric dimensions of the turbine flowpath and the given propulsive nozzle exit (throat) section area;

— the values of the basic flow parameters at various sections along the turbine flow path in the design regime;

— the division of the pressure ratios between the turbine and the propulsive nozzle in the regime being considered.

We shall examine the analysis technique for the example of the three-stage turbine, whose flowpath is shown in Figure 9.10.

A. Sequence of calculation of pressure ratio among turbine stages

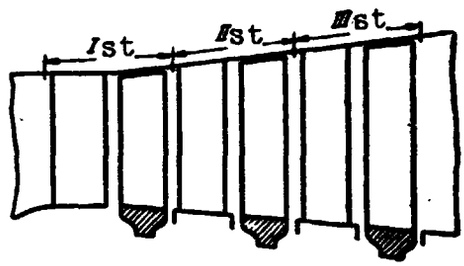

Figure 9.10. Schematic of turbine flow path

1. For the given value of π_c, we determine the pressure ratio in the last two stages $\pi^*_{(II+III)st} = p_2^{*\prime\prime}/p_2^*$, and in the first stage, $\pi^*_{I.st} = p_0^*/p_2^{*\prime\prime}$.

From the equation of flowrate through the second-stage stator and the propulsive nozzle exit section (throat), we obtain: /233

$$\pi^*_{(II+III)st}\sqrt{1-\left[1-\left(\frac{1}{\pi^*_{(II+III)st}}\right)^{\frac{k-1}{k}}\right]\eta^*_{(II+III)st}} = \frac{\sigma^*_{pn}}{(\sigma^*_s)_{II}}\cdot\frac{F_{pn}}{(F_s)_{II}}\cdot\frac{q(\lambda_{pn})}{q(\lambda_s)_{II}}. \tag{9.10}$$

In the first approximation in a comparatively wide range of π_c variation, the total pressure loss coefficients σ^*_{pn} and $(\sigma^*_s)_{II}$ and the relative flow density $q(\lambda_s)_{II}$ in the second-stage stator can be considered constant and equal to their values in the design regime.

Since in the design regimes, the pressure ratios in the turbine stage stators are critical or nearly so, for a small decrease of the pressure ratios in the stators, the function $q(\lambda_s)$ will remain practically constant. For example, with reduction of π_s from its critical value by 10%, $q(\lambda_s)$ decreases by less than 1%.

Then,

$$\pi^*_{(II+III)st}\sqrt{1-\left[1-\left(\frac{1}{\pi^*_{(II+III)st}}\right)^{\frac{k-1}{k}}\right]\eta^*_{(II+III)st}} = C_{II}q(\lambda_{pn}), \tag{9.11}$$

where

$$C_{II}=\frac{\sigma^*_{pn}}{(\sigma^*_s)_{III}}\frac{F_{pn}}{(F_s)_{III}}\frac{1}{q(\lambda_s)_{III}}.$$

For the value of $q(\lambda_{pn})$ known from previous calculation, we can use (9.11) or Figure 9.8 to determine the gas pressure ratio in the last two stages $\pi^*_{(II+III)st}$, and then in the first stage $\pi^*_{st} = \pi^*_T/\pi^*_{II+III)st}$.

2. We determine the pressure ratio in the third stage.

We assume in the first approximation that σ^*_{pn} and $(\sigma^*_s)_{III}$ are constant and equal to their values in the design regime. We take the parameter $q(\lambda_s)_{III}$ to be approximately constant or evaluate it with the aid of an available similar turbine characteristic. Then, we use the equation:

$$\pi^*_{III\,st}\sqrt{1-\left[1-\left(\frac{1}{\pi^*_{III\,st}}\right)^{\frac{k-1}{k}}\right]\eta^*_{III\,st}}=\frac{\sigma^*_{pn}}{(\sigma^*_s)_{III}}\frac{F_{pn}}{(F_s)_{III}}\frac{q(\lambda_{pn})}{q(\lambda_s)_{III}}\cong C_{III}q(\lambda_{p,x}); \tag{9.12}$$

or the nomogram of Figure 9.8 to determine the pressure ratio in the third stage $\pi^*_{III.st}$. /234

3. We determine the gas expansion ratio in the third stage based on the stage inlet total pressure and the stage exit static pressure. To this end, we determine $q(\lambda_2)_{III}$ at the stage exit from the flowrate equation:

$$q(\lambda_2)_{III}=\sigma^*_{pn}\frac{F_{pn}}{(F_2)_{III}}q(\lambda_{pn}),$$

where $(F_2)_{III}=(F_{2a})_{III}(\sin\alpha_2)_{III}$ [for $\alpha_2=80-100°\,(F_2)_{III}\simeq(F_{2a})_{III}$], and then $\pi(\lambda_2)_{III}$ and $\pi_{III.st} = \pi^*_{III.st}/\pi(\lambda_2)_{III}$.

4. We determine by successive approximations the change of $q(\lambda_s)_{III}$ with change of $\pi_{III.st}$ in comparison with its value in the design regime*. For this, we determine the parameter

$$A = \frac{1}{e_{st.d} + 1} \left(\frac{e_{cr.0}}{e_{cr}}\right)^{0.5}$$

where

$$e_{st.d} = \pi_{st.d}^{\frac{k-1}{k}}$$

$$e_{cr} = \frac{1 - \rho_d}{0.856 - \rho d} \text{ for } \rho_{cr.d} \approx \rho_d;$$

$\rho_{cr.d}$ — stage reaction corresponding to the critical pressure ratio in the propulsive nozzle;

$e_{cr.0} = e_{cr}$ — for reaction $\rho_d = 0.3$.

For the known value of $\pi_{III.st}$, calculated for the previously assumed value of $q(\lambda_s)_{III}$, we determine the parameter $A(\pi_{st} - 1)$, and then use Figure 9.11 to find $[\bar{q}(\lambda_s)]^2$ and the new value of $q(\lambda_s)'_{III} = q(\lambda_s)_{III}\,\overline{q(\lambda_s)}$.

We refine the value of the constant C_{III} and use Figure 9.8 to determine the new value of $\pi^*_{III.st}$, and then $\pi_{III.st}$, and so on, until refinement of $q(\lambda_s)_{III}$ does not lead to significant change of $\pi^*_{III.st}$. Usually, two or three approximations suffice.

5. We determine the pressure ratios in the second stage.

---

*Refinement of $q(\lambda_s)_{III}$ is made only for a significant change of $\pi_{III.st}$.

From the flow total parameters,

$$\pi^*_{II\,st} = \frac{\pi^*_{(II+III)st}}{\pi^*_{III\,st}}.$$

In accordance with the flowrate equation, we determine: /235

$$q(\lambda_2)_{II} = \frac{(F_2)_{III}}{(F_2)_{II}} q(\lambda_2)_{III} \frac{1}{\pi^*_{III\,st}\sqrt{1-\left[1-\left(\frac{1}{\pi^*_{III\,st}}\right)^{\frac{k-1}{k}}\right]\eta^*_{III\,st}}}.$$

From the gasdynamic function tables, we find $\pi(\lambda_2)_{II}$, and then $\pi_{II.st} = \pi^*_{II.st}/\pi(\lambda_2)_{II}$:

6. We determine $q(\lambda_2)_I$ at the first-stage exit:

$$q(\lambda_2)_I = \frac{(F_2)_{III}}{(F_2)_I} q(\lambda_2)_{III} \times$$
$$\times \frac{1}{\pi^*_{(II+III)st}\sqrt{1-\left[1-\left(\frac{1}{\pi^*_{(II+III)st}}\right)^{\frac{k-1}{k}}\right]\eta^*_{(II+III)st}}}.$$

From the tables, we find $\pi(\lambda_2)_I$, and then

$$\pi_{I.st} = \frac{\pi^*_{I\,st}}{\pi(\lambda_2)_I}.$$

7. From the values of π^*_{st}, π_{st}, and $q(\lambda_s)$ known from this calculation, we determine for each stage the gas pressure ratios in the stator and rotor:

$$\pi_s = \frac{1}{\sigma^*_s\,\pi(\lambda_s)} \text{ and } \pi_r = \frac{\pi_{st}}{\pi_s},$$

where

$$\pi_s = \frac{p^*_{0\,st}}{p_1},\quad \pi_r = \frac{p_1}{p_2};$$

$p^*_{0.st}$ — stage inlet total pressure; /236

p_1 — stator exit static pressure;

p_2 — stage exit static pressure

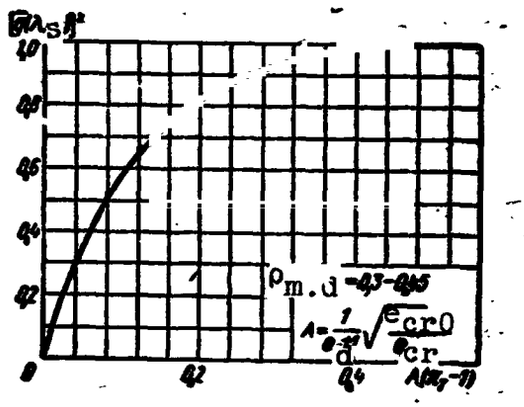

Figure 9.11 Relative change of square of flow density in the propulsive nozzle as function of gas expansion ratio in the turbine

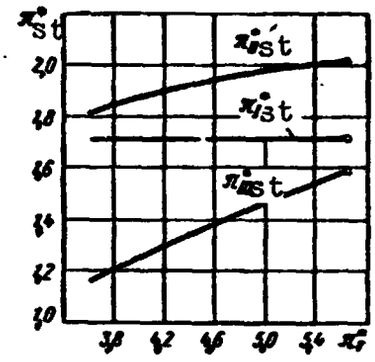

Figure 9.12. Division of pressure ratios between stages of multistage turbine in off-design regimes

Figure 9.12 shows the results of calculation of the division of the pressure ratios between the stages of a three-stage turbine as a function of the change of the overall gas expansion ratio in the turbine π_T^*. We see that with change of π_T^* by 40%, the pressure ratio in the first stage and in its elements remains practically unchanged. In the second and third stages, the pressure ratio decreases with decrease of π_T^*, and the most marked pressure ratio change takes place in the third stage.

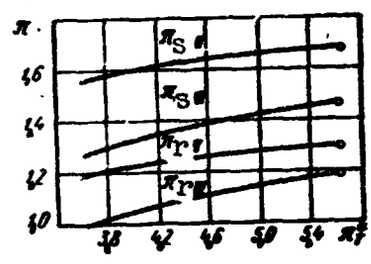

Figure 9.13. Division of pressure ratios between propulsive nozzle and rotor in the stages of a multistage turbine in off-design regimes

In accordance with the variation of π_{st}^*, there is change of the pressure ratios in the stator and rotor (Figure 9.13).

From the known division of the pressure ratios in the turbine stages and in their elements, we can determine the kinematic parameters of the stages and their efficiencies in the off-design regimes.

B. Calculation of turbine stage kinematic parameters and efficiencies in off-design regimes

We shall examine one of the possible analysis techniques, in which the basic data for the calculation are:

— the turbine inlet gas flow total parameters;

— the division of the pressure ratios between the turbine stages and their elements, calculated using the technique presented above; /237

— the turbine rotational speed (or circumferential velocity).

In this case, the calculation of the parameters in the first and following stages is made in the following sequence.

1. Using the known value of $\pi(\lambda_s)$ and the gasdynamic function tables, we determine $\lambda_{1\ c.ad}$.

2. We estimate the stator velocity coefficient ϕ. For the first stages, we can take $\phi = \phi_d$.

We find the reduced velocity:

$$\lambda_{1c} = \varphi \lambda_{1c\,ad}.$$

3. We find the stator exit static pressure:

$$p_1 = p_0^* \pi(\lambda_{1c\,ad});$$

the stator exit velocity

$$c_1 = a_{cr} \lambda_{1c} = 18{,}1 \sqrt{T_0^*} \lambda_{1c};$$

the stator exit flow angle

$$\alpha_1 = \alpha_{1p} + \Delta\alpha,$$

where $\alpha_{1p} = \arcsin\left(\frac{a}{t}\right)$;

$\Delta\alpha$ — flow deviation angle, found from the graph of $\Delta\alpha = f(\alpha_p, M_1)$, presented in Figure 5.5.

4. We determine the stator exit circumferential and axial velocities:

$$c_{1u} = c_1 \cos \alpha_1; \; c_{1a} = c_1 \sin \alpha_1;$$

the rotor inlet and exit circumferential velocity

$$u_1 \simeq u_2 = u = \frac{\pi D_m n}{60};$$

the circumferential component of the relative velocity at the rotor inlet

$$w_{1u} = c_{1u} - u;$$

the relative velocity at the rotor inlet

$$w_1 = \sqrt{c_{1a}^2 + w_{1u}^2};$$

the flow angle in the relative motion at the rotor inlet

$$\beta_1 = \arcsin\left(\frac{c_{1a}}{w_1}\right).$$

5. We find the gas total temperature at the rotor inlet: /238

$$T_{1w}^* = T_1 + \frac{w_1^2}{2310}, \text{ where } T_1 = T_0^* - \frac{c_1^2}{2310};$$

the reduced relative velocity at the rotor inlet

$$\lambda_{1w} = \frac{w_1}{18.1\sqrt{T_{1w}^*}};$$

the gas total pressure at the rotor inlet

$$p_{1w}^* = \frac{p_1}{\pi(\lambda_{1w})}.$$

6. We find the gasdynamic function $\pi(\lambda_{2w})=\frac{p_2}{p_{1w}^*}$, and then from the tables, we find $\lambda_{2\ w.ad}$;

the angle of attack at the rotor inlet

$$i=\beta_{1p}-\beta_1,$$

where $\beta_{1\ p}$ — is the design flow angle at the rotor inlet in the design regime.

7. We find the relative parameter $\bar{i}=\frac{i}{(\beta_1/\beta_{2p})(\beta_{1p}+\beta_{2p})}$, and then from the graph of $\psi/\psi_p=f(\bar{i})$, shown in Figure 9.6, we determine ψ/ψ_p and the velocity coefficient $\psi=(\psi/\psi_p)\psi_p$ *.

8. We find the reduced velocity:

$$\lambda_{2w}=\psi\lambda_{2w\ ad};$$

the rotor exit flow angle

$$\beta_2=\beta_{2p}+\Delta\beta,$$

where $\beta_{2p}=\arcsin a/t$;

$\Delta\beta$ — flow deviation angle in the rotor cascade (found from the graph of Figure 5.5);

the circumferential and axial components of the reduced velocity λ_{2w}

$$\lambda_{w_{2u}}=\lambda_{2w}\cos\beta_2;\ \lambda_{w_{2z}}=\lambda_{2w}\sin\beta_2;$$

the stage exit flow angle

$$\alpha_2=\operatorname{arctg}\frac{\lambda_{2z}}{\lambda_{w_{2u}}-(u_2/a_{cr}{}^2)};$$

For $D_{1\ m}-D_{2\ m}$; $\frac{u_2}{a_{cr2}}=\lambda_u\sqrt{\frac{\tau(\lambda_{1w})}{\tau(\lambda_{1c})}}$, where $\lambda_u=\frac{u_1}{18{,}1\sqrt{T_0^*}}$.

---

*The graph of $\psi/\psi_p=f(\bar{i})$ is t ken from [8].

9. We determine the reduced velocity at the stage exit: /239

$$\lambda_{2c} = \frac{\lambda_{2w} \sin \beta_2}{\sin \alpha_2};$$

the stage exit static pressure $p_2 = p_2^* \pi(\lambda_{2c})$;
the turbine stage reaction

$$\rho = \frac{L_{ad.r}}{L_{ad.st}} = \frac{T_1\left[1-(p_2/p_1)^{\frac{k-1}{k}}\right]}{T_0^*\left[1-(p_2/p_0^*)^{\frac{k-1}{k}}\right]}.$$

10. We determine the turbine stage efficiency:

adiabatic efficiency

$$\eta_{ad} = \varphi^2\psi^2(1-\rho)+\psi^2\rho-(1-\psi^2)(x^2-2x\varphi\cos\alpha_1\cdot\sqrt{1-\rho});$$

effective efficiency

$$\eta_r = 2x\left[\varphi\cos\alpha_1\cdot\sqrt{1-\rho}+\right.$$
$$\left.+\psi\cos\beta_2\cdot\sqrt{\rho+\varphi^2(1-\rho)-2x\varphi\cos\alpha_1\cdot\sqrt{1-\rho}+x^2}-x\right];$$

turbine stage adiabatic efficiency based on total parameters

$$\eta_r^* = \frac{\eta_r}{\eta_r+(1-\eta_{ad.T})}$$

11. We determine the turbine stage work:

$$L_{st} = 1155T_0^*\left[1-\left(\frac{1}{\pi_{st}^*}\right)^{\frac{k-1}{k}}\right]\eta_{st}^*;$$

the turbine stage exit total temperature

$$T_2^* = T_0^* - \frac{L_{st}}{1155}.$$

The basic parameters of the second and following stages are calculated in an analogous sequence. We then determine the efficiency of the entire multistage turbine:

$$\eta_r^* = \frac{L_r}{L_{ad.T}^*} = \frac{\sum L_{st}}{1155T_0^*\left[1-\left(\frac{1}{\pi_r^*}\right)^{\frac{k-1}{k}}\right]}.$$

This technique can be used to formulate a digital computer calculation program.

9.4. Example of Turbine Parameter Calculation in Off-Design Regimes

As an example, we shall determine the basic parameters of a single-shaft three-stage turbine in various regimes of its operation in a turboprop engine with regulation program: rotor speed n = const, engine exit (propulsive) nozzle area F_{pn} = const; propeller blade setting angle ϕ_p = var. /240

With this regulation program, the operating regime of the turbine and of the engine as a whole can be changed by varying the turbind loading by varying ϕ_p, and also by varying the flight speed and altitude.

In this example, we shall limit ourselves to examining variation of the basic turbine parameters by varying the propeller blade setting angle for the case of engine operation on the stand (with H = 0, V = 0).

The basic data for calculation of the turbine parameters are:

1) geometric dimensions of the turbine flow path and exit nozzle;
2) basic turbine parameters in the design regime;
3) compressor characteristic with lines T_0^*/T_H^* = const, where T_0^* is the turbine inlet gas temperature, T_H^* is the engine inlet total temperature.

The geometric dimensions and basic parameters of the turbine in the design regime are shown in Table 9.1.

TABLE 9.1.*

Parameter	Stage		
	I	II	III
Stage exit flow section area F_2, m^2	0,097	0,136	0,188
Stator throat area F_s, m^2	0,0257	0,0385	0,0755
Tip speed $\bar{u}_1 = u_2$, m/s	334	337	341
Angle α_{1p}	18°00′	19°50′	28°30′
Angle β_{1p}	55°40′	48°30′	61°20′
Angle β_{2p}	22°25′	26°40′	36°30′
Stator velocity coefficient ϕ	0,95	0,97	0,97
Rotor velocity coefficient ψ	0,945	0,945	0,95
Reduced velocity λ_{1c}	0,74	0,905	0,785

*Translator's note. Commas in numbers represent decimal points.

The exit nozzle area and velocity coefficient are $F_{pn} = 0.21\ m^2$, /241
$\phi_{pn} = 0.97$. In addition, for the assumed engine regulation program with given constant rotor speed, we know the turbine inlet gas temperature T_0^* dependence on the overall gas expansion ratio in the turbine and exit nozzle.

We make the calculation in the following sequence.

1. We determine the pressure ratio division between the turbine and the propulsive nozzle in the various turbine operating regimes (see section 9.3.1).

a) We determine the parameter:

$$C_I = \frac{\sigma^*_{pn}}{(\sigma^*_s)_I} \frac{F_{pn}}{(F_s)_I \cdot q(\lambda_s)_I} = \frac{0,99}{0,965} \cdot \frac{0,21}{0,0257 \cdot 0,9204} = 9,12,$$

where $(\sigma_s^*)_I = 0.965$ and $q(\lambda_s)_I = 0.9204$ are found from the values of ϕ_I and $(\lambda_{1\,c})_I$ in the design regime;

b) From Figure 9.8 for $C_I = 9.12$, and the values of the gas expansion ratio $\pi_d = \pi_c \cdot \sigma^*_{cc}$ used for the calculation, where $\sigma^*_{cc} = 0.96$, we determine the gas expansion ratio in the turbine π^*_T and the value of $q(\lambda_{pn})$ in the propulsive nozzle. We summarize the calculation results in Table 9.2.

TABLE 9.2.*

Parameter	Gas expansion ratio π_p						
	7,30	6,91	6,53	6,15	5,76	5,28	5,0
π^*_T	6,58	6,275	5,98	5,68	5,36	4,96	4,73
π_{pn}	1,110	1,100	1,091	1,082	1,075	1,063	1,058
$q(\lambda_{pn})$	0,588	0,564	0,538	0,515	0,489	0,455	0,436
$\pi^*_{(II+III)st}$	3,86	3,67	3,48	3,31	3,13	2,89	2,76
π^*_{Ist}	1,723	1,720	1,720	1,720	1,715	1,712	1,71
$q(\lambda_s)_{III}$	0,9456	0,9450	0,9400	0,935	0,925	0,914	0,906
π^*_{IIIst}	1,85	1,77	1,69	1,625	1,57	1,54	1,50
π^*_{IIst}	2,085	2,075	2,060	2,036	1,995	1,876	1,84
$q(\lambda_2)_{III}$	0,67	0,641	0,613	0,586	0,556	0,518	0,496
π_{IIIst}	2,095	1,980	1,870	1,773	1,700	1,650	1,595
$q(\lambda_2)_{II}$	0,5170	0,5165	0,5150	0,5115	0,4940	0,4700	0,4630
π_{IIst}	2,228	2,22	2,20	2,173	2,12	1,98	1,94
$q(\lambda_2)_I$	0,379	0,378	0,378	0,378	0,378	0,377	0,377
π_{Ist}	1,785	1,785	1,785	1,785	1,780	1,773	1,770
$q(\lambda_s)_I$	0,9204	0,9204	0,9204	0,9204	0,910	0,908	0,905
$(\pi_s)_I$	1,440	1,440	1,440	1,440	1,440	1,435	1,435
$(\pi_r)_I$	1,240	1,240	1,240	1,240	1,240	1,235	1,234
$q(\lambda_s)_{II}$	0,9894	0,9894	0,9894	0,9894	0,9894	0,9830	0,9800
$(\pi_s)_{II}$	1,70	1,70	1,70	1,70	1,70	1,65	1,63
$(\pi_r)_{II}$	1,310	1,306	1,294	1,278	1,247	1,200	1,190
$(\pi_s)_{III}$	1,475	1,473	1,460	1,446	1,423	1,400	1,385
$(\pi_r)_{III}$	1,420	1,337	1,270	1,190	1,144	1,071	1,028

*Translator's note. Commas in numbers represent decimal points.

2. We determine the pressure ratio division between the turbine stages (see section 9.3.2.A).

a) The pressure ratio in the last two stages.

We find the parameter:

$$C_{II}=\frac{\sigma^*_{pn}}{(\sigma^*_s)_{II}}\cdot\frac{F_{pn}}{(F_s)_{II}}\cdot\frac{1}{q(\lambda_s)_{II}}=\frac{0,99}{0,967}\cdot\frac{0,21}{0,0385}\cdot\frac{1}{0,980}=5,65,$$

and then, from Figure 9.8 for the given value of C_{II} and the previously obtained values of $q(\lambda_{pn})$, we find $\pi^*_{(II+III)st}$.

Since in the first and second stages the quantity $q(\lambda_s)$ remains constant or varies little over a wide range of π_d variation, the parameters C_I and C_{II} are taken to be constant for these stages in the considered range of π_d variation.

b) We determine the pressure ratio in the first stage:

$$\pi^*_{I.st}=\frac{\pi^*_{I}}{\pi^*_{(II+III)st}};$$

c) We determine the pressure ratio in the third stage.

In the first approximation, we determine the parameter:

$$C_{III}=\frac{\sigma^*_{pn}}{(\sigma^*_s)_{III}}\cdot\frac{F_{pn}}{(F_s)_{III}}\cdot\frac{1}{q(\lambda_s)_{III}}=\frac{0,99}{0,98}\cdot\frac{0,21}{0,0755\cdot 0,9456}=2,96,$$

and then, from Figure 9.8 for the values of π_d assumed in the calculation and the known values of $q(\lambda_{pn})$, we find $\pi^*_{III.st}$. /242

We determine $q(\lambda_2)$ at the third stage exit:

$$q(\lambda_2)_{III}=\sigma^*_{pn}\frac{F_{pn}}{(F_2)_{III}}q(\lambda_{pn})$$

and then,

$$\pi(\lambda_2)_{III} \text{ and } \rho_{III.st}=\frac{\pi^*_{III}st}{\pi(\lambda_2)_{III}}.$$

We use successive approximations to determine the change of $q(\lambda_s)_{III}$, and refine the values of $\pi^*_{III.st}$ and $\pi_{III.st}$.

In the example considered, two approximations were sufficient.

d) We determine the pressure ratio in the third stage in terms of total parameters:

$$\pi^*_{II.st} = \frac{\pi^*_{(II+III)st}}{\pi^*_{III st}};$$

e) We use the above technique to determine $q(\lambda_2)_{II}$ and $q(\lambda_2)_I$, and then $\pi_{II.st}$ and $\pi_{I.st}$.

In determining the pressure ratio division in the turbine and determining the parameter $q(\lambda_2)$, it is convenient to use the graph of $\pi_T^* = f(A)$, constructed from the expression

$$A = \pi_T^* \sqrt{1 - \left(1 - \frac{1}{\pi_T^{*0,25}}\right)\eta_T^*}$$

for various values of $\eta_T^* = 0{,}80 \div 0{,}93$.

We summarize the calculation results in Table 9.2.

3. We use the technique described above (see section 9.3.2) to determine the pressure ratios in the stator and rotor from the known values of π^*_{st}, π_{st}, $q(\lambda_s)$ for each stage. /243

4. We use the technique described above (see 9.3.2.B) to calculate the kinematic parameters in the turbine stages at the mean diameter, and determine the efficiencies of the individual stages and of the entire turbine. We summarize the calculation results in Table 9.3.

TABLE 9.3.*

Parameter	Gas Expansion ratio π_p						
	7,30	6,91	6,53	6,15	5,76	5,28	5,0
First stage							
$\varkappa_s$	1,44	1,44	1,44	1,44	1,44	1,436	1,435
λ_{1c}ad	0,781	0,781	0,781	0,781	0,781	0,77	0,76
φ	0,95	0,95	0,95	0,95	0,95	0,95	0,95
$\lambda_{1c} = \varphi\lambda_{1c}$ad	0,741	0,741	0,741	0,741	0,741	0,730	0,721
$(T_0^*)_I$, K	1310	1030	903	798	697	576	520
c_1, m/s	486	432	405	380	350	317	298
α_1, deg	18	18	18	18	18	18	18
$c_{1a} = c_1 \cos\alpha_1$, m/s	462	410	385	361	332	302	284
$c_{1u} = c_1 \sin\alpha_1$, m/s	150	133,5	125	117,3	108	98	92
$w_{1u} = c_{1u} - u_1$, m/s	128	76	51	27	−2	−32	−50
$w_1 = \sqrt{c_{1a}^2 + w_{1u}^2}$, m/s	198	153,3	135	120	108	103	105
$\beta_1 = \arcsin \frac{c_{1a}}{w_1}$	49°12′	60°35′	67°06′	78°00′	90°00′	107°15′	119°00′
$T_1 = T_0^* - \frac{c_1^2}{2310}$, K	1207	949	832	736	644	533	482
$T_{1w}^* = T_1 + \frac{w_1^2}{2310}$, K	1220	957	839	742	650	539	488
$\lambda_{1w} = \frac{w_1}{18,15\sqrt{T_{1w}^*}}$	0,274	0,248	0,239	0,236	0,243	0,274	0,297
$\pi(\lambda_{2w}) = \frac{(\pi_s)_I \pi(\lambda_{1w})}{\pi_{I\,st}}$	0,773	0,782	0,780	0,782	0,776	0,767	0,759
$i = \beta_{1p} - \beta_1$	6°28′	−4°55′	−11°26′	−22°20′	−34°20′	−51°20′	−63°20′
$\bar{i} = \frac{i}{(\beta_1/\beta_{2p})(\beta_{1p} + \beta_{2p})}$	0,0354	−0,0195	−0,0475	−0,0825	−0,1096	−0,137	−0,1583
ψ/ψ_p (from Fig. 9.6)	0,988	1,003	1,007	1,008	1,008	1,007	1,006
$\psi = \psi_p(\psi/\psi_p)$	0,933	0,948	0,950	0,950	0,950	0,950	0,950
$\lambda_{2w} = \psi(\lambda_{2w}ad)$	0,620	0,616	0,620	0,619	0,627	0,642	0,654
$\lambda_{2wr} = \lambda_{2w} \cos\beta_2$	0,573	0,570	0,573	0,572	0,580	0,593	0,604
$\lambda_{2wa} = \lambda_{2w} \sin\beta_2$	0,236	0,235	0,236	0,236	0,239	0,245	0,249
$\lambda_u = \frac{u_1}{18,15\sqrt{(T_0^*)_I}}$	0,509	0,575	0,604	0,653	0,698	0,768	0,808
$\frac{u_2}{a_{cr2}} = \lambda_u \cdot \sqrt{\frac{\pi(\lambda_{1w})}{\tau(\lambda_{1c})}}$	0,466	0,596	0,627	0,678	0,725	0,795	0,834
$\alpha_2 = \operatorname{arctg} \frac{\lambda_{2wa}}{\lambda_{2wu} - \frac{u_2}{a_{cr2}}}$	65°36′	96°20′	101°54′	114°24′	121°12′	129°34′	132°49′
$\eta_{ad.st}$	0,877	0,897	0,897	0,898	0,899	0,896	0,897
η_{st}	0,798	0,840	0,845	0,846	0,828	0,803	0,785
η_{st}^*	0,866	0,888	0,890	0,891	0,890	0,885	0,880

(Table continued on following page)

TABLE 9.3. (continued)

Parameter	Gas expansion ratio π_p						
	7,30	6,91	6,53	6,15	5,76	5,28	5,0
$T_2^* = (T_0^*)_I - (T_0^*)_I \left[1 - \left(\frac{1}{\pi_{I\,st}^*}\right)^{\frac{k-1}{k}}\right]\eta_{I\,st}^*$	1169	919	800	706	619	514	465
Second stage							
π_s	1,7	1,7	1,7	1,7	1,7	1,65	1,63
$\lambda_{1c\,ad}$	0,905	0,905	0,905	0,905	0,905	0,880	0,869
φ	0,975	0,964	0,96	0,954	0,950	0,948	0,945
$\lambda_{1c} = \varphi\lambda_{1c\,ad}$	0,885	0,873	0,869	0,863	0,860	0,834	0,821
$(T_0^*)_{II}$, K	1169	919	800	706	619	514	465
c_1, m/s	550	480	446	416	389	343	322
α_1	19°50′	19°50′	19°50′	19°50′	19°50′	19°50′	19°50′
$c_{1a} = c_1 \cos\alpha_1$, m/s	518	451	420	392	366	323	303
$c_{1u} = c_1 \sin\alpha_1$, m/s	187	163	151	141	132	116	109
$w_{1u} = c_{1u} - u_1$, m/s	181	114	83	55	29	−14	−34
$w_1 = \sqrt{c_{1a}^2 + w_{1u}^2}$, m/s	260	199	173	151	135	117	114
$\beta_1 = \arcsin\frac{c_{1a}}{w_1}$	46°03′	55°00′	60°42′	69°14′	77°42′	97°42′	106°36′
$T_1 = (T_0^*)_I - \frac{c_1^2}{2310}$, K	1038	819	714	631	553	463	420
$T_{1w}^* = T_1 + \frac{w_1^2}{2310}$, K	1067	836	727	641	561	469	426
$\lambda_{1w} = \frac{w_1}{18,15\sqrt{T_{1w}^*}}$	0,439	0,379	0,354	0,328	0,314	0,298	0,305
$\pi(\lambda_{2w}) = \frac{(\pi_s)_{II}\,\pi(\lambda_{1w})_{II}}{\pi_{II\,st}}$	0,683	0,705	0,718	0,736	0,754	0,794	0,797
$i = \beta_{1p} - \beta_1$	2°30′	−6°27′	−11°05′	−20°41′	−29°09′	−49°05′	−57°06′
$\bar{i} = \frac{i}{(\beta_1/\beta_{2p})(\beta_{1p} + \beta_{2p})}$	0,0191	−0,0086	−0,0633	−0,105	−0,131	−0,171	−0,191
ψ/ψ_p (from Fig. 9.6)	0,993	1,006	1,008	1,0085	1,0075	1,0040	1,0020
$\psi = \psi_p(\psi/\psi_p)$	0,938	0,95	0,952	0,952	0,951	0,948	0,946
$\lambda_{2w} = \psi\lambda_{2w\,ad}$	0,761	0,732	0,716	0,690	0,663	0,600	0,574
$\lambda_{2wa} = \lambda_{2w}\cos\beta_2$	0,681	0,654	0,640	0,615	0,590	0,535	0,511
$\lambda_{2wu} = \lambda_{2w}\sin\beta_2$	0,347	0,334	0,329	0,312	0,300	0,272	0,260
$\lambda_u = \frac{u_1}{18,15\sqrt{(T_0^*)_{II}}}$	0,545	0,614	0,658	0,698	0,765	0,818	0,860
$\frac{u_2}{a_{cr}^2} = \lambda_u\sqrt{\frac{\tau(\lambda_{1w})}{\tau(\lambda_{1c})}}$	0,570	0,642	0,690	0,732	0,803	0,855	0,898

(Table continued on following page)

TABLE 9.3. (continued)

Parameter	Gas expansion ratio π_p						
	7,30	6,91	6,53	6,15	5,76	5,26	5,0
$\alpha_2 = \operatorname{arctg} \dfrac{\lambda_{2ua}}{\lambda_{2u} - \dfrac{u_2}{a_{cr}^2}}$	72°14′	88°00′	98°37′	110°30′	125°21′	139°35′	146°08′
$\eta_{ad.st}$	0,899	0,907	0,904	0,896	0,892	0,889	0,886
η_{st}	0,812	0,828	0,825	0,820	0,785	0,725	0,685
η^*_{st}	0,886	0,900	0,895	0,890	0,877	0,864	0,853
$T^*_2 = (T^*_0)_{II} - (T^*_0)_{II}\left[1 - \left(\dfrac{1}{\pi^*_{II\,st}}\right)^{\frac{k-1}{k}}\right]\eta^*_{II\,st}$	993	780	680	603	532	449	408
Third stage							
π_s	1,475	1,473	1,460	1,446	1,423	1,400	1,385
λ_{1ead}	0,785	0,784	0,774	0,765	0,748	0,730	0,718
φ	0,966	0,970	0,970	0,970	0,970	0,950	0,930
$\lambda_{1e} = \varphi\lambda_{1ead}$	0,758	0,760	0,760	0,742	0,726	0,694	0,668
$(T^*_0)_{III}$, K	991	780	680	603	532	449	408
c_1, m/s	431	390	360	336	304	277	245
α_1	28°25′	28°25′	28°25′	28°30′	28°35′	28°40′	28°45′
$c_{1u} = c_1 \cos\alpha_1$, m/s	379	343	317	295	267	243	215
$c_{1a} = c_1 \sin\alpha_1$, m/s	205	186	171	160	146	133	118
$w_{1u} = c_{1u} - u_1$, m/s	38	−2	−24	−46	−74	−98	−126
$w_1 = \sqrt{c_{1a}^2 + w_{1u}^2}$, m/s	208	186	173	166	164	165	175
$\beta_1 = \arcsin \dfrac{c_1}{w_1}$	80°06′	90°	98°42′	105°12′	117°	126°12′	137°30′
$T_1 = (T^*_0)_{III} - \dfrac{c_1^2}{2310}$, K	910	714	624	554	492	416	382
$T^*_{1w} = T_1 + \dfrac{w_1^2}{2310}$, K	929	729	637	566	504	428	395
$\lambda_{1w} = \dfrac{w_1}{18,15\sqrt{T^*_{1w}}}$	0,378	0,380	0,378	0,385	0,402	0,439	0,485
$\pi(\lambda_{2w}) = \dfrac{(\pi_s)_{III}\,\pi(\lambda_{1w})_{III}}{\pi_{III\,st}}$	0,650	0,685	0,718	0,748	0,764	0,759	0,758
$i = \beta_{1p} - \beta_1$	1°14′	−8°40′	−17°22′	−2[illegible]°52′	−35°40′	−44°52′	−55°10′

(Table concluded on following page)

TABLE 9.3. (concluded)

Parameter	Gas expansion ratio π_p						
	7,30	6,91	6,53	6,15	5,76	5,28	5,0
$\bar{I} = \frac{i}{(\beta_1/\beta_{2p})(\beta_{1p}+\beta_{2p})}$	0,004	−0,0295	−0,065	−0,098	−0,175	−0,255	−0,497
ψ/ψ_p	0,9985	1,005	1,008	1,009	1,0035	0,994	0,967
$\psi = \psi_p(\psi/\psi_p)$	0,948	0,954	0,956	0,956	0,953	0,944	0,918
$\lambda_{2w} = \psi\lambda_{2w}$ ad	0,810	0,765	0,720	0,676	0,651	0,650	0,630
β_2	35°55′	36°30′	36°55′	37°15′	37°18′	37°18′	37°20′
$\lambda_{2wa} = \lambda_{2w}\cos\beta_2$	0,665	0,615	0,575	0,538	0,518	0,517	0,500
$\lambda_{2wu} = \lambda_{2w}\sin\beta_2$	0,475	0,455	0,431	0,410	0,395	0,394	0,382
$\lambda_u = \frac{u_1}{18,15\sqrt{(T_0^*)_{III}}}$	0,600	0,671	0,720	0,765	0,815	0,888	0,933
$\frac{u_2}{a_{cr}^2} = \lambda_u\sqrt{\frac{\tau(\lambda_{1w})}{\tau(\lambda_c)}}$	0,620	0,694	0,745	0,785	0,835	0,908	0,953
$\alpha_2 = \operatorname{arctg}\frac{\lambda_{2wa}}{\lambda_{2wu}-\frac{u_2}{a_{cr2}}}$	85°47′	99°51′	111°30′	121°04′	128°49′	133°48′	139°48′
$\eta_{ad.st}$	0,900	0,915	0,910	0,918	0,912	0,870	0,795
η_{st}	0,719	0,734	0,723	0,674	0,591	0,386	0,075
η^*_{st}	0,874	0,865	0,890	0,888	0,857	0,735	0,249
$T_2^* = (T_0^*)_{III} - (T_0^*)_{III} \times \left[1-\left(\frac{1}{\pi^*_{III st}}\right)^{\frac{k-1}{k}}\right]\eta^*_{III st}$	865	685	603	540	482	414	398
$\eta^*_{r\Sigma} = \frac{\sum L_{st}}{1155(T_0^*)_I\left[1-\left(\frac{1}{\pi^*_{\tau}}\right)^{\frac{k-1}{k}}\right]}$	0,90	0,908	0,905	0,902	0,889	0,833	0,700

*Translator's note. Commas in numbers represent decimal points.

We see from these tables that the division of the overall pressure ratio $\pi^*_{T\Sigma}$ in the turbine between the individual stages, obtained as a result of the calculation, has the same nature as that shown in Figure 9.12. With decrease of $\pi^*_{T\Sigma}$ from 6.58 to 4.7 (about 30%), the pressure ratio in the first stage and in its elements does not change. In the second stage, π^*_{st} decreases by 12%, and in the third stage — by 19%. There is a corresponding redivision of the pressure ratio in the stator and rotors of the last stages. /247 /248

Calculation of the kinematic parameters and efficiencies of the individual stages and of the turbine as a whole showed that, in the case of turbine operation in the turboprop engine system with reduction of $\pi^*_{T\Sigma}$ and corresponding reduction of the turbine inlet gas temperature (when the engine is throttled), there is marked restructuring of the flow in the turbine stages, particularly in the last stage. Comparison of the dependences of η^*_{st} on $\pi^*_{T\Sigma}$ shows that when the engine power is throttled (with reduction of $\pi^*_{T\Sigma}$ and T^*_0 with n = const), the efficiency of the last turbine stage changes most markedly. For example, with reduction of $\pi^*_{T\Sigma}$ from 6.58 to 4.7, the third-stage efficiency decreases from 0.874 to 0.240, while the second-stage efficiency decreases to 0.853, and that first stage efficiency — to 0.880. This marked reduction of the efficiencies of the last stage and of the turbine as a whole when throttling the engine (for small $\pi^*_{T\Sigma}$, T^*_0, and η = const) can be prevented by using regulation of the last-stage stator vanes.

APPENDIX I

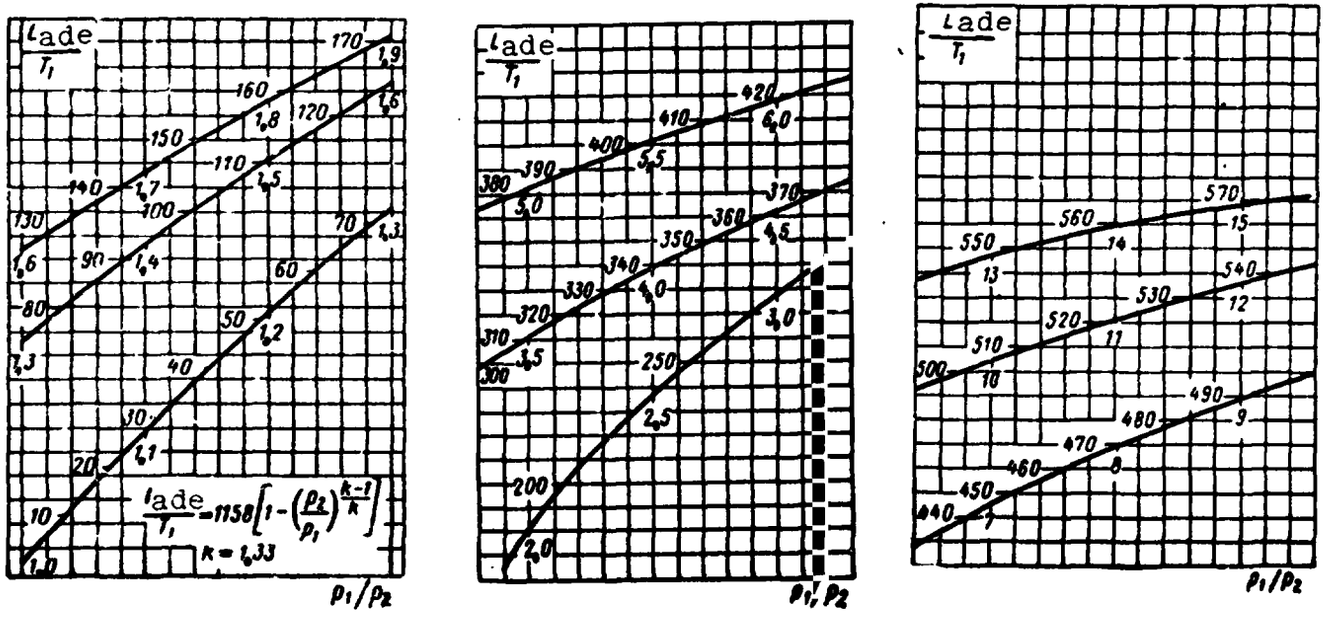

Figure 1. Ratio of adiabatic expansion work to initial gas temperature L_{ade}/T_1 as function of pressure ratio p_1/p_2

APPENDIX II

TABLE II.1. THERMAL CONDUCTIVITY OF MATERIALS $\lambda \cdot 10^3$, W/m·K*

Material	T, K										
	290	295	370	470	570	670	770	870	970	1070	1170
Nitridable CrNiT steels											
25Cr18Ni8W2 (EI946)	0,146	—	0,159	0,176	0,196	0,213	0,230	0,251	—	—	—
CrNiMo steels											
Cr17Ni5Mo3 (SN-3, EI925)	—	0,171	0,184	0,201	0,217	0,238	0,251	0,272	0,293	0,309	0,330
CrNi steels											
Cr18Ni9 (1Cr18Ni9, EYal)	0,159	—	0,163	0,180	0,188	0,201	0,213	0,238	0,255	0,268	0,268
Cr18Ni10Ti and Cr18Ni9Ti (1Cr18Ni9Ti, EYalTi)	—	—	0,163	0,176	0,188	0,205	0,217	0,234	0,247	0,263	0,284
0Cr18Ni12Nb (EI402)	—	—	0,159	0,176	0,192	0,205	0,221	0,230	—	0,263	—
1Cr21Ni5Ti (EI811)	—	—	0,176	0,180	0,192	0,201	0,230	0,272	0,301	0,351	0,368
EI654	0,121	—	0,134	0,146	0,159	0,176	0,192	0,213	0,226	0,242	—
EI759	0,113	—	0,125	0,142	0,159	0,184	0,201	0,221	0,238	0,262	0,294
CrNiMn steel with N											
Cr25Ni16Mn7NB (EI835)	—	—	0,150	0,163	0,176	0,192	0,209	0,221	0,238	0,255	0,276

(Table continued on following page)

TABLE II.1. (continued)

Material	T, K										
	200	295	370	470	570	670	770	870	970	1070	1170
Cr steels											
1Cr17Ni2 (EI268)	0,209	—	0,217	0,226	0,234	0,242	0,251	0,259	0,267	0,280	0,297
13Cr14NiWVBN (EI736)	0,196	—	0,209	0,221	0,230	0,230	0,259	0,267	0,276	—	—
1Cr12Ni2WMoV (EI961)	0,209	—	0,221	0,238	0,255	0,272	0,280	0,284	0,288	0,301	—
10Cr12NiWMoVN (EI962)	0,209	—	0,221	0,238	0,255	0,272	0,280	0,284	0,288	0,301	—
23Cr13NiWMoVN (EI388)(sheet)	—	0,192	0,201	0,213	0,226	0,238	0,255	0,267	—	—	—
CrMnNi steel											
4Cr15Ni7Mn782NoSi (EI388)	—	0,125	0,142	0,159	0,180	0,201	0,217	0,238	0,259	0,276	0,297
CrNiMn steel											
4Cr12Ni8Mn8MoVNb (EI481)	—	—	0,171	0,184	0,196	0,213	0,230	0,247	0,259	0,272	0,298
CrNi steels											
EI961L	—	0,188	0,196	0,213	0,230	0,238	0,251	0,259	0,263	0,272	—
VZhL10	—	0,130	0,138	0,150	0,163	0,176	0,192	0,209	0,221	0,226	0,234
EP126 (VZh100)	—	0,109	0,125	0,142	0,159	0,176	0,192	0,209	0,221	0,238	0,259

(Table continued on following page)

TABLE II.1. (continued)

Material	T, K										
	290	295	370	470	570	670	770	870	970	1070	1170
Ni-base alloys											
CrNi78Ti (Cr20Ni80Ti, EI435)	—	—	0,146	0,167	0,184	0,205	0,226	0,247	0,267	0,288	0,318
CrNi70Al (EI652)	—	0,117	0,125	0,138	0,155	0,171	0,188	0,209	0,230	0,247	0,267
CrNi60W (EI868, VZh98)	0,096	—	0,104	0,117	0,138	0,152	0,188	0,213	0,234	0,255	0,280
CrNi77TiAlB (EI437B)	0,125	—	0,138	0,155	0,171	0,188	0,209	0,234	0,251	0,280	0,309
EI437BU	0,125	—	0,138	0,155	0,171	0,188	0,209	0,234	0,251	0,280	0,309
CrNi77TiAl (EI437A)	—	0,113	0,125	0,142	0,159	0,180	0,201	0,221	0,242	0,267	0,293
CrNi70MoWTiAlNb (EI598)	—	—	0,113	0,129	0,146	0,159	0,188	0,205	0,217	0,242	0,263
CrNi70WMoTiAl (EI617)	—	—	0,096	0,113	0,130	0,150	0,171	0,192	0,217	0,242	0,272
EI867	0,088	—	0,104	0,130	0,150	0,168	0,188	0,201	0,217	0,230	0,247
EI929	0,088	—	0,104	0,121	0,142	0,163	0,184	0,205	0,226	0,242	0,267
EI220	—	—	0,096	0,113	0,125	0,146	0,159	0,180	0,196	0,213	0,234
ZhS6-KP	—	0,092	0,104	0,117	0,134	0,150	[illegible]	[illegible]	[illegible]	0,226	0,251
EP109 (VZh101)	—	—	0,100	0,113	0,134	0,150	0,167	0,184	0,201	0,221	0,242
ZhS6	—	0,105	0,113	0,125	0,138	0,155	0,176	0,196	0,217	0,238	0,268

(Table concluded on following page)

TABLE II.1. (concluded)

Material	T, K										
	290	295	370	470	570	670	770	870	970	1070	1170
Ni-base alloys											
ZhS6-K	0,084	—	0,096	0,117	0,134	0,155	0,180	0,196	0,213	0,230	0,251
ZhS6-KP	—	0,096	0,109	0,121	0,138	0,150	0,167	0,184	0,196	0,213	0,234
ZhS3 (EI618)	0,096	—	0,105	0,117	0,134	0,150	0,171	0,188	0,209	0,238	0,268
ANV300	—	0,092	0,100	0,113	0,130	0,146	0,163	0,180	0,196	0,217	0,242
VZh36-L1	—	0,075	0,088	0,105	0,125	0,138	0,146	0,159	0,184	0,209	0,236
VZh36-L2	—	0,113	0,125	0,138	0,155	0,171	0,188	0,205	0,222	0,238	0,255
High Cr steel											
Cr28NNi (EI657)	0,259	—	—	—	0,259	0,263	0,276	0,288	0,313	0,339	359

*Translator's note. Commas in numbers represent decimal points.

TABLE II.2. PHYSICAL PARAMETERS OF DRY AIR AT PRESSURE p = 100 kPa (735.5 mm Hg)*

Temperature, K	Thermal conductivity, $\lambda \cdot 10^3$ W/m·K	Dynamic viscosity, $\mu \cdot 10^6$ H·c/m^2	Temperature, K	Thermal conductivity, $\lambda \cdot 10^3$ W/m·K	Dynamic viscosity, $\mu \cdot 10^6$ H·c/m^2
400	33,8	22,86	900	62,0	39,73
500	40,7	26,88	1000	66,7	42,38
600	46,9	30,51	1100	71,5	44,83
700	52,4	33,84	1200	76,3	47,19
800	57,3	36,89	1300	—	49,54

*Translator's note. Commas in numbers represent decimal points.

APPENDIX III

COOLED TURBINE BLADES FOR AIRCRAFT ENGINES

Figure III.1 shows the cooling scheme for the turbine stages of the PWA JT9D twin-spool bypass engine. The turbine inlet gas temperature of this engine is 1443 K. The turbine has cooled first-stage stator vanes 4 and rotor blades 5, and second-stage stator vanes 6. /256

The air 3 is extracted downstream of the compressor 1, flows around the outside of the flametube, and is used to cool the turbine first-stage stator vanes 4 and second-stage stator vanes 6. The air is exhausted from the vane cooling passages into the flow path through slots along the entire length of the trailing edge.

This same air is fed to the turbine first-stage rotor blades 5 after flowing over the inner surface of the flame-tube. After cooling the rotor blades, the air is discharged from radial passages located inside the blades through the blade tip into the radial clearance and then into the turbine flow path. Air taken from a compressor intermediate stage flows through the cavity 2 to cool the last turbine stage rotors.

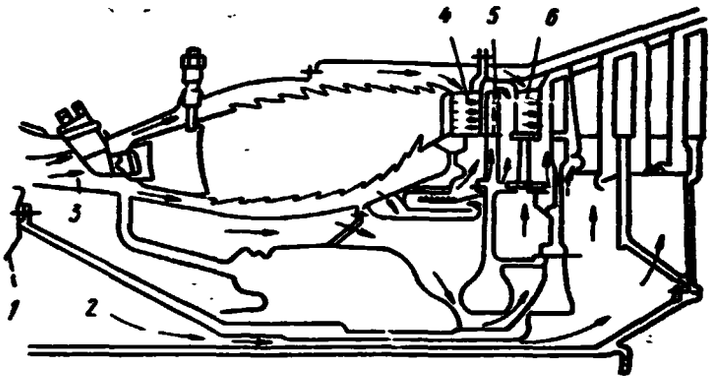

/257

Figure III.1. JT9D engine turbine

The first-stage stator vanes 1 (Figure III.2) are made from a cobalt-base casting alloy. The stator vane leading edge 2 is cooled by air jets which come through the holes 4 from the deflector 3 located inside the blade, and impinge on the inner surface of the vane. The deflector is a casting with the seating band 5 and protrusions on the surface, whose height determines the clearance between the deflector and the inner surface of the vane. These same protrusions improve convective heat transfer effectiveness by creating turbulent air flow.

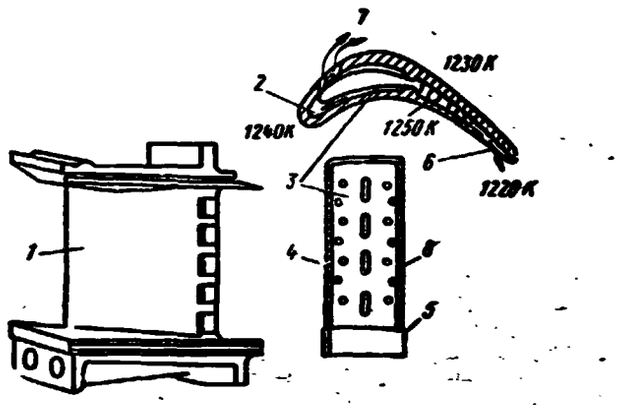

Figure III.2. JT9D turbine first-stage stator vane

The vane trailing edge is cooled by air coming from the inner cavity of the deflector through the continuous slot 8 and discharging from the slots 6 located on the concave side of the vane near the trailing edge. Holes 7 are provided on the back side of the vane near the leading edge for cooling air discharge in order to create film cooling of the back of the vane, and thus improve the cooling of the vane profile segment which is most highly loaded by the gas /258

forces. This cooling system provides practically uniform vane cross section temperature.

The second-stage stator vane (Figure III.3) with the inserted inner deflector 4 is made from a nickel-base casting alloy. The second-stage stator inlet gas temperature is 160° lower than that of the first stage. The vane is cooled convectively by jet impingement in the leading edge region 1, and by film cooling in the trailing edge segment 3.

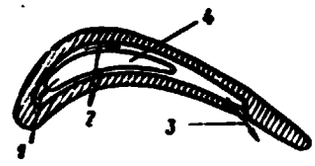

Figure III.3. JT9D engine turbine second stage stator vane

The first-stage rotor blade (Figure III.4) is also made from a casting alloy. Blade cooling is convective. The cooling air enters the root 1, and then the three-passage cooling system 2 of the profiled part of the blade.

After flowing through the radial passages, the air is discharged into the radial clearance from the blade tip 3. Local protuberances 4 are provided at the inlet to the central passage to cause turbulent flow and thereby intensify the heat transfer. Longitudinal ribs 5 are provided on the side walls of this passage, and they also intensify the heat transfer and increase the cooling surface area.

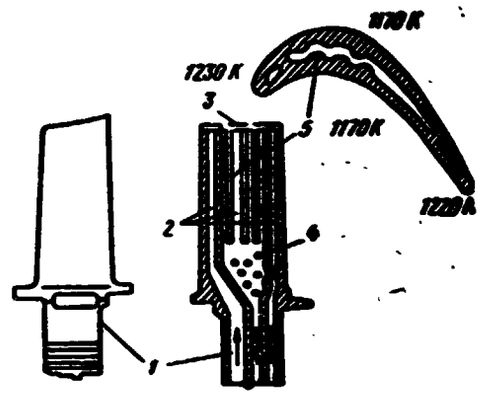

Figure III.4. JT9D engine turbine first-stage stator blade

Figure III.5 shows the changes made in the cooled blades produced by PWA in the course of several years. This figure shows that blades with purely convective cooling permit turbine inlet gas temperatures up to 1470 K (see Figure III.5a), blades with purely convective cooling and jet impingement of the air on the inner surface of the leading edge (see Figure III.5b) permit temperatures from 1470 to 1570 K, and blades with convective and film cooling of the leading and

trailing edges (see Figure III.5c) permit turbine inlet gas temperatures up to 1670 K.

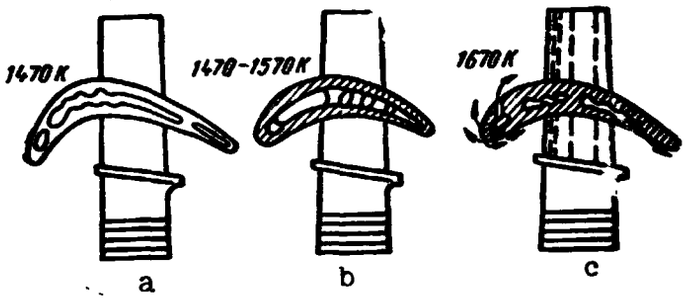

Figure III.5. Modification of PWA blades

Figure III.6 shows the scheme for cooling the first stage of the high-pressure turbine of the Rolls-Royce RB-211 bypass engine, in which the turbine inlet gas temperature is 1480 K, and also shows the design of the cooled rotor blade of this stage.

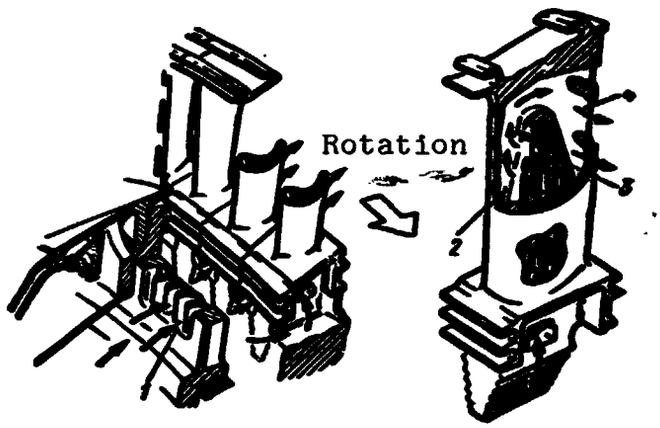

Figure III.6. Rolls-Royce engine turbine first-stage cooling scheme

The figure shows the guide vanes 1 of the pre-swirl cascade used to impart a circumferential velocity component in the direction of wheel rotation to the cooling air entering the root part of the rotor blade. This reduces the cooling air total /259 pressure losses during entry into the rotor blade and reduces the cooling air temperature. The rotor blade is cooled convectively, and is made from a casting alloy. Jet impingement of the air through the slot 2 in the cast inner deflector 3 is used to improve leading edge cooling, and longitudinal ribbing of the inner surface is used in the central part of the blade. The air discharges through the slots 4 along the trailing edge into the turbine flow path.

Figures III.7 - III.10 show the GE TF-39 bypass engine turbine blades. The turbine first-stage inlet gas temperature is 1560 K. The turbine first-stage stator vane (Figure III.7) uses both convective and film cooling.

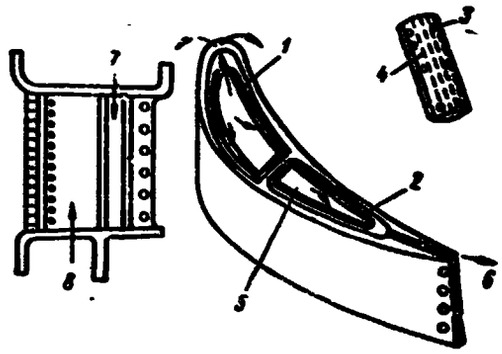

Figure III.7. TF-39 engine first-stage turbine stator vane

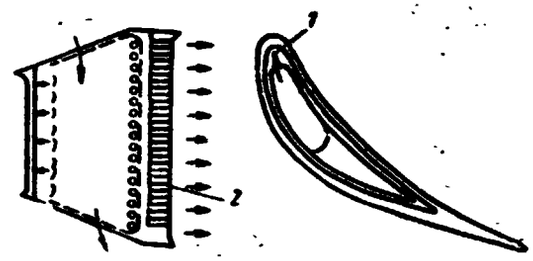

Figure III.8. TF-39 engine second-stage turbine stator vane

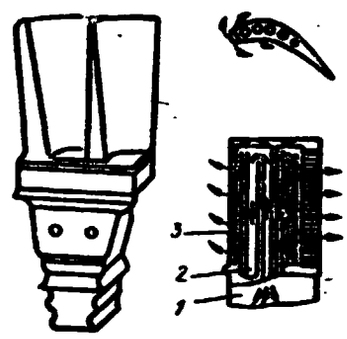

Figure III.9. TF-39 engine first-stage turbine rotor cooled blades

A distinctive feature of the first-stage stator vane is the fact that its interior is divided into two regions. The deflectors 1 and 2, respectively, are installed in the two regions and the side surfaces of the deflectors have numerous positioning protrusions 3 and small holes 4 to provide jet cooling of the inner surface of the vane. Air 7 from the intermediate compressor stage enters the inner cavity of the deflector 5, adjacent to the trailing edge, at a pressure lower than that in the leading-edge cavity 8, and is discharged into the flow path through the slots 6 in the trailing edge. /260

The second-state stator vane (Figure III.8) is cooled convectively with jet impingement of the cooling air 1 on the inner surface of the leading edge, i.e., with transverse flow of the cooling air relative to the vane length. The cooling air discharges through the trailing-edge passages 2 into the turbine flow path.

A feature of the first-stage rotor blade design (Figure III.9) is the fact that in this blade the profiled parts are dual, and are arranged pairwise on the same retention unit, in which there is a

distribution chamber 1 into which the cooling air is supplied. The air is directed from this chamber into the cooling passages 2 along both profiled parts. Thus, the large cross section area of the vane air suply passages make it possible to reduce the air leakage. The air splits into two passages upon entry into the profiled parts of the blade; one part of the air is fed to the passage for cooling the leading edge, the other part is fed to the trailing edge. Both streams follow a looping path along the radial passages, providing convective cooling of the profiled part. Then the cooling air impinges in the form of jets on the inner surface of the leading edge and thence passes through holes in the wall 3 onto the outer surface, and forms a protective air layer. The holes 3 are located along the entire length of the vane, and are angled to ensure reliable cooling of the leading edge.

Dual passages are also provided in the second-stage rotor blade (Figure III.10) to provide convective cooling. This system design is the same as in the first-stage blade — the radial passages in the middle part of the blade form air flow which is symmetric relative to the axis with three reversals of direction. In addition, straight flow passages are provided along the leading and trailing edges. After cooling the blade, the air is discharged through five holes from the blade tip into the radial clearance.

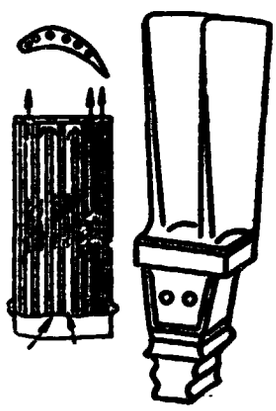

Figure III.10. TF-39 engine second stage turbine rotor cooled blades

All these passages are made by electro-erosive drilling. This technique makes it possible to drill several passages of different diameter simultaneously at a speed of 25 - 50 mm/min. The passages in the leading and trailing edge of the blade are made by anodic dissolution by electrolyte which is supplied from a slender glass tube.

In spite of the large number of small-diameter holes and the complexity of their

configuration, they do not clog during operation. Particles of dimension no more than 50 microns which enter the passages are ejected from the cleaning holes in the tip part of the blade. Moreover, by selecting the dimensions of these holes, we can regulate the hydraulic resistance of the cooling passages and ensure uniformity of the cooling air distribution among the blades. /261

The GE CF-6 bypass engine turbine blade with turbine inlet gas temperature 1530 - 1560 K uses the same cooling scheme as the TF-39 jet engine blade.

Figure III.11 shows two designs of the first-stage cooled rotor blade of the P-100 bypass engine of the PWA TF-30 family, which operates with turbine inlet gas temperature 1530 K.

A new modification is the blade with insert-type deflector and cooling air discharge through slots in the trailing edge. According to the manufacturer [34], efficiencies above 90% were obtained in tests of a turbine with these blades. This indicates that the blades with internal deflector and transverse cooling air flow are quite promising from the viewpoint of both cooling effectiveness and turbine efficiency.

The second-stage stator vane of this same engine (Figure III.12) has an internal insert-type deflector, and also has transverse flow of the cooling air with discharge of the latter from slots in the concave part of the blade along the trailing edge.

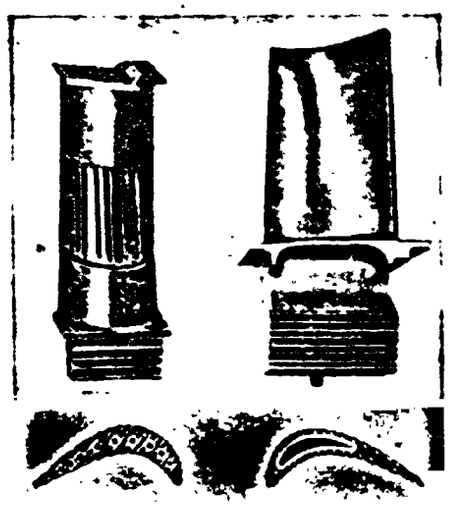

Figure III.11. Original (left) and new modification of the P-100 engine high-pressure turbine rotor blade

The above-mentioned turbine inlet gas temperatures are mass-average values and can characterize only approximately the temperature level of the gas flow around the stator vanes and rotor blades. For the same value of this temperature, there may be different degrees of nonuniformity of the temperature field T_{pat} in the combustion chamber exit gas flow (see section 6.5), and this means different maximal temperature of the gas approaching the stator vanes. This difference may be quite large (up to 100°) and depends on the combustion chamber efficiency and the magnitude of the air temperature rise in the combustion chamber.

Figure III.12. P-100 engine second-stage turbine stator vane

The temperature of the gas flowing around the rotor blades also differs from the mass-average turbine inlet gas temperature by the magnitude ΔT_{pat} and by the magnitude ΔT_w, which depend on the turbine stage loading, magnitude of the circumferential velocity, and other factors (see section 7.1).

APPENDIX IV

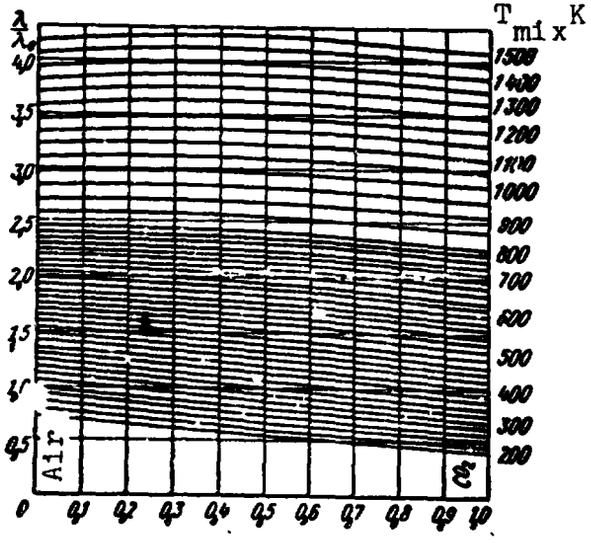

Figure IV. Relative thermal conductivity versus component ratio of air-CO_2 mixture for various values of T_{mix} (for air with T_0= 273 K and λ_0 = 24.116 · 10^{-3} W/(m·K)

APPENDIX V

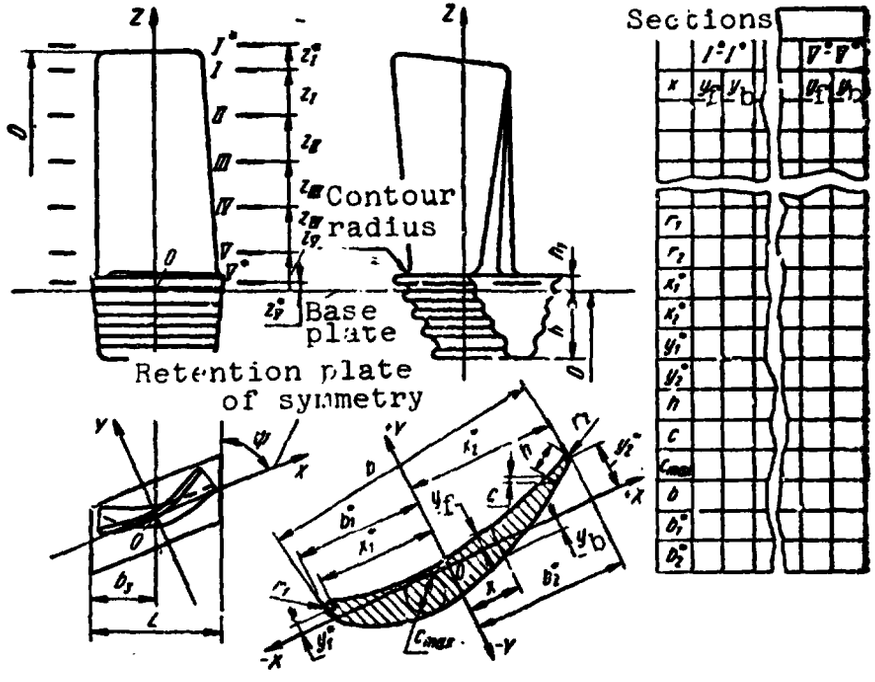

Figure V. Rotor blade coordinate system, location of blade profile dimensions, form of variable parameter table (dimensions and reference sections)

REFERENCES

1. Abiants, V. Kh. Teoriya gazovykh turbin rekativnykh dvigateleiy (Jet Engine Gas Turbine Theory). Moscow, Mashinostroyeniye Press, 1965, 310 pp. /264

2. Aronov, B. M. Profilirovaniye pera lopatok aviatsionnykh gazovykh turbin (Profiling Aircraft Gas Turbine Blades). Kuibyshev, Kuibyshev Aviation Institute Press, 1970, 168 pp.

3. Bodunov, M. N. and V. I. Lokay. Coefficient of Heat Transfer from Gas to Various Turbine Flow Path Elements. In the book: Vysokotemperaturnyye okhlazhdayemyye gazovyye turbiny (High-Temperature Cooled Gas Turbines). Moscow, Mashinostroyeniye Press, 1971, pp. 23-43.

4. Gurov, S. V. Issledovaniye intensivnosti okhlazhdeniya deflektornoy lopatki (Study of Deflector Type Blade Cooling Rate). Teploenergetika, No. 10, 1967, pp. 81 - 84.

5. Gikhman, A. A. and N. V. Ilyukhin. Osnovy ucheniya o teploobmene i techenii gaza s bol'shoy skorost'yu (Fundamentals of Heat Transfer in High-Velocity Gas Flow). Moscow, Mashgiz Press, 1951, 227 p.

6. Deich, M. Ye. and G. S. Samoylovich. Osnovy aerodinamiki osevykh turbomashin.(Fundamentals of Axial Turbomachine Aerodynamics). Moscow, Mashgiz Press, 1965, 428 pp.

7. Dobrokhotov, A. N. and A. V. Maksay. Teoriya aviatsionnykh gazovykh turbin (Theory of Aircraft Gas Turbines). Riga, RKVIAVU, 1955, 166 p.

8. Yemin, O. N. Kharakteristika i regulirovaniye aviatsionnykh turbin (Aircraft Turbine Performance and Regulation). Moscow, Moscow Aviation Institute, 1964, 126 pp.

9. Zhiritskiy, G. S., et al. Gazovyye turbiny aviatsionnykh dvigateley (Aircraft Engine Gas Turbines). Moscow, Mashinostroyeniye Press, 1971, 620 pp.

10. Zhuravlev, V. A. Use of Digital Electronic Computers to Profile Gas Turbine Blades. Izvestiya AN SSSR, OTN, Energetika i Transport, No. 1, 1963, pp. 72-77.

11. Zhuravlev, V. A. Analytic Construction of GTE Turbine Blade Profiles. In the book: Voprosy aerodinamiki i dinamicheskoy ustoychivosti ploskikh kompressornykh i turbinnykh reshetok (Aerodynamics and Dynamic Stability of Two-Dimensional Compressor and Turbine Cascades). Riga [Transactions of RKIIGA], No. 187, 1970, pp. 90 - 108.

12. Zysina-Molozhen, L. M. Calculation of the Thermal Boundary Layer in a Compressible Gas Stream. IFZh, Vol. 5, No. 6, 1962, pp. 12-15.

13. Kirillov, I. I. Teoriya Turbomashin (Turbomachine Theory). Moscow, Mashinostroyeniye Press, 1964, 510 pp.

14. Kopelev, S. Z., S. V. Gurov and M. V. Avilova-Shul'gina. Generalized Heat Transfer Relations in Transverse Cooling Flow Blades. Energomashinostroyeniye, No. 4, 1963, pp. 31-33.

15. Kopelev, S. Z. and V. G. Nesterenko. Influence of Wire Banding on Turbine Efficiency. In the book: Voprosy aerodinamiki i dinamicheskoy ustoychivosti ploskikh kompressornykh i turbinnykh reshetok (Aerodynamics and Dynamic Stability of Two-Dimensional Compressor and Turbine Cascades). Riga [Transactions of RKIIGA], No. 187, 1970, pp. 66-77.

16. Kopelev, S. Z, S. V. Gurov and M. V. Avilova-Shul'gina. Study of Hydraulic Resistance in Cooled Gas Turbine Blades. Teploenergetika, No. 9, 1970, pp. 36-39.

17. Kopelev, S. Z. Influence of Flow Kinematics in Turbine Stage on Efficiency. In the book: Voprosy aerodinamiki i dinamicheskoy ustoychivosti ploskikh kompressornykh i turbinnykh reshetok (Aerodynamics and Dynamic Stability of Two-Dimensional Compressor and Turbine Cascades). Riga [Transactions of RKIIGA], No. 187, 1970, pp. 79-89.

18. Kopelev, S. Z., Ya. L. Fogle and V. A. Zhuravlev. Profiling Turbine Blades. In the book: Proizvodstvo lopatok dvigateley (Engine Blade Production). Moscow, Oborongiz Press, No. 3, 1957, pp. 28-35. /265

19. Kopelev, S. Z., Ye. Ye. Likherzak and S. G. Lev. Losses in a Cascade with Injection Through the Leading Edge. In the book: Energeticheskoye mashinostroyeniye (Energetic Machine Design). Kharkov, Kharkov University Press, No. 16, 1973, pp. 38-40.

20. Kutateladze, S. S. Osnovy Teorii Teploobmena (Fundamentals of Heat Transfer Theory). Moscow-Leningrad, Mashgiz Press, 1962, 456 pp.

21. Mikheyev, M. A. Osnovy Teploperedachi (Fundamentals of Heat Transfer). Moscow-Leningrad, Gosenergoizdat Press, 1956, 392 pp.

22. Ratner, F. Z. Computer Calculation of Flow and Pressure Distributions in Gas Turbine Cooling Systems. In the book: Raschetnyye i eksperimental'nyye metody opredeleniya teplovogo sostoyaniya osnovnykh uzlov gazovykh turbin s vozdushnym oklazhdeniyem (Theoretical and Experimental Methods of Determining the Thermal Status of the Basic Components of

Air-Cooled Gas Turbines). Leningrad, Trudy TsKTI (Central Boiler and Turbine Institute), No. 29, 1970, pp. 153-193.

23. Stepanov, G. Yu. Gidrodinamika Reshetok Turbomashin (Hydrodynamics of Turbomachine Cascades). Moscow. Fizmatgiz Press, 1962, 512 pp.

24. Stechkin, B. S., et al. Teoriya Reaktivnykh Dvigateley Lopatochnye Mashiny (Jet Engine Theory. Compressors and Turbines). Moscow, Oborongiz Press, 1956, 548 pp.

25. Tikhonov. N. D. Off-Design Operating Regimes of Aircraft Gas Turbines. Riga [Trudy RKVIAVU], No. 18, 1957, 38 pp.

26. Tumanskiy, S. K. Turbojet Engines for High Speeds. Aviatsiya i kosmonavtika, No. 2, 1966, pp. 60 - 54.

27. Horlock, J.H. Osevyye turbiny (Axial-Flow Turbines). Moscow, Mashinostroyeniye Press, 1972, 210 pp.

28. Kholshchevnikov, K. V. Teoriya i raschet aviatsionnykh lopatochnykh mashin (Theory and Design of Aircraft Turbomachines) Moscow, Mashinostroyeniye Press, 1970, 609 pp.

29. Shvets. I. T. and Ye. P. Dyban. Vozdushnoye okhlazhdeniye rotorov gasovykh turbin (Air Cooling of Gas Turbine Rotors). Kiev, Kiev University Press, 1959, 349 pp.

30. Sherstyuk, A. N. Determining Losses in Turbine Cascades at Off-Design Angles of Attack. Izvestiya AN SSSR, OTN, Energetika i avtomatika, No. 2, 1960, pp. 18-21.

31. Schneider, P. J. Conduction Heat Transfer. Moscow. Foreign Literature Press, 1960, 478 pp.

32. Shnee, Y. I. and V. L. Grodzinskiy. Variation of Stage Reaction Under Variable Operating Conditions. In the book: Energeticheskoye mashinostroyeniye (Energetic Machine Design), No. 8, Kharkov, 1970, pp. 100-107.

33. Eigenson, L. S. Modelirovaniye (Modeling). Moscow, Promstroizdat Press, 1949, 238 pp.

34. Internal Combustion Engine (Japan), Vol. 9, No. 9, 1970, pp. 65-75.

35. Aviation Week, Vol. 95, No. 20, 1971, p. 23.

Translated for National Aeronautics and Space Administration under contract No. NASw 2483, by SCITRAN, P. O. Box 5456, Santa Barbara, California, 93108